

**POLITECNICO DI TORINO**

**Corso di Laurea Magistrale in  
Ingegneria Biomedica**

**Tesi di Laurea Magistrale**

**Design and manufacturing  
of bioprinted gellan gum-based constructs  
representative of the articular cartilage**



**Supervisors**

Prof. Gianluca Ciardelli  
Dr. Piergiorgio Gentile  
Prof. Chiara Tonda-Turo

**Candidate**

Michele Pistillo  
Matricola: s244210

**A.A. 2019/2020**



#### Declaration of work

I declare that this thesis is based on my own work and has not been submitted, in whole or in part, for another degree at any University or any other tertiary education. Information derived from published and unpublished works of others have been reported in the bibliography section.



## Abstract

Articular cartilage (AC) is a highly specialized tissue which exhibit topographical heterogeneity in terms of matrix composition and mechanical properties. Due to its avascular nature AC shows limited regenerative ability, therefore representing an excellent subject for tissue engineering (TE). Particularly, bioprinting is an emerging additive manufacturing technology that has already demonstrated its potential use in regenerative medicine and cartilage TE. It allows to recapitulate the tissues microstructure by a controlled deposition of “bioinks”, suspensions of cells alone or encapsulated in biomaterials. As cells source, mesenchymal stem cells and chondrocytes, both naturally found in AC, are mainly selected. Hydrogels are largely used as biomaterials for their ability to resemble soft tissues extracellular matrix (ECM), providing an ideal micro-environment for the embedded cells survival, proliferation and differentiation. Hydrogels are produced from synthetic and natural polymers, including gellan gum (GG), a biocompatible polysaccharide that has gained interest in cartilage TE because of its structural similarity to cartilage glycosaminoglycans (GAGs) and chondrogenic potential.

The aim of this work was the design and manufacturing of 3D constructs mimicking AC by extrusion bioprinting. Particularly, this thesis objectives (OBJ) were: the synthesis and characterisation (physico-chemical, morphological, mechanical) of methacrylated GG-based hydrogels subjected to a dual physical and photo-chemical crosslinking (OBJ1); the subsequent biofabrication via Rokit INVIVO bioprinter of *in vitro* constructs (OBJ2) and biological characterisation of cell-laden constructs in terms of cells viability and AC tissue formation (OBJ3). The final stage of this work dealt with the manufacturing of osteoarthritis (OA) *in vitro* models, via culturing healthy models in cytokine-enriched culture medium, for future analysis on novel OA therapeutic treatments. Firstly, the success of GG methacrylate (GGMA) synthesis was demonstrated through FTIR and XPS analysis. Then, 4 photo-curable hydrogels were prepared: pure GGMA 2% w/v (GG2) and 3% w/v (GG3), and GGMA (respectively 2% w/v and 0.75% w/v) combined with 5% w/v manuka honey (GG/MH) and 10% w/v gelatin (GG/GEL). Gelation analysis at room temperature showed that GG3 and GG/GEL underwent sol-gel transition in ~1 minute, while GG2 and GG/MH in ~3 minute. Water uptake (WU) analysis demonstrated the strong hydrophilic nature of these hydrogels, reaching WU values up to ~1950%. Morphological analysis evidenced that they had an interconnected porous morphology with a mean pore diameter in the range 100-200  $\mu\text{m}$ , suitable for AC applications.

Similarly, mechanical analysis showed that hydrogels had a compressive Young's modulus between ~25 and ~16 kPa, comparable to other natural hydrogels found in literature. GG2 and GG/MH hydrogels were selected as bioinks encapsulating human TERT immortalised stem cells differentiated into chondrocytes (Y201-C;  $7 \times 10^6$  cells/ml). The double-crosslinked bioinks were successfully printed into stable constructs. Live/Dead assay demonstrated high cell viability for both bioprinted constructs, while immunostaining analysis of cells nuclei and cytoskeleton evidenced that cells appeared not uniformly dispersed in GG/MH constructs. The GAGs quantification assay showed that Y201-C GAGs production increased over time in both hydrogels. Finally, scanning electron microscopy analysis showed that cells exhibited a typical chondrocytes rounded-shaped morphology and tended to aggregate in both healthy and pathological GG2 constructs.



## Acknowledgements

Questo lavoro segna la fine del mio percorso come studente del Politecnico di Torino, che ha visto come tappa finale l'attività di tesi svolta presso la Newcastle University. Questi anni sono stati intensi e turbolenti, e nonostante varie difficoltà mi hanno arricchito moltissimo. Desidero ringraziare tutte le persone che mi hanno supportato e affiancato durante questo percorso.

Ringrazio il Prof. Gianluca Ciardelli, relatore della tesi, per la sua disponibilità e per avermi permesso di intraprendere l'attività di tesi all'estero.

Grazie al Dr. Piergiorgio Gentile, correlatore della tesi, per avermi seguito costantemente e aiutato sia nella realizzazione della tesi sia durante il mio periodo di permanenza all'estero. Ringrazio la Prof. Tonda Turo, correlatrice, per avermi indirizzato nella scelta dell'argomento di tesi.

Ringrazio Annachiara, per la sua pazienza e gentilezza, per avermi supportato scrupolosamente nella stesura della tesi, e per avermi guidato passo dopo passo durante la mia esperienza in laboratorio.

Un pensiero va ai miei amici conosciuti prima del percorso universitario Fabio, Miky, Riccardo, Giulia e Asia. Non siete mai stati distanti.

Grazie alla Prof. Bozzani, per essere stata una delle prime persone a credere in me.

Ringrazio calorosamente tutti i miei coinquilini, per avermi fatto sentir parte di una famiglia. Grazie ad Alessio, amico con cui ho condiviso i primi anni, le prime difficoltà e i primi momenti felici da studente fuori sede. Grazie a Saverio, che mi ha fatto sempre sentire a casa. Grazie a Daniele, a cui devo tante risate.

Un grazie sentito va agli amici conosciuti in collegio, che mai mi hanno fatto sentire solo. In particolare, ringrazio Piernicola, Giorgio e Anita, per i momenti preziosi vissuti insieme. Grazie a Luca, per il modello di dedizione che ha rappresentato. Ringrazio Paolo, capace di risollevare l'umore anche grazie alla sua cucina. Grazie a Giammarco, il miglior vicino di stanza che potessi desiderare.

Grazie di cuore anche ai miei compagni di corso, che hanno reso più lievi gli impegni universitari. Grazie a Cesare, per la sua sincera amicizia ed esempio di tenacia. Grazie a Marco, per la sua generosità. Grazie a Elena, Alessandra e Michele, con cui ho frequentato lezioni e passato momenti gioiosi. Grazie anche a Gerardina per il suo entusiasmo ed energia contagiosi. Grazie anche a Francesco, Assunta e Valeria, compagni di corso del primo anno che sono rimasti vicini.

Infine, ringrazio profondamente i miei genitori, mia sorella e i miei nonni. Grazie per avermi sempre sostenuto, per avermi confortato nei momenti difficili e soprattutto per avere avuto fiducia in me. Siete le forti radici che mi sostengono. A voi dedico questo lavoro.



# Table of Contents

<b>Abstract</b> .....	<b>III</b>
Acknowledgements.....	VI
List of Figures .....	XI
List of Tables.....	XII
List of Abbreviations .....	XII
<b>Chapter 1: Introduction</b> .....	<b>1</b>
1.1 Cartilage biology and function in the human body.....	1
1.1.1 Articular cartilage formation and chondrogenic signalling molecules .....	3
1.1.2 Structure, functions and composition of adult articular cartilage .....	5
1.1.3 Ultra-Structure of adult articular cartilage.....	8
1.1.4 Biomechanical properties .....	11
1.2 Articular cartilage changes in osteoarthritis .....	14
1.2.1 Surgical and cell-based treatments for articular cartilage repair.....	17
1.2.2 Tissue engineering application in cartilage treatment.....	21
1.3 3D <i>in vitro</i> models .....	25
1.3.1 3D <i>in vitro</i> models to mimic cartilage development .....	27
1.3.2 Modelling cartilage degenerative processes.....	29
1.3.3 3D <i>in vitro</i> models fabrication techniques .....	31
1.4 3D Bioprinting.....	32
1.4.1 Process and approaches .....	33
1.4.2 3D Techniques classification.....	35
1.4.3 Limits and prospects .....	38
1.5 Bioinks for 3D Bioprinting .....	39
1.5.1 Bioink properties and bioprinting parameters relationships .....	40
1.5.2 Hydrogel properties.....	42
1.6 Gellan gum-based hydrogels and their application in 3D bioprinting .....	51
1.6.1 Overview of Gellan Gum.....	51
1.6.2 Gellan gum methacrylate .....	56
1.6.3 Gellan gum-based bioinks for 3D bioprinting.....	58
1.7 Cell source for cartilage tissue engineering .....	60
<b>1.8 Aim and objectives of the thesis</b> .....	<b>64</b>
<b>Chapter 2: Materials and Methods</b> .....	<b>66</b>
2.1 Materials.....	66

2.2 Hydrogels preparation .....	66
2.2.1 GGMA synthesis .....	66
2.2.2 GGMA-based hydrogels preparation .....	66
2.3 Hydrogel Characterisation .....	68
2.3.1 GG and GGMA Chemical characterisation .....	68
2.3.2 GG and GGMA Thermogravimetric analysis (TGA) .....	69
2.3.3 Physical Characterisation .....	69
2.3.4 Hydrogel Morphological analysis .....	70
2.3.5 Mechanical characterisation .....	71
2.4 Cell culture .....	72
2.5 Bioprinting.....	72
2.5.1 Hydrogel printability evaluation .....	72
2.5.2 Bioink preparation.....	73
2.5.3 3D Bioprinting and <i>in vitro</i> cell culture of constructs .....	73
2.5.4 Cell viability after printing.....	74
2.5.5 Cell morphology and distribution .....	75
2.5.6 OA induction in bioprinted 3D <i>in vitro</i> models .....	75
2.5.7 GAGs quantification (AlcianBlue) .....	76
2.5.8 Bioprinted constructs morphological analysis (SEM) .....	76
2.6 Statistical analysis .....	77
<b>Chapter 3: Results .....</b>	<b>79</b>
3.1 Hydrogel Characterisation .....	79
3.1.1 Chemical Characterisation .....	79
3.1.2 Thermal characterisation .....	82
3.1.3 Physical Characterisation .....	83
3.1.4 Morphological analysis.....	84
3.1.5 Mechanical characterisation .....	87
3.2 Bioprinting.....	89
3.2.1 Hydrogels printability evaluation .....	89
3.2.2 Bioprinted construct: cells viability.....	90
3.2.3 Cell morphology and distribution in GGMA-based printed bioinks.....	91
3.2.4 GAGs quantification (AlcianBlue) .....	92
3.2.5 Bioprinted constructs morphological analysis .....	93
<b>Chapter 4: Discussion .....</b>	<b>96</b>

4.1 Hydrogel synthesis and characterisation .....	96
4.2 Bioprinting .....	102
<b>Chapter 5: Conclusion and future directions .....</b>	<b>110</b>
Appendix: Immunofluorescence analysis .....	113
<b>Bibliography.....</b>	<b>116</b>

## List of Figures

Figure 1.1: Scanning electron microscope image of a chondrocyte .....	2
Figure 1.2: Histology of the three types of cartilage .....	3
Figure 1.3 Development of the growth plate and bone formation .....	4
Figure 1.4 Hyaluronan and aggrecans forming a proteoglycan aggregate .....	8
Figure 1.5 Ultra-structure of articular cartilage .....	10
Figure 1.6 Viscoelastic response of articular cartilage under compression.....	13
Figure 1.7: Articular cartilage changes during osteoarthritis.....	17
Figure 1.8: Articular cartilage defect treatments .....	20
Figure 1.9 Cartilage tissue engineering .....	22
Figure 1.10: Osteoarthritis 3D <i>in vitro</i> models .....	31
Figure 1.11 Typical 3D printing fabrication phases .....	35
Figure 1.12: The main three techniques of 3D bioprinting .....	36
Figure 1.13: Relationships between bioink properties and printing parameters. ....	42
Figure 1.14: Chemical structure of acylated and deacylated gellan gum .....	52
Figure 1.15: Gellan gum polymer configuration during gelation process.....	54
Figure 1.16: Schematic drawing of gellan gum methacrylation reaction .....	57
Figure 1.17: Schematic illustration of GelMA-GG bioprinting and photo-crosslinking.....	59
Figure 2.1: Digital photo of the samples used for the water uptake test .....	70
Figure 2.2: Digital photo of a GG/GEL sample during unconfined compression test .....	71
Figure 3.1: FTIR-ATR spectra of GG and GGMA.....	80
Figure 3.2: High resolution XPS analysis of GG and GGMA.....	81
Figure 3.3: TG and dTG curves of GG and GGMA.....	82
Figure 3.4: Water uptake analysis relevant to GG3, GG2, GG/MH and GG/GEL hydrogels.....	84
Figure 3.5: eSEM images of GG3, GG2, GG/MH and GG/GEL hydrogels .....	85

Figure 3.6: Pore size distribution of GG3, GG2, GG/MH and GG/GEL hydrogels. ....	86
Figure 3.7: Mean pore diameter of GG3, GG2, GG/MH and GG/GEL hydrogels.....	87
Figure 3.8: Stress-strain curves of GG3, GG2, GG/MH and GG/GEL hydrogels.....	88
Figure 3.9: Compression Young's modulus of GG3, GG2, GG/MH and GG/GEL hydrogels.....	88
Figure 3.10: GGMA-based hydrogel printability assessment .....	90
Figure 3.11: Live/Dead confocal microscopy volume rendering of printed Y201-C.....	91
Figure 3.12: Immunostaining images of Y201-C .....	92
Figure 3.13: GAGs secretion quantitative analysis of Y201-C.....	93
Figure 3.14: Scanning electron microscopy images of bioprinted constructs.....	94
Figure A: Immunofluorescence images of Y201-C.....	114

## List of Tables

Table 1: Types of collagen found in articular .....	7
Table 2: Stimulating factors used in cartilage tissue engineering .....	24
Table 3: Comparison of the main 3D Bioprinting techniques.....	38
Table 4: Hydrogels used for cartilage tissue engineering.....	51
Table 5: Cell sources employed in cartilage tissue engineering .....	63
Table 6: Composition and code names of the prepared GGMA-based hydrogels.....	68
Table 7: Attribution of GG and GGMA FTIR-ATR absorption peaks.....	80
Table 8: Atomic percentage of GG and GGMA obtained through XPS.....	81
Table 9: Gelation time of the prepared GGMA-based systems.....	83

## List of Abbreviations

3D (Three-Dimensional)

A% (Atomic Concentration)

AAOS (Academy of Orthopaedic Surgeons)

AC (Articular Cartilage)  
ACI (Autologous Chondrocyte Implantation)  
AM (Additive Manufacturing)  
AMIC (Autologous matrix-induced chondrogenesis)  
BMPs (Bone morphogenetic proteins)  
BMSCs (Bone Marrow-derived Mesenchymal Stem Cells)  
BSA (Bovine Serum Albumin)  
CAD (Computer Aided Design)  
CAM (Computer Aided Manufacturing)  
Coll II (Collagen Type II)  
CPCs (Cartilage Progenitor Cells)  
CS (Chondroitin Sulphate)  
CT (Computed Tomography)  
CTE (Cartilage Tissue Engineering)  
DAPI (4', 6- Diamidino-2-Phenylindole)  
dH<sub>2</sub>O (Distilled Water)  
DMEM (Dulbecco's Modified Eagle Medium)  
dTG (Derivative Thermogram)  
ECM (Extracellular Matrix)  
ESCs (Embryonic Stem Cells)  
eSEM (Environmental Scanning Electron Microscope)  
EthD-1 (Ethidium Homodimer-1).  
EtOH (Ethanol)  
FBS (Fetal Bovine Serum)  
FDM (Fused Deposition Modelling)  
FTIR (Fourier Transform Infrared Spectroscopy)  
FTIR-ATR (Fourier Transform Infrared Spectroscopy - Attenuated Total Reflectance)  
GAGs (Glycosaminoglycans)  
GelMA (Gelatin-Methacryloyl)  
GFs (Growth Factors)  
GG (Gellan Gum)  
GGMA (Gellan Gum Methacrylate)

GMP (Good Manufacturing Procedure)  
HA (Hyaluronan)  
HBSS (Hanks' Balanced Salt Solution)  
HCl (Hydrochloric Acid)  
HDMS (Hexamethyldisilazane)  
ICRS (The international Cartilage Repair Society)  
IF (Immunofluorescence)  
IGFs (Insulin-like Growth Factors)  
IL-1 $\beta$  (Interleukin 1 $\beta$ )  
IL-6 (Interleukin 6)  
iPSCs (Induced Pluripotent Stem Cells)  
KS (Keratan Sulphate)  
LbL (Layer by Layer)  
MA (Methacrylic Anhydride)  
MACI (Matrix-Induced Autologous Chondrocyte Implantation)  
MRI (Magnetic Resonance Imaging)  
MSCs (Mesenchymal Stem Cells)  
M<sub>w</sub> (Molecular Weight)  
NaOH (Sodium Hydroxide)  
NSAIDs (Nonsteroidal Anti-Inflammatory Drugs)  
PBS (Phosphate Buffered Saline)  
PCL (Polycaprolactone)  
PCM (Pericellular Matrix)  
PCR (Polymerase Chain Reaction)  
PEG (Poly-Ethylene Glycol)  
PEGDA (Poly-Ethylene Glycol Diacrylate)  
PFA (Paraformaldehyde)  
PGs (Proteoglycans)  
PLGA (Poly(Lactic-Co-Glycolic Acid))  
RT (Room Temperature)  
SBF (Simulated Body Fluid)  
SEM (Electron Scanning Microscopy)

SLA (Stereolithography)

TE (Tissue Engineering)

TERT (Telomerase Reverse Transcriptase)

TG (Thermogram)

TGA (Thermogravimetric Analysis)

TGF- $\beta$  (Transforming Growth Factor-Beta)

TNF- $\alpha$  (Tumour Necrosis Factor-Alpha)

UV (Ultra Violet)

VEGFs (Vascular Endothelial Growth Factors)

XPS (X-ray Photoelectron Spectroscopy)

Y201 (Human TERT Immortalised Bone Marrow Stromal Cell)

Y201-C (Y201-chondrocytes)



# Chapter 1: Introduction

## 1.1 Cartilage biology and function in the human body

Cartilage is a specialised viscoelastic connective tissue generated over the course of the embryonic stage of human body development and constitutes a support for bone formation during skeletal development (Camarero-Espinosa *et al.*, 2016). Cartilage shows semitransparency, elasticity, flexibility and toughness. It is present in joints, ears, nose, the rib cage, the throat and between vertebral discs (ParviziMD and K.KimMD, 2010). Cartilaginous tissues form moreover callus, xyphoid, fracture mandibular condyle, as well as sphenoccipital synchondrosis, and costochondral junction (Boyan, Doroudi and Schwartz, 2011). Cartilage is pressure resistant, possess a high fluid percentage and presents low oxygen demand (Hall, 2005). Cartilage coats the surface of joints in order to decrease frictional effects that may give rise to damages, enables bones to slide on top of one another and to perform rotational movements. (ParviziMD and K.KimMD, 2010). This tissue is composed by water, specialised cells called chondrocytes, and extracellular matrix (ECM) which contains mainly collagen and proteoglycans. The most abundant collagen is type II collagen (Coll II). Depending on the histological aspect and the matrix composition cartilage is commonly divided into three principal types: articular or hyaline cartilage, elastic cartilage, and cartilage (Figure 1.2) (Mescher, 2016). Cartilage ECM, according to the cartilage type, can be mineralised or not. Chondrocytes synthesize and deposit ECM. They are surrounded by pericellular matrix (PCM) and ECM and they are located individually or in small isogenous group in regions of cartilage called *lacunae* (Figure 1.1, (Hall, 2005)). Several chondrocytes continuously divide during life, but in certain type of cartilage, such as articular cartilage, less than one per cent of the chondrocyte population consists of dividing chondrocytes (Hall, 2005). Human cartilage in adults has no blood vessels, lymphatic vessels and nerves (Shetty *et al.*, 2014). Because of its avascular nature and low cellular density cartilage shows limited regenerative ability, therefore this tissue represents an excellent subject for tissue engineering (Chung and Burdick, 2008a; Camarero-Espinosa *et al.*, 2016).

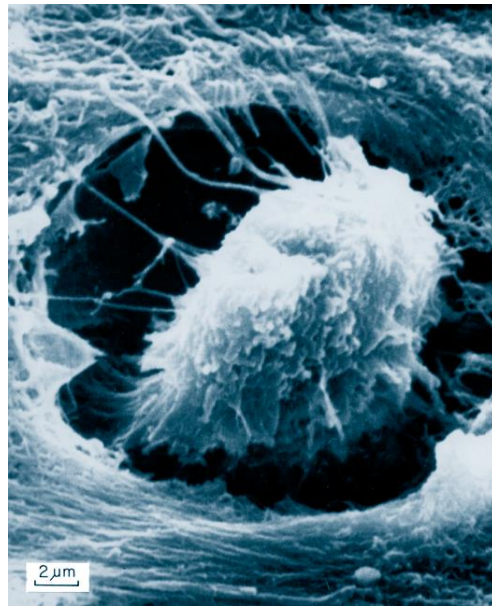


**Figure 1.1:** Scanning electron microscope image of a chondrocyte inside a lacuna of the articular cartilage of a human patella (Hall, 2005)

Each cartilage type shows different mechanical, biochemical and structural characteristics, developed in order to bear different mechanical stresses (Camarero-Espinosa *et al.*, 2016). Fibrocartilage is located in zones of the body that need to withstand high tensile and compressive forces such as meniscus, symphysis, ligaments and intervertebral discs, where provides a lubricated cushioning that attenuate local stresses (ParviziMD and K.KimMD, 2010). Fibrocartilage is the toughest type of cartilage and may be considered a combination of connective tissue and hyaline cartilage and exhibit different forms depending on his location in the human organism. In this type of cartilage chondrocytes may form linear-shaped clusters while the surrounding ECM is usually scarce. One of the most relevant feature of this type of cartilage is the presence of high quantity of collagen type I, which interact with collagen type II to create a dense mesh (Camarero-Espinosa *et al.*, 2016). Hyaline cartilage is the most common type of cartilage in the human body, covers the bone surface of joints (where it is usually named articular cartilage) (Pavelka and Roth, 2010) , forms a temporary skeletal structure during embryonic development and is also located inside bones, where support bone formation processes (ParviziMD and K.KimMD, 2010). Hyaline cartilage can be found at the level of hip, elbow, shoulders, larynx, trachea, bronchi, ribs and nose (Camarero-Espinosa *et al.*, 2016). This type of cartilage, excluding hyaline cartilage of joints, is surrounded by a cover of connective tissue called perichondrium, which supports his sustenance (Mescher, 2016). Hyaline cartilage in adults can bear up to approximately 3.5 times the body weight at

the level of the knees (Camarero-Espinosa *et al.*, 2016). Elastic cartilage is considered a flexible yet strong tissue and is located at the auricle of the ears, epiglottis and numerous tubes (e.g. larynx) (ParviziMD and K.KimMD, 2010). Elastic cartilage, which appears yellow, maintain the shape and provides elasticity of soft tissues and organs. It shows similarities with hyaline cartilage but contains a higher concentration of elastin and network of fibrils made by type II collagen. Elastic cartilage possesses a perichondrium comparable to the one of articular cartilage (Mescher, 2016)

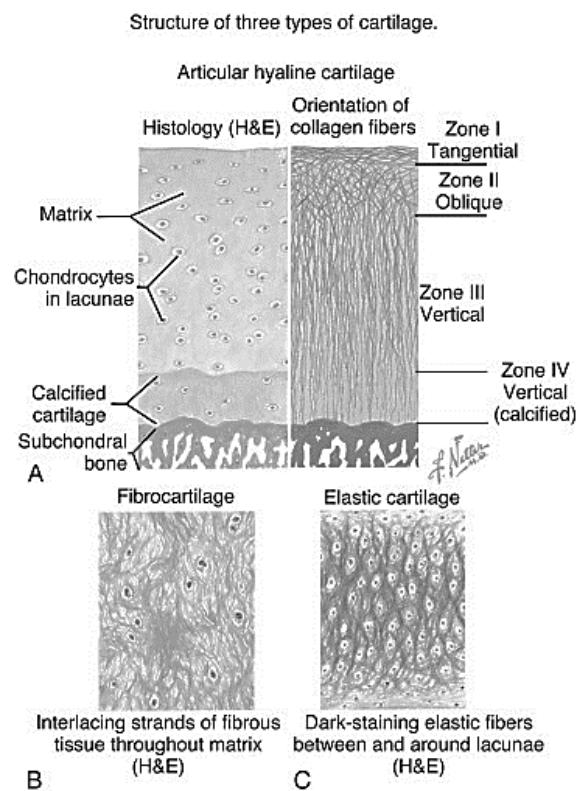


**Figure 1.2:** Histology (Hematoxylin and eosin staining) of the three types of cartilage: articular cartilage(A), fibrocartilage(B) and elastic cartilage(C). (Ovalle and Nahirney, 2008)

### 1.1.1 Articular cartilage formation and chondrogenic signalling molecules

Mesoderm, endoderm and ectoderm are the three different germ layers generated during embryogenesis. Mesenchyme derives from mesoderm, the middle embryonic layer, and contains mesenchymal stem cells (MSCs). After 4 weeks of gestation, MSCs give rise to the elements of appendicular skeleton (Hall and Miyake, 1992). Cartilage develops from MSCs in a process called chondrogenesis. Firstly, through a process called condensation, MSCs assume a rounded morphology, undergo to cell-ECM and cell-cell interactions and aggregate (DeLise,

Fischer and Tuan, 2000; Mescher, 2016). Then MSCs differentiate into chondrocytes that in 4-7 weeks form the cartilaginous anlage producing a large amount of ECM components (such as PGs and collagen type II, IX and XI). (Camarero-Espinosa *et al.*, 2016; Kwon *et al.*, 2016a). At this point two different lineages are formed. Chondrocyte in the central zone of the anlage becomes hypertrophic and synthesise type X collagen. Then, in a process called endochondral ossification, they form the epiphyseal ossification centre from where joint development occurs. Cells in the edge of the anlage becomes lifelong chondrocytes that will eventually form mature articular cartilage (Kwon *et al.*, 2016a).

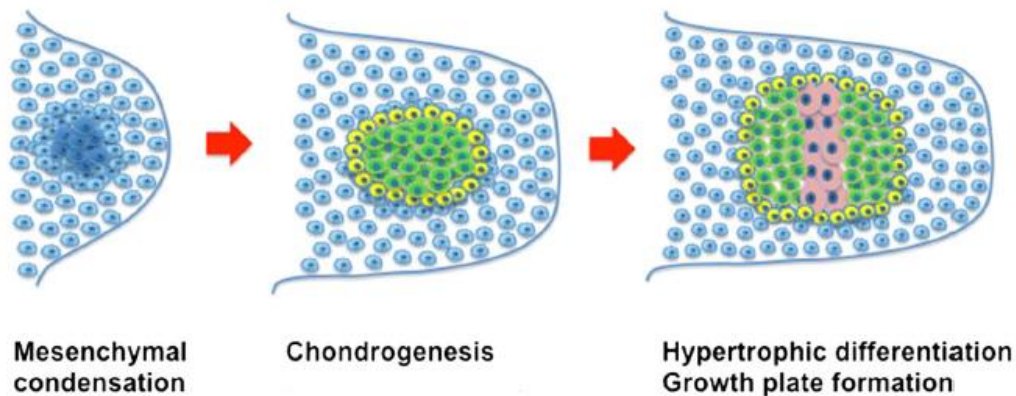


**Figure 1.3** Formation of the cartilaginous anlage during cartilage development. Mesenchymal stem cells (blue) aggregates during condensation. Then the cells differentiate into chondrocytes (green) and pericondium cells are likewise formed (yellow). In the hypertrophic phase cells in the central region become hypertrophic (pink) and give rise to the bone growth plate. (Kwon *et al.*, 2016a)

A wide range of signal, such as growth factors (GFs) and transcription factors, influences and regulate chondrogenesis. Among many transcriptional factors, SOX-9 plays a crucial role in chondrogenesis. SOX-9 presence is fundamental during mesenchymal condensation and stimulate chondrocyte proliferation. SOX-9 may be used as a marker of chondrocyte phenotype preservation and collagen type II and aggrecans production (João T. Oliveira, Santos, *et al.*, 2010; Yang *et al.*, 2018). It has also a role in endochondral ossification and interacts with other chondrogenic pathways controlled by molecules such as transforming growth factor-beta (TGF-  $\beta$ ). Bone morphogenetic proteins (BMPs) induce MSCs differentiation, promote cell proliferation and the formation of the growth plate. BMPs effect on cartilage formation is mediated by SOX family proteins, and BMPs stimulates SOX-9 expression (Zehentner, Dony and Burtscher, 1999; Pogue and Lyons, 2006). TGF- $\beta$  molecules

encourage the expression of cartilage-specific gene such as collagen II, stimulate the production of ECM components and cell division during early stages of chondrogenesis and suppress the differentiation into hypertrophic cells during the final phases of the process (Zhang *et al.*, 2004; Kwon *et al.*, 2016a). Insulin-like growth factor (IGF) is also involved in MSCs chondrogenesis and has a key role in the survival of chondrocytes (Demoor *et al.*, 2014; Kwon *et al.*, 2016a).

### **1.1.2 Structure, functions and composition of adult articular cartilage**

AC is fundamental for the functioning of the musculoskeletal system. It sharply reduces frictions produced between articular surfaces during motion and allows loads distribution over a wider area, dissipating and decreasing stresses on subchondral bone (Cohen, Foster and Mow, 1998). Human AC shows resiliency and high resistance to compression, showing an elastic compressive modulus ranging from 240 kPa to 1 MPa (Beck *et al.*, 2016a), even if has a thickness of just few millimetres (1 - 7 mm) (Mangine, Rauch and Middendorf, 2012) and in optimal conditions ensures the functioning of the joint into old age. From a macroscopic point of view AC seems not to be a complex tissue. It shows low metabolic activity and under changes of mechanical stress level has slow responsiveness. However, morphological and biological in depth studies revealed that AC is characterised by several intricate interactions between cells and ECM and a sophisticated matrix framework (Buckwalter and Mankin, 1998). Chondrocytes, which represent about the 1-5 % of the total AC volume, are involved in the synthesis and maintenance of ECM and their shape. Chondrocyte can form small “cell nests” in cartilage areas called *lacunae* (Parvizi, 2010). Chondrocyte dimension and concentration changes according to the AC zone to which they belong and their metabolic exchanges occur by diffusion (Buckwalter, JA ; Mankin,HJ; Grodzinsky, 2005; Bhosale and Richardson, 2008a). It has been estimated that normal adult human AC possess a mean concentration of nearly 10 thousand cells per mm<sup>3</sup>, or ~10 million cells/mL, and that chondrocytes have a mean diameter of about 13 µm (Hunziker, Quinn and Häuselmann, 2002) and a Young’s modulus of approximately 0.6 kPa (Guilak, 2000). They have limited replicative potential, and this is reflected in the low regenerative ability of cartilage. Every chondrocyte produces and is concerned with the turnover of the surrounding ECM and they respond to different kind of stimuli, both physical and biochemical, such as hydrostatic pressure and growth factors (Sophia Fox, Bedi and Rodeo, 2009). Other key features of chondrocytes are the absence of

cell-to-cell contacts, the ability to survive on hypoxic conditions and the production of enzymes specialised in the degradation of their own ECM (Bhosale and Richardson, 2008a). The ECM gives protection to cells from mechanical forces, stores GFs and cytokines, influences the diffusion rate of waste products and nutrients and has a role in the signal transduction for the chondrocytes. Also, ECM deformation generates biochemical electrical and mechanical stimuli that influences cell's activity via electro-/mechano- transduction (Bhosale and Richardson, 2008a). AC matrix is composed by two different phases: the first one is represented by fluid (mostly water) and the second one consisting is dense mesh formed by the interaction of different macromolecules such as collagen and PGs (Buckwalter, JA ; Mankin,HJ; Grodzinsky, 2005) constituting from sixty five to eighty per cent of the wet weight of cartilage. The pH value of the matrix is about 7.4 and pH changes can lead to matrix infrastructure alteration (Bhosale and Richardson, 2008a). AC fluid, formed by water and dissolved electrolytes such as mobile cations ( $Ca^{2+}$ ,  $K^+$ ,  $Na^+$  and  $Cl^-$ ) and gases, is the most abundant component representing approximately 80% of the wet weight of the tissue. AC fluid allows waste and nutrient exchange between the tissue and synovial fluid, which represent the nutrition source of chondrocytes. The movement of nutrients, waste product, gases and electrolytes takes places through mass-transport and diffusion caused by AC strain (Cohen, Foster and Mow, 1998; He *et al.*, 2014; Camarero-Espinosa *et al.*, 2016).

Regarding the AC solid phase, col II is the most abundant collagen type found in the tissue and make up nearly the 50% of the dry weight of AC. Collagen fibres provides high tensile resistance and their arrangement changes through the depth of the tissue. Collagen I and collagen X are other collagen type present in the tissue in lower quantity than Coll II. Collagen I is located mainly on the superficial layer of cartilage, is a marker associated with de-differentiation of chondrocytes often occurring in 2D *in vitro* culture (Oliveira *et al.*, 2009) and the ratio between Coll II with collagen I can be used as a marker of chondrogenesis. Collagen X is predominantly found in the deepest zone of the tissue near the subchondral bone and it is estimated to be involved in the matrix mineralization process of AC (Eyre and Wu, 1995) and is frequently synthesized by hypertrophic chondrocytes, a not favourable condition when attempting to reproduce AC like ECM (Oliveira *et al.*, 2009). Other forms of collagen present in smaller amount are collagen VI, collagen IX and collagen XI (Table 1) (Eyre and Wu, 1995).

Collagen type	Structure	% of total collagen content	Distribution
I	Fibril forming	≈ 0	Only in the superficial zone
II	Fibril forming	9.5	Throughout the tissue
VI	Short - helix	0 - 1	Concentrated in the pericellular matrix
IX	Short - helix	1	Throughout the tissue, associated with type II (cross-linking)
X	Short - helix	1	Deep and calcified zones
XI	Fibril forming	3	Throughout the tissue, associated with type II (cross-linking)

**Table 1:** Types of collagen found in articular cartilage (Camarero-Espinosa *et al.*, 2016)

PGs are the second most abundant macromolecules after collagen and represents the 15-40% of the dry weight of AC. PGs are formed by many linear polysaccharide side chains, predominantly glycosaminoglycans (GAGs), covalently attached to a “core protein” through a serine residue. The most abundant GAGs found in AC are keratan sulphate (KS) and chondroitin sulphate (CS), while dermatan sulphate and hyaluronan (HA) are found in lower concentration (Camarero-Espinosa *et al.*, 2016). Along PGs chains a high number of sulphate and carboxyl groups are present, which becomes negatively charged in physiological conditions giving PGs a strong hydrophilic nature, allowing these macromolecules to repulse each other and to apply a swelling pressure on the surrounding collagen fibrils. Plus, electric repulsion donates to GAGs a typical brush-like structure (Cohen, Foster and Mow, 1998; March and Little, 2010). The presence of a high negative charge gives to PGs the ability to block the movement of large molecules through the tissue and allows the diffusion of molecules with a low molecular weight (Labat-Robert, Bihari-Varga and Robert, 1990). Aggrecan is the most diffused proteoglycan in AC made of a protein core possessing three globular domains (G1, G2 and G3) and 3 linear interglobular domains. Aggrecan has the ability to bind HA molecules, the largest GAGs synthesized by cells in AC, thanks to a specialised “link protein” forming the so called “proteoglycan aggregates” (Figure 1.4) (Cohen, Foster and Mow, 1998). HA lacks of sulphate group and is not linked to PGs as a side chain but represent a central large core of the proteoglycan aggregates (Thakker *et al.*, 2017). These enormous aggregates have a molecular weight between 1 and 2 million Da (March and Little, 2010). Interestingly, it has been observed that with aging proteoglycan aggregates becomes larger,

CS concentration diminishes and KS concentration increases (Lehman, 2011). AC in addition contains at lower concentration proteoglycan such as syndecan, glypican, perlecan, decorin and biglycan (Camarero-Espinosa *et al.*, 2016). The remaining molecules found in AC are lipids, glycoproteins, such as lubricin (which is involved in the lubrication of the superficial zone of the tissue) and fibromodulin (which contribute to the preservation of collagen fibrils), non-collagenous ECM protein such as anchorin, fibronectin and chondrocalcin (Kuettner, 1992).

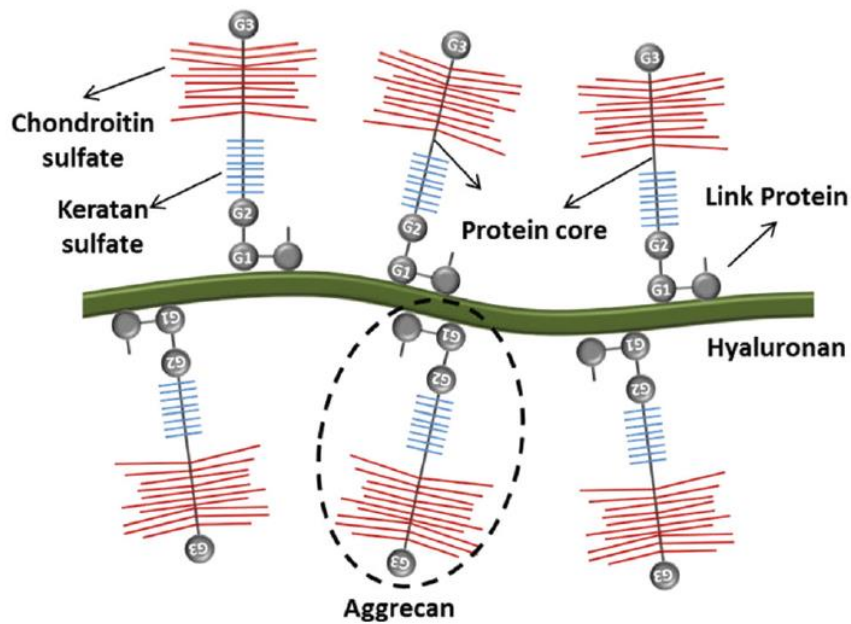


**Figure 1.4** Hyaluronan and aggrecans interact each other to form a proteoglycan aggregate. The binding site of keratan sulphate and chondroitin sulphate is the interglobular region between G2 and G3. Link proteins stabilize the aggregate stability. Thanks to negatively charged GAGs repulsion, this macromolecule shows a bottle-brush configuration (Camarero-Espinosa *et al.*, 2016).

### 1.1.3 Ultra-Structure of adult articular cartilage

As mentioned before, AC is a structured tissue that exhibit relevant variability through its depth in terms of collagen fibrils orientation, PGs allocation, matrix composition and mechanical response. Plus, chondrocytes organization, morphology, content, metabolic activity, and specific marker expression differ in different zones of the tissue. It is known that AC topographical heterogeneity is predominantly caused by biomechanical load (Brama *et al.*, 2009). AC is typically seen as a four layered structure. From the articular surface to the subchondral bone, the four zones are known as superficial or tangential zone, middle or transitional zone, deep zone and calcified zone (Figure 1.4). On the top of tangential zone AC is covered by a thin (few hundred nanometres) protein layer called *lamina splendens*, which

is created by the continuous deposition of synovial fluid proteins on AC surface. *Lamina splendens* provides a lubrication surface and reduces frictions, but nowadays its specific function is still not clear (Camarero-Espinosa *et al.*, 2016; Armiento *et al.*, 2018).

The superficial zone appears to be the thinnest layer of AC and represent the 10-20% of the full thickness of the tissue. (Camarero-Espinosa *et al.*, 2016). In this zone the PGs content is relatively low while collagen concentration, water content and permeability reach their peak value. It is composed by elongated and flattened chondrocytes that are disposed parallel to the articular surface and secrete lubricating proteins. Chondrocytes represent approximately the 2.6% of the total volume of the layer (Hunziker, Quinn and Häuselmann, 2002) Chondrocytes are surrounded by thickly clustered collagen fibrils also oriented parallel to the joint surface. This structure makes the superficial zone critical for shear and tensile toughness of the tissue (Bhosale and Richardson, 2008a). Collagen fibrils provide a sort of “filter” that reduce the entrance of large molecules from synovial fluid to the tissue separating AC from the immune system. Plus, the most abundant proteins that can be found in this zone are clusterin, lubricin and Del-1 (Di Bella *et al.*, 2015). Damages to the superficial layer jeopardise mechanical properties and lubrication ability of the tissue and may cause a fast wearing-down process, moreover AC may unleash biochemicals that promote an inflammatory or immune reaction (Buckwalter, JA ; Mankin,HJ; Grodzinsky, 2005; He *et al.*, 2014).

The transitional zone comprises from 40 to 60% of total AC thickness. Its name is derived from its structural and compositional features that generates an “anatomic bridge” between deep and tangential zones. Middle zone chondrocytes exhibit a rounded morphology and a lower content compared to superficial zone (Bhosale and Richardson, 2008a; Sophia Fox, Bedi and Rodeo, 2009; Camarero-Espinosa *et al.*, 2016). In this zone cells occupy nearly the 2% of the whole volume (Hunziker, Quinn and Häuselmann, 2002). This zone has thicker collagen fibrils that are poorly packed and randomly disposed. Overall there is an increase of PG concentration and a decrease of collagen and water content in relation to superficial zone ECM (Buckwalter, JA ; Mankin,HJ; Grodzinsky, 2005). The middle zone shows a higher compressive modulus than superficial zone (Pearle, Warren and Rodeo, 2005) and represents the first defensive stand against compressive loads of the tissue (Sophia Fox, Bedi and Rodeo, 2009). In the middle layer cartilage oligomeric matrix protein and cartilage intermediate layer protein can be found (Di Bella *et al.*, 2015).

The deep zone, also called radial zone, takes its name by its radial-oriented constituents and represents approximately the 30% of the total AC volume (Pearle, Warren and Rodeo, 2005; Sophia Fox, Bedi and Rodeo, 2009). Collagen fibres possess the largest radius and their axis are perpendicularly oriented to the articular surface, contributing to give to this zone a high compression strength. Cells forms columnar fashions parallel to collagen fibrils and synthesize lower concentration of collagen II (Eggl, Hunziker and Schenk, 1988; Sophia Fox, Bedi and Rodeo, 2009). This zone possess a lower cell density and water content than in the previous two zones, while has the maximum content of PGs and highest compressive modulus (Buckwalter, JA ; Mankin,HJ; Grodzinsky, 2005; Pearle, Warren and Rodeo, 2005).

The calcified zone is visibly separated from the deep zone by a thin border called “tidemark”. Chondrocytes in this region are smaller than other cells in AC and in certain areas they are totally embedded into calcified ECM. These cells have a low metabolic activity and produces collagen X (Buckwalter, JA ; Mankin,HJ; Grodzinsky, 2005; Bhosale and Richardson, 2008a). The calcified zone contains hydroxyapatite and act as a protective shielding reducing the mechanical gradient between cartilage and bone (Camarero-Espinosa *et al.*, 2016).

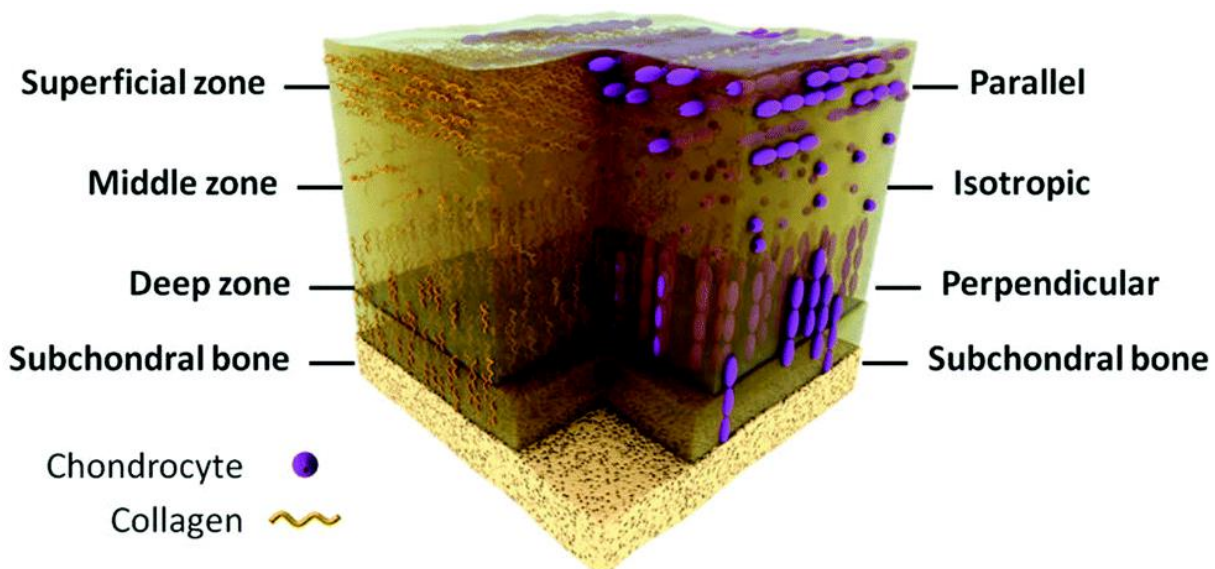


**Figure 1.5** Schematic drawing of the ultra-structure of articular cartilage displaying chondrocyte morphology and disposition and collagen fibrils orientation (Camarero-Espinosa *et al.*, 2016)

AC structure changes not only through its depth but also as a function of the radial distance from cells. Chondrocytes are surrounded by the pericellular matrix (PCM), composed by the

glycocalyx and the pericellular capsule. PCM may be considered as a 2 micrometres wide rim of ECM and serves as a hydrodynamic cushion protecting chondrocytes from mechanical stress (Poole, 1997; Poole et al., 1987). PCM contain PGs and non-collagenous proteins such as decorin and anchorin. Collagen type II small fibrils, collagen type VI and collagen IX are also found in this region (Youn *et al.*, 2006; Bhosale and Richardson, 2008a). The territorial matrix surrounds the PCM and singular or clustered chondrocytes. Collagen fibrils in this region form a collagenous “basket” that provides an additional protection from mechanical impacts to cells (Bhosale and Richardson, 2008a). Territorial matrix composition is similar to the one of interterritorial matrix but with smaller collagen fibres. The remaining ECM volume of the tissue, that is also the widest region, is known as interterritorial matrix. This region contains PG aggregates and the thickest collagen fibrils (Hunziker, Michel and Studer, 1997; Bhosale and Richardson, 2008a).

#### **1.1.4 Biomechanical properties**

Mechanical properties of AC are influenced by the interplay of its main components: interstitial fluid, PGs and collagen (Mansour, 2003). Since the tissue possess an heterogeneous organization, it shows nonlinear and anisotropic mechanical properties (R K Korhonen *et al.*, 2002). Collagen fibres provide high tensile properties to AC, but they are weak in compression resistance because of their diameter/length ratio (Cohen, Foster and Mow, 1998). The collagen network has a major role in instantaneous deformation (Mizrahi *et al.*, 1986) and his orientation affects the tensile behaviour of the tissue (Cohen, Foster and Mow, 1998). PGs mainly provide compressive stiffness to AC give to the tissue (R K Korhonen *et al.*, 2002). Negative charges on PGs create the “fixed charge density” (FCD) that give rise to an ionic imbalance between the tissue and the external environment. FCD reaches its maximum value in the deep zone and decreases in the superficial zone (Schinagl *et al.*, 1997). The mobile ion disequilibrium generates a high osmotic pressure, named “Donnan osmotic pressure” that helps to maintain AC highly hydrated, influences ion mobility and affects apparent mechanical properties of the tissue (Lu and Mow, 2008). When AC undergoes physiological compression, the charge repulsion of PGs prevents the deformation and allows the restoration of the initial shape of the tissue (March and Little, 2010). Fluid flow through AC deeply influences the mechanical behaviour of the tissue. A fluid flow through AC occurs when the tissue is deformed or after the application of an external pressure (Linn and Sokoloff, 1965; Maroudas

and Bullough, 1968) and its passing through the tissue give rise to frictional resistances and dissipations which mainly generates the viscoelastic response of AC. The “biphasic model of cartilage” is one of the most famous theory used to describe the viscoelastic behaviour of cartilage under compression. In this theory AC is regarded as composed of two different phases: the “solid phase”, and the “fluid phase”. (Lu and Mow, 2008). While the fluid phase is generally considered incompressible and inviscid, the solid phase is seen as an elastic material (Mow *et al.*, 1980). According to this model, the interaction of three main internal forces (the stress developed by the solid phase deformation, the pressure of the interstitial fluid and the frictional forces between the two phases) balances the external forces applied on the tissue and give rise to the viscoelastic behaviour of AC (Lu and Mow, 2008). Other noteworthy theories used to describe the biomechanical properties of AC are elastic (Hayes *et al.*, 1972), viscoelastic (Parsons and Black, 1977) and triphasic (Lai, Hou and Mow, 1991) models. When physiologically deformed, the superficial layer of AC undergoes to the lowest level of hydrostatic pressure and highest level of strain, otherwise the hydrostatic pressure reaches his maxim value and a negligible strain is observed at the level of the deep zone. Under constant loading AC shows creep behaviour. At the beginning the tissue undergoes a steep deformation and a relatively large volume of interstitial fluid is extruded from the cartilage. Then the deformation rate decreases until the load is balanced, and a mechanical equilibrium is reached: in this situation both fluid flow and displacement cease (Fig 1A). When a constant displacement is applied to cartilage, the tissue exhibits a stress-relaxation response: firstly the displacement results in a sharp stress increase until a peak is reached, then the stress gradually diminishes until equilibrium (Fig. 1B) (Cohen, Foster and Mow, 1998).

The most common tests used to investigate biomechanical properties of AC are confined and unconfined compression test, indentation test and stress-relaxation test (Boschetti *et al.*, 2004). Compression test is conducted by placing the material sample on a support and applying a compressive uniaxial force on it through a load cell and a compression plate (or a porous filter). The compressive force is measured in function of the displacement of the compressed specimen. The same experimental set-up is used to perform a compression creep test, but in this methodology the sample is compressed by a constant load. In a stress relaxation test a displacement is applied at a constant rate to the surface of the sample. When the fixed displacement value is reached, the sample undergoes to a constant deformation until a desired compression level is obtained. During compressive creep and stress-relaxation tests

the compressive force is recorded in function of time (Cohen, Foster and Mow, 1998). Indentation test represents an interesting option to compression test (Hayes and Mockros, 1971). In this methodology the load is applied via a circular and rigid indenter tip, whose diameter is generally smaller than 800  $\mu\text{m}$ . An indentation test allows to test in situ material properties: AC is not removed from its underlying bone, so the test is performed in an environment closer to a physiological situation, moreover this methodology does not need special sample preparation such as microtoming tissue (Boschetti et al., 2004). Confined and unconfined compression tests are influenced by PGs swelling pressure, while indentation test measurements are affected not only by PGs swelling pressure but also by the contribution of collagen tensile resistance (R. K. Korhonen *et al.*, 2002).

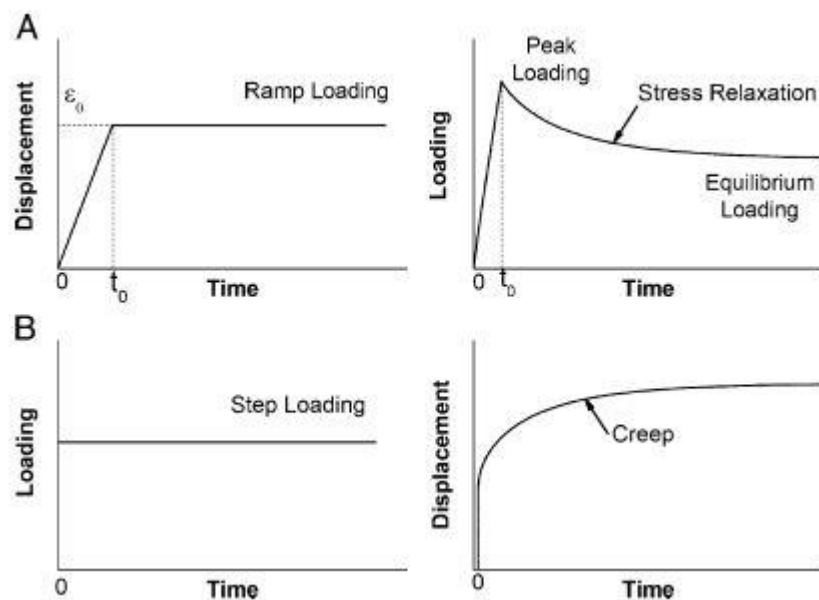


**Figure 1.6** Viscoelastic response of articular cartilage under compression. Stress-relaxation test is performed by compressing at a constant rate the sample until a desired strain value  $\xi_0$  is reached at  $t_0$ . After  $t_0$  the strain is kept constant and the stress start to decrease until mechanical equilibrium is obtained (A). Typical Creep curve obtained by applying a constant load to the specimen. After a rapid rise, a gradual non-linear increment of the displacement is observed until mechanical equilibrium (B).

Compression test is typically employed to assess the Young's modulus, also called elastic modulus ( $E$ ), and the equilibrium Young's modulus (measured when mechanical equilibrium is reached). Unconfined compression test is used to optically evaluate the Poisson ratio ( $\nu$ ) of cartilage, while creep compression test and stress-relaxation test are employed to evaluate the permeability ( $k$ ) of the tissue (Lu and Mow, 2008). Permeability is described as the ability of a fluid to flow through a porous and permeable material like AC and it's inversely related

with the frictional resistances caused by the passage of the fluid. AC shows a non-linear permeability behaviour. When the tissue undergoes to deformation or to an external compressive load application the value of permeability decline because of the decreases of ECM pore size (Cohen, Foster and Mow, 1998). Permeability in normal cartilage is in the range of  $10^{-16} \text{ m}^4/\text{Ns}$  and its value is lowest in AC deep layer and highest at the level of superficial layer, allowing a relatively high interstitial fluid flow near the joint end (Maroudas and Bullough, 1968). The Poisson's ratio of cartilage has a value ranging from approximately 0 to 0.4. This is a noticeable information since the tissue was assumed to be incompressible ( $\nu = 0.5$ ) in early researches (Lu and Mow, 2008). Young's modulus of articular cartilage is a measure of the stiffness of the tissue and is generally calculated as the slope of the elastic region (by dividing the measured stress with the strain of the specimen during a compression test at the end of the linear region) (Scalzone et al., 2019) Compressive Young's modulus of AC ranges from 240 to 1000 kPa (Beck *et al.*, 2016b) and its value increase with the increase of GAGs content and FCD value, so from the superficial zone to the deep zone of the tissue (Schinagl *et al.*, 1997). Young's modulus gradient in AC from the superficial to the deep zone may also be related to a higher collagen concentration and collagen fibres dimension in the middle and deep zones of the tissue (Muir, Bullough and Maroudas, 1970). In humans, equilibrium tensile modulus of knee AC appears to be higher (10.1 MPa) in the superficial zone, where the concentration of collagen fibrils is the highest and, than in the middle zone where its value drops to 5.4 MPa (Akizuki *et al.*, 1986). Elastic moduli determined via indentation are influenced by the indenter radius and are typically higher than those obtained from compression test (R. K. Korhonen *et al.*, 2002). Finally it should be noted that the displacement rate of testing may impact the measure of mechanical properties of the tissue (Huang *et al.*, 2005).

## **1.2 Articular cartilage changes in osteoarthritis**

Cartilage degeneration may lead to the generation of various medical conditions, such as heterotopic ossification, fibrodysplasia, achondroplasia and osteoarthritis (OA) (Bhattacharjee *et al.*, 2015). Osteoarthritis (OA), also named degenerative joint disease, is a disorder related to all the components of the joints. OA is generally described as an outcome of impaired cartilage homeostasis, caused by the accumulation of oxidative stress and dysfunctional organelles in the tissue (Haseeb and Haqqi, 2013). Two of the principal features of the

condition are modifications of the subchondral bone and the progressive breakdown of AC (Heinegård and Saxne, 2011). OA epidemiology is still not totally clear and is influenced by the interaction of different elements such as genetic, biochemical and biomechanical factors. Different studies suggested that the pathobiology of OA is more complicated than a simple bone or cartilage condition (Cope *et al.*, 2019). OA is regarded as a social and financial burden and represents one of the main causes of disablement and physical pain across the globe (Glyn-Jones *et al.*, 2015). It is estimated that worldwide approximately the 18% of women and the 10% of men aged over 60 years suffer of this condition (Woolf and Pfleger, 2003), while in the United States of America nearly the 80% of people over the age of 65 have OA (Mansour, 2013). The main OA clinical symptoms are joint dysfunction (tenderness stiffness or also locking), swelling and pain (Kean, Kean and Buchanan, 2004; Felson, 2006). One of the main clinical issue of the disease is that OA becomes evident just when is in an advanced phase (Heinegård and Saxne, 2011). The leading risk factor of the disease may be divided in “systematic factors” (age, bone mineral density, obesity, genetics) and “biomechanical factors” (muscle weakness, joint injury or misalignment) (Frontera *et al.*, 2020). OA treatments are mainly intended to alleviate the pain and ameliorate joint functions, without preventing the start or the progression of the condition (Zhang *et al.*, 2008; Maldonado and Nam, 2013). The principal therapies for OA may be divided in non-pharmacological, pharmaceutical and surgical treatments. The primary non-pharmacological measures suggested by American Academy of Orthopaedic Surgeons (AAOS) are light aerobic and aquatic exercises, moderate strengthening activities for muscles and weight reduction programs (Kalamegam *et al.*, 2018; DeRogatis *et al.*, 2019). Currently the most diffused pharmaceutical prescription are paracetamol, corticosteroid injection, tramadol and nonsteroidal anti-inflammatory drugs (NSAIDs) (Kloppenburger and Berenbaum, 2020). When the disease reaches a late phase, knee or hip joint replacement are valid surgical strategies, but the implants do not have a lifelong duration and patients need medical follow-up (Lane and Schnitzer, 2012; Kloppenburger and Berenbaum, 2020). Therefore, it is important to develop therapies aimed to prevent or to halt the onset of OA instead of proceeding with a surgical intervention at the final phases of the disease. For this reason, treatments focused on cartilage regeneration are under investigation in order to give further treatment alternatives to patients (Jiang, Lin and Tuan, 2017). It is essential for scientific research to focus on a clear comprehension of the mechanism

underlying OA and the events that occur at its start and progression (Setton, Elliott and Mow, 1999).

During OA development AC may be subjected to microscopically changes targeting ECM architecture and composition. It has been observed that aggrecan and PGs concentration decrease, while collagen content increase. These changes are reflected by the altered mechanical properties of the tissue. With OA, tensile modulus, compressive modulus and shear resistance of cartilage decrease, so the tissue undergoes to larger strains when exposed to mechanical stress (Setton, Elliott and Mow, 1999) and AC shows an higher permeability that cause an increase in water content up to approximately 90% (Bhosale and Richardson, 2008a). Chondrocytes activity is also impaired, in fact these cells synthesise more collagen type I compared to their healthy counterpart (Maldonado and Nam, 2013), and presents low levels of SOX-9 (João T. Oliveira, Santos, *et al.*, 2010). During the progression of the disease cells within the superficial zone cells tend to agglomerate while chondrocytes in the radial and calcified zones experience apoptosis (W. Zhang *et al.*, 2016). OA chondrocytes synthesise a large variety of inflammatory proteins including interleukin 1 $\beta$  (IL-1 $\beta$ ) and interleukin 6 (IL-6), and tumour necrosis factor TNF- $\alpha$ . Matrix degrading enzymes, such as aggrecan degrading enzymes ADAMTS 4 and 5 and collagenases MMP1 and MMP13, are also overexpressed (Fig 1.7) (Glyn-Jones *et al.*, 2015). Also, chondrocyte death with characteristics of apoptosis have been found in OA animal models (Musumeci *et al.*, 2011).

As above mentioned, OA affects all structures of the joints. Besides AC progressive loss of structure and functionality, OA may cause calcification and aberrant hypertrophy (W. Zhang *et al.*, 2016). OA is also associated with inflammation. Different studies reported the presence of mononuclear cells such as macrophages and T-cells in the synovial membrane of OA patients (Haywood *et al.*, 2003; Benito *et al.*, 2005; Sakkas and Platsoucas, 2007). Other changes in OA joints are reported in Figure 1.7.

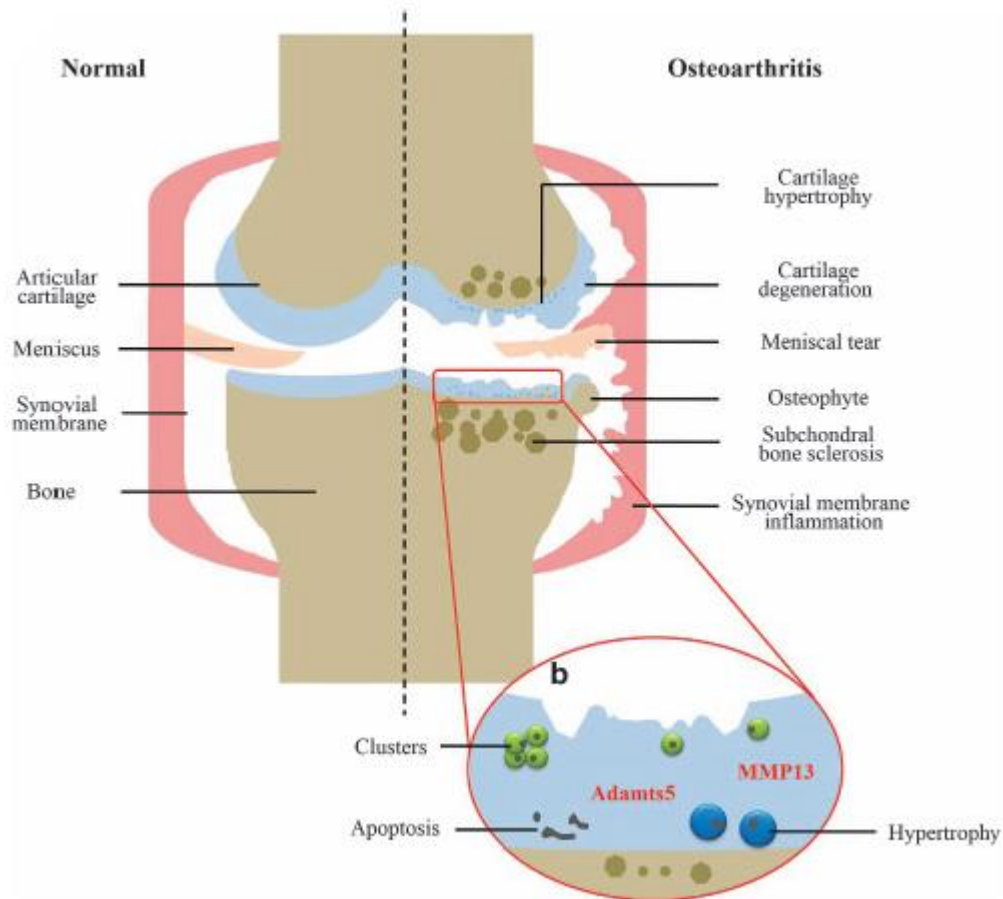


**Figure 1.7:** Articular cartilage and synovial joint changes during the progression of osteoarthritis

### 1.2.1 Surgical and cell-based treatments for articular cartilage repair

As mentioned before, AC possess limited intrinsic regenerative ability being an a-vascular tissue. Given this, AC degenerative diseases such as OA frequently occurs in human adults (Correa and Lietman, 2017). AC impairments may occurs as a consequence of joint impacts or as a result of degenerative conditions caused by intra-articular fracture (Perdisa *et al.*, 2019). The clinical purposes of AC repair are to enhance the functionality of the joints and to reduce symptomatic pain (Redman *et al.*, 2005).

Articular cartilage lesions may occur in various joint as a result of micro-traumatic or traumatic events or concurrently to damages of other joint tissues including crucial ligament and menisci. The international Cartilage Repair Society (ICRS) have created a code for the evaluation of cartilage injuries gravity and a consequent guideline for clinical decision, where five different levels of AC injuries are determined depending on their location and size (Jiang, Lin and Tuan, 2017). AC lesions may also be distinguished, according to their depth, in partial thickness or chondral defects and full thickness or osteochondral defects. Partial thickness

lesions do not penetrate to the underlying bone. Their aspect is similar to the small cracks and crevices observed in OA early phases. Chondral defects fail to heal naturally. Osteochondral lesions penetrate to the subchondral bone influencing the activity of the cells residing in the bone marrow such as MSCs and provoking the formation of a fibro-cartilaginous tissue biochemically different from the native AC (Redman *et al.*, 2005). Typically cartilage surgical treatments are focused on repairing lesions whose size is inferior to 4 cm<sup>2</sup> in order to avoid the onset of degenerative processes and OA (Kwon *et al.*, 2019). Bone marrow stimulation techniques, based on a surgical penetration to the subchondral bone, are among the earliest methods developed to stimulate the formation of new cartilaginous tissue (Bhosale and Richardson, 2008a). Between them, the most notable are subchondral drilling or debridement (Mitchell and Shepard, 1976), spongialization (Ficat *et al.*, 1979), arthroscopy chondroplasty (Friedman *et al.*, 1984) and microfracture (Steadman, Rodkey and Rodrigo, 2001). Microfracture (Fig 1.8) became an interesting method because is regarded as an inexpensive, short and relatively easy procedure and it's used to manage small AC lesions (<2.5 cm<sup>2</sup>) (Mollon *et al.*, 2013). In a single surgical operation, the AC lesion is removed and cleaned, thereafter a 2-4 mm deep perforation of subchondral bone is performed. Bone marrow MSCs migrate to the lesion site and a fibril clot is formed, that will eventually remodel into fibrocartilage, which as described in chapter 1.1, has a different structure and composition compared to the hyaline and is not able to bear properly the loads acting at joint level (Bae, Yoon and Song, 2006). The effectiveness of this treatment is affected by many factors such as size of the lesion, body mass index and age of the patient (Mithoefer *et al.*, 2009). Although microfracture is the most used methods between sportsmen (Bhosale and Richardson, 2008) and is considered as the golden standard for many clinicians, the neo-cartilaginous tissue becomes mechanically vulnerable and generally fail after two years after the intervention (Makris *et al.*, 2015). A relatively new alternative to microfracture is represented by augmented bone marrow stimulations techniques, based on the co-administration of GFs, the use of a-cellular scaffold or micronized cartilage ECM (Albright and Daoud, 2017).

Mosaicplasty (Matsusue, Yamamuro and Hama, 1993), also called osteochondral auto- or allograft transfer, consists in the delivery of cylindrical plugs of mature osteochondral tissue (including AC and subchondral bone) at the level of the chondral defects. Osteochondral autograft samples (Fig 1.8) are harvested from low weight bearing regions of AC (e.g. lateral

trochlea), so this technique is limited to small chondral lesions. The main benefit of this methodology is that autologous grafts can bear mechanical stresses after a short post-operative time, reducing the rehabilitation period (Kwon *et al.*, 2019). The major drawbacks are donor site morbidity, mechanical mismatch and lack of integration between osteochondral grafts and surrounding tissues (Clair, Johnson and Howard, 2009). Osteochondral allografts (Fig 1.8) are obtained from cadaveric donor, so larger size defects can be treated. However allogenic tissue may cause disease transmission and possess a questionable viability, also mechanical and size/depth mismatch between allograft and surrounding tissues may occurs (Mollon *et al.*, 2013). Other notable alternatives to classic allograft are particulated juvenile allograft (DeNovo NT), cryopreserved osteochondral allograft (Cartiform) and fresh osteochondral allograft (ProChondrix) (Fig 1.8), but their efficiency has yet to be demonstrated (Hinckel, Gomoll and Farr, 2017).

Cell-based therapies are biological treatments based on the introduction of cells into the human body in order to cure age-related or degenerative pathologies. They represent a novel therapeutic approach and have the potential to change the future of disease management (Mobasheri *et al.*, 2014). The use of cell based repair techniques is usually expensive and needs the availability of furnished facility where *in vitro* cell culture may be performed (Carson, 2018). Currently cell-based cartilage repair methods are widely used to treat large chondral lesion (> 4cm<sup>2</sup>). Autologous chondrocyte implantation (ACI) (Brittberg *et al.*, 1994) is a double-stage methods. During the first step autologous chondrocytes are harvested by biopsy from joint regions that bears low loads. Then cells are expanded *in vitro* to reach a population of 12 – 48 million chondrocytes. During the second phase, the expanded chondrocytes are re-implanted *in vivo* into the debrided tissue lesion and covered by a patch. The main benefits of this technique are the prevention against viral infection and immune response by using autologous chondrocytes and the small size biopsy that reduce the onset of complication at the donor site. However ACI requires a long recovery period (up to a year) (Makris *et al.*, 2015), plus graft delamination and periosteal hypertrophy may occur (Mollon *et al.*, 2013). Moreover chondrocyte de-differentiation during the *in vitro* expansion shall be considered (Mobasheri *et al.*, 2014). Matrix-Induced Autologous Chondrocyte Implantation (MACI) (Dunkin, 2013) is a variant of the previous technique and consists in seeding the harvested chondrocyte in a scaffold before the transplantation. MACI (Fig 1.8) is the most diffused scaffold-plus-cell based methods for AC treatment in clinical practice. Scaffold are produced using various biomaterials

such as collagen type I and type III or mixtures of hyaluronan and synthetic polymers (Makris *et al.*, 2015; Camarero-Espinosa *et al.*, 2016). Ebert *et al.* in a study reported that, 5 years after MACI treatment, approximately the 90% of the surveyed was satisfied about pain reduction and enhanced joint function. However, MACI remains an expensive procedure and its superiority of MACI over other AC surgical treatments is unproved. Plus, clinicians tend to prefer techniques that need just a single operation over ACI and MACI (Makris *et al.*, 2015; Ebert *et al.*, 2017; Kwon *et al.*, 2019).

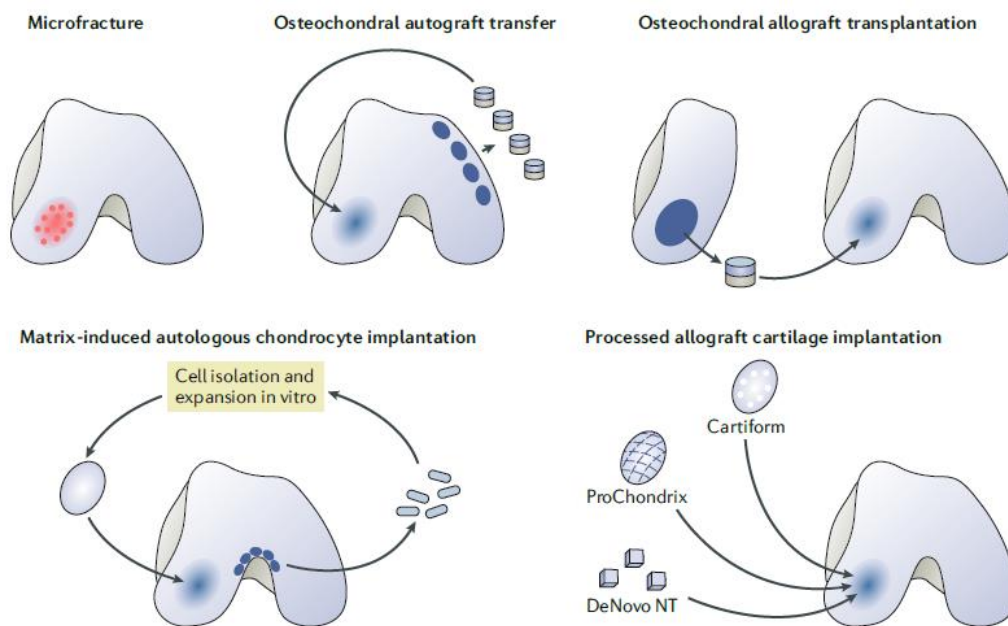


**Figure 1.8:** Articular cartilage defect treatments (Kwon *et al.*, 2019)

Stem cells represent a promising option for the treatment of diseased cartilage thanks to their chondrogenic potential and self-renewal ability. Among them, the most relevant type used in cartilage repair are MSCs. MSCs show an apparent anti-inflammatory activity and may be obtained from different tissue including adipose tissue, bone marrow, bone and muscles. Bone marrow derived MSCs (BMSCs) are the most promising option for cartilage cell therapies considering their high chondrogenic potential and easy availability. Recently, bone marrow aspirate concentrate (BMAC), that contain BMSCs and high concentration of chondrogenic GFs, has been investigated for the management of cartilage focal defects. BMAC has been used as an independent technique or as an adjuvant (e.g. BMAC-augmented microfracture). Despite various question about BMAC remains, for instance optimal timing of injection and

optimal cell density, this technique has demonstrated good clinical outcomes (Cotter *et al.*, 2017). Other stem cell type used in cartilage repair are Embryonic Stem Cells (ESCs) and Induced Pluripotent Stem Cells (iPSCs) (Jiang, Lin and Tuan, 2017). Nowadays no surgical or pharmaceutical therapies can totally restore AC to its initial state (Cucchiaroni and Madry, 2019). Surgical treatments are insufficient to block OA development and progression, thus has speeded up the research and development of alternative tissue engineering treatments (Kwon *et al.*, 2019).

### **1.2.2 Tissue engineering application in cartilage treatment**

As mentioned before, there is no long-term treatment method for OA and therefore poor outcomes in the long run. In this scenario, tissue engineering (TE) has gained interest over the last three decades representing a new hope in address current treatment problems (Francis *et al.*, 2018). The first definition of TE was given by Langer and Vacanti during 1993. The authors described TE as “an interdisciplinary field which applies the principles of engineering and life sciences toward the development of biological substitutes that restore, maintain, or improve tissue function” (Langer and Vacanti, 1993). The general TE principle involves the association of living cells with a synthetic, natural or bio-artificial support to create a 3D construct that has mechanical, structural and functional properties equal to a desired tissue (Kim and Evans, 2005). The main tools used to develop a bioengineered construct, known as “tissue engineering triad”, are cells, a supporting biomaterial and biological or environmental stimuli (Chung and Burdick, 2008a). The classic TE approach consist in the collection of primary cells from the patient and the subsequent seeding on a 3d matrix/scaffold, that provide support to cells. Then, the construct is developed undergoing to different physical and biochemical stimuli provided by a bioreactor in a controlled environment. After an *in vitro* maturation phase, where cells start to proliferate and to produce ECM, the construct is transplanted in the patient triggering a tissue repair process (Caddeo, Boffito and Sartori, 2017). Cartilage tissue engineering (CTE) (Fig. 1.9) ideal construct should fill the tissue defect, have structural and compositional features similar to the ones of ECM and hold cells *in situ* (You, B Frank Eames and Chen, 2017). CTE first attempts lead to the generation of engineered construct that resembled hyaline cartilage but with inferior mechanical properties (Schulz and Bader, 2007). Therefore, in the last years the research focused particularly on the mechanical features of the construct (Francis *et al.*, 2018).

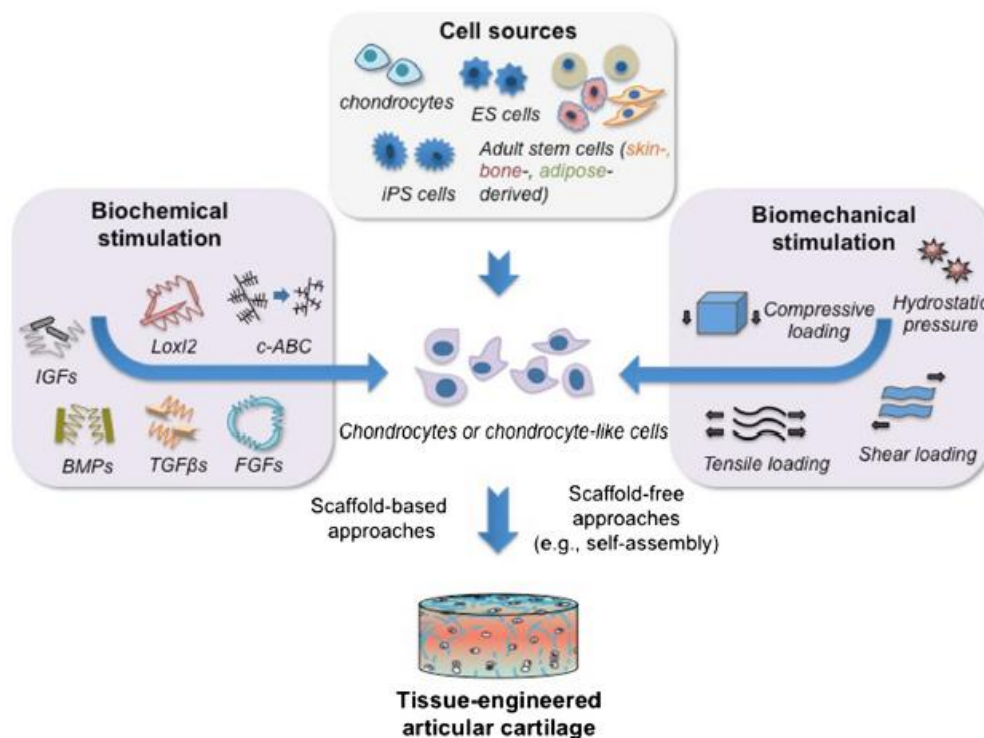


**Figure 1.9** Cartilage tissue engineering. Abbreviation: ES cells (embryonic stem cells), iPS cells (induced pluripotent stem cells). (Kwon *et al.*, 2016a).

Ideally the chosen cell source should be autologous, easily isolated and expanded *in vitro*, it should produce a large amount of hyaline cartilage-like. Plus, de-differentiation processes should be avoided (Kock, Van Donkelaar and Ito, 2012). The “gold standard” cell type for CTE has yet to be identified (Chung and Burdick, 2008a) but most studies have been focused on MSCs and chondrocytes (Vinatier and Guicheux, 2016). In TE cells are usually seeded into a biocompatible and biodegradable scaffold, which provides a support that replicate the feature of the desired tissue ECM. An optimal scaffold should: i) have a controlled degradation in time, ii) permit the diffusion of waste substances and nutrients, iii) provide a mechanical support on the defect site, iv) stimulate cell viability, proliferation and ECM synthesis, v) integrate with the nearby tissues and as mentioned above vi) assume the size of the defect (Chung and Burdick, 2008a).

The most critical design features of a CTE scaffold, the ones that determine the success or the failure of the implant construct, are biocompatibility, porosity, mechanical strength, and the ability to maintain a chondrocytic type or to promote the differentiation of stem cells (Camarero-Espinosa *et al.*, 2016). A study reported that chondrocytes showed preferential proliferation when cultured in construct with pore size between 200  $\mu\text{m}$  and 500  $\mu\text{m}$  (Lien, Ko

and Huang, 2009), while matrices with a pore size of at least 200  $\mu\text{m}$  were used to induce chondrogenesis to different stem cell sources (Loh and Choong, 2013). Smaller pores, with a diameter inferior to 30  $\mu\text{m}$ , allows nutrients and waste products transport (Bonifacio, Cochis, Cometa, Scalzone, *et al.*, 2020). The presence of a gradient porosity enhances cell mobility during regenerative processes and is essential for AC defects treatment in CTE (van Tienen *et al.*, 2002).

Various polymeric materials have been used to create scaffold for cartilage regeneration, both synthetic and natural, in forms of fibrous meshes, hydrogels, foams or sponges (Chung and Burdick, 2008a). Natural polymers used for CTE includes collagen, gelatin, CS, HA, alginate, cellulose, agarose, chitosan, silk and fibrin glue (Francis Suh and Matthew, 2000; Li and Zhang, 2005; Müller *et al.*, 2006; Wang *et al.*, 2006; Lien, Li and Huang, 2008; Ko *et al.*, 2009; Scotti *et al.*, 2010; Hoyer *et al.*, 2014; Singh, Bhardwaj and Mandal, 2016). Synthetic polymers used in the same field include polyurethanes, poly( $\alpha$ -esters), poly(ethyleneglycols), poly(propylene fumarates), poly(NiPAAm), poly(vinyl alcohol) (Sittinger *et al.*, 1996; An *et al.*, 2001; Martens, Bryant and Anseth, 2003; Liao *et al.*, 2007; Skaalure, Chu and Bryant, 2015). Natural polymers for CTE usually shows good biocompatibility and led to a proper chondrogenic response. On the other hand, they are often hard to process in the desired shapes and their functionalization is also a difficult process. The main advantages of the synthetic polymers for CTE are the ease of processing, their good mechanical properties and the possibility of controlling their degradation kinetics by modifying their composition. However synthetic polymers are not bioactive so they are not able to induce cell attachment, proliferation and differentiation processes (Camarero-Espinosa *et al.*, 2016).

A large variety of signaling molecules, including GFs, have been explored in CTE for the proliferation and differentiation of different cell type and for improving the mechanical properties of the construct (Kwon *et al.*, 2016a). These molecules have been used singularly or in combination with results dependent on scaffold nature, cell type and culture condition (Chung and Burdick, 2008a). The most important biomechanical stimuli, used both for cartilage homeostasis and improve mechanical properties of the construct, are compression, shear and hydrostatic pressure (Kwon *et al.*, 2019). Stimulating factor investigated for CTE are summarized in Table 2.

Stimulating factor	Reference
Biochemical and biophysical stimuli	
BMPs	Bessa et al., 2008
c-ABC	Natoli et al., 2009
FGFs	Martin et al., 2001; Murakami et al., 2000
Hyaluronan	Goodstone et al., 2004
IGFs	Fukumoto et al., 2003; Vetter et al., 1986
Kartogenin	Sun et al., 2018
LOXL2	Makris et al., 2014
Oxygen tension	Malda et al., 2003
TGF- $\beta$ s	Bosetti et al., 2012; Kim et al., 2003
Mechanical stimulations	
Compression loading	Davisson et al., 2002; Démarteau et al., 2003
Hydrostatic pressure	Carver and Heath, 1999; Mizuno et al., 2002
Shear loading	Jin et al., 2001; Waldman et al., 2003
Tensile strain	Fan and Waldman, 2010

**Table 2** Stimulating factors used in cartilage tissue engineering

Despite of their function, scaffold utilization may also lead to stress-shielding, toxic degradation products release, impediments to remodelling and altered cell phenotype (Athanasίου *et al.*, 2013). For these reason, scaffold-free techniques for CTE have gained attention during the last years (Hu and Athanasίου, 2006). An interesting scaffold-free approach for CTE is represented by the production and implantation of autologous chondrocyte spheroids, also called “chondrospheres” (Schubert *et al.*, 2009; Meyer *et al.*, 2012). Cell-free material based for CTE have gained interest since methods for isolating, proliferating and differentiate cells are expensive and timely (Simon and Jackson, 2018). Autologous matrix-induced chondrogenesis (AMIC) is an example of cell-free technique and can be done in a single surgical operation (Benthien and Behrens, 2010).

Currently, no strategy for AC repair have succeeded to finely recapitulate the function and the architecture of the native tissue (Walter, Ossendorff and Schildberg, 2019). The clinical translation of engineered construct for cartilage repair continues to face difficulties. CTE problems include low mechanical properties of construct compared to native tissues, phenotypic instability and inflammation after implantation, poor integration with the nearby tissues and the need of obtaining a sufficient number of autologous cells (Kwon *et al.*, 2016a, 2019). Another principal bottlenecks in the clinical translation of TE construct is the lack of standardised processes complying with good manufacturing procedure (GMP). Plus,

standardization of product-approval procedures should be simplified from country to country (Makris *et al.*, 2015; Barbara J. Klotz *et al.*, 2016).

### **1.3 3D *in vitro* models**

The main aim of TE is the generation of constructs to induce specific regenerative processes in the patient's body. However, TE approaches have gained interest for the possibility to produce *in vitro* models of healthy and pathological tissues/organs. It is important to note that if a scaffold is designed for a 3D *in vitro* model, is recommended but is not strictly required to exactly match the mechanical properties of the native tissue since there is not a subsequently implantation *in vivo* (You, B Frank Eames and Chen, 2017). Also, the degradation behaviour and the absolute dimensions of the construct are not so relevant (Haycock, 2011). These models provide a novel platform for different application, such as drug screening, novel therapies development and for studying tissue development processes and disease onset and progression underlying mechanisms (Caddeo, Boffito and Sartori, 2017; Moroni, Burdick, *et al.*, 2018). *In vitro* CTE construct have gained interest for their potential use for the investigation of chondrogenesis processes (Freed, Martin and Vunjak-Novakovic, 1999) and for the production of OA *in vitro* models (Francioli *et al.*, 2011).

In addition to their scientific relevance in biological and medical research, *in vitro* models are beneficial from an ethic and economic point of view. Animal models are a key instrument in biological research and in some cases are the only reasonable approach. For instance, it is generally accepted that murine models will remain indispensable for toxicological and pharmacokinetic evaluation of novel drugs for decades ahead (Imparato, Urciuolo and Netti, 2015). On the other hand, the 3Rs principle (Russell and Burch, 1959) of reducing, refining and replacing animal experiments is encouraging researchers to recognize the animal welfare importance and is required wherever possible by European legislation. The use of animal models for drug development may be extremely expensive and time consuming (Hartung, 2008). Moreover, these models have a limited predictive power because of differences among species and may not properly reproduce feature such as human tumour microenvironment and autoimmune disease (Imparato, Urciuolo and Netti, 2015). In native tissues, cells are surrounded by a complex 3D micro-environment that allows cell-cell and cell-ECM interactions and provides biochemical and biophysical cues, regulating their activities, including proliferation, differentiation and migration (Murphy and Atala, 2014a; Das *et al.*, 2016). The

crucial requirement of *in vitro* tissue models is the proper biomimicry of the natural micro-environment of the native tissue (Cho *et al.*, 2019). The replication of this sophisticated environment in a 2D cell culture is clearly difficult. 2D tissue models may lead to un-physiological changes of nuclei morphology, gene expression and protein synthesis (Knight and Przyborski, 2015). 3D cell cultures show significant differences from traditional 2D cell cultures in nutrient diffusion, cellular mechanics, cell-cell interaction (Edmondson *et al.*, 2014), cell motion and apoptosis (Duval *et al.*, 2017). As an example, OA chondrocytes isolated from human cartilage and cultured in a 3D poly(ethylene glycol) diacrylate (PEGDA) based hydrogel are more resistant to apoptosis when compared to a control 2D culture (Musumeci *et al.*, 2011). Different studies demonstrated 3D scaffolds led cells to arrange in different morphologies than cells cultured on 2D substrates (Miyagawa *et al.*, 2011) and to encourage greater cell aggregation and proliferation than 2D models (Caddeo, Boffito and Sartori, 2017). Furthermore, 3D culture influences cells differentiation, de-differentiation. For instance, in 2D cultures differentiated chondrocyte phenotype is unstable, they lose their round shape, reduce their production of Coll II and aggrecan and increase type I collagen synthesis while in 3D *in vitro* models chondrocytes tend to not de-differentiate due to their more physiological production and storage of bioactive molecules (Oliveira *et al.*, 2009; Caron *et al.*, 2012; Hemmati-Sadeghi *et al.*, 2019).

Unlike animal models, 3D *in vitro* models allows to identify and to control biochemical and cellular factors responsible for the formation and progression of different diseases, including OA, in order to develop new methods of intervention (Sun, Wang and Kaplan, 2011; Caddeo, Boffito and Sartori, 2017). Additionally, 3D *in vitro* integration model may be exploited to study the mechanisms regulating construct integration for osteochondral lesions treatment (Theodoropoulos *et al.*, 2011). For all these reasons, 3D *in vitro* models may better recapitulate the *in vivo* environment of the correspondent tissue if compared to the classic 2D *in vitro* culture models (Cho *et al.*, 2019) and may represent a bridge between classic monolayer cell cultures and *in vivo* models (Khademhosseini *et al.*, 2006) and also between animal models and clinical trials (Griffith and Swartz, 2006).

During the last two decades, several 3D *in vitro* models have been developed, including transwell systems (Wang *et al.*, 2015), cell sheets (Asakawa *et al.*, 2010), cellular spheroids (Ramaiahgari *et al.*, 2014), organoids (Lancaster *et al.*, 2013), and micro-fluidic tissue/organ on chip (Huh *et al.*, 2010). 3D *in vitro* model have been also exploited for cancer research. One

of the most common *in vitro* 3D tumour models, used for drug screening, is represented by cancer cells spheroids. The main limitation of this model is the absence of the complex tumour micro-environment, that includes blood vessels and neural networks. To overcome this problem, biofabrication techniques, treated in the next chapter, may be used to produce more sophisticated tumour models (Moroni, Burdick, *et al.*, 2018). One of the main limitation of 3D *in vitro* models deals with the choice of the optimal cell source, and in particular the difficulty to isolate human primary cells and culture them *in vitro* for a long time (Caddeo, Boffito and Sartori, 2017). Using patient-derived cells could lead in the future to the development of personalized medicine, dealing with the identification of patient-specific treatments (Vanderburgh, Sterling and Guelcher, 2017). However, the pressing necessity to develop validation methods to examine the reproducibility and affability of 3D *in vitro* model represent an important challenge for the future (Ahadian *et al.*, 2018).

### **1.3.1 3D *in vitro* models to mimic cartilage development**

The “developmental engineering” paradigm is a recently introduced concept that aims to replicate, to a certain extent, processes and mechanisms occurring during organogenesis and tissue formation in order to develop engineered constructs (Lenas, Moos and Luyten, 2009). The cell types used in the context of CTE are ESCs and adult human MSCs, while different biochemical and physical stimuli are exploited to activate organogenesis pathways (Bhattacharjee *et al.*, 2015).

3D scaffold-free culture methods, such as high-density micro mass and pellet culture, may induce strict cell-cell contact and mimic cellular condensation processes. For example, MSCs may undergo chondrogenesis if cultured in micro mass pellets (Johnstone *et al.*, 1998). On the other hand, scaffold free methods show various drawbacks such as poor mechanical properties, uncontrollable shapes, inadequate dimensions (Wang *et al.*, 2005), the formation of a necrotic core inside the aggregates, the presence of diffusion gradient that may cause lack of homogeneity in cell phenotype and a scarce control of culture condition. Microfluidic systems allow to overcome some of these limitations and to generate 3D scaffold free cell aggregates in a controlled environment. For instance, by providing a continuous laminar flow, these systems eliminate the presence of diffusional gradients ensuring a control over nutrients and oxygen supply (Titmarsh *et al.*, 2011; Bhattacharjee *et al.*, 2015).

Scaffold-based 3D *in vitro* models of cartilage development comprises the use of hydrogels, fibrous meshes and porous scaffolds. Collagen based hydrogels may promote cell aggregation and induce chondrogenesis. In an *in vitro* study, Zhang *et al.* reported that collagen type I based hydrogel itself promoted MSCs chondrogenesis and lead them to generate neo-cartilage tissue without the use of exogenous GFs. These effects appear to be influenced by the degradation and contraction of the hydrogel (Zhang *et al.*, 2012). Alginate beads hydrogel 3D models lead to chondrogenic differentiation of human MSCs. Plus, this model allows a homogeneous cell positioning, shows a better diffusion of nutrients if compared to pellet models and encourage cartilage ECM production. The main drawback of this model is the low cell adhesion (Häuselmann *et al.*, 1992; Kavalkovich *et al.*, 2002). Silk based scaffold are highly biocompatible, have excellent mechanical properties and cell-controlled degradability. A highly porous silk-based scaffold was used for a 3D culture of human MSCs. Interestingly, after three weeks of cultivation, MSCs fully differentiated generating a zonal structure similar the native AC one (Wang *et al.*, 2005). Also, CS based hydrogels appear to have chondrogenic effects on human MSCs (Varghese *et al.*, 2008).

In order to promote chondrogenic processes, different groups encapsulated within 3D scaffold different biochemical signals such as TGF- $\beta$ s, FGF-2, and HA. For instance, TGF- $\beta$ s was incorporated in different matrices including micro-sphere made of poly (lactic-co-glycolic acid) (PLGA), chitosan and gelatin (Lee *et al.*, 2004; Holland, Tabata and Mikos, 2005; DeFail *et al.*, 2006), polyethylene glycol (PEG) and fibrin hydrogels (Huang *et al.*, 2002; Sridhar *et al.*, 2014). An interesting option is represented by the possibility to incorporate peptides within scaffolds by covalent bonding, for examples collagen mimetic peptides were encapsulated into PEGDA hydrogels to enhance chondrogenesis (Lee *et al.*, 2008). Interestingly, hypoxic conditions were shown to promote chondrogenesis in bone marrow MSCs (Tian *et al.*, 2013) and in ESCs (Koay and Athanasiou, 2008). Gosh *et al.* developed a 3D *in vitro* model of mesenchymal condensation to assess the influence of morphological and mechanical features on chondrogenesis in the presence of TGF- $\beta$ s. In this study, different nano-fibrous silk-based scaffold were producing via electrospinning by tuning fibres diameter, obtaining different construct stiffness. Human MSCs appeared to migrate and aggregate on “soft” scaffolds, mimicking their *in vivo* behaviour during chondrogenesis and demonstrating cells sensitiveness to the surrounding environment stiffness and morphology (Ghosh *et al.*, 2009).

### 1.3.2 Modelling cartilage degenerative processes

For what concerns OA research, both *in vivo* and *in vitro* models have been developed in the past (Guzman *et al.*, 2003; Grenier, Bhargava and Torzilli, 2014). Animal models may be useful to understand long-time effects of cartilage degeneration but inevitably failed to represent human pathobiology (Pritzker, 2011). Many OA *in vitro* models have been designed centred on different OA-associated factors (Bhattacharjee *et al.*, 2015), but the two most commonly used models are load-based models and cytokine-based models (Johnson, Argyle and Clements, 2016). Load-based OA *in vitro* models may replicate traumatic injury-induced OA (Huser and Davies, 2006) or may focus on mechanical stress on cartilage through static and dynamic loading (Sauerland, Raiss and Steinmeyer, 2003; Davies *et al.*, 2004). Cytokine-based OA *in vitro* models are very common and generally properly understood. These models are typically easy to manage and inexpensive. IL-1 $\beta$  and TNF- $\alpha$  are the most used cytokines in OA *in vitro* models. In OA synovial fluid IL-1 and TNF concentration measures is highly variable between experiments and are respectively inferior to 2 ng/ml and 3 ng/ml (Johnson, Argyle and Clements, 2016). The quantities used in the correspondent *in vitro* models are generally much more elevated: IL-1 $\beta$  and TNF- $\alpha$  concentrations may rise respectively at up to 100 ng/ml and 50 ng/ml (Macrory *et al.*, 2009; Gabriel *et al.*, 2010). The latter condition is applied in order to shorten the time needed for OA *in vitro* study, since usually the disease evolution *in vivo* occurs in several years (Weber *et al.*, 2019). Other molecules such as vascular endothelial GFs (VEGFs), IL-6 and IL-8 are rarely exploited. A more *in vivo* like synergistic effect may be obtained by using a combination of different cytokines (Johnson, Argyle and Clements, 2016).

Different 3D *in vitro* OA models have been developed during the last decade. Pellet chondrocyte culture is the most diffused 3D OA *in vitro* model. However these models do not mimic properly the *in vivo* OA conditions, because of limited cellular density and poor proliferative ability of chondrocyte in the native tissue (Yeung *et al.*, 2019). Miyaki *et al.* produced human MSCs pellet to study microRNA-140 expression pattern during chondrogenesis and comparing it to the one of healthy and OA chondrocytes (Miyaki *et al.*, 2009). Weber *et al.* developed a scaffold free cytokine-induced model generated by human MSCs. In this work, MSCs were cultured for three weeks to produce 3D cartilage transplant via mechanical stimulation. Subsequently the constructs were cultured with TNF- $\alpha$  and IL-1 $\beta$  enriched medium to simulate OA condition *in vivo* (Weber *et al.*, 2018). In a study, human osteoarthritic chondrocytes were micro-encapsulated into collagen-based microsphere. The

construct were exposed to different external factors (serum-free medium, TGF- $\beta$  and hypoxia) to assess phenotypic changes of chondrocytes in order to assess the ability of this model to constitute a 3D *in vitro* model for the screening of novel OA therapeutics (Yeung *et al.*, 2019). In another cytokine-induced OA model, healthy chondrocytes were cultured in 3D PEGDA hydrogels and exposed to IL-1 $\beta$ . Cells ECM production decreased as well as Coll II and aggrecan gene expression while collagen type I and MMP13 gene expression increased (Coburn *et al.*, 2013). Sun *et al.* developed a new 3D *in vitro* OA model by culturing human chondrocytes within a silk scaffold in presence of TNF- $\alpha$  and IL-1 $\beta$  or macrophage enriched medium. Interestingly, macrophage conditioned medium induced an increase of aggrecan expression and a downregulation of Coll II expression (Sun, Wang and Kaplan, 2011). Jutila *et al.* created an OA *in vitro* model to study the relevance of PCM stiffness for cells mechano-transduction during normal and pathological condition. Since PCM stiffness decreases in OA condition, chondrocytes were encapsulated in two agarose-based hydrogels at different polymeric concentration. Then, the cellular response to mechanical loading was assessed, demonstrating that gel stiffness affects chondrocyte behaviour (Jutila *et al.*, 2015). Galuzzi *et al.* produced a IL-1 $\beta$  induced OA 3D *in vitro* model using two different cell source (nasal and articular chondrocytes) and five different cell culture methods: alginate beads, decellularized ECM, alginate beads and decellularized ECM, pellet and decellularized ECM, silk/alginate microcarriers and decellularized ECM (Fig 1.10). The authors preferred beads and microcarriers models since pellet culture need a high number of cells and is very time consuming. According to authors, alginate and silk/alginate scaffolds may be easily produced and stored via cryopreservation and represent a cheap and ready-to-use platform for OA drug screening (Galuzzi *et al.*, 2018). In the future, a potential requirement for a OA 3D *in vitro* model may be a spatial and temporal controlled release of signalling molecules in order to recapitulate human pathogenesis (Bhattacharjee *et al.*, 2015).

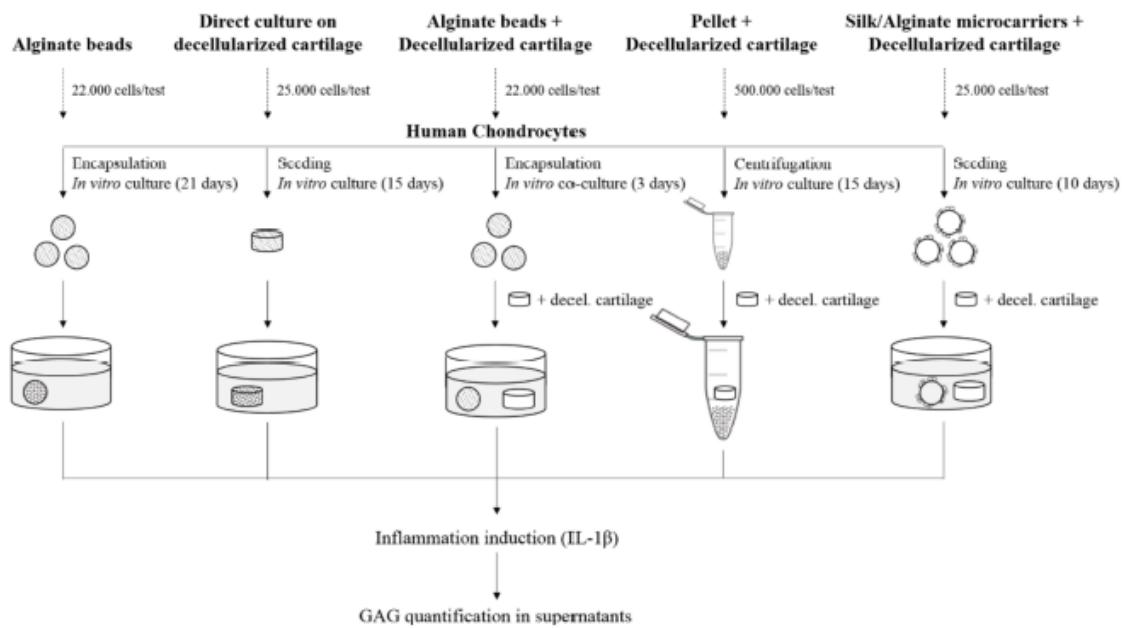


**Figure 1.10:** Schematics of Galuzzi *et al.* experimental setup. Five different OA 3D *in vitro* model were creating considering different type of matrix, culture times and number of cells per test (Galuzzi *et al.*, 2018).

### 1.3.3 3D *in vitro* models fabrication techniques

The classic TE approach to design a 3D *in vitro* model consist in i) choosing an appropriate porous scaffold with a structural architecture, mechanical properties and surface properties similar to the desired tissue, ii) selecting the optimal cell source to embed in the designed scaffold and iii) deciding the appropriate stimulating factors and eventually designing a bioreactor which will provide them (Caddeo, Boffito and Sartori, 2017). For what concerns scaffold fabrication methods, TE scaffolding techniques developed for regenerative medicine may be used to produce 3D *in vitro* models (Caddeo, Boffito and Sartori, 2017). Scaffold fabrication techniques may be classified into two categories: additive manufacturing (AM) and conventional techniques (Santos, Almeida and Bártolo, 2013). Conventional techniques include solvent casting and particulate leaching, phase separation, freeze drying, melt moulding, gas foaming, fibre bonding and electrospinning. However, these techniques have a limited control over the cell positioning and construct microarchitecture , in terms of pore size, interconnectivity and distribution (Pereira, Almeida and Bártolo, 2013; Vanderburgh, Sterling and Guelcher, 2017). In addition, some of the above-mentioned techniques are not able to incorporate biological cues and cells because they work in presence of harsh conditions such as high temperature or using organic solvents (Santos, Almeida and Bártolo, 2013). To

fabricate 3D models of complex tissue high temporal and spatial resolutions are needed (Moroni, Burdick, *et al.*, 2018).

AM refers to a class of processes based on the bottom-up production of a solid construct from a 3D model data by the aggregation of materials, usually in a layer-by-layer (LbL) fashion (Mota *et al.*, 2015). Contrarily to the conventional techniques, AM methods give the opportunity to properly control the internal microarchitecture and external shape of constructs, also ensuring the reproducibility of these features and the scalability from the tissue plate to the anatomic scale (Melchels *et al.*, 2012). Interestingly, it is possible to obtain anisotropic mechanical properties, in order to mimic zonal architecture of AC, by varying the structure of each layer (Woodfield *et al.*, 2005). The increasing speed of AM machines gives the opportunity to manufacture constructs for high throughput drug screening (Vanderburgh, Sterling and Guelcher, 2017). AM technologies used in CTE are stereolithography (SLA), fused deposition modelling (FDM), powder bed fusion processes, inkjet printing and bioprinting (Santos, Almeida and Bártolo, 2013).

## **1.4 3D Bioprinting**

Biofabrication represents an emerging additive manufacturing research field that deals with the generation of functional bio-constructs with a complex hierarchical architecture in an automated way and their associated tissue-maturation processes (Groll *et al.*, 2016). Bioprinting is a biofabrication technology that allows to recapitulate the microstructure of different tissues by a controlled, accurate and simultaneous deposition of various cell type, molecules and biomaterials (Mandrycky *et al.*, 2016). This technique allows the production of constructs with pre-programmed structures and pattern, based for instance on converted medical image, and thus with high reproducibility, potentially enabling high-throughput fabrication (Gungor-Ozkerim *et al.*, 2018). More specifically, the positioning of cell-laden biomaterials is controlled by digital information from 3D computed aided design (CAD) files (Cho *et al.*, 2019). Even if bioprinting is a relatively new technology, it has already demonstrated its potential use in regenerative medicine. It was used for the production of various living 3D *in vitro* tissue models, including heart (Y. S. Zhang *et al.*, 2016), kidney (Homan *et al.*, 2016), skin (Min *et al.*, 2018), liver (Knowlton and Tasoglu, 2016), lung (Horváth *et al.*, 2015), blood vessels (Kolesky *et al.*, 2016), several *in vitro* disease model (Ma *et al.*,

2018) and it has also been exploited for the production and transplantation of several tissues (Murphy and Atala, 2014a; Ozbolat, Peng and Ozbolat, 2016). To date, one of the most promising bioprinting device called “Biopen” enables the potential use of this technology during surgical operation, directly on the repairing site (O’Connell *et al.*, 2016).

The term “bioink” is used to describe biomaterials processed during bioprinting that may encapsulate cells and/or bioactive molecules (Moroni, Boland, *et al.*, 2018). Hydrogels are largely used for this aim due to their ability to provide an aqueous environment to cells and, more specifically, are also promising in CTE (You, B. Frank Eames and Chen, 2017). Cells are typically embedded in bioinks at a concentration on the order of  $1 \times 10^7$  cells per millilitre, concentration corresponding to roughly  $\leq 5\%$  total bioink volume (Moroni, Boland, *et al.*, 2018) and interestingly similar to the volume concentration of AC chondrocyte observed *in vivo* (Buckwalter, JA ; Mankin,HJ; Grodzinsky, 2005). At these densities, the presence of cells does not significantly affect the rheological properties of bioinks during extrusion (Cheng *et al.*, 2008). In addition to hydrogels, other types of bioink used in bioprinting processes are tissue spheroids, cell pellets, tissue strands, microcarriers and decellularized ECM (Hospodiuk *et al.*, 2017). Hydrogels and cells for CTE will be discussed in detail in the next chapters.

#### **1.4.1 Process and approaches**

The whole bioprinting process may be divided in three stages: i) pre-processing, which includes imaging and the choice of process approach, biomaterials and cell type, ii) processing and iii) post-processing (Fig. 1.11) (Murphy and Atala, 2014a). In the pre-processing phase 3D anatomical data are collected in order to reproduce the targeted tissue structure (Duval *et al.*, 2017). Medical imaging techniques, including computed tomography (CT) and magnetic resonance imaging (MRI), are then exploited to generate CAD files and computer aided manufacturing (CAM) models. A manufacturing file created from CAD/CAM models and usually converted in STereoLitography (STL) file format, is eventually transmitted to the 3D printer. Printing paths are generated by “slicing” STL files in 2D layers, which have a thickness ranging from 100 to 500  $\mu\text{m}$  depending on the machine resolution and bioink properties (Mandrycky *et al.*, 2016). The processing step deals with the printing of the designed structure with an appropriate bioink. The post-processing step involves the culturing and maturation of the engineered tissue inside an incubator or a bioreactor, to simulate *in vivo* conditions, and subsequent *in vitro* testing and/or implantation. To date, bioprinting process is not highly automated, thus various manual operations may lead to a slow manufacturing speed and a

relatively high chance of errors (Mandrycky *et al.*, 2016; Basu and Ghosh, 2017). Three key approaches for 3D bioprinting can be distinguished: biomimicry, biologic self-assembly and mini-tissue modular building blocks. Biomimicry approach deals with the ideal replication of cellular and extra cellular components of a tissue. To this aim, a tissue replication up to the microscale is required and so a deep understanding of the target tissue composition, architecture, cells and ECM arrangement. Cell laden hydrogel can mimic native anatomy, however ECM production, hydrogel degradation and cell proliferation must be taken in account for the functional success of the construct (Murphy and Atala, 2014a; Dhawan *et al.*, 2019). The biological self-assembly approach take inspiration from embryonic organ development processes. Autonomous self-assembly exploit the ability of early cellular components of a developing tissue to conduct the neo tissue histogenesis, regulating its structure, and functional properties. An interesting application of this approach is the bioprinting of self-assembling cellular spheroids, and their subsequent fusion and cellular organization. For example, cellular spheroids have been bio-printed on collagen-based bio-paper sheets LbL to obtain tubular structures (Mironov, Prestwich and Forgacs, 2007; Pati, Gantelius and Svahn, 2016). The last approach deals with the concept of “mini-tissues”, that are defined as the smallest functional blocks of a tissue (e.g. lobules represent liver’s mini tissues). Mini tissues may be produced in modules and then assembled to form more complex constructs by rational design or self-assembly methods. 3D bioprinting may be used to produce mini tissue and to assemble them to fabricate 3D living structures. An interesting example of mini tissue is represented by tissue strands, cylindrical building block used as a bioink for bioprinting. Tissue strands are produced packing at a high concentration cells inside hollow alginate tubule. After cellular aggregation occurs, alginate tubule are dissolved via de-crosslinking agents (Akkouch, Yu and Ozbolat, 2015; Yu *et al.*, 2016)

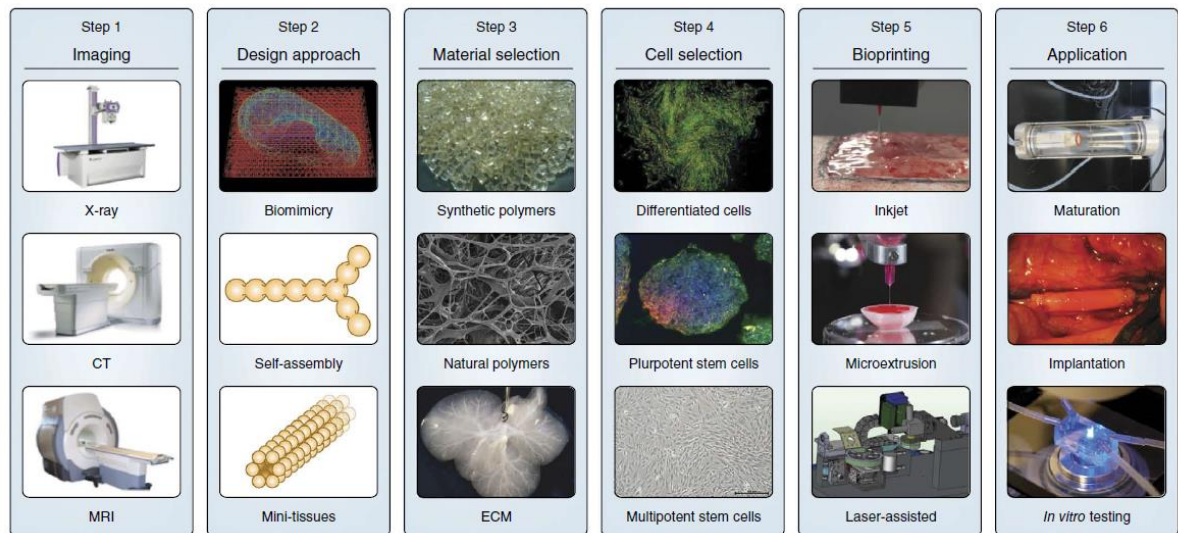


**Figure 1.11** Typical 3D printing fabrication phases. Clinical imaging techniques may be used to generate the 3D model of the construct. Design approach includes biomimicry, self-assembly and mini tissues. engineered constructs may need a maturation stage before implantation, or alternatively can be used as 3D models. Step 3 to 5 will be discussed later. Some (Murphy and Atala, 2014a)

#### 1.4.2 3D Techniques classification

3D bioprinting technique can be primary classified into three methods based on the working principle: extrusion-based, laser-assisted and droplet/inkjet-based printing. A concise comparison of these methods is provided in Table 3.

Laser-assisted printing (Fig. 1.12 A) is a bioprinting strategy that utilizes laser-based modalities to induce bioink release. The main components are a pulsed laser source, a laser focusing tool, a donor layer, and a collector for the positioning of bioink droplets. The donor layer is composed by an upper “ribbon” structure, consisting in a metallic laser-energy absorbing layer (e.g. gold or titanium), and bottom bioink solution film. The absorption layer prevents direct interaction between bioink and the laser. During the printing process the laser beam is focused on a small area of the ribbon, inducing a temperature increase that generates a high-pressure bubble, causing the ejection of a small droplet of the underneath suspended bioink (Mandrycky *et al.*, 2016; Huang *et al.*, 2017). The main advantages of this technique are high resolution (the droplet volume can be controlled in a range of 10 - 7000 pl) (Pati, Gantelius and Svahn, 2016), the possibility to use higher cell concentration than inkjet printing and relatively high viscous bioink, and an high cell viability (due to the lack of a nozzle and the non-contact printing). However, laser assisted printers are expensive, the procedure is time

consuming and the manipulation of the laser system is complex, plus side effects of laser exposure on cell are not yet fully understood (Mandrycky *et al.*, 2016).

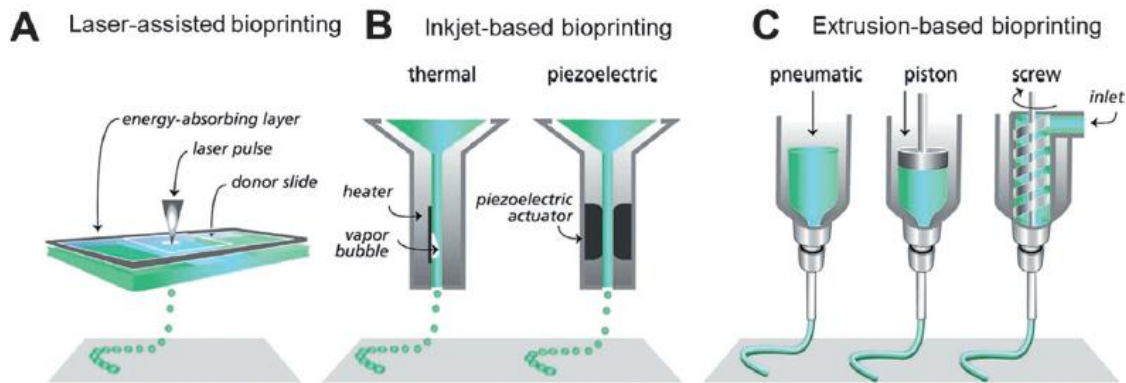


**Figure 1.12:** The main three techniques of 3D bioprinting: A) laser assisted printing, B) inkjet-based printing, C) extrusion-based printing (Pati, Gantelius and Svahn, 2016)

Inkjet based printing (Fig. 1.12 B) was the first developed method used in TE (Tuan, Boland and Tuli, 2002) and shows similarities to traditional 2D inkjet printing (Singh *et al.*, 2010). It is a non-contact technique that consists in depositing small volume ink drops (Pati, Gantelius and Svahn, 2016). A hydrogel pre-polymer solution embedding living cells is loaded in the ink cartridge, representing the bioink reservoir, that is directly connected to the printer head (Mandrycky *et al.*, 2016). To date four different inkjet-based printing techniques exist, respectively named piezoelectric, thermal, electrostatic, acoustic inkjet printing. The first two are also the most used for cell-based construct manufacture. Thermal inkjet printers electrically heat the printer head up to 300°C, producing a high-pressure air pulse that leads to the ejection of bioink droplets from the nozzle (Ihalainen, Määttä and Sandler, 2015; Huang *et al.*, 2017). The short duration of the heating leads to a low overall temperature rise (5-10 °C) that does not have a relevant impact on cell viability and molecule stability. Thermal inkjet printing is an economic and rapid technique, but shows various drawbacks including frequent nozzle clogging and poor droplet directionality (Murphy and Atala, 2014a). Piezoelectric inkjet printers contain a piezoelectric crystal that generates a mechanical pressure when voltage is applied. The generated pressure extrudes bioink droplets outside the nozzle. The main drawback of this method is the working frequency range (15-25 kHz) that causes cell damage and membrane lysis. Thus, thermal inkjet printing is more suitable for TE applications (Huang *et al.*, 2017). Overall, inkjet printing main advantages are low cost, high

working speed high resolution, and relatively high cell viability. On the other hand, inkjet printing main limitations are low material viscosity and cell concentration. (Murphy and Atala, 2014a; Mandrycky *et al.*, 2016).

Extrusion-based printing (Fig. 1.12 C) is regarded as the most suitable 3D bioprinting technique for the production of living constructs with high cell concentration (Malda *et al.*, 2013) and is the most used bioprinting methods for the fabrication of CTE constructs, being involved in approximately 85% of publications (Mouser *et al.*, 2017). This technique may be seen as a modification of inkjet printing in order to extrude more viscous bioinks (Huang *et al.*, 2017). Among all the bioprinting methods, because of the extrusion mechanism and larger nozzle dimensions, extrusion based printing possess the highest flexibility (Hospodiuk *et al.*, 2017). Usually, extrusion bioprinting systems are composed by a temperature-controlled bioink dispensing system and stage (one or both able to moves along *x*, *y*, and *z* direction), a light source that provides illumination and/or curing for photo-crosslinkable hydrogel-based bioinks, and optional video camera and humidifier (Murphy and Atala, 2014a). Extrusion printers function by automated extrusion of bioink, that is deposited on a collector plate through the extrusion head. Differently from the previous methods, extrusion bioprinting enables the printing of continuous cylindrical bioink filaments by applying a continuous pressure (Ozbolat and Hospodiuk, 2016) and allows to operate at room or physiological temperature (Kumar *et al.*, 2016). 3D extrusion printers may be classified in base of their dispensing systems, that can be pneumatic (air force pump) or mechanical (piston or screw-based). While mechanical dispensing systems allows a more accurate control over the bioink disposition than pneumatic bioprinters (that suffers of a delay of the compressed gas volume), the latter have higher pressure capabilities (Murphy and Atala, 2014a). Screw-based bioprinting enable a more accurate spatial control, but may damage cells during the process (Dababneh and Ozbolat, 2014). Extrusion bioprinting have a good compatibility with various types of biomaterials and bioink, including cell spheroids, with a wide range of viscosities. These systems often have more than a printing head, enabling the deposition of different bioinks at the same time (Huang *et al.*, 2017). As mentioned before, the main advantage of this techniques is the possibility to deposit high viscous bioink with high cell concentration, creating constructs with clinically relevant sizes (Pantani and Turng, 2015). However, cells experience mechanical stress during printing, that are thought to decrease cells viability. Increasing nozzle diameter and/or reducing dispenser pressure may increase cell survival but

at the expense of a diminished processing speed and resolution (Murphy and Atala, 2014a). Other drawbacks are nozzle clogging, relative slow printing speed and scarce resolution since the filament thickness is limited by the extrusion to approximately 200  $\mu\text{m}$ . Plus, hydrogel-based bioinks utilization may be complex because of gelation requirements and, after printing, cells may suffer dehydration and shortage of nutrients (Dhawan *et al.*, 2019).

	3D Bioprinting technique			Reference
	Inkjet	Extrusion	Laser-assisted	
Cost	Low	Medium	High	(Jones, 2012)
Preparation time	Low	Medium-low	Medium-high	(Murphy and Atala, 2014a)
Processing speed	Fast	Slow, 10 $\mu\text{m/s}$ to 700 mm/s	Medium, 200 to 1600 mm/s	(Hözl <i>et al.</i> , 2016; Cho <i>et al.</i> , 2019)
Material viscosity	3.5 to 12 mPa/s	30 to above $6 \times 10^6$ mPa/s	1 to 300 mPa/s	(Chang <i>et al.</i> , 2011; Guillemot <i>et al.</i> , 2010;)
Cell viability	>85%	80% to 90%	>95%	(Catros <i>et al.</i> , 2011; Hözl <i>et al.</i> , 2016)
Cell density	Low, $<10^6$ cells/ml	High, cell spheroids	Medium, $10^8$ cells/ml	(Murphy and Atala, 2014a)
Resolution	High, 10 to 50 $\mu\text{m}$	Medium, 200 to 1000 $\mu\text{m}$	High, 10 to 100 $\mu\text{m}$	(Ozbolat and Yu, 2013; Hözl <i>et al.</i> , 2016)

**Table 3** Comparison of the main 3D Bioprinting techniques

### 1.4.3 Limits and prospects

The first drawback of 3D bioprinting is the limited resolution to accurately recapitulate the ultrafine tissue architecture and organization. Currently, only laser-assisted approaches can reach a micro-scale resolution (Cho *et al.*, 2019). Also, two big challenges are represented by the need of increasing printing speed and scaling up. Cells viability decrease as printing time increase and to date reported works are widely based on small construct sizes (Ma *et al.*, 2018). Material selection remain a key concern for bioprinting, and incorporating multiple materials is often challenging. Bioink preparation may last weeks due to biomaterial production and cell expansion (Mandrycky *et al.*, 2016). Standardization and optimization of the printing processes, in order to ensure sterility and minimize manual handling in the respect of Good Manufacturing Practice, are also needed (Mouser *et al.*, 2017). The optimization of

the printing process also involves the choice of appropriate printing parameters, including deposition speed, dispenser and chamber temperature, nozzle diameter, dispenser travel speed, single layer height. Moreover, the success of 3D bioprinting is affected by the selection of design parameters, such as fill density, pore dimension, overall porosity (Basu and Ghosh, 2017). All the three bioprinting techniques have difficulties in printing hollow structures and there is a lack of reliable methodologies to print pre-vascularised tissues (Mandrycky *et al.*, 2016). Finally, the biofabrication of engineered construct need a large number of cells, that are often difficult to obtain (Moroni, Boland, *et al.*, 2018).

TE is a highly multidisciplined field, thus advances of both research and technology in medicine, chemistry, material science, engineering and biology are necessary to overcome 3D bioprinting limits and realize complex 3D *in vitro* models (Mandrycky *et al.*, 2016; Huang *et al.*, 2017). Even if great progresses have been achieved in biomaterials development for TE, relatively few advances for 3D bioprinting biomaterials development have been made (Hospodiuk *et al.*, 2017). An interesting future perspective is represented by 4D bioprinting, a biomimetic technology that takes inspiration from natural shape morphing systems, like nastic plants. Simplistically, 4D bioprinting adds the fourth dimension of time to 3D bioprinting. This technology theoretically exploits the combination of “smart” materials compatible with 3D printing (e.g. supramolecular hydrogels or shape memory biomaterials) and time-dependent external stimuli during printing process and/or tissue maturation. This technology will ideally enable the production of a wide variety of constructs with sophisticated structure and high resolution (Sydney Gladman *et al.*, 2016; Hendrikson *et al.*, 2017).

## **1.5 Bioinks for 3D Bioprinting**

3D bioprinting processes often involves the utilization of biomaterials as a vehicle for cell loading and to provide scaffolding for cells. The materials used for 3D bioprinting may be divided in two categories. The first one includes curable polymers produced via thermal processes and often used as scaffolds. In this case, cell seeding occurs after the printing process of the scaffold. The second category deals with bioink based on materials capable to store large water quantities, loaded with viable cells and other components such as biomolecules and drugs, including hydrogels (Pati, Gantelius and Svahn, 2016).

### 1.5.1 Bioink properties and bioprinting parameters relationships

The choice of a suitable material for 3D bioprinting and its performance in specific applications depend on different properties. Firstly, biocompatibility should be considered. The bioprinted material must be cytocompatible and non-immunogenic, while its degradation products should be non-toxic and should not elicit negative effects during in vitro maturation phase (Atala and Yoo, 2015). The printability refers to the ability of a bioink to be accurately deposited, by applying small printing pressures inferior to 3 bars, and to maintain the designed 3D structure with structural fidelity over time. Printability is influenced by processing parameters, such as nozzle diameter and crosslinking methods, and by material characteristics such as viscosity, surface tension and rheological properties. There is a lack of standardization to quantify printability, a qualitative analysis may be performed by comparing the printed structure to the CAD file geometry (Ballyns *et al.*, 2009; He *et al.*, 2016; Zhuang *et al.*, 2019). Bioink's gelation kinetics are also crucial for the preservation of 3D structure, during the process the printed material should stabilize in the least time possible (Basu and Ghosh, 2017). Material should be selected based on the required mechanical properties of the construct, crucial for the maintenance of the 3D geometry and ideally matching those of the target tissue (Murphy and Atala, 2014b). If the construct is designed for implantation, the degradation rate should ideally match the rate of neo-tissue formation (Raghunath *et al.*, 2007). Viscosity is a key parameter, affecting the cell encapsulation and sedimentation within hydrogels (Zhuang *et al.*, 2019), and is influenced by temperature, polymer concentration and molecular weight (You, B Frank Eames and Chen, 2017). Shear-thinning behaviour, by which the viscosity decrease as shear rate increase, is also a desirable bioink characteristic, especially for extrusion based bioprinting processes (Guvendiren, Lu and Burdick, 2012; Cho *et al.*, 2019). Also pseudo-plasticity, a form of shear-thinning, is a favourable rheological property for bioprinting (Melchels *et al.*, 2014). Bioinks used for extrusion bioprinting should show flow interruption immediately after deposition (Müller *et al.*, 2015). Furthermore, standardization of bioink formulation represents a pressing need for various bioprinting applications (Gungor-Ozkerim *et al.*, 2018).

As mentioned in section 1.4.3, the main printing parameter include deposition speed, dispenser and chamber temperature, nozzle diameter, printing pressure and printing time. These parameters are related to bioink properties and together affect loaded cells' viability and function. Every time a novel bioink is developed, a new set of printing parameters and

material properties should be optimized considering the chosen cell type (Panwar and Tan, 2016). Figure 1.13 summarizes the relationship between bioink properties, processing parameters and cell laden bioinks. In general a good viscosity lead to an appropriate printability and shape fidelity, however high viscous bioink requires significant extrusion forces that may expose the embedded cells to elevate shear stresses (Melchels *et al.*, 2014; You, B Frank Eames and Chen, 2017). For instance, it has been reported that chondrocyte behaviour is impaired when cells are exposed to shear stresses higher than approximately 160 Pa (Müller *et al.*, 2017). Viscosity appears to be a limiting factor for bioinks miscibility with cells (Mouser *et al.*, 2016a). Plus, bioinks with high viscosity and high polymer concentration may compromise cell viability, proliferation and mobility (Malda *et al.*, 2013). As well as shear stresses, also increased residence times of cell within the needle tip may damage cells during bioprinting processes (Paxton *et al.*, 2017a). Cell viability decreases by diminishing nozzle diameter, raising dispensing force and with the increase of printing time, since cells are exposed for more time to the printer chamber environment that may be not completely sterile. Regarding temperature sensitive hydrogels, cell viability increases if nozzle and/or chamber temperature are raised up to a threshold temperature of 37°C (Panwar and Tan, 2016). The printing process may affect various function of embedded cell, but in many cases cells viability is the only assessment performed to evaluate bioink's and process quality. Thus, more extensive biological test should be conducted for better evaluations (Mouser *et al.*, 2020)

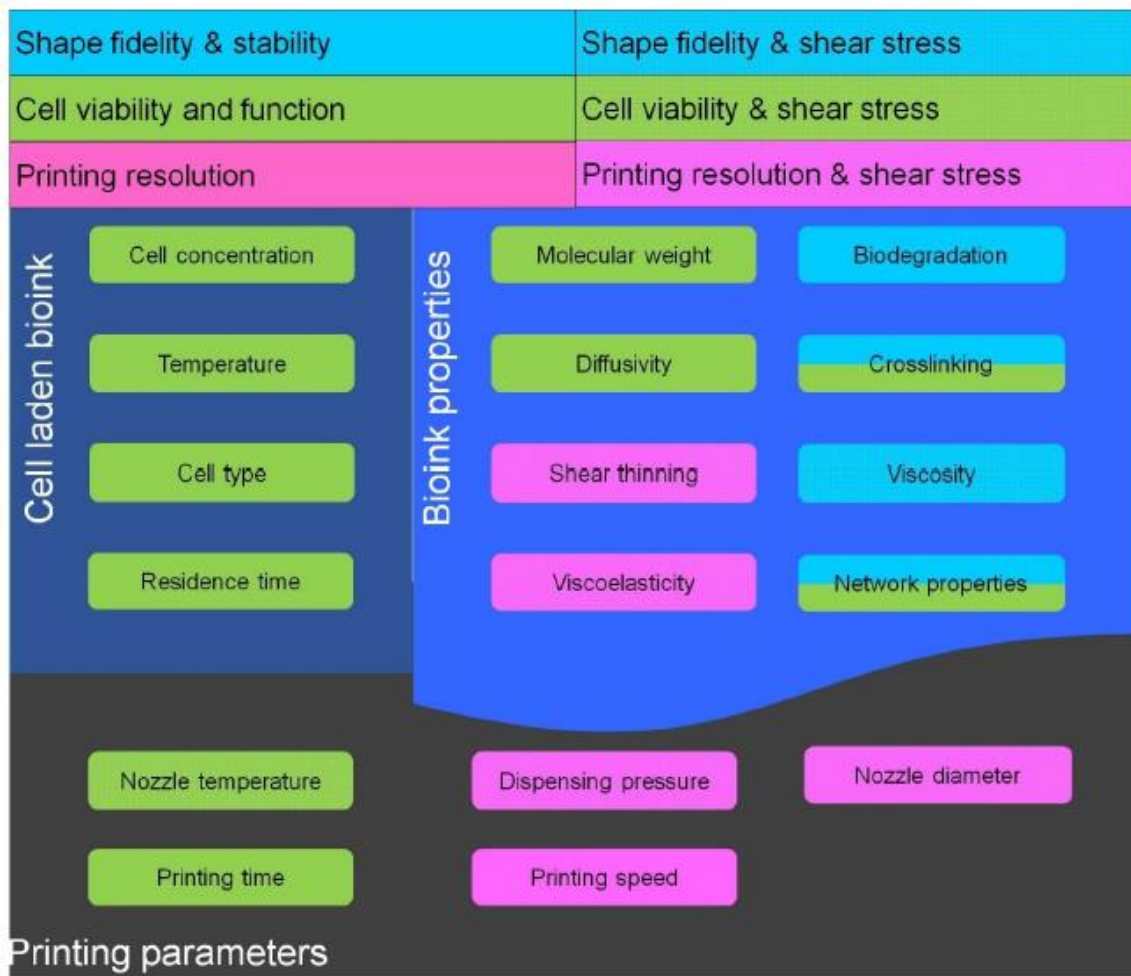


**Figure 1.13:** Relationships between bioink properties and printing parameters.

### 1.5.2 Hydrogel properties

Hydrogels are the most used material to produce living 3D constructs via bioprinting (Pantani and Turng, 2015). These are attractive biomaterials for TE consisting in hydrophilic polymer capable of hold large volume of water, retaining it up to a thousand time their dry weight, usually forming crosslinked 3D networks that can extensively swell but not dissolve in aqueous environments (Ahmed, 2015). As scaffolds, they enable an efficient nutrient, gas and waste transport and, owing to their highly hydrated environment, resemble soft tissue ECM more than other polymeric materials, providing an ideal micro-environment for cell proliferation and differentiation (Raghunath *et al.*, 2007; Zhu and Marchant, 2011). Hydrogels mechanical and biochemical features, as well as composition and architecture may be finely tuned to adapt to different biomedical application (Yue *et al.*, 2015). For instance, hydrogel mechanical strength may be controlled by varying polymer concentration (Krogstad *et al.*, 2013). Interestingly, hydrogels may show mechanical, lubricating, and swelling properties like native

AC. Subsequently, they may promote chondrocyte adhesion (Cushing and Anseth, 2007) and, due to their viscoelastic nature, they allow an efficacious load transfer to chondrocytes involving mechano-transduction processes. Moreover, hydrogel 3D network lead cells to assume a rounded morphology, promoting or maintaining chondrogenic phenotype (Spiller, Maher and Lowman, 2011).

The main hydrogel-based bioink used for CTE are reported in Table 4. Hydrogels are typically categorised, according to their material source, in natural and synthetic hydrogels and both classes have been used for bioprinting applications (You, B Frank Eames and Chen, 2017). In general, hydrogels produced from natural polymers, such as collagen and chitosan, exhibit excellent biocompatibility and biodegradability and possess bioactive motifs. They possess the potential to support chondrogenic growth, proliferation and cartilage formation (Spiller, Maher and Lowman, 2011; Yang *et al.*, 2017). Natural hydrogel used as bioink may derive from plants or animals, the latter type generally supporting better cell adhesion and growth (Panwar and Tan, 2016). Two of the main drawbacks of natural hydrogel are limited control of their degradation kinetic (Yang *et al.*, 2017) and low mechanical properties: hydrogels may be not sufficiently strong for application in load-bearing sites in the body (Levato *et al.*, 2014). Furthermore, some of natural hydrogels are not very suitable in terms of printability, and efforts have been made to overcome this problem by exploiting chemical modification or by mixing different natural materials (Cho *et al.*, 2019). Synthetic hydrogels possess superior mechanical resistance, reproducible composition, and interesting tailorable properties such as biodegradability. They are biocompatible but often show limited bioactive properties, including cell adhesiveness. However, they can be functionalised or combined with natural hydrogels to promote a better control over cell functions (Pantani and Turng, 2015; Yang *et al.*, 2017).

Hydrogels for biomedical applications may be produced, according on polymers distinctive characteristics and/or the presence of functional groups, via various crosslinking processes. Crosslinking mechanism are generally classified in i) physical and ii) chemical or covalent crosslinking, each one resulting in hydrogels with different properties. Physical crosslinking is typically obtained by varying environmental factors including pH, temperature, and ion concentration. For example, multivalent cations may be used at different concentrations to form physical crosslinks between polysaccharides molecules, generating gels with various mechanical strengths (Kaklamani *et al.*, 2014). Physical crosslinking involves molecular

structure changes, polymer chains entanglements and/or generation of weak bonds such as hydrogen bonds or hydrophobic interactions, leading to phase transition and the formation of a reversible semi-stable network (Chung and Burdick, 2008b; Yang *et al.*, 2017). Chemical crosslinking reactions deals with the interactions between two or more functional groups located on two different polymers that gives rise to covalent bonds, leading to the formation of a stable polymer network (Berger *et al.*, 2004). Covalent crosslinking reactions may be induced by various methods including introduction of crosslinking agents (Maitra and Shukla, 2014), dehydrothermal treatments (Ozeki and Tabata, 2005), and ultraviolet light irradiation (Mironi-Harpaz *et al.*, 2012). Photopolymerization is one of the most used chemical crosslinking methods. During the process, in the presence of a photo-initiator, monomers or oligomers forms a stable polymeric network when exposed to light irradiation (Hospodiuk *et al.*, 2017). Photo-crosslinkable hydrogels represent interesting materials for 3D bioprinting since they allow rapid crosslinking reactions under mild and cytocompatible conditions. Photopolymerization may occur during or just after the deposition of bioprinted filaments to stabilize them (Pantani and Turng, 2015). The second option can compromise the quality and limit the size of the construct since ultraviolet light may not homogeneously illuminate large structures (Levato *et al.*, 2014). Both chemical and physical crosslinking are exploited to improve shape fidelity and increase mechanical strength (Panwar and Tan, 2016). Controlling the network crosslinking density, for instance through UV exposure time, allows to tune various hydrogel characteristics, including shape fidelity, mechanical strength, diffusion coefficient, degradation profile and swelling ability. The swelling ratio, that can be interpreted as of a hydrogel capacity to absorb water, is connected to the crosslinking density (Spiller, Maher and Lowman, 2011) and to charge density (Okay, 2009). High crosslinking degree lead to lower swelling ratio and hydrogel pore diameter compromising the diffusion of nutrients and waste product, thus affecting cell proliferation, migration and ability to homogeneously colonize a scaffold (Malda *et al.*, 2013; Levato *et al.*, 2014). If there is no mechanical stimulation, the main characteristics that influence neo cartilage tissue formation in CTE constructs appears to be crosslinking density (Spiller, Maher and Lowman, 2011). Crosslinking processes are also important for cell encapsulation; for what concerns photopolymerization the photo-initiator concentration, light exposure time and intensity must be optimized since cytocompatibility may be compromised by prolonged UV light exposure and possible cytotoxic effect of radicals produced by the dissociation of photo-initiator (Mironi-Harpaz *et al.*, 2012).

However, it has been reported that UV exposure time may have a negligible effect on bioprinted cell viability, mainly affecting printing resolution (Zhuang *et al.*, 2019). The presence of embedded cells may influence hydrogel rheological properties, such as viscosity (Billiet *et al.*, 2014), and mechanical properties (Hölzl *et al.*, 2016). For instance, chondrocyte encapsulation within agarose hydrogels results in higher tensile and compression equilibrium modulus than acellular constructs with the same polymer concentration (Buckley *et al.*, 2009).

Alginate is a natural anionic polysaccharide derived from brown seaweeds, extensively used as a hydrogel for biomedical application due to its relatively low cost, biocompatibility and mild gelation process. Alginate gelation is obtained by ionic crosslinking at room temperature in the presence of divalent cations such as  $\text{Ca}^{2+}$  (Yang *et al.*, 2017). This polysaccharide is bioinert and lacks of cell binding domains, but it is possible to combine alginate with other hydrogel (Panwar and Tan, 2016) or to chemically modify it in order to enhance cell adhesion (Jia *et al.*, 2014). Because of its shear thinning behaviour, good printability, versatility, and fast gelation alginate hydrogels are one of the most investigated systems in 3D bioprinting (Unagolla and Jayasuriya, 2020), however even after crosslinking alginate forms relatively soft gels making difficult the generation of multi layered constructs (Panwar and Tan, 2016). Alginate may be bioprinted as a sacrificial material for the fabrication of anatomically shaped cartilage constructs (Visser *et al.*, 2013). A chondrocyte-embedding bioink composed by alginate and polycaprolactone (PCL) was used to fabricate a 3D scaffold (Kundu *et al.*, 2015). Alginate hydrogels appear to support growth and proliferation of embedded chondrocytes, to maintain chondrogenic phenotype (Yang *et al.*, 2017), and to promote the formation of neo cartilage with similar mechanical characteristics to native tissues (Lima *et al.*, 2006). Similarly to alginate, agarose is a polysaccharide refined from marine algae. It is largely exploited for the production of electrophoresis membranes and in TE due to its gelling properties (Gasperini, Mano and Reis, 2014). Agarose forms hydrogel by thermal induced physical crosslinking. This material solidifies at low temperatures, while becomes solution at temperature ranging from 20°C to 70°C (Hospodiuk *et al.*, 2017). As with alginate, agarose possess good biocompatibility but lacks of cell adhesion moieties (Tanaka *et al.*, 2016). Agarose hydrogels represent suitable bioinks for 3D printing because of their easily controlled physical properties, moreover after gelation constructs exhibit good stability and excellent thickness (Hospodiuk *et al.*, 2017; Cho *et al.*, 2019). Because of its thermosensitive characteristic agarose hydrogels can be exploited as sacrificial materials for the production of

hollow channels within bulk constructs (Norotte *et al.*, 2009). It has been reported that agarose hydrogels possess notable biomechanical characteristics such as viscoelasticity similar to those of cartilage; they are able to maintain chondrogenic phenotype of encapsulated cells, as well as promote chondrogenic differentiation of embedded MSCs (Yang *et al.*, 2017).

Chitosan is a cationic linear amino polysaccharide obtained from deacetylation of chitin, refined from various renewable sources including crustacean shells and mushrooms (Croisier and Jérôme, 2013). It is a promising material for TE because of its good biocompatibility, antibacterial activity, wound healing properties, and biodegradability. Plus, its chemical structure is similar to that of human GAGs and it forms hydrogel with a viscosity suitable for bioprinting process (Dai *et al.*, 2011; Panwar and Tan, 2016). Chitosan gelation may be obtained via enzymatic (Jin *et al.*, 2009), ionic (Pierog, Gierszewska-Drużyńska and Ostrowska-Czubenko, 2009) or chemical crosslinking (Goycoolea *et al.*, 2003), the latter strategy is performed through chitosan derivatives, chemically modified to expose specific functional groups (Yang *et al.*, 2017). Chitosan drawbacks includes low cell adhesion property (Hsu *et al.*, 2004), relatively rapid dissociation under physiological conditions, weak mechanical integrity (Panwar and Tan, 2016). Furthermore, chitosan based bioinks possess reduced printability and unstable mechanical features (Montembault *et al.*, 2006), limiting the use of this biomaterial for the fabrication of large scale constructs (Geng *et al.*, 2005). In order to increase printability and shape fidelity, chitosan may be used in combination with other polymers such as alginate and agarose (Panwar and Tan, 2016).

Carboxymethyl cellulose is a semi-flexible polymer refined from cellulose, and can form thermo-sensitive hydrogel by adjusting its features such as molecular weight and degree of methylation. The gelation of carboxymethyl cellulose water solution occurs at temperature below 37°C (Kobayashi, Huang and Lodge, 1999; Thirumala, Gimble and Devireddy, 2013). Nanocellulose-based bioinks were used to create via 3D bioprinting patient specific auricular cartilage tissue, with the resulting structures showing good cell viability, shape fidelity and mechanical integrity (Ávila *et al.*, 2016). Cellulose may be used also in combination with other polymers to create composite bioinks. For instance, nanocellulose alginate-based bioinks were used for the bioprinting of human chondrocytes, the fabricated constructs were shown to possess excellent mechanical properties and to preserve cell viability (Markstedt *et al.*, 2015).

HA, previously described in section 1.1.2, has been largely investigated in TE because of its capacity to form flexible hydrogel. HA is extremely biocompatible and biodegradable, plus HA aqueous solutions are highly viscous, making HA suitable for bioprinting applications (Cho *et al.*, 2019). HA based bioinks possess slow gelation rate and limited mechanical characteristics; therefore HA molecules are often chemically modified with photo-crosslinkable functional groups (e.g. methacrylate groups) to enable photo-crosslinking and improve rheological and mechanical properties (Hospodiuk *et al.*, 2017). For the same reasons, HA based bioink are often mixed with other polymers, including gelatin and alginate (Unagolla and Jayasuriya, 2020). As scaffolds, HA based hydrogels stimulate chondrocytes to produce Coll II, CS and aggrecan; moreover, they support both in vitro and in vivo early MSCs differentiation onto chondrogenic lines and the formation of neo cartilaginous tissues (Yang *et al.*, 2017).

Fibroin is a natural polymer, obtained by removing the sericin coating from silk, in turn produced by spiders and silkworms such as *Bombyx mori* (Kundu *et al.*, 2013). Silk fibroin represent an attractive biomaterial due to its good biocompatibility, high elasticity, robust mechanical characteristics, slow degradation rate and low immunogenicity (Vepari and Kaplan, 2007). Fibroin hydrogels are produced by different methods involving a molecular conformation change. Gelation of fibroin is obtained via different processes including sonication, lyophilization, additions of ions and photo crosslinking after chemical modification (Cho *et al.*, 2019). Silk based bioinks high viscosity can lead to nozzle clogging during the printing process, however this limit may be overcome by using recombinant spider silk based bioinks (Panwar and Tan, 2016). Fibroin hydrogels support chondrocyte proliferation and chondrogenesis (Zhao *et al.*, 2013a), however is desirable to enhance chondrocyte adhesion by introducing RGD sequence in fibroin chemical structure (Kambe *et al.*, 2010). Collagen is one of the most exploited material for biomedical application because of availability, processability and biocompatibility (Cho *et al.*, 2019). Collagen type I is the mostly investigated collagen type for the production of bioinks for 3D bioprinting (Unagolla and Jayasuriya, 2020). At low temperatures collagen type I solutions remain in a liquid state, while undergoes gelation at neutral pH or raising up temperatures. However, collagen-based bioink processing is difficult because of low gelation rate: at 37°C gel formation lasts more than ten minutes, also leading to a non-homogeneous cell distribution (Hospodiuk *et al.*, 2017). Collagen hydrogels possess low mechanical properties and there are limitations for the production of bulk constructs via 3D bioprinting because of reduced mechanical stability (Cho

*et al.*, 2019). Plus, it has been reported that collagen type I hydrogels enhance in vitro chondrogenesis and ECM production and MSC chondrogenic differentiation (Yang *et al.*, 2017).

Gelatin is a biomaterial obtained by denaturation of collagen extensively used in pharmaceutical and food industries (Hospodiuk *et al.*, 2017). Gelatin preserve in its structure the bioactive sequences of collagen, including RGD motifs and metalloproteinase sensitive degradation sites, while showing lower antigenicity (Barbara J Klotz *et al.*, 2016). Other principal advantages of gelatin are low cost, biocompatibility, non-toxic degradation products and simple processability (Gungor-Ozkerim *et al.*, 2018). Gelatin solutions, as opposed to collagen, undergoes gelation via thermosensitive crosslinking at temperatures lower than 30°C (Yang *et al.*, 2017). Gelatin may be used as an additive to other bioinks to improve their printability, mechanical properties and enhance cell adhesion and proliferation (Axpe and Oyen, 2016). However, the main limitations for the use of gelatin in biomedical applications are fast enzymatic degradation, gel dissolution at 37°C and the consequent reduced mechanical stability (Raucci *et al.*, 2019), thus gelatin is rarely used in its natural form as a bioink (Hospodiuk *et al.*, 2017). Moreover, gelatin based bioink exhibit poor bioprinting resolution (Panwar and Tan, 2016). To solve these problems, gelatin may be covalent crosslinked without prior chemical modification by using aldehydes or genipin, the second one being less cytotoxic; on the other hand this approach does not allow a precise control over crosslinking density, so chemically modified gelatin has gained interest for 3D printing applications (Barbara J. Klotz *et al.*, 2016). Gelatin chemically modified with methacryloyl functional groups (GelMA) represent an attractive material for TE because of its bioactivity, tuneable mechanical properties (Barbara J. Klotz *et al.*, 2016), low immunogenicity and biocompatibility (Loessner *et al.*, 2016). GelMA undergoes photo-crosslinking when exposed to UV radiations, and the final characteristics of the hydrogel are affected by parameters like light exposure time and intensity (Barbara J. Klotz *et al.*, 2016). GelMA is widely used as a bioink embedding different cell type for various TE applications (Unagolla and Jayasuriya, 2020). GelMA bioinks has been used for 3D bioprinting of CTE constructs with chondrocytes and MSCs; chondrocytes exhibit good viability one day after printing, while MSCs cells underwent chondrogenic differentiation after few weeks (Yang *et al.*, 2017). However, GelMA hydrogels mechanical properties are not good enough for cartilage repair applications; to address this limitation various method have been proposed, including alternated printing with

PCL (Unagolla and Jayasuriya, 2020). Other worth mentioning natural hydrogels used for CTE are decellularized ECM (dECM) based hydrogels and fibrin-based hydrogels (Roseti *et al.*, 2018).

PEG and Pluronic® are the two most exploited synthetic polymers for 3D bioprinting (Gopinathan and Noh, 2018). PEG is a biocompatible and hydrophilic polyether, extensively investigated as a hydrogel for TE and drug delivery applications (Zustiak and Leach, 2010). PEG can be prepared with linear or branched structures, is very versatile and its mechanical properties are easily tailorable (Panwar and Tan, 2016). PEG-based bioink possess good mechanical characteristics that generally lead to good printability and shape stability of the obtained constructs (Gungor-Ozkerim *et al.*, 2018). PEG can be used in combination with other materials for 3D printing applications in order to enhance the mechanical features of the deposited structure (Hockaday *et al.*, 2012). However, PEG is a bioinert material, so it needs to be mixed with other bioactive hydrogels (Gungor-Ozkerim *et al.*, 2018) or to be functionalized with cell adhesion motifs like RGD (Chimene *et al.*, 2016). PEG hydrogels support chondrocyte and MSCs proliferation, and also promote MSCs chondrogenic differentiation in presence of GFs and mechanical loading (Yang *et al.*, 2017). Similarly to gelatin, PEG is widely used also in its photo-crosslinkable forms PEG-diacrylate (PEGDA) and PEG-tetracrylate (PEGTA) (Gungor-Ozkerim *et al.*, 2018). Pluronic® is a thermo-sensitive block copolymer used in different biomedical fields including 3D bioprinting. Pluronic® bioinks possess good printability, shear thinning behaviour. However, when used as a bioink, high polymeric concentrations are needed to ensure acceptable rheological properties for extrusion bioprinting. This compromise its ability to support long term cell viability, limiting its direct use. This synthetic polymer can be modified to include photo-crosslinkable groups in order to increase mechanical integrity that is generally poor (Müller *et al.*, 2015). Pluronic® has been extensively used as a sacrificial bioink, because he liquefies at temperature inferior to 4°C (Gungor-Ozkerim *et al.*, 2018).

	Advantages in CTE	Crosslinking type	Polymer concentration (w/v)	Printability	Advantages in 3D bioprinting	Drawbacks
<b>Alginate</b>	Maintain chondrogenic phenotype Support chondrocyte proliferation	Ionic	1 to 2%	High	Fast gelation  Mild gelation process conditions  Low cost	Low cell adhesion  Difficult to print multilayer structures  Mechanically unstable for prolonged culture
<b>Agarose</b>	Maintain chondrogenic phenotype  Stimulate MSCs chondrogenic differentiation	Thermal	0.3% to 2%	High	Good stability of bioprinted structures  Can be used as a sacrificial material	Low cell adhesion
<b>Chitosan</b>	Structurally similar to cartilage GAGs  Maintain chondrogenic phenotype  Support chondrocyte proliferation  Stimulate adipose stem cells and MSCs chondrogenic differentiation	Enzymatic  Ionic  Chemical	1.5% to 3%	Low		Slow gelation rate  Low mechanical stability
<b>HA</b>	Cartilage ECM component  Extensively investigated as a biomaterial for CTE  Stimulate MSCs chondrogenic differentiation  Stimulate synthesis of cartilage ECM components  Enhance cartilage tissue formation <i>in vitro</i> and <i>in vivo</i>	Photochemical (after functionalization)  Enzymatic (after functionalization)  Physical	2% to 6%	Average	High viscosity	Poor mechanical properties  Slow gelation rate
<b>Silk Fibroin</b>	Support chondrocyte proliferation  Stimulate MSCs chondrogenic differentiation Low immunogenicity	Various	5% to 10% (With PEG)  3% (Recombinant)  10% to 17% (With gelatin)	Average	Robust mechanical properties	Rheology optimization required Nozzle clogging  Limited cell adhesion
<b>Collagen</b>	Cartilage ECM component  Support MSCs proliferation and chondrogenic differentiation  Stimulate chondrocyte proliferation and ECM formation	Thermal  pH-mediated	0.223% to 0.3%	High	High cell adhesion	Slow gelation  Limited mechanical properties and stability

<b>Gelatin</b>	Rarely used for CTE application	Thermal	10% to 20%	Average	Low cost	Limited mechanical properties
		Enzymatic			High cell adhesion	Reduced resolution
		Covalent (aldehydes, genipin)			Additive to enhance cell functions	Additive to enhance mech. properties
<b>GelMA</b>	Promote neo-cartilage ECM production by chondrocyte and chondroprogenitor cells	Photochemical	5% to 20 %	High	High cell adhesion	
	Promote MSCs chondrogenic differentiation				Additive to enhance cell functions	Additive to enhance mech. properties
<b>PEG-based</b>	Support chondrocyte and MSCs proliferation	Photochemical	10% to 20%	High	Good mechanical properties and stability	Low cell adhesion
<b>Pluronic®</b>	Support chondrocyte growth with chitosan	Thermal	10% to 20%	High	Can be used as a sacrificial material	Poor mechanical properties
		Photochemical				Low cell adhesion

Additional references: Beldowski et al., 2018; Chawla et al., 2018; Demirtaş et al., 2017; Duarte Campos et al., 2015; Gopinathan and Noh, 2018; Jin et al., 2009; Levato et al., 2017; Montembault et al., 2006; Petta et al., 2018; Rodriguez et al., 2017; Schacht et al., 2015; Ye et al., 2014; Zheng et al., 2018

**Table 4:** Hydrogels used for CTE and their characteristics as bioink

## 1.6 Gellan gum-based hydrogels and their application in 3D bioprinting

### 1.6.1 Overview of Gellan Gum

Gellan gum (GG) is a hydrolysable natural polymer identified by CP Kelco (San Diego, USA) in 1978. GG large availability and ability to form transparent and acid resistant gels enabled its use as suspending agent or additive in food and cosmetic industries, and it has been FDA and EU(E418) approved for these applications. Moreover, GG has been employed for different biomedical and pharmaceutical purposes, including nasal, gastric, ocular drug delivery, wound healing and dental cavity filling applications (Cameron J. Ferris *et al.*, 2013; Osmatek, Froelich and Tasarek, 2014; Costa *et al.*, 2018). Moreover, it has received attention for its utilization in TE field, predominantly for cartilage repair (Melchels *et al.*, 2014). GG has been investigated for its potential in intervertebral disc repair, and cartilage and bone regeneration due to its fast gelation, non-toxicity, ease of functionalization, biodegradability, processing under mild conditions and structural similarity to native cartilage GAGs (because of the presence of glucuronic acid in its repeating unit). Some of the available GG products for clinical and non-clinical applications are Gelzan®, Gel-Gro® and KELCOGEL® (J. T. Oliveira, Martins, *et al.*, 2010a; Costa *et al.*, 2018).

GG is a linear anionic exopolysaccharide formed by a repeating tetrasaccharide sequence containing 1,3- $\beta$ -D glucose, 1,4- $\beta$ -D glucuronic acid, 1,4- $\beta$ -D glucose and 1,4- $\alpha$ -L-rhamnose, and is refined from the fermentation of *Sphingomonas paucimobilis* (ATCC 31461) (Silva-Correia *et al.*, 2013; Agibayeva *et al.*, 2020), a bacterium that lives on *Elodea Canadensis* algae (Bacelar *et al.*, 2016). GG repeating unit possess side carboxyl group, that may be exploited for functionalization. GG can be found at different degree of acetylation forms (Figure 1.14). GG acetylated form (high acyl GG) is the native state of the polysaccharides, and its repeating units contain glycerate and acetate functional groups. GG deacetylated form (low acyl GG), in which the acyl groups are removed by alkaline hydrolysis, is the most used GG type for TE applications because of its relatively simple production and processing (Stevens *et al.*, 2016a). Both GG types form thermoreversible hydrogel. Native GG forms opaque, soft and elastic gels, while low acyl GG forms hard and brittle gels, but transparent (J. T. Oliveira, Martins, *et al.*, 2010a). High acyl GG has a molecular weight ( $M_w$ ) between 1 and 2 MDa, while low acyl form's one is included between 200 kDa and 1 MDa (Dave and Gor, 2018).

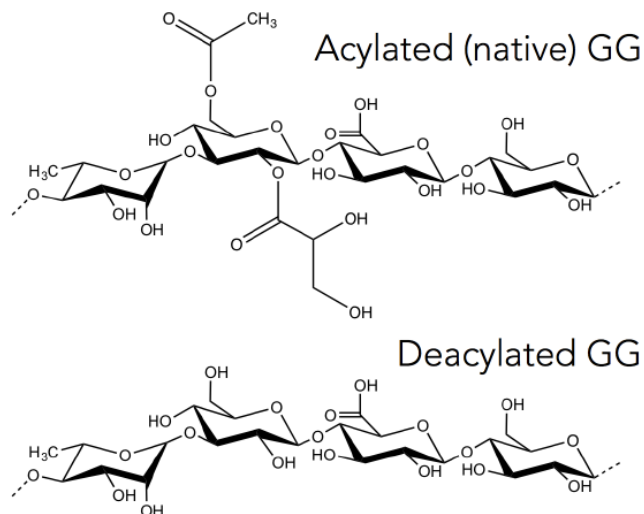


**Figure 1.14:** Chemical structure of the repeating tetrasaccharide unit of acylated and deacylated Gellan Gum (GG) (Stevens *et al.*, 2016a).

As stated before, GG can form thermoreversible gels (Figure 1.15). At high temperature GG exists in its sol phase (e.g. 80°C, 1% w/v) showing a random coil structure. By decreasing temperature down to the coil-helix transition temperature ( $T_m$ ), a reversible conformational transition from random coil to double-helix occurs, that is an essential precondition for GG

physical crosslinking (J. T. Oliveira, Martins, *et al.*, 2010a). The helices are tied through inter- and intra-chain hydrogen bonds. Thereafter, during the sol-gel transition, the double-helices structure aggregates to form a stabilized conformation, consisting in anti-parallel double-helices forming oriented bundles named “junction zones”. Different junction zones are connected by single helix chains, together generating the hydrogel 3D polymeric network (Quinn *et al.*, 1993; Morris, Nishinari and Rinaudo, 2012). Various works have reported that the gelation of this polysaccharide depends on various factors, including GG molecular weight and concentration, and solution pH (Costa *et al.*, 2018).  $T_m$  raises as GG concentration increase, and the increase of GG molecular weight promote the coil-helix transition. By reducing pH, helices aggregation and stabilization are enhanced by reducing the negative charge of GG carboxyl side groups and thus shielding electrostatic repulsion between chains. (Morris, Nishinari and Rinaudo, 2012). Also, GG gelation is strongly related to the concentration and type of introduced salt cations. For instance,  $T_m$  is increased by the presence of cations. Similarly to pH reduction, the presence of monovalent cations such as  $\text{Na}^+$  and  $\text{K}^+$  diminishes negative side groups repulsion promoting the formation of junction zones and the subsequent gelation. On the other hand, divalent cations such as  $\text{Mg}^{2+}$  and  $\text{Ca}^{2+}$  promote gelation much more significantly than monovalent ones because they generate “direct bridges” between helices by binding pairs of carboxyl groups. GG gel forming ability is advantageous for TE applications, since gelation may be obtained simply by adding standard cell culture medium (Alpha-modified minimum essential medium), that typically contains milli-molar concentration of divalent cations (Smith *et al.*, 2007; J. T. Oliveira, Martins, *et al.*, 2010a).

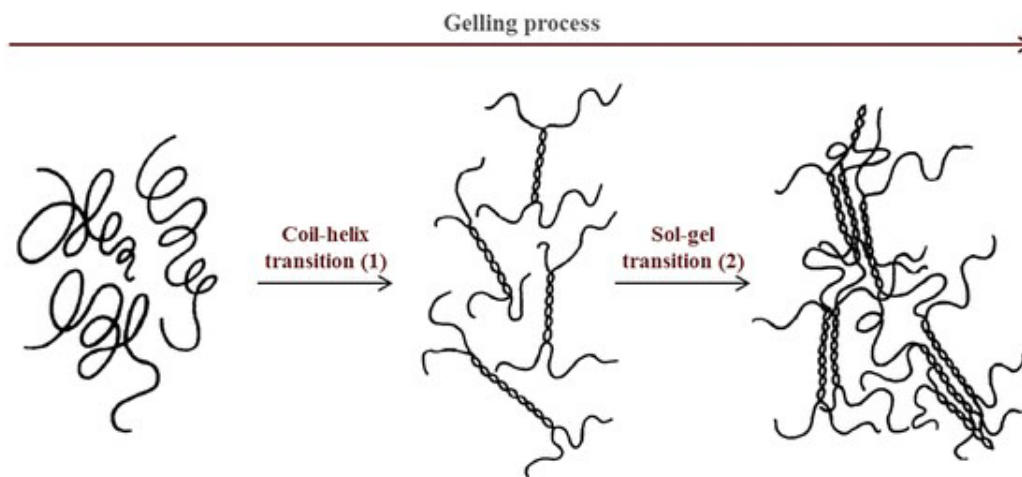


**Figure 1.15:** Schematic illustration of Gellan Gum polymer configuration during gelation process (Costa *et al.*, 2018)

In addition to gelation properties, GG possess other interesting characteristics for biomedical applications. GG-based hydrogels exhibit transparency, a favourable feature for encapsulated cells analysis, and apparently no inhibitory effects on polymerase chain reaction (PCR) analysis. GG mechanical properties can be tailored by varying polymer concentration as well as cations type and amount (Cameron J. Ferris *et al.*, 2013). GG elasticity may be tuned by controlling cation concentration and also by altering GG molecular weight employing, for instance, ultrasonication (Stevens *et al.*, 2016b). GG can be used as an injectable biomaterial by controlling its sol-gel transition at physiological temperature and pH and it has been found to provoke limited inflammation *in vivo*. GG-based hydrogels allow a simple preparation of homogeneous cell suspension by mixing hydrogel and cells at a temperature above sol-gel transition temperature, at which it shows very low values of viscosity. For instance, it has been reported that an efficacious chondrocytes encapsulation in GG hydrogel may be performed at 41 – 42°C, considering a sol-gel temperature of approximately 39°C and a gelation time of about 20 seconds. Furthermore, by using simple processing technologies such as solution casting and freeze-drying, the polysaccharide can be processed in different structures and shape (e.g. membranes, fibres, porous scaffolds) (J. T. Oliveira, Martins, *et al.*, 2010a; Bacelar *et al.*, 2016). If compared with other natural polymers, this polysaccharide attains similar mechanical properties as agar and gelatin with lower polymer concentration (Lozano, Stevens, Brianna C. Thompson, *et al.*, 2015). GG hydrogel degradation behaviour in PBS has been investigated *in vitro*. Gels reported a weight loss of approximately 15% of their starting weight

after more than 160 days. The degradation rate may be influenced by the presence of enzymes or alkaline conditions (Stevens *et al.*, 2016b). In this scenario, degradation rate can be controlled by incorporation of enzymatically labile segments in the polymer chains (Bacelar *et al.*, 2016).

Several works have proven the chondrogenic potential of GG-based hydrogels, showing their ability to sustain chondrocytes proliferation and production of ECM components (Costa *et al.*, 2018). Encapsulated chondrocytes typically exhibit a rounded shape, and they may exploit GG chains as a glucose source, gradually creating open spaces in the polymer network (J. T. Oliveira, Martins, *et al.*, 2010a). GG based constructs have been investigated as injectable cell carriers, incorporating various cell type including chondrocytes, MSCs, and adipose stem cells (Osmatek, Froelich and Tasarek, 2014). In a *in vivo* study, human chondrocytes embedded GG hydrogels have been transplanted in a murine model. These gels sustained cell proliferation and ECM synthesis, and chondrocytes aggregated in clusters of two-three cells after few weeks (Oliveira *et al.*, 2009). Plus, it has been reported that GG hydrogels support *in vitro* chondrogenesis of synovium derived MSCs (Fan *et al.*, 2010)

Although GG physical hydrogels possess various advantages for TE applications, there are a number of limitations that should be considered. In some cases, processing and gelation temperatures may compromise embedded cell viability (Costa *et al.*, 2018). At physiological cationic concentration, the sol-gel transition occurs at temperature above 42°C (Bacelar *et al.*, 2016). However, possible solutions to diminish gelling temperature is decrease GG molecular weight through oxidation (Gong *et al.*, 2009) or functionalize GG chains with thiol and carboxymethyl groups (Bacelar *et al.*, 2016) . GG hydrogels tend to become mechanically weaker and to gradually dissolve *in vivo* due to the exchange of divalent cations with monovalent cations (Coutinho *et al.*, 2010a). Plus, extrusion processes may compromise GG physical hydrogel stability. It has been reported that extrusion of GG solution through 1.7 mm diameter needle lead to mechanical instability of the gel probably caused by shear forces disruption of junction zones (Smith *et al.*, 2007). Like other polysaccharide such as alginate and agarose, GG lacks cell adhesion motifs. The limited cell adhesion on GG can be also attributed to the presence of negative charges and to its high hydrophilicity (Bacelar *et al.*, 2016). On the other hand, different approaches have been investigated to solve this problem. Different authors have blended GG hydrogels with bioactive materials like HA and fibronectin. Interestingly, GG blending with gelatin, obtaining through enzymatic binding or genipin-

mediated crosslinking, enhance both cell adhesion and mechanical strength of GG (Stevens *et al.*, 2016b). Another main issue of physical GG hydrogels is represented by their limited mechanical properties. It has been estimated, through dynamic compression analysis at 1Hz, that the compression modulus of 0.7% w/v GG disc was about 38 kPa (J. T. Oliveira, Martins, *et al.*, 2010a). Various strategies have been examined to improve GG mechanical performances. Low acyl GG and high acyl GG were combined in order to optimize the resulting hydrogel stiffness (Lee *et al.*, 2011). GG blending with inorganic materials including hydroxyapatite (Manda-Guiba *et al.*, 2012), bioactive glass nanoparticles (Gantar *et al.*, 2014), calcium phosphate (Douglas *et al.*, 2016) and gold nanorods (Vieira *et al.*, 2015) has been investigated to reinforce the resulting hydrogels. An interesting approach to improve GG mechanical properties and also providing it antibacterial characteristics consists in combining GG with inorganic clay (mesoporous silica) and Manuka honey (Bonifacio, Cochis, Cometa, Scalzone, *et al.*, 2020). Other reported strategies for mechanical reinforcement deal with GG blending with sulphated HA (Cencetti *et al.*, 2011), PLGA microspheres (Park *et al.*, 2015) and GG combination with poly- $\epsilon$ -caprolactone electrospun fibres (Thorvaldsson *et al.*, 2013) or wet spun chitosan fibres (Liu *et al.*, 2013).

### **1.6.2 Gellan gum methacrylate**

In addition to the various approaches reported in last section, GG chemical modification strategies are used to overcome some problems of GG hydrogels, leading to lower gelation temperature, superior mechanical characteristics, and enhanced bioactivity (Costa *et al.*, 2018). GG can be easily modified thanks to the presence in the repeating unit of a carboxyl group and multiple hydroxyl groups, providing new functionalities to the polysaccharides (Bacelar *et al.*, 2016). For instance, it has been reported that chemical functionalization of GG with short peptides containing RGD motifs improve cell adhesion, and covalent binding of GG with prednisolone can be exploited to provide anti-inflammatory characteristics to GG (Stevens *et al.*, 2016b).

One of the most investigated chemical modification of GG is methacrylation, employed to introduce methacrylate side groups on the polysaccharide backbone. Gellan gum methacrylate (GGMA) is typically synthesized by using methacrylic anhydride (MA) (Shin, Olsen and Khademhosseini, 2014; Pacelli *et al.*, 2016). The reaction with MA groups causes

the formation of covalent bonds between the MA and hydroxyl groups in each repetitive unit of GG. The presence of these functional groups enables GG gelation mechanism via photo crosslinking, in addition to the characteristic thermoreversible one. Indeed, when GGMA is exposed to UV light, the double bonds of MA groups react each other generating the chemical crosslinking. As stated in section 1.5.2, photo-crosslinking reactions need the presence of a photo-initiator and light irradiation, usually in the UV band (Bacelar *et al.*, 2016). GGMA-based hydrogels exhibit highly tailorable mechanical, physical and degradation characteristics, controlled by tuning the type of crosslinking method and the methacrylation degree of the polymer (Coutinho *et al.*, 2010a), and is most often employed for the production of load bearing engineered tissues such as cartilage (Stevens *et al.*, 2016b). Methacrylation degree can be tuned by varying the amount of methacrylic anhydride during GGMA preparation, and it has established that methacrylation increase GG hydrophobicity (Agibayeva *et al.*, 2020).

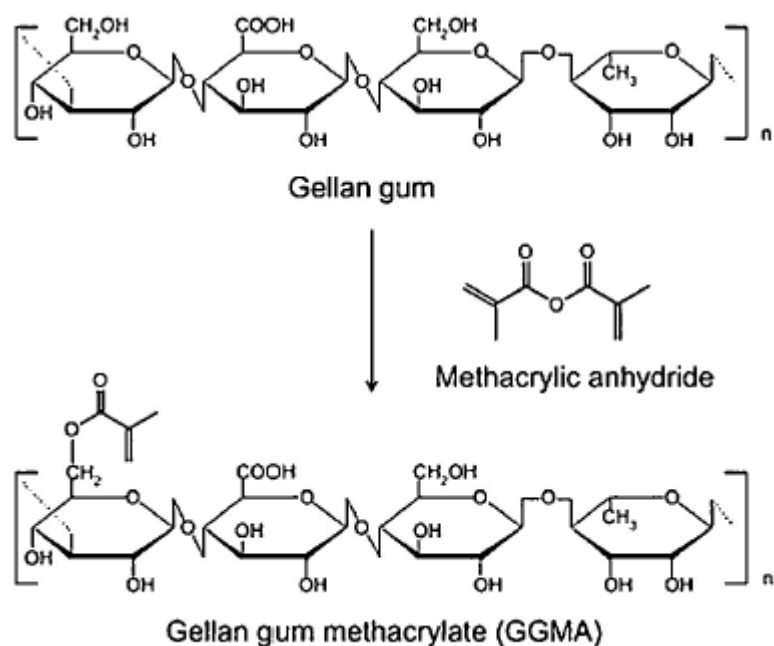


**Figure 1.16:** Schematic drawing of low acyl GG methacrylation reaction (Osmatek, Froelich and Tasarek, 2014)

It has been proven that GGMA-based hydrogels exhibit superior mechanical properties and structural stability than GG-based hydrogels, and they possess a Young's Modulus ranging from 0.15 to 148 kPa, dependently on the gelation method used (Coutinho *et al.*, 2010a). Chemically modified GG hydrogels possess lowered sol-gel transition temperature (Yang *et al.*,

2017) and, similarly to GG, GGMA can be blended with other biomaterials, such as gelatin (Shin, Olsen and Khademhosseini, 2012) and HA (Khang *et al.*, 2015) to enhance cell adhesion. *In vitro* and *in vivo* studies showed that GGMA retain GG biocompatibility, supporting good cell encapsulation with excellent viability and without elicit cytotoxic effect (Shin, Olsen and Khademhosseini, 2012; Silva-Correia *et al.*, 2013; Bacelar *et al.*, 2016). Mechanical properties of GGMA hydrogels can be further strengthened by the incorporation of laponite<sup>®</sup> nanoclay, also enabling the modulation of GGMA swelling behaviour for a controlled drug release kinetic (Pacelli *et al.*, 2016). Interestingly, Bartnikowski *et al.* reported that, under UV light exposure, lateral MA groups showed a cytoprotective effect on chondrocyte when GGMA was used as photo crosslinkable hydrogel systems (Bartnikowski *et al.*, 2015).

### **1.6.3 Gellan gum-based bioinks for 3D bioprinting**

For what concerns 3D printing, GG-based hydrogels have been employed as bioinks in various works. GG hydrogel exhibit interesting features for 3D bioprinting, including good gelling ability and shear thinning behaviour (Wu *et al.*, 2018). GG can be combined with other materials in order to obtain bioinks with enhanced rheological properties and to improve printability (Gungor-Ozkerim *et al.*, 2018). For instance, GG was added to GelMA at optimised salt concentration to create a bioink with enhanced printability and rheological properties (Figure 1.17). The bioink supported encapsulated chondrocytes viability, showed pseudo-plasticity, and the addition of increasing GG concentrations caused a gradual compression modulus rise. Plus, the mixture between these two biomaterials resulted in a viscosity increase, probably caused by the interaction between GG negatively charged carboxyl groups and GelMA protonated lysine residues. This bioink experienced a three-step gelation mechanism. The first step was caused by the electrostatic interactions explained before, the second one was represented by the thermal crosslinking obtained by decreasing temperature, and the third step consisted in GelMA photo-crosslinking by UV light exposure (Melchels *et al.*, 2014).

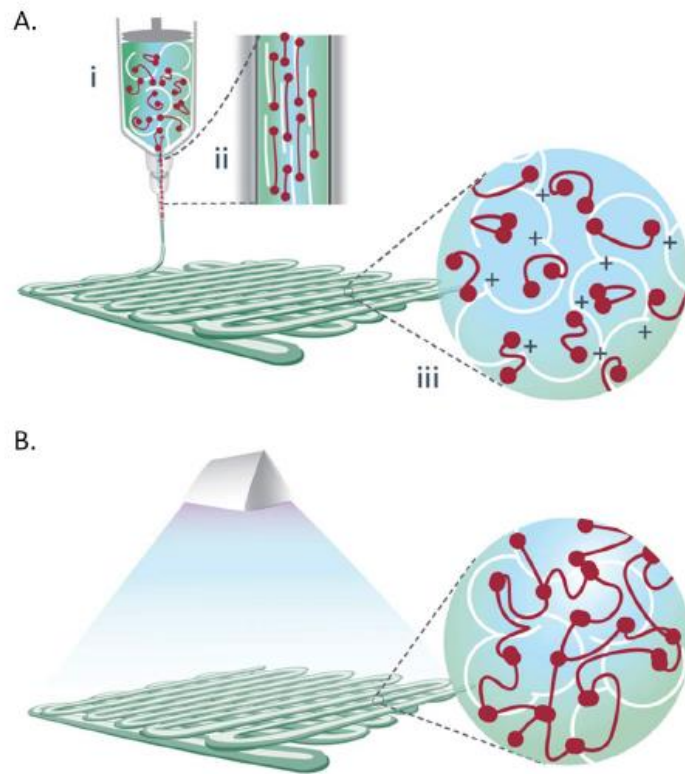


**Figure 1.17:** Schematic illustration of GelMA-GG bioprinting (A) and photo-crosslinking (B). In the extrusion chamber, GG molecules (in white) undergoes cationic-induced crosslinking generating a momentary network (i). During extrusion, the pseudo-plastic behaviour of the gel is caused by the alignment of GG chains and GelMA chains (in red) to the flow direction (ii). Upon deposition, GG chains re-established their previous conformation (iii) and, after photo curing, GelMA molecules generate a permanent network (Melchels *et al.*, 2014).

A GelMA-GG-based bioink containing MSC laden polylactic acid microcarriers was also investigated. The presence of microcarriers enhanced the bioink printability and mechanical properties of the bioprinted structure, whilst supporting cell adhesion, osteogenic differentiation, and bone-like ECM production. Interestingly, the presence of GG did not relevantly influence cell differentiation, and the authors recommended not to use MSCs laden GelMA bioinks for the fabrication of cartilage constructs, since cells may easily undergo osteogenic differentiation (Levato *et al.*, 2014). In a study, different murine cell lines (C2C12, PC12 and L929) were embedded in surfactant-modified GG microgel based-bioinks and inkjet bioprinted. The bioink showed good printability and supported cell viability, preventing cell settling phenomenon that may hinder the printing process (Cameron J Ferris *et al.*, 2013). A bioink composed of RGD-modified GG and containing primary cortical neuros was used to generate a multi-layered 3D *in vitro* model recapitulating brain microstructure. The construct sustained cell viability, proliferation, and ability to form neural networks. Also, it was found

that the printing process did not affected cell viability and shape after comparing them to the same cells in casted controls (Lozano, Stevens, Brianna C. Thompson, *et al.*, 2015). GG was combined with alginate and cartilage ECM particles (BioCartilage, Arthrex) to form a novel bioink. Various 3D constructs, including meniscal, nasal, vertebral discs and auricular grafts based on CT images or computer models. The hydrogel gelation was obtained by co-extrusion of a cation loaded support solution. The bioink showed shear-thinning behaviour and good shape fidelity, also enabling a low-pressure printing. The printed cellular constructs showed discrete mechanical strength, with a tensile modulus of approximately 116 kPa. Moreover, after *in vitro* culturing with TGF- $\beta$ 3 supplementation, biological analysis revealed that the bioink supported embedded bovine chondrocytes viability, proliferation, and hyaline-like ECM production (Kesti *et al.*, 2015). Also, GG was used in combination with PEGDA to create a photo-crosslinkable cell-laden bioink for 3D extrusion bioprinting. The bioink showed appreciable rheological properties and printability, additionally the obtained constructs exhibited good cell viability, shape fidelity and stability, enabling the fabrication of human-scale nose and ear models (Wu *et al.*, 2018). In another work, 3D extrusion bioprinting was employed to study GG mechanical properties and degradation behaviour by creating constructs with different porosity surface area to mass ratio. Degradation behaviour was tested in phosphate buffered saline (PBS) and simulated body fluid (SBF). It was revealed that the degradation rate is higher in 3D GG constructs with greater porosity, and that the compression modulus of these constructs tend to rise with degradation in SFB, probably due to the presence of cations in the fluid (Yu, Kaonis and Chen, 2017).

## **1.7 Cell source for cartilage tissue engineering**

As mentioned in section 1.2.2, the ideal cell source for CTE has yet to be determined (Levato *et al.*, 2017). Chondrocytes, stem cells, progenitor cells, fibroblast and genetically modified cells have all been investigated for their potential in cartilage repair. A list of various cell type used in CTE is summarized in Table 5. On the other hand, MSCs and chondrocytes remain the two most used cell type in the CTE applications (Vinatier and Guicheux, 2016).

ESCs show pluripotency and extremely high proliferative ability, but their use is limited by complex ethical and political concerns (Kwon *et al.*, 2016b). When employed for TE applications, ESCs are often differentiated in chondrogenic cells by culturing them as 3D

embryoid bodies (Koay, Hoben and Athanasiou, 2007). In a study, PCL scaffolds seeded with chondrogenic cells derived from ESCs, were implanted *in vivo* in murine models and lead to the formation of neo cartilage tissues (Fecek *et al.*, 2008).

iPSCs, stem cells that can be obtained through reprogramming of somatic cells, do not suffer the ethical problems of ESCs, and have been used for CTE after purifying and inducing their differentiation into chondrocytes. iPSCs represent an interesting and copious cell source for TE and, if autologous, can be employed for the fabrication of patient-specific *in vitro* OA models (Diekman *et al.*, 2012). Differentiated iPSCs, encapsulated in a nanocellulose and alginate composed bioink, have also been used in the context of 3D bioprinting for the fabrication of cartilaginous constructs (Nguyen *et al.*, 2017).

Cartilage progenitor cells (CPCs) represent a little subpopulation of cartilage cells, comprising about 0.1-1% of total cell number, and can be found mainly in AC superficial zone. They are similar to MSCs in terms of potency and self-renewal ability *in vitro* and are involved in cartilage repair processes upon damages, cartilage development processes and OA molecular changes. CPCs can be used as a complementary cell source for the fabrication of CTE constructs. Levato *et al.* have encapsulated CPCs in a GelMA-based hydrogel and bioink, in combination with chondrocyte and MSCs, to evaluate their potential for cartilage regeneration, (Bhattacharjee *et al.*, 2015; Levato *et al.*, 2017). Also, CPCs were encapsulated in a GelMA-GG based bioink to fabricate via 3D bioprinting the superficial layer of a two-zone cartilage construct (Mouser *et al.*, 2020).

Adult chondrocytes can be obtained from different sources including AC, auricular cartilage, nasal septum, and costal cartilage. For what concerns AC regeneration, hyaline cartilage sources are recommended (Vinatier and Guicheux, 2016). Two of the main issues of chondrocyte use in TE are the low availability of donor sites and their scarce concentration in native tissues (Scalzone *et al.*, 2019). For these reasons, once isolated, chondrocytes usually need to be expanded *in vitro*, and this step may induce de-differentiation (Chung and Burdick, 2008a). When cultured in monolayer, these cells tend to lose their phenotype (Vinatier and Guicheux, 2016) and a rise in collagen type I expression can be manifested (Kwon *et al.*, 2016b). The large majority of works employ chondrocyte isolated from full thickness cartilage biopsy, however zonal chondrocyte subpopulations have been used to recapitulate the layered ultrastructure of AC (You, B. Frank Eames and Chen, 2017).

MSCs are adult multipotent stem cells that can be isolated from various tissues, including AC, bone marrow, synovium, muscle, periosteum, adipose tissues, deciduous teeth, trabecular bone, and peripheral blood (Chen, Rousche and Tuan, 2006; You, B. Frank Eames and Chen, 2017). MSCs possess excellent proliferative ability, self-renewal capacity, high-plasticity, and can induce anti-inflammatory and immunosuppressive effect. Plus, they can be expanded *in vitro* (Mouser *et al.*, 2020) and have the potential to differentiate into various cell types, including chondrocytes, adipocytes, osteoblast, myogenic cells and neural cells (Filardo *et al.*, 2016; Kwon *et al.*, 2016b; Vinatier and Guicheux, 2016). MSCs chondrogenic differentiation can be manipulated *in vitro* by the addition of specific GFs, including TGF- $\beta$ 1, TGF- $\beta$ 3, FGF-2 and IGF-1 (Kwon *et al.*, 2016b). Among MSCs, synovial derived stem cells show the highest chondrogenic potential (Koga *et al.*, 2008). However, it has been reported that these cells, when implanted *in vivo*, can undergo hypertrophic differentiation and promote endochondral ossification (Mouser *et al.*, 2020). Plus, when human MSCs are cultured *in vitro*, they undergo replicative senescence after 20-40 passages. To overcome this problem, human MSCs can be immortalized through the insertion of human telomerase reverse transcriptase (TERT). The transfection can be achieved by using lentivirus including TERT gene (Bischoff, Makhijani and Yamaguchi, 2012).

Recently, MSCs and chondrocytes have been used in combination, representing an interesting alternative approach for CTE. When these cells are co-cultured, they influence each other behaviour. More specifically, chondrocyte may promote MSCs chondrogenic differentiation, and at the same time MSCs encourage chondrocytes proliferation and inhibit de-differentiation (Scalzone *et al.*, 2019). In the context of 3D bioprinting, chondrocytes are more employed than stem cells for the fabrication of engineered cartilage tissue (You, B. Frank Eames and Chen, 2017).

Cell Type	Reference
Cartilage Progenitor Cells	(Mouser <i>et al.</i> , 2020)
Fibroblasts	(Sommar <i>et al.</i> , 2010)
Chondrocytes	
Articular Chondrocytes	(Wang <i>et al.</i> , 2006)
Auricular Chondrocytes	(Yamaoka <i>et al.</i> , 2006)
Costal Chondrocytes	(Kusuhara <i>et al.</i> , 2009)
Nasoseptal Chondrocytes	(J. T. Oliveira, Martins, <i>et al.</i> , 2010b)
Stem cells	
Embryonic Stem Cells	(Fecek <i>et al.</i> , 2008)
IPSCs	(Nguyen <i>et al.</i> , 2017)
Adipose derived MSCs	(Onofrillo <i>et al.</i> , 2018)
Bone marrow MSCs	(Wayne <i>et al.</i> , 2005)
Synovial MSCs	(Ando <i>et al.</i> , 2007)
Umbilical Cord derived MSCs	(Wang <i>et al.</i> , 2009)

**Table 5:** Cell sources employed in cartilage tissue engineering

## 1.8 Aim and objectives of the thesis

The aim of this thesis was to design and manufacture 3D *in vitro* constructs representative of AC both in of healthy and pathological state. Particularly, this thesis is focused on biomimicking the middle zone of the AC tissue. The relative objectives are listed below:

- 1) Synthesis and characterization of 4 different GG-MA based hydrogels in terms, physico-chemical properties (FTIR, XPS, TGA, gelation time and water uptake) morphology (eSEM), mechanical properties (unconfined compression test) and printability. This thesis is part of a cooperation between Politecnico di Torino and Newcastle University and the part of the activity is based on GG-based hydrogel printing experimental results obtained by Annachiara Scalzone during her PhD work.
- 2) Fabrication of a healthy AC *in vitro* construct through bioprinting with RokIt INVIVO bioprinter of two bioink formulations based on two selected hydrogel compositions and Y201-C.
- 3) Biological characterization of the obtained cells-laden constructs in terms of cell viability, distribution and AC tissue production.

In conclusion, this thesis dealt with the manufacturing of a pathological *in vitro* AC model for future analysis on novel OA therapeutic treatments. Starting from the healthy constructs, OA condition was induced in the biological environment by the addition of specific cytokines. An evaluation of chondrogenic performance in terms of GAGs production and cell morphology (SEM) was performed. This part of the work was intended as an initial stage of a more exhaustive work that will be carried on in in the future.



## Chapter 2: Materials and Methods

### 2.1 Materials

The ultrapure water (dH<sub>2</sub>O) employed throughout the experiments was obtained with a Milli-Q® Integral system equipped with a BioPak ultrafiltration cartridge (Millipore, Merck). All the materials were bought from Sigma Aldrich (UK), unless otherwise stated.

### 2.2 Hydrogels preparation

#### 2.2.1 GGMA synthesis

GGMA powder was obtained through the reaction of GG and MA as outlined by Coutinho *et al.* (Coutinho *et al.*, 2010b). Firstly, a TRIS buffer solution (1M) was prepared by adding 12.11 g of Tris base (Trizma® base) to 80 ml of dH<sub>2</sub>O under stirring. Hydrochloric acid (HCl) (reagent grade 37%) was slowly added under stirring to adjust the buffer pH to 8.5, and additional dH<sub>2</sub>O was included to reach a final volume of 100 ml. pH measurements were carried out by utilizing a digital pH-meter (FiveEasy® Plus pH/mV bench meter, Mettler Toledo). Then, 1 g of low acyl GG powders (Gelzan® CM, M<sub>w</sub>:1MDa) was dissolved within the buffer solution (1% w/v) at 90°C for approximately 30 minutes under energetic agitation in order to obtain a clear homogeneous solution. The temperature of GG dispersion was reduced to 50°C and 8 ml of MA were added. The solution was left for 4 hours at the same temperature under constant stirring, and the pH was maintained at 8.5 with 1M sodium hydroxide (NaOH). The obtained solution was dialyzed in dH<sub>2</sub>O (minimum thrice per day) using dialysis cellulose membranes (M<sub>w</sub> cut off 12–14 kDa) at 4°C for at least 72 hours to eliminate the non-reacted MA. Finally, the obtained product was frozen overnight at -20°C and subsequently freeze dried (Alpha 1-2 LDplus, CHRIST, Germany) at -50°C and 0.04 mBa for at least four days in order to obtain pure GGMA powders. GGMA lyophilized powders were stored in vacuum chambers.

#### 2.2.2 GGMA-based hydrogels preparation

Four different GGMA-based hydrogel formulations were prepared, and their physico-chemical properties were assessed. The first two compositions were based on pure GGMA hydrogel at different polymer concentration: GGMA 2% w/v (GG2) and GGMA 3% w/v (GG3). The third hydrogel (GG/MH) was prepared by combining GGMA with MH (Manuka Guard®, Medical grade12+, MGO 400) (GGMA 2% w/v, MH 5% w/v), while the last hydrogel (GG/GEL) was

obtained by blending GGMA 0.75% w/v with gelatin (type A from porcine skin) 10% w/v. In order to conducting biological experiments, GGMA freeze-dried hydrogel were sterilized under UV lamp for 1 hour. The nomenclature and composition of the obtained hydrogels are summarized in Table 6.

For the hydrogel preparation, GGMA lyophilized powders were dissolved in dH<sub>2</sub>O at the proper concentration specified in Table 6, under constant stirring for about 15-20 minutes until a homogeneous solution was obtained. For the GG/MH sample, MH was added to the GGMA solution, when homogenous at the specified concentration, as reported by Bonifacio et al. (Bonifacio et al., 2020b). Then the solution temperature was increased to 60°C and the photoinitiator LAP (Lithium phenyl-2,4,6-trimethylbenzoylphosphinate) was added at 0.1 w/v concentration and left to dissolve under stirring overnight. GG/GEL hydrogels were produced by firstly diluting GG2 or GG3 solutions with dH<sub>2</sub>O in order to obtain a final GG concentration of 0.75% w/v. Gelatin powders (10% w/v) were added to GG solution at 50°C under constant stirring. 1M HCl and 1M NaOH solution were added drop by drop to the system to adjust pH. The solution pH was set to 7.5, since it has been reported that the genipin crosslinking rate of gelatin reached its peak around this pH value (Lu *et al.*, 2019). A genipin solution (10% w/v) was obtained by dissolving 20 mg of genipin powders (Challenge Bioproducts Ltd.) in 200 µl of 70% ethanol using a laboratory vortex (IKA, Germany). The genipin solution was then added to gelatin-GG solution under stirring in order to obtain a final genipin/gelatin concentration of 1.5% w/w. All hydrogels were finally stored at 4°C in a fridge and contained in laboratory vials covered from light. Cylindrical samples, used for mechanical, morphological and water uptake analysis, were obtained. To do so, hydrogel solutions were casted in a multi-well plate, crosslinked at RT under UV light (365 nm wavelength, UV LED total power: 6W) for about 10 minutes, covered by Dulbecco's Modified Eagle Medium (DMEM, Gibco) and stored in incubator at 37°C. Prior to use, DMEM was removed and samples were left overnight in the fridge to solidify, and subsequently cut with a hollow puncher to obtain cylinder-shaped specimens.

Hydrogel Code	GGMA content (%w/v)	MH content (%w/v)	Gelatin content (%w/v)
GG2	2	-	-
GG3	3	-	-
GG/MH	2	5	-
GG/GEL	0.75	-	10

**Table 6:** Composition and code names of the prepared GGMA-based hydrogels.

## 2.3 Hydrogel Characterisation

### 2.3.1 GG and GGMA Chemical characterisation

#### 2.3.1.1 Fourier Transform Infra-Red Spectroscopy (FTIR) Analysis

Fourier transform infrared spectroscopy with attenuated total reflectance (FTIR-ATR) test was conducted to evaluate the success of GG methacrylation. Both GG and GGMA spectra were acquired by using Spectrum Two™ spectrometer provided of a horizontal ATR zinc selenide crystal (PerkinElmer Inc., US) and the samples were positioned in contact with it. The analysed samples were GG raw powders and GGMA freeze-dried powders. FTIR spectra were recorded in absorbance mode, considering a wavelength window from 550 to 4000  $\text{cm}^{-1}$  with a resolution of  $4\text{cm}^{-1}$ .

#### 2.3.1.2 X-ray Photoelectron Spectroscopy (XPS) Analysis

GG raw powders and GGMA freeze-dried hydrogels underwent a second spectroscopic analysis via X-ray Photoelectron Spectroscopy (XPS) to quantitatively assess the elemental composition of biomaterials surface. The specimens were investigated by a scanning microprobe PHI 5000VersaProbe II (Physical Electronics, US), provided of an  $\text{AlK}\alpha$  X-ray radiation source, in high power mode. XPS high resolution spectra (pass energy of 29.35 eV) and survey scans (pass energy of 117.4 eV) of  $\text{C}_{1s}$  was obtained in “Fixed analyzer transmission” mode, with an analysis base pressure of  $10^{-9}$  mbar. Spectrum analysis was conducted using the MultiPak software (v.9.9.0). The atomic quantification, expressed as atomic concentration (A%), was carried out by using normalized peak area. The peak area normalization was performed in light of empirically derived sensitivity factors of the MultiPak library.

### 2.3.2 GG and GGMA Thermogravimetric analysis (TGA)

GG raw powders and GGMA freeze dried powders thermal stability were investigated by thermogravimetric analysis (TGA) in a N<sub>2</sub> atmosphere, considering a temperature range between 30 and 800°C and a 20 °C/min temperature rate, with a TGA-400 instrument (PerkinElmer Inc.). Both thermogram (TG) curves and derivative thermogram (dTG) curves were obtained and TGA Pyris software was exploited to analyse information.

### 2.3.3 Physical Characterisation

#### 2.3.3.1 Gelation time

The gelation time of the four hydrogel compositions was qualitatively measured in duplicate by using the “tube inverting” test (Scalzone *et al.*, 2019), within a 24-well plate (inner diameter = 15.6 mm, Corning® Costar® TC-Treated Multiple Well Plates). Hydrogel gelation time was measured at room temperature (RT; 20°C), under UV light, in the presence or absence of DMEM. The radiation was generated by the UV led (365 nm wavelength, 6W) of the 3D bioprinter (INVIVO, ROKIT HEALTHCARE, South Korea). For each composition, 800 µl of solution were poured into a separate well with or without the addition of 300 µl of DMEM. Culture medium was added after 1 minute of UV irradiation, in order to prevent the liquid to penetrate within the gel. Every 60 seconds, up to 10 minutes, the multi-well plate was inverted vertically for approximately 10 seconds to visually inspect samples deformation caused by their flow. The gelation time was defined as the time when no flow of the sample was monitored.

#### 2.3.3.2 Water uptake analysis

A water uptake (WU) test was performed in order to assess the ability of the four hydrogels to swell and retain water. At this regard, cylinder-shaped photo-crosslinked samples of about 6 mm diameter and 5 mm height (Figure 2.1) were firstly frozen at -20°C overnight and freeze-dried at -50°C and 0.04 mBa for two days to remove the water. Freeze-dried samples were weighted and singularly soaked in separate bijoux vials filled with 3ml of phosphate buffered saline (PBS). Samples were incubated at 37°C and each one was weighted before dipping and after 30, 90 minutes, 3, 5, 7, 24 and 48 hours. The weight was measured after delicately wipe samples with laboratory tissue papers to remove the excess PBS on their surface. To determine the WU percentage, the following formula was used (Scalzone *et al.*, 2019):

(Eq.1)

$$WU(\%) = \frac{W_f - W_0}{W_0} \times 100$$

In this equation,  $W_0$  represent the specimen weight measured before the first immersion in PBS, while  $W_f$  is the weight of the sample measured at the considered time point. For each hydrogel composition, WU measurements were performed in triplicate.



**Figure 2.1:** Digital photo of the cylindrical hydrogel samples used for the water uptake test in triplicate. This photo was taken at the end of the test. Samples shown from the top to the bottom of the image are: GG3(1), GG2(2), GG/GEL(4). Scale bar = 1cm.

### 2.3.4 Hydrogel Morphological analysis

The internal microstructure and morphology of the UV-crosslinked and lyophilized hydrogels was investigated by using environmental scanning electron microscopy (eSEM) after the WU test. To this end, the cylindrical samples were longitudinally cut in halves with a laboratory scalpel, attached on aluminium stabs by carbon tape in order to expose the longitudinal internal section, and finally gold coated by using a sputter coater (Bio-Rad). Then, electron scanning microscopy (SEM) images were acquired at 35X and 100X magnification with 20kV accelerating voltage (XL30 FEG Philips). These images were subsequently analysed by using an image processing program (ImageJ v1.46) to evaluate hydrogel pore size distribution. A 35X magnification SEM binarized image of each hydrogel composition was analysed. For each image, the diameter of at least 30 pores, whose morphology was approximated to ellipses,

was determined as the mean value of the bigger and smaller internal diameter. For every hydrogel composition, average pore diameter was calculated over all of the pores measured. Results were analysed using Microsoft® Excel software.

### 2.3.5 Mechanical characterisation

To evaluate hydrogel mechanical properties, an unconfined compression test was performed on UV-crosslinked cylindrical samples (5 mm height, 6 mm diameter) by using a mechanical testing machine (EZ SX, Shimadzu). For each hydrogel composition, three specimens were tested at RT. Samples were positioned between two platens, with the one on the top coupled with a 20N load cell. Then, they were compressed at a head speed of 0.5 mm/s, with a preload of 0.1N, until a displacement value of about 40% of the sample's original height was reached (Figure 2.2). The force was divided by the sample's superficial area in order to obtain the applied stress, while strain was calculated by normalizing the displacement to the initial height of the sample. Measurements were recorded using Trapezium X software (EZ SX, Shimadzu) and results were analysed using Microsoft® Excel software. The compressive Young's Modulus (E) was calculated as the slope of the linear region (ranging from 0-10% strain) of the obtained stress/strain curves.

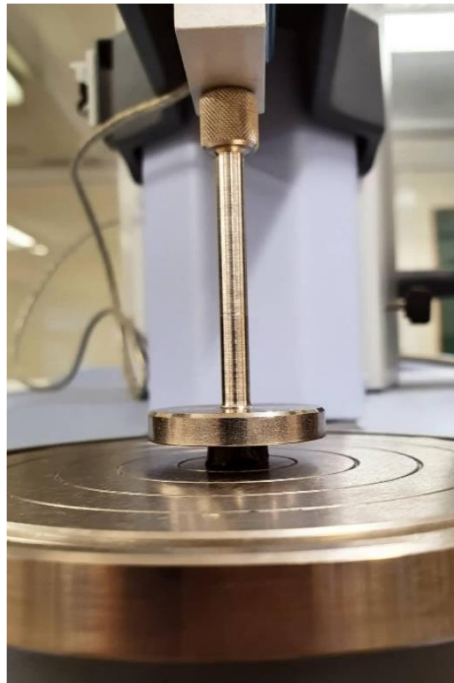


**Figure 2.2:** Digital photo of a GG/GEL cylindrical sample during unconfined compression test performed with a mechanical testing machine (EZ SX, Shimadzu). This particular specimen had a Young's modulus of 20.03 kPa.

## 2.4 Cell culture

Y201 cells were gently provided by prof P. Genever (York University) and previously differentiated into chondrocytes (Y201-C) by culturing them in the presence of chondrogenic media (serum free DMEM with P/S supplemented with 10 ng/ml TGF- $\beta$ 3 (Gibco), 50  $\mu$ g/ml L-Ascorbic acid-2-phosphate, 1%ITS+1, 40 $\mu$ g/ml L-Proline and 100 nM Dexamethasone). Y201-C were cultured in DMEM/F-12 supplemented with 10% v/v foetal bovine serum (FBS) and 1% v/v penicillin/streptomycin in T175 cell culture flask (Thermo Fisher Scientific Inc.) at 37°C and in a humidified atmosphere with 5% CO<sub>2</sub>. Y201-C were expanded in vitro until reaching an adequate number for the following experiments. Cells were passaged when they reached approximately 90% confluence using trypsin-EDTA dissociation and culture medium was replaced three times per week.

## 2.5 Bioprinting

### 2.5.1 Hydrogel printability evaluation

The printability of each hydrogel composition (without embedded cells) was evaluated by using a 3D micro-extrusion bioprinter, equipped with a temperature control system connected to the syringe bio-dispenser and the printbed. GG-MA based solutions were loaded within a tip-cap closed end syringe, that was subsequently inserted in the syringe dispenser. 25-gauge dispensing tips (1/2" Straight Cannula Blunt End Dispensing Tips, FISNAR) was used as dispensing nozzle. NewCreatorK software was used to generate a GCode for 3D grid-shaped structures of 3-4 layers (20 x 20 mm) and to control the hydrogel deposition. Filaments of subsequent layers were deposited perpendicularly with respect to the underneath layer. Strands were extruded on rectangular microscope glass slides, fastened with tape on glass petri dishes. Before printing, x, y and z calibration was performed manually: x-y offset was adjusted to position the dispenser tip to the bed centre, while z offset was calibrated to obtain 0.1-0.2 mm distance between the needle and the bed. When the extruded filament showed poor attachment to the substrate, the z offset was diminished. Printing parameters, including dispenser and bed temperature, printing speed, layer height and fill density, were optimised for each hydrogel composition. When the corner of the grid resulted rounded, printing speed was decreased (Paxton *et al.*, 2017a). The printing process occurred under UV light (365 nm wavelength) generated by the bioprinter UV LED (total power: 6W). After the

deposition of each layer, the construct was covered with DMEM/F-12 (Gibco) medium, manually added with a pipette in order to obtain a double-crosslinked network: chemically and physically. The fabricated constructs were post-cured under the same UV light source for approximately five minutes. Hydrogels' printability was assessed considering various factors, including the shape of the hydrogel at the nozzle (when a droplet formed the nozzle temperature was decreased) shape fidelity the printed structures, continuous and stable strands extrudability, the absence of filament deposition interruption and corrugation, the presence of nozzle clogging events, gelation kinetic and crosslinking uniformity (Mouser *et al.*, 2016b; Tonda-Turo *et al.*, 2020).

### **2.5.2 Bioink preparation**

After evaluating hydrogels printability, GG2 and GG/MH composition were selected to produce cell laden bioinks. Bioinks were made by mixing cells and hydrogels. GG2 and GG/MH solutions were prepared as described in section 2.2.2. In order to obtain sterile GGMA-based solutions, all the laboratory instruments involved in the process and GGMA powders were sterilized under a UV lamp for 30 minutes. Y201-chondrocytes encapsulation was obtained by gently pipetting and mixing a concentrated cell suspension with GGMA-based hydrogel solutions, using a 100  $\mu$ L pipette tip at RT. The process was performed avoiding the formation of air bubbles. A final concentration of  $7 \times 10^6$  cell/mL was obtained, and the cell-laden hydrogels were loaded within tip-cap closed 12 ml printing syringes.

### **2.5.3 3D Bioprinting and *in vitro* cell culture of constructs**

The same 3D INVIVO micro-extrusion bioprinter was exploited for the fabrication of 3D *in vitro* models. Before the printing process, the printer cabinet and all components involved in the procedure were sterilized with 70% v/v ethanol. The bioink-loaded syringes were placed into the printing carriage of the 3D bioprinter and the 25-gauge tip caps used. Both GG and GG/MH cell-embedded solutions were processed. Filaments were extruded on a glass petri dish. NewCreatorK software was used to generate simple box-shaped 3D constructs of 5-6 layers (approximately 4 x 4 x 1 mm, total volume 100 – 150  $\mu$ l per sample) and to control the bioink deposition. The calibration procedure and hydrogel crosslink were conducted as described in section 2.5.1. Culture medium was added after the deposition of each layer. The bioink was

deposited under UV light (365 nm wavelength, UV LED total power: 6W) with a printing speed of 4-5 mm/s. The same value was selected for the bottom layer speed and the printbed speed (XY movements). A layer height of 0.2 mm, inferior to nozzle inner diameter in order to foster contact between adjacent printed layers (Kosik-Kozioł *et al.*, 2017), was set. The temperature of the bed was set between 30 and 34 °C, while the temperature of the syringe dispenser was set between 35°C and 38°C. 3D bioprinted constructs are referred as their relative hydrogel code name with the addition of the suffix “H”: (i) GG2-H and (ii) GG/MH-H. Immediately after the printing process, 3D constructs were moved with a spatula and placed singularly on the bottom of well of a 48 multi-well plate. Afterwards, 1 ml of cell culture medium DMEM/F-12 was added to each well and constructs were incubated at 37°C and 5% CO<sub>2</sub> in order to carry out biological characterisation tests. Culture medium was refreshed 3 three times per week.

#### **2.5.4 Cell viability after printing**

Live/dead staining (LIVE/DEAD® Cell Imaging Kit, Life Technologies, Thermo Fisher Scientific, UK) was exploited to evaluate the viability of GG2 embedded Y201-chondrocytes. The used fluorescence-based kit is composed by two components: calcein AM and ethidium homodimer-1 (EthD-1). The first one was used to stain living cells in green (ex/em 494/517 nm), while the second one to label dead cells in red (ex/em 528/617 nm). The staining solution was obtained by diluting 2 µM calcein AM and 4 µM EthD-1 in PBS. After removing the culture medium, 3D printed constructs were washed with PBS and 500 µl of staining solution was added to each scaffold. Then, constructs were incubated covered from light at 37°C for 20 minutes. The viability of GG/MH embedded cells was assessed by using NucBlue® Live ReadyProbes® Reagent (Invitrogen, Thermo Fisher Scientific, UK). This reagent exploits Hoechst 33342 nuclear stain that emits blue light (ex/em 360/460 nm) when bound to DNA of living and dead cells. The staining solution was created by diluting 4 µM EthD-1 (LIVE/DEAD® Cell Imaging Kit, Life Technologies, Thermo Fisher Scientific, UK) and 2 drops/ml of NucBlue®, according to manufacturer’s guide, with PBS. Then, the same staining protocol followed for GG2 construct was taken. For both GG2 and GG/MH bioprinted constructs, the viability of encapsulated Y201-chondrocytes was assessed at 24 and 72 hours after printing. Also, the same test was performed on GG2 encapsulated cells at 3 hours in order to directly evaluate the effects of the printing process on cells. Cell viability analysis were carried out at the stated timepoints using a Nikon A1R inverted confocal microscope, by setting constant lightness and

scan parameters. Specifically, volume rendering images acquired at 10X magnification with a Z-stack of 15  $\mu\text{m}$  along the whole thickness of the bioprinted constructs by utilizing a Galvano scanner and 3D-reconstructed with a maximal projection algorithm. Finally, images were analysed employing NIS-Elements software (Nikon).

### **2.5.5 Cell morphology and distribution**

The distribution and morphology of encapsulated Y201-C in GG2 and GG/MH bioprinted hydrogels was visualized by immunostaining after 7 days of culture. Cell nuclei were stained in blue by using 4', 6- diamidino-2-phenylindole (DAPI), while rhodamine-phalloidin was used to detect cytoskeleton F-actin (red). After removing culture medium, cell-laden constructs were washed twice with pre-warmed PBS and fixed in pre-warmed 4% w/v paraformaldehyde (PFA) solution in PBS for 30 minutes at 4°C. Bioprinted hydrogels were washed in PBS, and permeabilization was performed by washing constructs three times with 0.1% v/v Tween20® solution in PBS (PBS-Tween). Then, constructs were covered for 20 minutes at RT with a rhodamine-phalloidin solution created by diluting 1:100 phalloidin-tetramethylrhodamine B isothiocyanate in PBS-Tween. Thereafter, hydrogels were re-washed twice with PBS-Tween and immersed for 10 minutes at RT in a DAPI solution, prepared by diluting 1:2500 DAPI (Vector Laboratories) in PBS-Tween. Finally, hydrogels were rinsed twice again with PBS-Tween and images were acquired using a Nikon A1R inverted confocal microscope at 10X magnification as detailed in section 2.5.4.

### **2.5.6 OA induction in bioprinted 3D *in vitro* models**

In order to induce OA condition and obtain 3D pathological *in vitro* models, the bio-printed systems were cultured with the addition of specific cytokines to the culture medium. Then, the feasibility of the bioprinted hydrogels as *in vitro* model was evaluated. In particular, the formation of neo cartilaginous or OA tissue was investigated by immunofluorescence (IF) analysis for Coll II production, by Alcian Blue staining for the accumulations of GAGs and by histological analysis via immunohistochemistry (IHC). Finally, SEM analysis were carried out to study cell morphology and distribution within the hydrogel. Cytokine-based OA *in vitro* models were obtained by culturing the bioprinted 3D cell-laden constructs in the presence of a cytokine cocktail. The latter was obtained by adding IL-6, IL-1 $\beta$  and TNF- $\alpha$ , respectively at a

concentration of 10, 1 and 1 ng/ml, to DMEM/F-12 cell culture medium. The cytokine concentration ratio 10:1:1 was chosen considering the levels of IL-6, IL-1 $\beta$  and TNF- $\alpha$  in advanced OA synovial fluid (Sohn *et al.*, 2012). As described in section 2.8.3, the bioprinted constructs were moved within a multi-well plate and singularly covered with 1ml of cytokine cocktail to induce OA condition. Constructs were incubated at 37°C and 5% CO<sub>2</sub> and the cytokine-based medium was changed three times per week. Pathological *in vitro* models are referred as their relative 3D bioprinted constructs code name with the addition of the suffix “P”: (i) GG2-P and (ii) GG/MH-P.

### **2.5.7 GAGs quantification (AlcianBlue)**

Alcian blue staining (pH = 2) was exploited to determine the deposition of GAGs in the cell-embedded healthy and pathological models at day 7 and 14. Firstly, after being washed twice with PBS, constructs were fixed in pre-warmed 4% w/v PFA for 30 minutes at 4°C. Constructs were covered with 1% w/v Alcian Blue solution, prepared by dissolving Alcian blue powders in 3% w/v acid acetic, and left covered from light at RT for 30 minutes. Samples were rinsed repeatedly with dH<sub>2</sub>O until the blue staining in excess was visibly removed. A quantitative GAGs production evaluation was conducted. 6M guanidine hydrochloride solution was prepared by dissolving guanidine hydrochloride (6M) in 50 mL of dH<sub>2</sub>O. 500  $\mu$ l of guanidine hydrochloride solution was added to each Alcian Blue stained sample and constructs were left covered from light on a shaking plate for 4 hours at RT to extract the stain. Then, 50  $\mu$ l of supernatant were taken in triplicate from each construct and placed in a 96-clear bottom well plate. Other 50  $\mu$ l of guanidine hydrochloride solution was added to each well. Reading was performed at 630nm in absorbance (values expressed in OD) with a Filter-based multi-mode microplate reader

### **2.5.8 Bioprinted constructs morphological analysis (SEM)**

SEM analysis were carried out to monitor the morphology and distribution of Y201-chondrocytes within GG2-H and GG2-P constructs at day 14. Firstly, constructs were washed twice in PBS and fixed in pre-warmed 2% v/v glutaraldehyde for 30 minutes at 4°C. Then, samples were washed twice in 0.4M sodium cacodylate buffer (pH = 7.4). Constructs underwent de-hydration at 4°C in ascending ethanol grades (EtOH; v/v in dH<sub>2</sub>O): 15 minutes

in 25%, 50%, 70% and 80% EtOH, 15 minutes in 95% EtOH twice, and 4 times in 100% EtOH for 15 minutes covered by filter paper. Subsequently, samples underwent various critical point drying steps through increasing hexamethyldisilazane (HMDS) concentration at RT: 15 minutes 5 drops of HMDS in EtOH 100%, 15 minutes HMDS 50% v/v in EtOH 100%, and three times 100% HMDS for 10 minutes. Constructs were fixed on aluminium stubs with Achesons Silver ElectroDag and sputter-coated with gold by using a Polaron E5000 SEM Coating unit (Quorum Technologies, UK). SEM images were acquired at various magnification with 8kV accelerating voltage.

## **2.6 Statistical analysis**

Statistical analysis were performed via ANOVA One-way or two-way analysis of variance (Turkey's multiple comparison test) by using a GraphPad® 8.4.3. For each condition, tests were carried out three times, unless otherwise specified. Data were reported as mean values  $\pm$  standard deviation. Differences between groups were considered significant for  $p < 0.05$ . Single (\*), double (\*\*), triple (\*\*\*) and quadruple (\*\*\*\*) asterisks indicated respectively  $p < 0.05$ ,  $p < 0.01$ ,  $p < 0.001$  and  $p < 0.0001$ .



## Chapter 3: Results

This chapter is divided in two main parts: the first one focus on the characterisation of the hydrogels (chemical, thermal and physical), while the second part deals with the biological characterisation of the bioprinted constructs.

### 3.1 Hydrogel Characterisation

#### 3.1.1 Chemical Characterisation

##### 3.1.1.1 FTIR Analysis

FTIR-ATR spectra of GG powders and GGMA lyophilized powders were measured in the range 4000 - 550  $\text{cm}^{-1}$  in order to confirm the methacrylation process (Figure 3.1). Characteristic GG absorption peaks, reported in Table 7, were observed in both GG and GGMA spectra at 1035  $\text{cm}^{-1}$ , 1410  $\text{cm}^{-1}$ , 1620  $\text{cm}^{-1}$ , 2920  $\text{cm}^{-1}$  and 3420  $\text{cm}^{-1}$ . As regards to GGMA spectrum, the distinctive C=O stretching vibration absorption peak of MA ester bond appeared at 1740  $\text{cm}^{-1}$ , while the peak at 1535  $\text{cm}^{-1}$  were assigned to C–C stretching (Figure 3.1 insert, Table 7). However, the absorption peak at 1635  $\text{cm}^{-1}$ , typical of C=C bond of MA, was not clearly distinguished (Figure 3.1 insert).

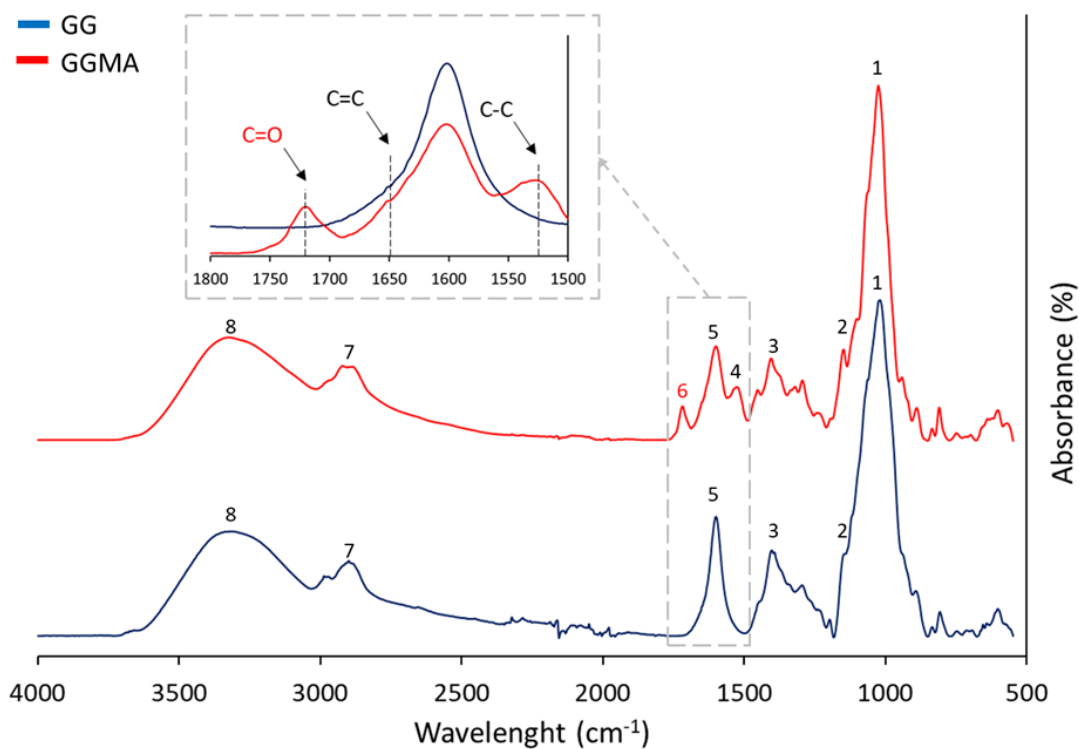


**Figure 3.1:** FTIR-ATR spectra of GG powders and GGMA lyophilized powders. The insert shows a zoom on the wavelength band where peaks relative to the introduction of MA were noticed. Peaks assignment is listed in Table 7.

Peak number	Wavelength (cm <sup>-1</sup> )	Assignment
1	1035	C-O stretching
2	1220	C-C stretching
3	1410	Symmetric COO <sup>-</sup> stretch
4	1535	C-C stretching
5	1620	Asymmetric COO <sup>-</sup> stretch
6	1740	(ν C=O) ester carbonyl stretch
7	2920	C-H stretch
8	3420	O-H stretch

**Table 7:** Attribution of GG and GGMA FTIR-ATR absorption peaks illustrates in Figure 3.1 (Silva-Correia *et al.*, 2011; Agibayeva *et al.*, 2020)

### 3.1.1.2 XPS analysis

XPS was employed to study the surface composition of GG powders and GGMA lyophilized powders. The elemental composition of the investigated samples expressed as A% was listed in Table 8.

Sample	C <sub>1s</sub> (A%)	O <sub>1s</sub> (A%)	N <sub>1s</sub> (A%)
GG	56.9	40.1	1.9
GGMA	71.9	25.2	2.0

**Table 8:** Atomic percentage (A%) of GG powders and GGMA lyophilized powders obtained through XPS analysis.

The results showed the major presence of carbon (C<sub>1s</sub>) and oxygen (O<sub>1s</sub>) in both GG and GGMA samples. It is noticeable that the carbon percentage increased from 56.9% for GG to 71.9% for GGMA, whilst oxygen amount decreased from 40.1% for GG to 25.2% for GGMA. In both composition a small amount of nitrogen (N<sub>1s</sub>) of around 2% was detected. For simplicity, the presence of elements between 0.3 and 1% was not reported.

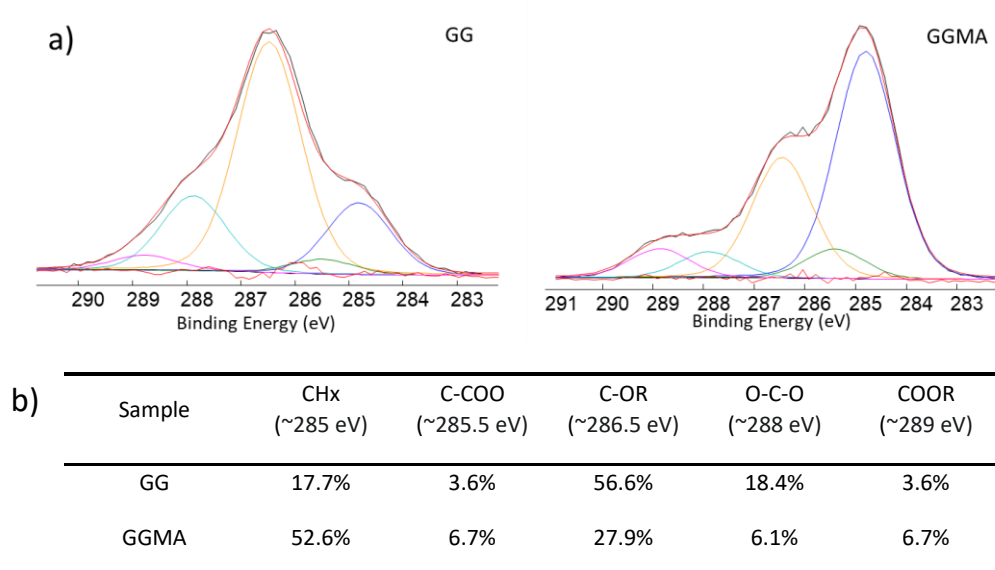


**Figure 3.2:** High resolution XPS analysis of GG and GGMA. Curve fitting of high resolution C<sub>1s</sub> spectrum of GG (left) and GGMA (right) (a). Bond percentage and relative binding energy of the investigated samples (b).

High resolution XPS of carbon ( $C_{1s}$ ), reported in Figure 3.2 (a), was carried out, and the signal was de-convoluted into five spectra related to the following functional groups: CHx (binding energy: 284.8 eV), C-COO (binding energy: 285.4 eV), C-OR (binding energy: 286.5 eV), O-C-O (binding energy: 287.9 eV) and COOR (binding energy: 288.9 eV). The table in Figure 3.2 (a) showed, for each sample, the associated peak area percentage (%) of considered chemical species. The major differences in bonds percentages between GG and GGMA were the following: CHx increased from 17.7% in GG to 52.6% in GGMA; C-COO also grew from 3.6% in GG to 6.7% in GGMA; C-OR was found at 56.6% in GG and diminished to 27.9% in GGMA; O-C-O decreased from 18.4% in GG to 6.1% in the methacrylated form; COOR increased from 3.6% to 6.7% in GGMA.

### 3.1.2 Thermal characterisation

GG powders and GGMA lyophilized powders thermal stability was studied through TGA. The relative TG and dTG spectra are displayed in Figure 3.3. The first GG weight loss of approximately 13%, appeared from 30°C to 180°C, whilst the initial 11% weight loss of GGMA occurred in a narrower range, between 30°C and 120°C. The main degradation step of GG occurred between 230°C and 520°C, with a relative weight loss of approximately 60% and a peak temperature of 262°C. GGMA showed a major weight loss of nearly 65% in a temperature range of 120–530°C, in a degradation step composed by two overlapping peaks at 232°C and 252°C. Only GG spectrum displayed a third degradation step, with a moderate weight loss of 16% occurring at around 600°C.

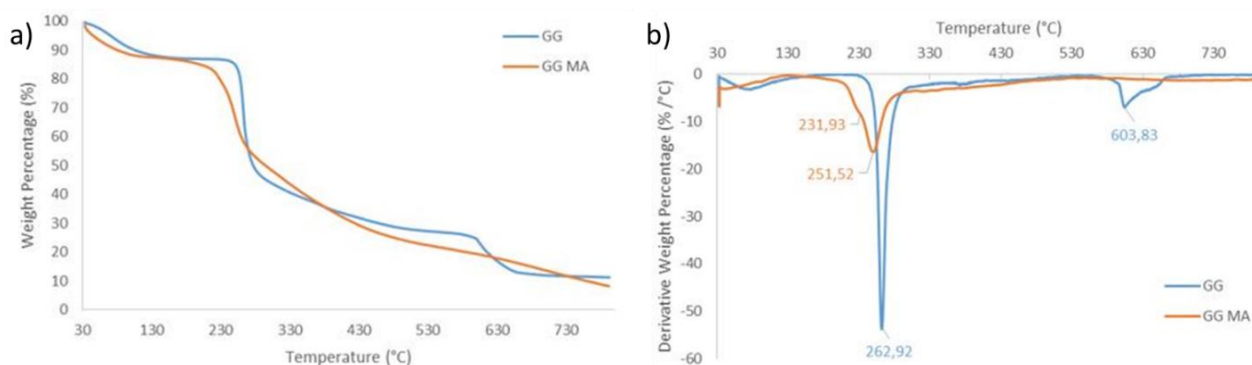


**Figure 3.3:** TG (a) and dTG (b) curves between 30°C and 800°C of GG powders (blue) and GGMA lyophilized powders (orange).

### 3.1.3 Physical Characterisation

#### 3.1.3.1 Gelation time

A simple inversion test was conducted at RT to qualitatively estimate the gelation time of a-cellular GGMA-based hydrogels and to investigate the effect of the addition of MH and gelatin. Table 9 reports the gelation time under UV light (365nm, UV LED total power: 6W) of the investigated systems with or without the presence of cell culture medium. The test was conducted on the four aforementioned GGMA based hydrogels: GG2 (2%w/v GGMA), GG3 (3%w/v GGMA), GG/MH (2%w/v GGMA; 5%w/v MH), and GG/GEL (0.75%w/v GGMA; 10%w/v gelatin). Considering a time window of 10 minutes, both GG2 and GG/MH systems did not undergo gelation without the presence of cell culture medium. At the same conditions, GG3 and GG/GEL showed a sol-gel transition time of about one minute. When cell culture medium was added, GG3 and GG/GEL gelation time remained the same, while GG2 and GG/MH underwent sol-gel transition within  $\approx$  3 minutes. As regards to pure GGMA-based hydrogels (GG2 and GG3) the gelation time in both conditions was negatively correlated with the polymer concentration. Moreover, between GG3 and GG/GEL and between GG2 and GG/MH no differences in terms of gelation time were noticed.

Composition	Gelation time, no medium (min)	Gelation time with medium (min)
GG3	~ 1	~ 1
GG2	> 10	~ 3
GG/MH	> 10	~ 3
GG/GEL	~ 1	~ 1

**Table 9:** Gelation time of the prepared GGMA-based systems (800  $\mu$ l) under UV light (365 nm, 6W) at RT (20-25°C) with or without the addition of cell culture medium (DMEM, 300  $\mu$ l). Test was performed in duplicate.

#### 3.1.3.2 Water uptake analysis

Figure 3.4 illustrates the water uptake (WU) capacity of the freeze-dried GGMA-based hydrogels at different time points after 30 minutes, 90 minutes, 3 hours, 5 hours, 7 hours, 24 hours and 48 hours. As highlighted in Figure 3.4 insert, all hydrogel compositions swelled

immediately after their soaking in PBS. GG2, GG3, GG/MH and GG/GEL exhibited a steep WU increase within 3 hours, respectively reaching a value of  $1682 \pm 110 \%$ ,  $1434 \pm 57 \%$ ,  $675 \pm 32 \%$  and  $440 \pm 41 \%$ . At this point, GG2, GG3 and GG/MH samples showed a slower water uptake rate, achieving a WU value of respectively  $1956 \pm 10 \%$ ,  $1544 \pm 64 \%$  and  $772 \pm 48 \%$  within 24 hours, then a WU plateau was detected after 48 hours of immersion. As regards to GG/MH, after 3 hours of analysis the WU value remained approximately stable up to 48 hours. Overall, GG2, GG3 and GG/GEL hydrogels showed a similar WU evolution, with a steep rise at the beginning of the test, followed by a more gradual rise to reach an equilibrium value after two days. On the other hand, GG/MH sample WU percentage, after the initial rapid increment, remained nearly constant. Also, MH-based hydrogels and GG/GEL reached a lower WU% compared to bare GGMA-based hydrogel (GG2 and GG3). In particular, at equal concentration of GGMA (GG2 and GG/MH), the addition of MH led to a WU% drop.

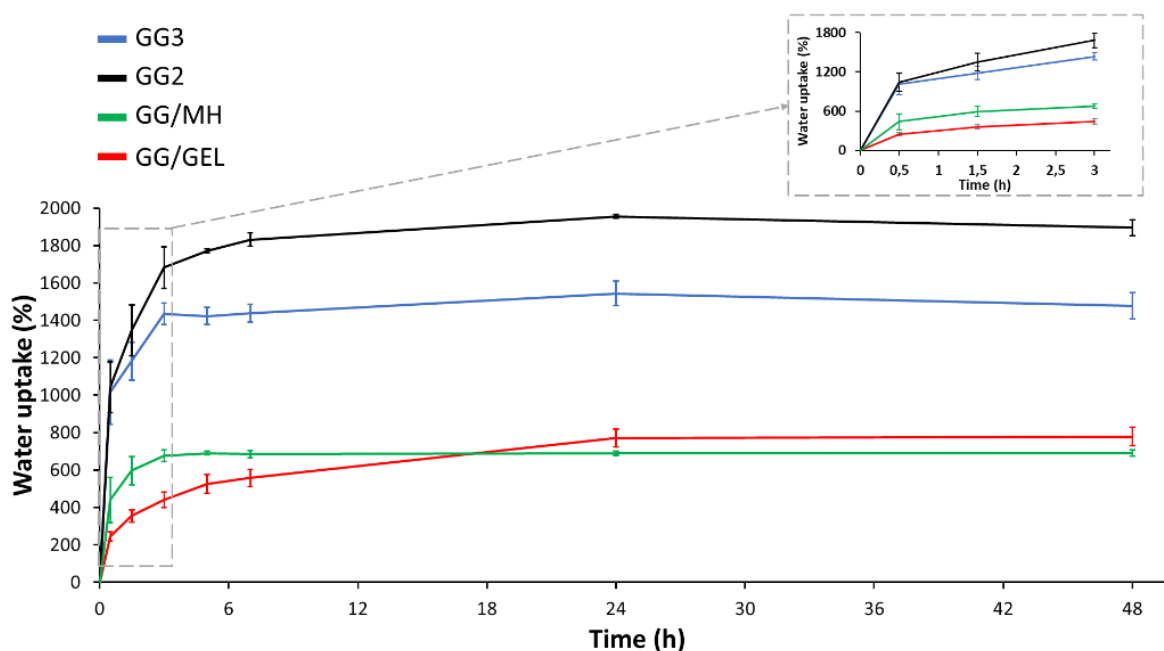


**Figure 3.4:** Water uptake (%) analysis up to 48 hours relevant to GG3, GG2, GG/MH and GG/GEL freeze-dried hydrogels. Measurements were performed in PBS at 37°C. The insert illustrates the water uptake profile in the first three hours of analysis. Values are expressed as mean  $\pm$  standard deviation ( $n = 3$ ).

### 3.1.4 Morphological analysis

GGMA-based hydrogels surface morphology post-water uptake test was investigated using SEM. The influence of GGMA concentration and the effect of gelatin and MH on the internal microstructure was evaluated. From the acquired SEM images (Figure 3.5) it was observed

that all the compositions have an anisotropic porous microstructure. GG3, GG2 and GG/MH (Figure 3.5 a, b, c) appeared possessing a well interconnected framework, clearly displayed at 100x magnification, with irregular (circular and elliptical) pore shape. The addition of MH did not lead to a considerable changes on GGMA hydrogel microarchitecture. GG/GEL structure revealed a more defined pore morphology, with larger pore size compared to the other compositions (Figure 3.5 d). Also, GG/GEL samples appeared to have smoother pore surface compared to the other formulations.

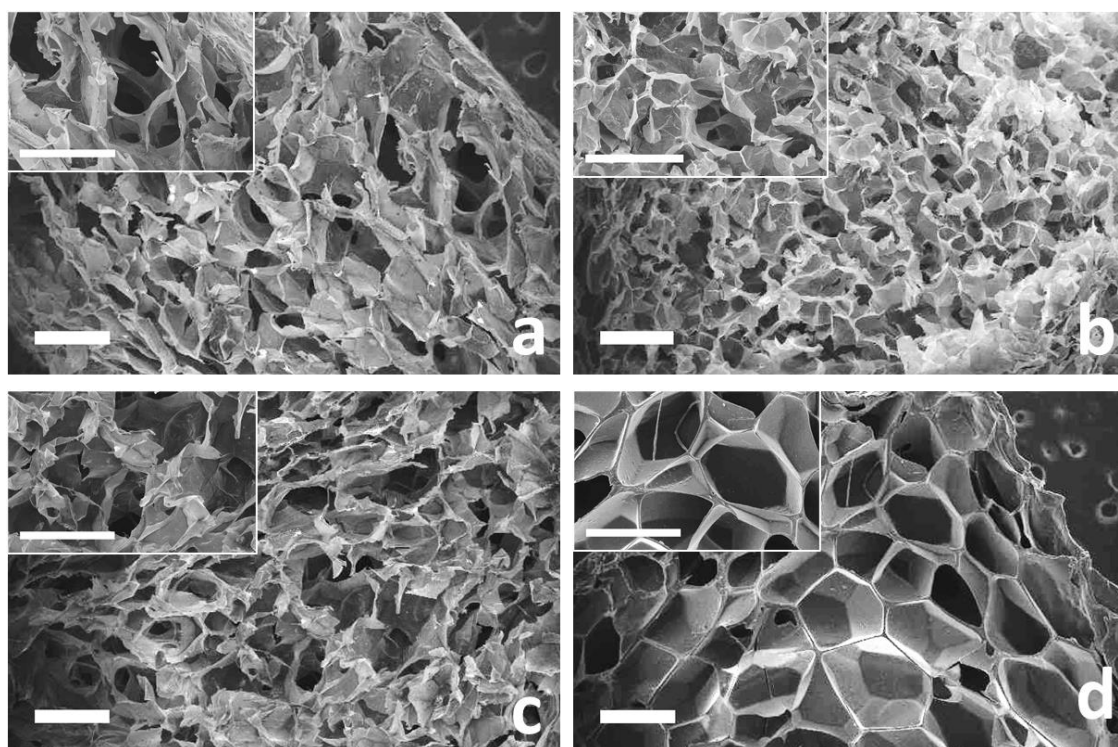


**Figure 3.5:** Environmental scanning electron microscopy (eSEM) representative images illustrating the cross-section morphology of the freeze-dried GGMA-based hydrogels at 35x and 100x (upper left inset). (a) GG3; (b) GG2; (c) GG/MH; (d) GG/GEL. Scale bar = 500  $\mu\text{m}$ .

Differences in pore diameters between the four hydrogels, calculated as described in section 2.3.4, were observed. Hydrogels showed multiple length scale porosities (Figure 3.6). In the case of GG3 hydrogel, more than 30% of pores had a diameter between 100 – 150  $\mu\text{m}$ , nearly 25% of pores showed a diameter between 50 – 100 or 150 – 200  $\mu\text{m}$ , about 12% of pores had a diameter between 200 – 250  $\mu\text{m}$ , and around 5% of pores exhibited a diameter between 250 – 300  $\mu\text{m}$ . Regarding GG2 hydrogel, more than 40% of the pores had a diameter between 50 -100  $\mu\text{m}$  and 100 – 150  $\mu\text{m}$ , nearly 7% of pores had a size between 200 – 250  $\mu\text{m}$  and the

remaining 4% of pores were in 250 -300  $\mu\text{m}$  diameter range. As regards to GG/MH, around 45% of pores were in 100 – 150  $\mu\text{m}$  diameter range, about 30% and 15% of the pores had respectively a diameter between 50 – 100  $\mu\text{m}$  and 150 – 200  $\mu\text{m}$  and about 3% of pores showed a size between 200 – 250  $\mu\text{m}$ . Concerning GG/GEL, around 30% of the pores were in the 150 – 200  $\mu\text{m}$  or 100 – 150  $\mu\text{m}$  diameter range, about 20% of the pores had a diameter between 300 – 400  $\mu\text{m}$ , 15% of the pores showed a diameter between 200 – 250  $\mu\text{m}$  and nearly 3% had a size between 50 – 100  $\mu\text{m}$  and 250 – 300  $\mu\text{m}$ . Overall, most of GG3, GG2 and GG/MH pores had a diameter inferior to 200  $\mu\text{m}$ . GG2 and GG/MH showed the narrowest pore diameter distribution, ranging from 50 to 250  $\mu\text{m}$ , whilst GG/GEL pore size distribution was the largest one.

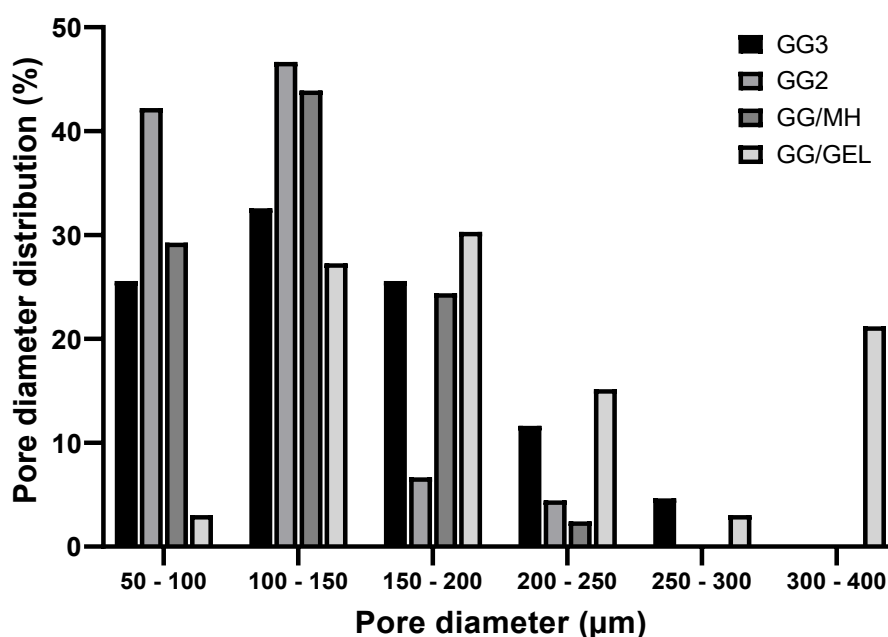


**Figure 3.6:** Bar chart illustrating the percentage distribution of pore sizes of prepared hydrogels (GG3, GG2, GG/MH and GG/GEL). Pores diameter ranges are: 50- 100  $\mu\text{m}$ ; 100-150  $\mu\text{m}$ ; 150-200  $\mu\text{m}$ , 200-250  $\mu\text{m}$ , 250-300  $\mu\text{m}$  and 300-400  $\mu\text{m}$ .

Figure 3.7 shows the mean pore diameter of the four hydrogel compositions. GG3, GG2 and GG/MH possessed respectively an average pore diameter value of 146, 108 and 124  $\mu\text{m}$ , with a considerable statistical difference ( $p < 0.05$ ) between GG3 and GG2 values. GG/GEL had a mean pore size of 207  $\mu\text{m}$ , higher than the other values and statistically different ( $p < 0.0001$ ). The addition of MH at equal concentration of GGMA (GG2 and GG/MH) did not lead to a

statistical difference of mean pore size. Overall, all compositions showed a mean pore diameter between approximately 100 and 200  $\mu\text{m}$ .

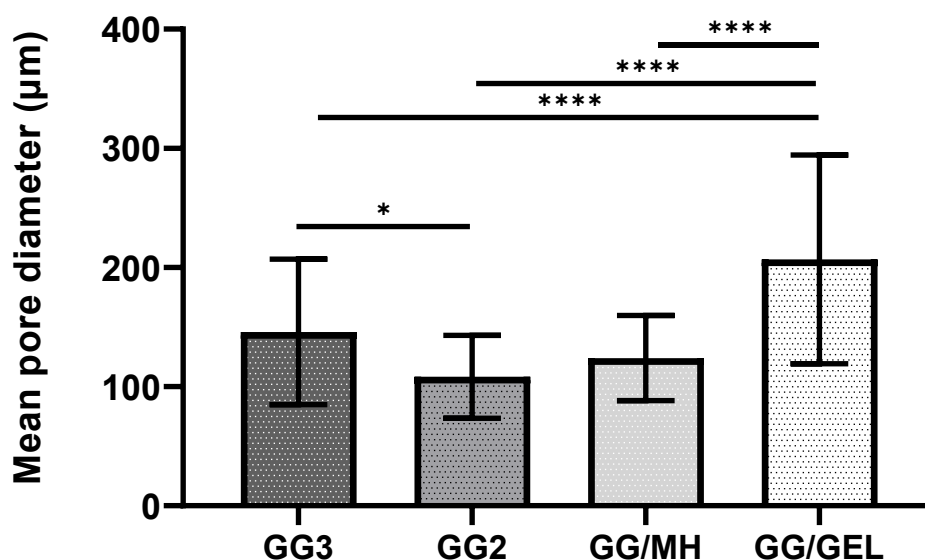


**Figure 3.7:** Bar chart illustrating the mean pore diameter of the four GGMA-based hydrogels (GG3, GG2, GG/MH and GG/GEL). Data are presented as mean  $\pm$  standard deviation (minimum  $n = 30$ ). Statistical significance is shown as \* ( $p < 0.05$ ) and \*\*\*\* ( $p < 0.0001$ ).

### 3.1.5 Mechanical characterisation

The mechanical properties of the prepared hydrogels were investigated through unconfined uniaxial compression test. Figure 3.8 illustrates the representative stress-strain curves of the GGMA-based hydrogels. All hydrogel compositions exhibited a limited linear elastic region, ranging approximately between 0 – 10% strain. Every GG2 tested sample underwent breakage at a compressive strain value of approximately 27% (Figure 3.7). GG2/MH and GG/GEL curves showed a similar evolution, with a modest increase of the compressive stress after the linear region. On the other hand, in relation to the other compositions, GG3 samples exhibited a sharply increase of the compressive stress after roughly 10% strain (Figure 3.7).

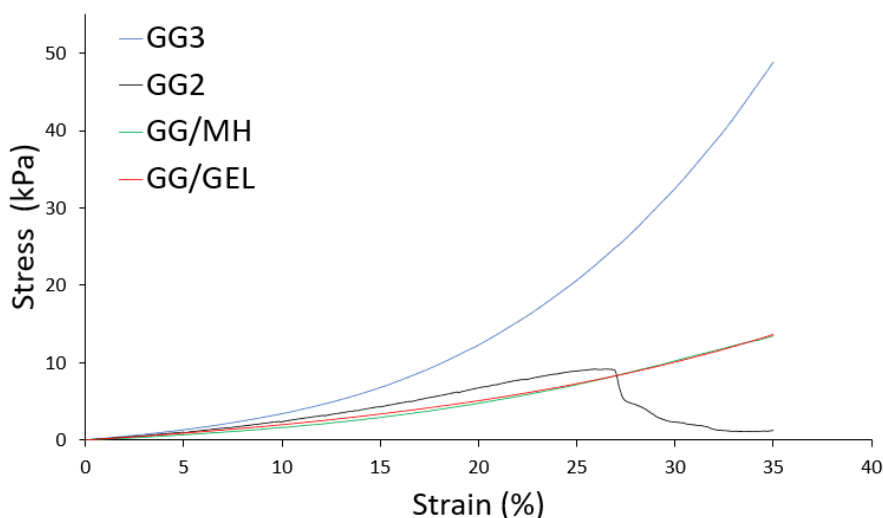


**Figure 3.8:** Representative stress-strain curves of the GGMA-based hydrogels compressed at a strain of 0 -35%. For each composition, the shown curve was calculated with one of the three tested cylindrical sample.

The linear stress strain curves were then exploited to determine E modulus of GGMA-based hydrogels, computed as the slope of the linear region. GG3, GG2, GG/MH and GG/GEL showed respectively an E of about  $24.6 \pm 1.8$  kPa,  $19.7 \pm 1.2$  kPa,  $16.2 \pm 2.8$  kPa and  $18.0 \pm 1.6$  kPa (Figure 3.9). GG3 showed the highest value of E, statistically different from GG/GEL ( $p < 0.05$ ) and GG/MH ( $p < 0.05$ ), that exhibited the lowest E value. Interestingly, no statistical difference was observed between GG2 and GG/MH.

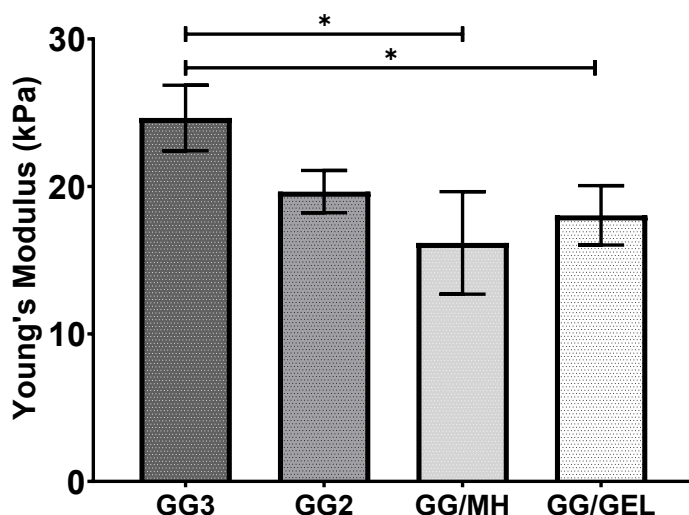


**Figure 3.9:** Compression Young's modulus (E) of the four hydrogels. E was calculated as the slope of the linear region of the stress-strain curves. Data are expressed as mean  $\pm$  standard deviation ( $n = 3$ ). Statistical significance is indicated as \* ( $p < 0.05$ ).

## 3.2 Bioprinting

### 3.2.1 Hydrogels printability evaluation

A visual qualitative assessment of the printability of each hydrogel formulation, without embedded cells, was performed. The selection of printing parameter range was based on previous GG-based hydrogel printing experiments performed by Annachiara Scalzone during her PhD work. In particular, for each experiment the substrate temperature was set between 28 and 35 °C, the temperature of the syringe was adjusted in a range of 34 – 38 °C and the printing speed was select between 2 – 5 mm/s. The travel speed value (x-y speed at which the bed moved) was set equal to the printing speed value (speed at which the hydrogel was extruded) to avoid over-deposition (printing speed > travel speed) or under-deposition of material (printing speed < travel speed). GG3 showed an enhanced viscosity with respect to GG2. In most of the trials when GG3 came into contact with the collecting plate, this underwent an instantaneous sol-gel transition. However his hydrogel was not always easily extruded, and sometimes a non-continuous strand deposition was observed. Concerning GG/GEL, it appeared to be the most viscous system, leading to unsuccessful printed structures. Also, GG/GEL was not homogeneously crosslinked. Moreover, during GG3 and GG/GEL printing, frequent nozzle clogging events were experienced. For the reasons stated above, these two hydrogels (GG3 and GG/GEL) were not selected as potential cell-laden bioinks and were not carried out in the further experiments.

As regards to GG2 and GG/MH, the second hydrogel appeared to be more viscous than the first. Both hydrogels were successfully printed: consistent filaments deposition, continuous and stable strands extrudability and the absence of filament deposition interruption were observed. The extruded filaments were homogeneously UV crosslinked and underwent a fast gelation when came in contact with the bed, allowing a precise positioning and retaining their shape. The table showed in Figure 3.10 (a) reports the optimized printing parameters used for the deposition of GG2 and GG/MH filaments. As a demonstration of GG2 and GG/MH ability to form multi-layered structures, 3D grid shaped structures of 3-4 layers (20 x 20 mm), with a 10% fill density were printed. Figure 3.10 (b) shows top view of a three-layered grid shaped GG2 construct. Even if DMEM was not added, the structure showed good shaped fidelity in respect with the GCode 3D model.

a) **Printing parameters**

Nozzle size (Gauge)	T syringe (°C)	T bed (°C)	Printing speed (mm/s)	Travel speed (mm/s)	Bottom speed (mm/s)	Layer height (mm)	Fill density (%)
25	36-38	30-34	5	5	5	0.15	10

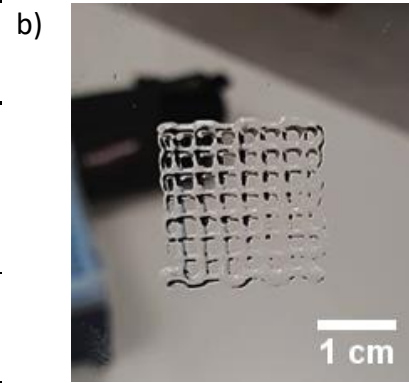


**Figure 3.10:** GGMA-based hydrogel printability assessment. (a) Experimentally optimised printing parameters used for GG2 and GG/MH deposition. (b) Digital photo showing the top view of a 3-layered GG2 printed grid-shaped construct, with a 10% fill density.

In order to fabricate cell laden constructs by using GG2 and GG/MH, the temperature of the bed was set between 30 and 34 °C, while the temperature of the syringe dispenser was set between 35°C and 38°C. The printing process was performed with a bioink composed by GG2 or GG/MH hydrogel with embedding Y201-C ( $7 \times 10^6$  cells/ml). On average, every time the bioprinting process was performed, 6 – 8 box shaped sample of 5 - 6 layers (approximately 150 - 200  $\mu$ l per sample) were fabricated. The duration of the printing process was approximately 5 - 6 minutes. After their deposition, samples were mechanically stable enough to be manipulated with a spatula, enabling their removal from the bed and positioning on the bottom of well of a 48 multi-well plate. No delamination was experienced during the manipulation of the samples.

### 3.2.2 Bioprinted construct: cells viability

Live/dead assay was performed after printing at different time points in order to qualitatively evaluate cell viability over a 72h culture period and to examine the effect of the printing process on Y201 chondrocytes. GG2 embedded live cells were stained in green, whilst dead cells were stained in red (Figure 3.11 a). Since it was observed that MH absorbed green light, live cells encapsulated in GG/MH hydrogel were stained in blue, while dead cells were stained in red (Figure 3.11 b). As regards to GG2, at three hours after printing most of embedded cells were viable, showed a round-like shape and tended to agglomerate. As can be clearly seen in Figure 3.11 (a), the number of living cells sharply increased over time and cells maintained their rounded morphology. Furthermore, after 72 hours of culture few dead cells were visible.

Concerning GG/MH, at 24 and 72 after printing cells showed a rounded morphology. Moreover, at each time point the vast majority of Y201-C were viable and only few dead cells were found (Figure 3.11 b). Overall, at 72 hours after printing, Y201-C viability was comparable between GG2 and GG/MH hydrogels.

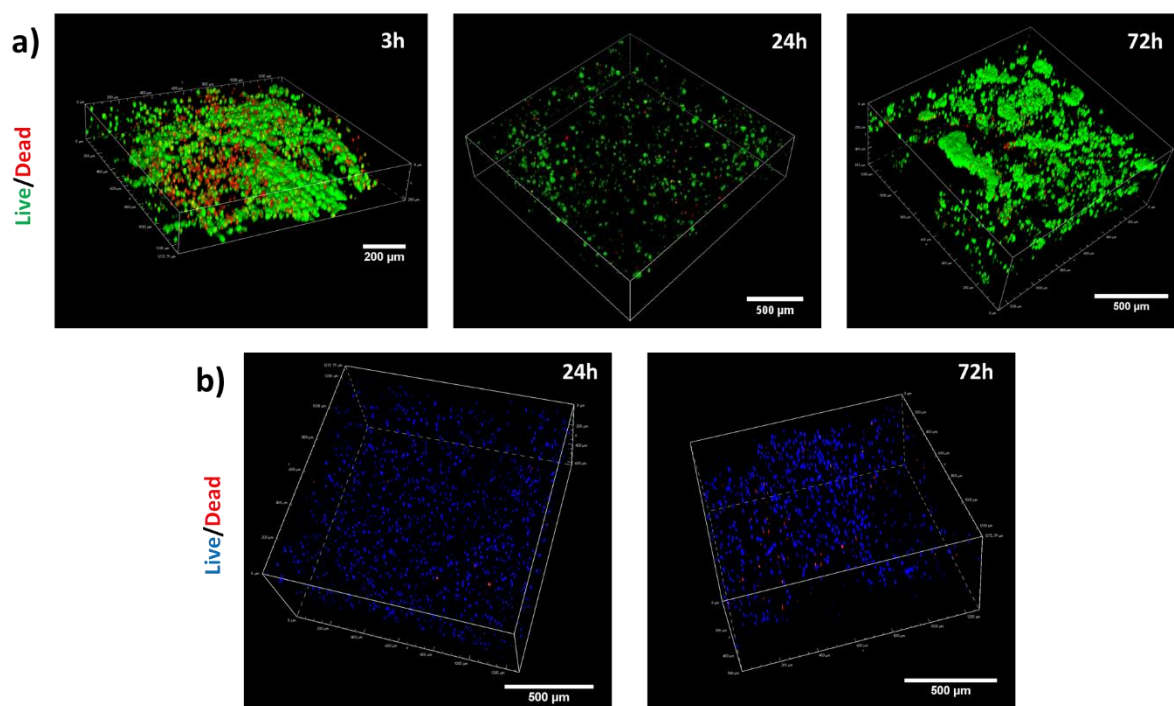


**Figure 3.11:** Live/Dead confocal microscopy volume rendering of printed Y201-Chondrocytes (10x Magnification, Z-stack of 15  $\mu\text{m}$ ). (a) Viability of cells embedded within GG2 hydrogel by bioprinting at 3, 24 and 72 hours after printing. Live cells were stained in green and dead cells in red. (b) Viability of cells embedded within GG/MH hydrogel by bioprinting at 24 and 72 hours after printing. Live cells were stained in blue and dead cells in red/purple.

### 3.2.3 Cell morphology and distribution in GGMA-based printed bioinks

Confocal microscopy was employed at day 7 after printing to qualitatively assess Y201-C morphology, distribution and cytoskeleton organization within GG2 and GG/MH bioinks. Both 2D immunostaining images and volume stacks were obtained (Figure 3.12). Cell nuclei were stained in blue (DAPI) and cytoskeleton f-actin was labelled in red (Rhodamine-phalloidin). GG2 and GG/MH hydrogels demonstrated a good Y201-C affinity, in terms of nuclei integrity. In both compositions, few isolated nuclei without a surrounding cytoskeleton, visualised as blue dots, were detected in both hydrogels. As regards to cell morphology and disposition, Y201-C embedded in both hydrogel compositions showed a round morphology with no sign

of spreading. Cells tended to aggregate in both bioprinted constructs. However, cells within GG/MH hydrogel formed bigger cluster when compared with Y201-C in GG2, where smaller cell clumps were observed. Finally, Y201-C exhibited a different disposition within the two hydrogel. Cells appeared to be distributed evenly throughout GG2 hydrogel, while they were not uniformly dispersed within GG/MH, may be due to GG/MH hydrogel non-homogeneity.

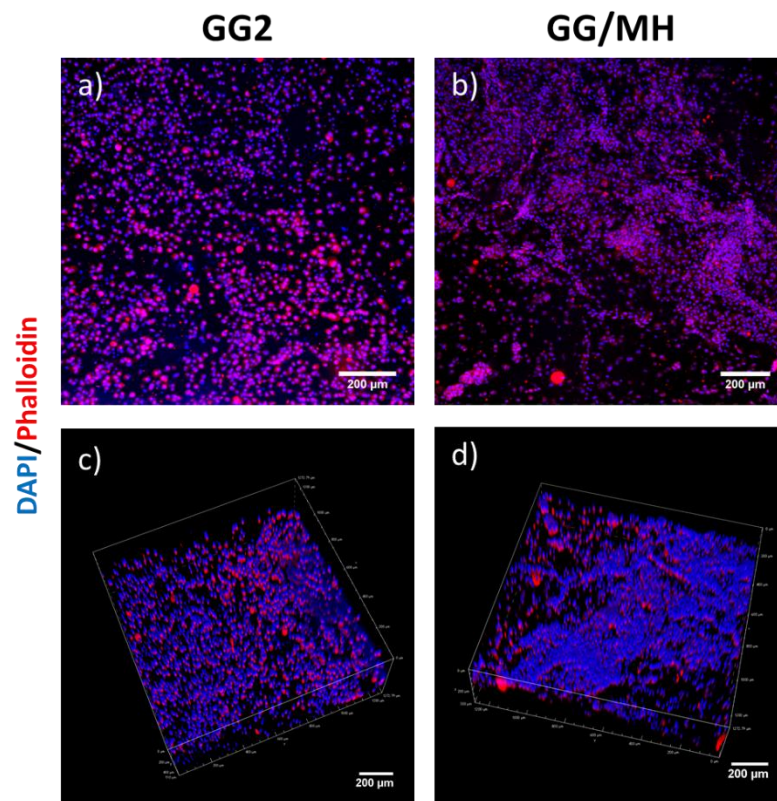


**Figure 3.12:** Immunostaining images and confocal microscopy 3D rendering of Y201-chondrocytes at day 7 after printing. Cell nuclei were stained in blue (DAPI) and f-actin is visualized in red (Rhodamine-phalloidin). (a-b) Immunostaining images of cells encapsulated in GG2 (a) and GG/MH (b) bioinks. (c-d) Volume stack of cells embedded in GG2 (c) and GG/MH (d) bioinks (10x Magnification, Z-stack of 15 µm). Scale bar = 200 µm.

### 3.2.4 GAGs quantification (AlcianBlue)

The GAGs content of the healthy and pathological *in vitro* bioprinted constructs was quantitatively determined at day 7 and 14 through GAGs quantification assay (AlcianBlue and guanidine hydrochloride). Figure 3.13 illustrates the absorbance, proportional to GAGs content, of the four investigated constructs. At day 7, GG/MH-H revealed the highest GAGs content. Moreover, the GAG's amount in GG/MH-based constructs was higher in the healthy model than the pathological one, while in GG2-based models showed an opposite trend. At day 14, GG/MH-P revealed the highest absorbance value, statistically different from GG/MH-

H ( $p < 0.0001$ ). Furthermore, in GG2-H GAGs content was higher than the one in GG2-P and GG/MH-H and statistically different ( $p < 0.01$ ,  $p < 0.5$ ). Overall, from day 7 to day 14 GG2-H and GG/MH-P showed respectively a sharply absorbance value increase of about 3- and 2-fold. In contrast, GG2-P GAGs content appeared to decrease from day 7 to day 14, whilst in GG/MH-H construct's GAGs production slightly increased over time.

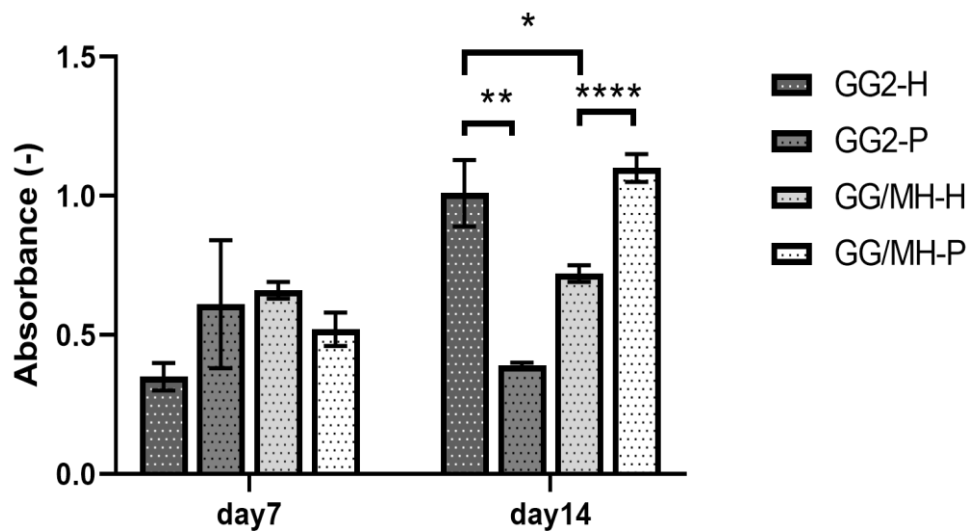


**Figure 3.13:** GAGs secretion quantitative analysis performed with guanidine hydrochloride (AlcianBlue, reading at 630 nm). The bar graph represents results obtained at day 7 and day 14 of GG2-H, GG2-P, GG/MH-H and GG/MH-P. Statistical significance is shown as \* ( $p < 0.05$ ), \*\* ( $p < 0.01$ ) and \*\*\*\* ( $p < 0.0001$ ).

### 3.2.5 Bioprinted constructs morphological analysis

SEM investigation was conducted to assess the morphological differences between healthy and pathological bioprinted GG2-based constructs. Figure 3.14 illustrates the hydrogel microstructure and cell organization of GG2-H (Figure 3.14 a, b) and GG2-P (Figure 3.14 c, d) at day 14 after printing. After two weeks of cell culture, both healthy and pathological GG2-based constructs did not retain the porous microstructure observed in section 3.1.4 in absence of Y201-C. At higher magnifications, the hydrogel surface of both constructs appeared to be irregular and showed the presence of ripples and bulges. As can be seen in Figure 3.14, several Y201-C were found within the two constructs after two weeks of culture. Both GG2-H and GG2-P were apparently populated by a comparable number of cells. Y201-C were completely entrapped within the hydrogel and maintained a spherical shape with a diameter  $>10 \mu\text{m}$ .

Furthermore, cells were not uniformly distributed throughout the hydrogel matrix and showed a tendency to form bunch-shaped clusters in both GG2-H and GG2-P models. Since Y201-C were covered by the hydrogel, the secreted ECM was not clearly discernible. However ECM protuberances, indicated by a white arrow, can be observed around a Y201-C within GG2-H (Figure 3.14 b). Finally, in GG2-P cluster of regular-shaped crystalline structures, with a size inferior to 5  $\mu\text{m}$  can be observed (Figure 3.14 d). The nature of these structures was not clear and needed further investigations.

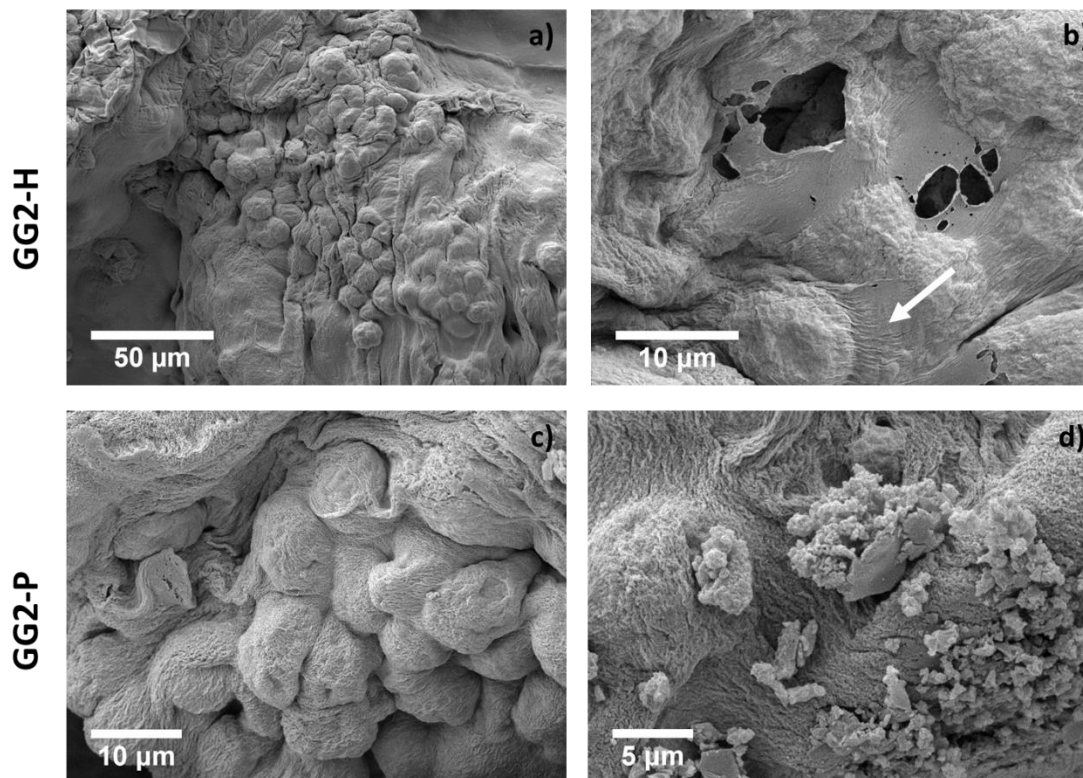


**Figure 3.14:** Scanning electron microscopy (SEM) images of bioprinted 3D constructs. (a, b) GG2-H construct after 14 days of culture in DMEM/F-12 medium. White arrow (b) indicated the presence of subtle threads around a Y201-C. (c, d) GG2-P construct after 14 days of culture in cytokine-based medium. Magnification were respectively: 1360x, 6710x, 5050x and 8730x.



## Chapter 4: Discussion

### 4.1 Hydrogel synthesis and characterisation

Hydrogels are the most used biomaterial to produce living 3D constructs via bioprinting. In general, natural hydrogels exhibit excellent biocompatibility and biodegradability (Spiller, Maher and Lowman, 2011; Levato *et al.*, 2014; Pantani and Turng, 2015; Yang *et al.*, 2017). GG is a biocompatible polysaccharide that possess interesting characteristics for biomedical applications, such as transparency and simple preparation, and that has gained attention in CTE because of its structural similarity to cartilage GAGs and chondrogenic potential. Moreover, GG hydrogels exhibit interesting features for 3D bioprinting, including good gelling ability and shear thinning behaviour (João T. Oliveira, Gardel, *et al.*, 2010; Cameron J Ferris *et al.*, 2013; Costa *et al.*, 2018; Wu *et al.*, 2018). One of the main drawback of GG hydrogels is represented by their limited mechanical properties, however this issue may be addressed through methacrylation. The presence of MA functional groups enables GG gelation mechanism via photo crosslinking, in addition to the characteristic thermo-reversible one, enabling the control over mechanical and physical characteristics of the hydrogel. For these reasons, GGMA has been employed for the production of load bearing engineered tissues such as cartilage (Coutinho *et al.*, 2010b; Bacelar *et al.*, 2016; Stevens *et al.*, 2016b).

In this work, the success of the reaction between GG powders and MA was demonstrated through FTIR-ATR and XPS analysis. In both GG and GGMA FTIR spectra peaks between 1300 - 1400  $\text{cm}^{-1}$  may be attributed to C-H bending. Compared to bare GG, GGMA showed variations in terms of chemical bond-related peaks: in particular, after the chemical modification two new peaks respectively at 1535  $\text{cm}^{-1}$  (attributed to assigned to C-C stretching) and at 1740  $\text{cm}^{-1}$ . Surprisingly, the unreacted C=C double bond peak at 1635  $\text{cm}^{-1}$ , related to the methacrylate side groups, was not clearly discernible in GGMA spectrum presumably due to its overlapping with the absorption peak at 1620  $\text{cm}^{-1}$  ( $\text{COO}^-$  stretch). However, the presence of an absorption peak at around 1740  $\text{cm}^{-1}$  in GGMA spectrum, corresponding to stretching of the C=O of the methacrylate side groups, whose absorbance value is directly proportional to the methacrylation degree (intended as the concentration of MA involved during GGMA synthesis), proved the success of GG derivatization (Coutinho *et al.*, 2010b; Silva-Correia *et al.*, 2011; Pacelli *et al.*, 2015; Xu *et al.*, 2018; Agibayeva *et al.*, 2020). From the XPS analysis, it was found that the main elements contained in both GG and GGMA sample were oxygen and

carbon, the primary elements present in GG polymeric chains (Figure 1.16), with a very small contribution of nitrogen (Table 8). The small amount of nitrogen (N1s) in both compositions may be attributed to small contamination that can be occurred during the synthesis or analysis of the material. For simplicity, the presence of elements between 0.3 and 1% was not reported. Also, the detected atomic percentages the evaluated samples were similar to those reported in literature. Moving towards to carbon high resolution spectrum it was noticeable the increase of the CHx bond percentage (C-H, ~285 eV) after methacrylation, that may be attributed to aliphatic carbon of MA. On the other side, the lower bond percentage of C-OR peak (~286.5 eV) in GGMA in respect to GG, may be associated to the loss of a C-OH specie during the formation of covalent bonds between the MA and OH groups in each repetitive unit of GG. Also, the COOR peak (~288.5 eV), typical of C=O species, had a higher bond percentage in GGMA in respect to GG. This can be associated to the presence of the C=O species in the side MA groups. All these results taken together re-confirmed the success of GGMA synthesis (Coutinho *et al.*, 2012; Bonifacio *et al.*, 2017; De Giglio *et al.*, 2018).

Four different GGMA-based photo-curable hydrogels were prepared: pure GGMA 2% w/v (GG2) and 3% w/v (GG3), and GGMA (respectively 2% w/v and 0.75% w/v) combined with 5% w/v MH (GG/MH) and 10% w/v gelatin (GG/GEL). As aforementioned, GGMA was chosen as a bioink to allow a double crosslinking, physical and photochemical, and also because its relatively little presence in literature. MH was introduced in order to exploit its viscosity and antibacterial activity, thus increasing GGMA-based hydrogels viscosity and E value and reducing the risk of contaminations (Maria A Bonifacio *et al.*, 2018; Bonifacio, Cochis, Cometa, Scalzone, *et al.*, 2020). Gelatin, a low-cost natural polymer largely exploited for biomedical applications, was used as a GGMA additive to improve its printability, mechanical properties and enhance cell adhesion and proliferation (Shin, Olsen and Khademhosseini, 2012; Axpe and Oyen, 2016; Gungor-Ozkerim *et al.*, 2018).

The gelation time of the four investigated hydrogels and the effect of the addition of MH or gelatin were qualitatively estimated through tube inverting test (Table 9) at RT, when chemically crosslinked via photo-curing or with the addition of a second physical ionic crosslinking. In the first condition, when exposed to UV irradiation, GG2 and GG/MH samples did not experience the sol-gel transition within 10 minutes, while GG3 and GG/GEL hydrogels displayed a gelation time of about 1 minute. As regards to pure GGMA hydrogel, the decrease of gelation time was negatively correlated with the polymer concentration. On the other hand,

the short gelation time of GG/GEL may be due to the combined effect of the physical crosslinking of gelatin due to the presence of genipin occurring at RT, and the photo-crosslinking of GGMA (Lien, Li and Huang, 2008). The addition of divalent ions (present in DMEM cell culture medium) was previously exploited as a methodology to physical crosslink GG-based hydrogel at temperatures lower than sol-gel transition temperature, which is around 36°C according to rheological analysis previously performed by Annachiara Scalzone during her PhD work (Lozano, Stevens, Brianna C Thompson, *et al.*, 2015). In presence of DMEM cell culture medium, manually added after 1 minute of UV irradiation in order to prevent the liquid to penetrate within the gel, GG3 and GG/GEL gelation behaviour remained the same, while GG2 and GG/MH gelation time sharply decreased to approximately 3 minutes. Interestingly, at the same GGMA concentration (2% w/v) the addition of 5% w/v MH to did not qualitatively change the gelation behaviour of the system with or without the presence of cell culture medium. These results were expected, since cell culture medium typically contains milli-molar concentration of divalent cations that promote GG physical crosslinking by generating “direct bridges” between polymer chains by binding pairs of carboxyl groups and thus induced a combination of physical and chemical crosslinking (double crosslinking) (Smith *et al.*, 2007; J. T. Oliveira, Martins, *et al.*, 2010a). It is important to note that it is challenging to exactly determine the gelation point of a hydrogel with the tube inverting test and various factors as the solution volume, the shape of the container and the solution pH may influence it (Morris, Nishinari and Rinaudo, 2012; Gering, 2015; Szymańska *et al.*, 2015).

Water uptake ability is a fundamental characteristic of hydrogels, crucial for assessing the application of these systems in TE field, and is connected to the nutrient absorption during *in vitro* culture (Gentile *et al.*, 2017; Kim *et al.*, 2019). Biomaterials showing high water uptake ability can closely resemble the hydrophilic nature of ECM. However, excessive swelling levels may result detrimental for hydrogels mechanical stability and, in the case of transplanted materials, may cause damages to the surrounding tissues. Generally, the water uptake ability of a hydrogel is affected by its 3D architecture and is inversely proportional to its crosslinking degree (Gentile *et al.*, 2016; Kosik-Kozioł *et al.*, 2017; Kouhi *et al.*, 2020; Pitarresi *et al.*, 2020; Scalzone *et al.*, 2020). The investigated hydrogels swelled very rapidly and exhibited a steep WU boost within 3 hours. A similar behaviour, was observed in MH - GG composite hydrogels by Bonifacio *et al.* (Maria A. Bonifacio *et al.*, 2018). It has been reported that the hydrogel swelling phenomenon occurs in aqueous solution in approximately 6 hours, and in this time

the crosslinking bond forces are balanced by the osmotic pressure of the solution (Gentile *et al.*, 2017). In our study, after 3 hours, GG2 (2%w/v GGMA), GG3 (3%w/v GGMA), and GG/GEL (0.75%w/v GGMA, 10% w/v gelatin) hydrogels showed a gradual WU% value rise to reach an equilibrium value after two days, while the WU% value of GG/MH (2%w/v GGMA, 5%w/v MH) remained nearly constant. We found that pure GGMA-based hydrogel (GG2 and GG3) showed a higher WU% as compared to GG/MH and GG/GEL. This may be partially attributed to a greater GGMA chains flexibility that is limited by the presence of MH and gelatin. This result may be influenced by higher material content of GG/MH sample and by the hydrophobic nature of MH. GG chains interact with MH via hydrogen bonds, diminishing the amount of free lateral carboxyl groups. More specifically, it has been reported that the reduced swelling behaviour of GG after the addition of MH may be caused by a lower number of available GG lateral carboxyl groups, that normally form hydrogen bond with water molecules (Mohd Azam and Amin, 2017; Sasikala, Rathinamoorthy and Dhurai, 2018). On the other side, the relatively low WU ability of GG/GEL may be due to the increase of hydrogel weight caused by the presence of gelatin and the additional gelatin crosslinking with genipin, that provides to the sample a higher crosslinking degree and superior stability in PBS. In a study, Lien *et al.* reported that 10% w/v gelatin hydrogel crosslinked with genipin reached, at equilibrium, a WU% value of approximately 500% (Lien, Li and Huang, 2008). In this work we observed that GG/GEL reached, after 48 hours, a WU% value of nearly 700%. Therefore it is plausible that the WU behaviour of GG/GEL was predominantly influenced by gelatin. Interestingly, GG2 WU trend in PBS (pH = 7.4) appeared to be similar to the one of a ionic crosslinked GGMA hydrogel at the same concentration (2% w/v) (Silva-Correia *et al.*, 2013). GG2 had the highest swelling ability, reaching an equilibrium WU value of approximately 1950% and this is not surprising considering that the swelling ability of a hydrogel is inversely proportional to polymer concentration, as higher presence of material reduces the void space of the system (Beck *et al.*, 2016a). This result can be also attributed to a larger amount of hydrophobic MA side groups of GG3 in respect to GG2 and is consistent with the findings reported by Xu *et al.*, that demonstrated that higher degree of methacrylation resulted in reduced swelling response (Coutinho *et al.*, 2010b; Xu *et al.*, 2018). Overall, the WU analysis demonstrated that the investigated hydrogels had a strong hydrophilic nature resembling the one of ECM, with the capacity to retain large amount of PBS, while maintaining their stability in aqueous environment for 48 hours.

Then, the internal morphology of freeze-dried GGMA-based hydrogels was investigated after WU in order to simulate the hydrated condition of the human body. Native AC possess a gradient porous microarchitecture that promotes specific cell behaviours such as proliferation, matrix production and migration (Raghunath *et al.*, 2007; Caddeo, Boffito and Sartori, 2017). Both pore size and pore interconnectivity play an important role, providing a large surface area for cell adhesion, supporting effective cell waste removal and nutrients diffusion and influencing the tissue regeneration effectiveness (Raghunath *et al.*, 2007; Zhang *et al.*, 2014). As can be clearly seen in Figure 3.5, all freeze dried GGMA-based hydrogels obtained in this works showed a porous microarchitecture with interconnected cavities resembling an interconnecting “open-cell” architecture. As regards to GG3 and GG2, the two hydrogels showed a similar internal morphology (Figure 3.5 a and b). The increased GGMA concentration lead to a mean pore diameter increment (Figure 3.7) and to a different pore size distribution. Surprisingly, when compared to GG2, GG3 exhibited a higher percentage of pores with a diameter higher than 150  $\mu\text{m}$  and a lower proportion of pores smaller than 150  $\mu\text{m}$ . Visually, when comparing GG2 (Figure 3.5 b) and GG/MH (Figure 3.5 c), the addition of MH in the hydrogel composition did not significantly change the internal microarchitecture of the samples. No statistical difference in mean pore size and pore diameter distribution interval (50-250  $\mu\text{m}$ ) between GG2 and GG/MH was observed (Figure 3.7). On the other hand, when compared to GG2, the MH introduction reduced the number of pores size < 150  $\mu\text{m}$  and increased the percentage of those with a diameter between 150 – 200  $\mu\text{m}$  (Figure 3.6). As can be observed in Figure 3.5 d, the presence of gelatin remarkably affected the hydrogel microstructure. Pore morphology appeared to be more regular when compared to the other three compositions. The internal pore shape and architecture were visually similar to the one of pure gelatin freeze-dried sample observed in other works present in literature (Van Vlierberghe *et al.*, 2007; Lien, Li and Huang, 2008). This can be explained by the GG/GEL higher gelatin concentration (10% w/v) than GGMA one (0.75% w/v). Also, GG/GEL had the highest mean pore size, statistically different from the other three values (Figure 3.17) and this is consistent with findings reported in another work in which, the addition of 2mg/ml of collagen (from which gelatin is derived) to GGMA led to a noticeable increase of the hydrogel pore size (Chen *et al.*, 2018). Furthermore, when compared to the other formulations, GG/GEL showed the largest pore diameter distribution, ranging from 50 to 400  $\mu\text{m}$ , and approximately 70% of the pores had a diameter exceeding 150  $\mu\text{m}$ . The pore size distribution of the

investigated hydrogels, ranging from 50 to 400  $\mu\text{m}$ , proved that they possessed an hierarchical porosity, mimicking the one of native AC (Harley *et al.*, 2006; Gerhardt and Boccaccini, 2010). It has been stated that the presence of a gradient porosity enhances cell mobility during regenerative processes and is essential for AC defects treatment in CTE. Also chondrocytes showed preferential proliferation when cultured in construct with pore size between 200  $\mu\text{m}$  and 500  $\mu\text{m}$ . In another study, Xia *et al.* reported that a chitosan – gelatin scaffold showing a pore size ranging from 60 to 200  $\mu\text{m}$  was suitable for CTE applications (van Tienen *et al.*, 2002; Xia *et al.*, 2004; M. Iliescu, C.D. Hoemann, M.S. Shive, A.Chenite, 2008; Lien, Ko and Huang, 2009; Loh and Choong, 2013). Overall, in light of the aforementioned information, we can say that the investigated hydrogels showed an interconnected porous morphology with a mean pore size in the range 100-200  $\mu\text{m}$  suitable for both cells migration and nutrient transport in AC regeneration. It is fundamental to highlight that we did not perform an evaluation of the porosity degree, a key parameter that affects mechanical properties and swelling behaviour of hydrogels (Nandagiri *et al.*, 2011).

Finally, mechanical properties of the four systems were evaluated via unconfined compression test. It is well known and recommended that the mechanical properties of the designed TE construct should ideally mimic the one of the target tissue (Murphy and Atala, 2014b; Gering *et al.*, 2019). Mechanical properties are fundamental features in preserving the structural stability of the construct. In general, high porosity degree result in reduced mechanical properties, and the water uptake ability of a hydrogel is negatively correlated with its compression modulus. Also, it is widely known that natural hydrogel possess low mechanical properties, showing a E value less than 100 kPa (Kelly *et al.*, 2013; Gantar *et al.*, 2014; Xu *et al.*, 2018; Scalzone *et al.*, 2020). The stress strain curves of the four hydrogels (Figure 3.8) showed that hydrogels did not underwent breakage when a 35% strain was reached, except for GG2 that broke at around 27% of strain. This may denote a good load bearing capacity of the investigated gels (Bonifacio, Cochis, Cometa, Gentile, *et al.*, 2020). GG3 showed the highest value of E ( $24.6 \pm 1.8$  kPa), statistically different from GG/GEL ( $p < 0.05$ ;  $18.0 \pm 1.6$  kPa) and GG/MH ( $p < 0.05$ ;  $16.2 \pm 2.8$  kPa), that exhibited the lowest E value (Figure 3.9), while GG2 E value was  $19.7 \pm 1.2$  kPa. Several authors reported that the compressive modulus of engineered constructs often appeared to rise as the mean pore size declined. Considering pure GGMA hydrogels, even if GG3 mean pore size was lower than GG2's one, GG3 compressive modulus was higher than the one of GG2. This was reflected also in a lower GG3 WU ability. It

is known that higher polymer concentrations often results in superior mechanical properties (Ciardelli *et al.*, 2010; Krogstad *et al.*, 2013). Human AC has an E value ranging from 240 kPa to 1 MPa, while typically natural hydrogels exhibited an E value of at least a order of size less than the native tissue. Overall, the investigated hydrogels exhibited an E mean value between approximately 16 and 25 kPa comparable to other natural hydrogels for soft tissue and/or cartilage regeneration (Zhao *et al.*, 2013b; Beck *et al.*, 2016a; Scalzone *et al.*, 2020). Our finding agreed with other GG based hydrogels E value indicated in scientific literature, according to the used crosslinking method, ranged from approximately 150 Pa to 148 kPa. It has been hypothesized that the increased E value found in gels with higher GGMA concentration may be due to the formation of larger amount of chain entanglements and to the presence higher number of aggregated helix structures (Coutinho *et al.*, 2010a; da Silva *et al.*, 2014; Pereira *et al.*, 2018). It is noticeable that, at the same GGMA concentration, the incorporation of MH did not lead to an increase of E (Figure 3.9). This result is in contrast with the finding of Bonifacio *et al.* who observed that the incorporation of MH (2%w/v) lead to a rise of the compressive modulus of a GG-based hydrogel (2%w/v GG) (Maria A Bonifacio *et al.*, 2018). As stated in section 1.5.2, gelatin may be used as an additive to hydrogels to enhance their printability and mechanical properties. More specifically, the increased mechanical properties may be partially attributed to ionic interactions between the GG lateral carboxyl group and the side amino group of gelatin (Barbani *et al.*, 2012; Axpe and Oyen, 2016). However, we found that GG/GEL showed a lower E mean value than GG2. Maybe, the larger mean pore diameter of GG/GEL contributed to this result. Interestingly, we observed that GGMA concentration influenced E more than the introduction of gelatin and MH.

## 4.2 Bioprinting

Bioprinting is an additive manufacturing technology that allows to recapitulate the microstructure of different tissues by a controlled, accurate and simultaneous deposition by a controlled deposition of bioinks (Mandrycky *et al.*, 2016). Typically, a time-consuming phase of the development process of a novel bioink is the optimization of the hydrogel composition and printing parameters. The selected bioink formulation should possess a viscosity suitable for the extrusion through the available bioprinter, which in the case of this work is Rokit INVIVO (Paxton *et al.*, 2017b). For these reasons, we performed a printability test on the four

different GGMA-based hydrogel. As largely described in literature, increasing polymer concentration or adding supporting material lead to the formation of denser and more viscous bioinks (Axpe and Oyen, 2016; Rencsok *et al.*, 2017). In this perspective, MH and gelatin were added respectively to GGMA (GG/MH and GG/GEL) in order to increase the bioink viscosity and enhance the hydrogel printability. Visual qualitative assessment of the shape fidelity may be considered a relatively quick way to discern results obtained by printing bioink composed of different concentration of a hydrogel composition (Ribeiro *et al.*, 2018). Thus, a visual qualitative assessment of the printability of each bioink formulation, without embedded cells, was performed. As mentioned in section 2.5.1, particular attention was paid to various factors, including continuous and stable strands extrudability, the absence of filament deposition interruption, the presence of nozzle clogging events, gelation kinetic and crosslinking uniformity. Several attempts were carried out in order to achieve a satisfactory printability; however the printing parameters optimization phase was speeded up thanks to previous GG-based hydrogel printing experimental results obtained by Annachiara Scalzone during her PhD work. The investigated a-cellular hydrogels were printed by using a 25-gauge nozzle, and printing parameters were set in the ranges summarized in the table reported in Figure 3.10 a. It has been reported that the post-printing UV curing may reduce constructs size since the light may not penetrate homogeneously the printed structure (Levato *et al.*, 2014). In the present work, this issue was avoided by inducing chemical crosslinking during the filament extrusion through UV exposure via UV lamp provided in the Rokit INVIVO printer. As for the not printed hydrogels. The obtained bioprinted structures were subjected to a dual crosslinking method: physical (obtained via the manual addition of cell culture medium) and chemical (photo-crosslinking). GG3 formulation was considered too viscous. Even if in most of the trials GG3 underwent an instantaneous gelation when deposited on the collecting plate, this gel was not always easily extruded, and sometimes a non-continuous strand deposition was observed. GG/GEL formulation appeared to be the most viscous one, leading to unsuccessful printing due to frequent nozzle clogging events, and because at the selected dispenser temperature range, it became too firm hindering the eventual filament deposition. In particular, GG/GEL appeared to be non-uniformly crosslinked. This may be due to gelatin-gelatin physical crosslinking, that occurred at different degree partially depending on the local temperature of the solution within the syringe. For the reasons stated above, GG3 and GG/GEL were not selected as cell-laden bioinks. As regards to GG2 and GG/MH, the second hydrogel

appeared to be more viscous than the first. Both hydrogels were successfully printed. The extruded filaments were homogeneously UV crosslinked and underwent a fast gelation when came in contact with the bed. Both GG2 and GG/MH printed gels exhibited a transparent aspect, typical of GG, with the difference that the addition of MH made the second hydrogel more yellowish (Cameron J. Ferris *et al.*, 2013). As a demonstration of GG2 and GG/MH printability 3D gridded structures were printed. As clearly seen in Figure 3.10 b, even if DMEM was not added, the printed GG2 construct good shaped fidelity in respect with the GCode 3D model. The fidelity in the central part of the grid was superior than at the edges. The lower accuracy in these zones may be related to hydrogel accumulation were the filaments changed their angle (Sodupe-Ortega *et al.*, 2018).

After the success of Y201 MSCs differentiation into Y201-C, these were chosen as cell source because of their ease of in vitro expansion, availability and ability to avoid senescence (Bischoff, Makhijani and Yamaguchi, 2012; Mouser *et al.*, 2020). Y201-C were therefore encapsulated within GG2 and GG/MH hydrogels to fabricate bioprinted constructs. As mentioned in section 1.4, one of the main advantage 3D printing is the possibility to create construct with high cell concentration: cells are typically embedded in bioinks at a concentration in the order of  $1 \times 10^7$  cells/ml (Pantani and Turng, 2015; Moroni, Burdick, *et al.*, 2018). In this work, Y201-C were embedded at a concentration of  $7 \times 10^6$  cells/ml in order to recapitulate the chondrocyte concentration in the middle layer (Hunziker, Quinn and Häuselmann, 2002). As regards to printing parameters, the bed temperature was set between 30 and 34 °C, while the dispenser temperature was set between 35°C and 38°C, in order to allow the sol-gel transition and also to preserve cell viability. Purging the needle before bioprinting may increase the spatial homogeneity of cell density during the bioink deposition and may reduce cell sedimentation. Also, It is well known that increased residence times of cell within the needle tip may decrease cell viability (Paxton *et al.*, 2017a; Dudman *et al.*, 2020). On average, every time the bioprinting process was performed, 6 – 8 cell-laden constructs were fabricated, and the duration of the printing process may be considered relatively short (~ 5 minutes). Also, during the printing process, cell culture medium was added after the deposition of each layer not only to allow physical crosslinking but also to prevent drying effects of the bioinks and to increase the survival rate of the bioprinted cells. Finally, bioprinted GG2 and GG/MH were stable enough to be manipulated without experiencing delamination, to enable their deposition in a 48 multi-well plate for cell culture.

Live/dead assay was performed after printing at different time points with the aim to qualitatively evaluate cell viability, to assess the cytocompatibility of the bio-printed hydrogels, over a 72h culture period. In order to assess the direct effect of the cells encapsulation process, crosslinking mechanism and printing processes on Y201-C viability, the test was also conducted three hours after the construct fabrication. Live - dead volume rendering images were acquired with a Z-stack of 15  $\mu\text{m}$ , in order to set a planar height value close to the mean diameter of AC chondrocytes (Hunziker, Quinn and Häuselmann, 2002). As can be clearly seen in Figure 3.11 a, most of GG2 embedded Y201-C survived the printing process. Few dead cells were found, possibly for cell damages occurring during the cell mixing with the hydrogel and to the harmful effect of the shear forces on cells generated within the nozzle during the bioink extrusion. Apparently, UV exposure had a limited effect on Y201-C viability and this results corroborates with results reported by Coutinho *et al.* (Coutinho *et al.*, 2010b; Kesti *et al.*, 2015; Paxton *et al.*, 2017b). Moreover, MA lateral groups may have partially contributed to protect cells during the photo-crosslinking process: indeed, it was reported that, under UV light exposure, lateral MA groups showed a cytoprotective effect on chondrocyte when GGMA was used as photo cross-linkable hydrogel systems (Bartnikowski *et al.*, 2015). The number of GG2 embedded living Y201-C increased over time and cells, and after 72 hours of culture few dead cells were visible. Hydrogels composed by GG and MH have been previously demonstrated to be cytocompatible, and so GGMA-based hydrogels (Silva-Correia *et al.*, 2013; Maria A. Bonifacio *et al.*, 2018; Bonifacio, Cochis, Cometa, Gentile, *et al.*, 2020; Bonifacio, Cochis, Cometa, Scalzone, *et al.*, 2020). Concerning GG/MH, at 24 and 72 after printing the vast majority of Y201-C were viable and only few dead cells were found (Figure 3.11 b). This result may suggest that the addition of MH did not hinder cell viability. Moreover, at 72 hours after printing, Y201-C viability was comparable between GG2 and GG/MH hydrogels. Overall, the high cell viability of cells after 24 and 72 hours may indicate that GG2 and GG/MH hydrogels provided a hydrated artificial 3D environment, resemble soft tissue ECM, enabling an efficient nutrient, gas and waste transport and thus cell culture.

After Y201-C viability evaluation, confocal microscopy was used at day 7 after printing to qualitatively characterise Y201-C distribution and morphology in bioprinted constructs (Figure 3.12). GG2 and GG/MH hydrogels demonstrated a good Y201-C affinity, in terms of nuclei integrity. In both compositions, few isolated nuclei without a surrounding cytoskeleton, visualised as blue dots, were detected in both hydrogels. This may be associated with the

presence of a small number of dead cells and corroborates with the live/dead results at day 3 (Figure 3.11) (Müller *et al.*, 2017). Y201-C embedded in both hydrogel compositions showed a round morphology, similar to the one observed within AC middle layer. In other works, different cell type showed a similar round morphology when encapsulated in GG – or GGMA – based hydrogels (da Silva *et al.*, 2014; Camarero-Espinosa *et al.*, 2016; Oliveira *et al.*, 2016; Pereira *et al.*, 2018). Cells tended to aggregate in both bioprinted constructs during the culture time. However, cells within GG/MH hydrogel formed bigger cluster when compared with Y201-C in GG2 and were not uniformly dispersed, this may be due to GG/MH hydrogel non-homogeneity. Y201-C aggregation may be considered a remarkable finding and may be caused by the interconnected microstructure of GG2 and GG/MH (Figure 3.5 b and d) that provide a suitable environment for cell migration and interaction.

The final part of the thesis dealt with the manufacturing of *in vitro* OA model for future analysis on novel OA therapeutic treatments. Only few preliminary test, in which the respective healthy models were used as reference, were performed on these constructs: indeed this part of the work was intended as an initial stage of a more exhaustive work that will be carried on in the future. Cytokine-based OA *in vitro* models for OA research are very common and generally properly understood. IL-1 $\beta$  and TNF- $\alpha$  are the most used cytokines in OA *in vitro* models while IL-6 is more rarely used. In this work, cytokine-based OA *in vitro* models were obtained by culturing the bioprinted 3D cell-laden constructs in the presence of a cytokine cocktail, obtained by adding IL-6, IL-1 $\beta$  and TNF- $\alpha$ , respectively at a concentration of 10, 1 and 1 ng/ml, to DMEM/F-12 cell culture medium. The cytokine concentration ratio 10:1:1 was chosen considering the levels of IL-6, IL-1 $\beta$  and TNF- $\alpha$  in advanced OA synovial fluid, in which IL-1 and TNF concentration are respectively inferior to 2 ng/ml and 3 ng/ml. It must be noted that our chosen cytokine concentrations were lower than the ones usually used for OA *in vitro* studies, where IL-1 $\beta$  and TNF- $\alpha$  concentrations may rise up to 100 ng/ml and 50 ng/ml in order to shorten the time needed for OA evolution (Macrory *et al.*, 2009; Gabriel *et al.*, 2010; Sohn *et al.*, 2012; Johnson, Argyle and Clements, 2016; Weber *et al.*, 2019).

An analysis of GAGs synthesis (Figure 3.13) was performed in order to assess Y201-C ability to produce hyaline-like ECM in healthy and pathological bioprinted constructs. Other test, including an analysis on Coll II production (see appendix) and immunohistochemistry are in progress. However, it is important to note that the investigation of healthy and pathological *in vitro* models does not represent a fundamental part of this work. As described in section

1.1.2, since they are components of PGs, GAGs are considered key elements of AC matrix and their content may be used to relatively quantify the aggrecan concentration in ECM. During OA development AC may be subjected to microscopically changes targeting ECM composition. It has been observed in OA conditions aggrecan and other PGs concentration decrease. Matrix degrading enzymes, such as aggrecan degrading enzymes ADAMTS 4 and 5 and collagenases MMP1 and MMP13, are also overexpressed (Bhosale and Richardson, 2008a; Glyn-Jones *et al.*, 2015). Also, PGs degradation may lead to GAGs release, and GAGs concentration in the synovial fluid may be used to monitor OA progression (ALWAN *et al.*, 1991; Squires *et al.*, 2003). In this work, as regards to healthy models, GAG production appeared to increase with culture time: from day 7 to day 14, GG/MH-H construct's GAGs content slightly rose, whilst GG2-H showed a sharply GAGs content increment of about 3-fold. This result may prove that PGs were synthesized by Y201-C in both GG2 and GG/MH constructs during 14 days of culture. In the same time window, considering OA models, GG/MH-P embedded cells GAGs production increased of about 2- fold, while GG2-P GAGs content appeared to decrease. At day 7, GG/MH-H revealed the highest GAGs content, higher than the one of GG/MH pathological model. Moreover, at day 14, in GG2-H GAGs content was higher than in GG2-P. These results are in line with the decreased ECM GAGs presence in OA condition. In contrast, at day 7 the GAG content was higher in the GG2 pathological model than in the healthy one, and at day 14 GG/MH-P GAGs content was higher than the one of GG/MH-H. Of course these conflicting results will need further investigations. Overall, these finding may suggest that Y201-C embedded in GGMA-based constructs were able to produce a cartilage-like ECM after being printed during a 14 day-culture period. Also, as aforementioned, OA may lead to GAGs release in the synovial fluid. In the future, further test to quantify GAGs released in the cell culture medium will be carried out.

Finally, SEM analysis were carried out to characterise Y201-C morphology and organization within GG2-H and GG2-P bioprinted constructs after two weeks of *in vitro* culture (Figure 3.14). In the future, SEM analysis will be carried out also on GG2 (day 1) and GG/MH (day 1 and 14) healthy and pathological models to evaluate morphological and organizational differences of these constructs over time. Both GG2-H and GG2-P constructs did not retain the internal porosity (Figure 3.14), and this morphological modification may be an undesired effect caused by the dehydration process of the samples (Fergg, Keil and Quader, 2001; Autissier *et al.*, 2010). After two weeks of cell culture, both GG2-H and GG2-P were apparently

populated by a comparable amount of rounded Y201-C entrapped within the GGMA-based hydrogels and showed a spherical morphology with a diameter  $>10\ \mu\text{m}$ , a value similar to the one of human chondrocytes. This may be considered a good results, since it has been demonstrated that preserving cell roundness during culture is a key characteristics for regulating chondrocytes gene expression and the production of Coll II (Hunziker, Quinn and Häuselmann, 2002; Kosik-Kozioł *et al.*, 2017). Y201-C showed a tendency to form bunch-shaped clusters in both healthy and pathological GG2-based constructs. This last finding reinforces the assumption that GG2-based bioinks provide a suitable environment for cell migration and interaction. A similar result was reported by Oliveira *et al.* who observed that chondrocytes embedded in GG-based hydrogels formed clusters after 14 days of *in vitro* culture. They also stated that these aggregations may be beneficial for the synthesis of a hyaline-like ECM (J. T. Oliveira, Martins, *et al.*, 2010b). Also, it has been reported in scientific literature that chondrocyte proliferation and aggregation in the so called “chondrocyte clusters” can be described as OA-related events. However, in GG2-P no distinctive hypertrophic cells with larger diameter were observed, thus these speculations need further investigations (der Mark *et al.*, 1992; Pullig *et al.*, 2000). Since in both constructs Y201-C were totally covered by the hydrogel, the secreted ECM was not clearly discernible. However ECM threads were distinguished around a Y201-C within GG2-H (Figure 3.14 b, white arrow), and this may be associated to cell production of ECM (Pitarresi *et al.*, 2020). Finally, in GG2-P cluster of regular-shaped crystalline structures, with a size inferior to  $5\ \mu\text{m}$  were detected (Figure 3.14 d). Maybe their appearance was caused by contaminations occurred during the dehydration process. However, the nature of these structures is not clear and need further investigations. Overall, these results were in line with immunostaining findings, confirming that GG2 and GG/MH hydrogels preserved cells viability up to 14 days of culture and promoted Y201-C aggregation. These constructs supported the maintaining of a chondrogenic rounded cell phenotype and appeared to promote Y201-C ECM synthesis. These findings may reinforce the assumption that these hydrogels provide an appropriate 3D environment to cells for CTE applications.



## Chapter 5: Conclusion and future directions

In this work, GGMA-based bioprinted constructs representative of AC has been investigated. The success of the GGMA synthesis, obtained through methacrylation of GG powders, was demonstrated via FTIR-ATR and XPS analysis. Four different photo-curable hydrogels were prepared: pure GGMA 2% w/v (GG2) and 3% w/v (GG3), and GGMA (respectively 2% w/v and 0.75% w/v) combined with 5% w/v manuka honey (GG/MH) and 10% w/v gelatin (GG/GEL). MH was introduced in order to enhance GGMA printability, mechanical properties and to reduce contaminations risks, while gelatin was used as additive to improve GGMA printability, mechanical properties and enhance cell adhesion and proliferation. Gelation analysis at RT were performed under photochemical and double (photochemical and ionic) crosslinking. Under double crosslinking, GG3 and GG/GEL gelation time remained unchanged when compared to the one under photochemical crosslinking (~3 minute), while GG2 and GG/MH gelation time decreased to ~3 minute. These results demonstrated the short gelation time of hydrogels useful for bioprinting applications. WU analysis demonstrated that the four hydrogels had a high hydrophilic behaviour resembling the one of AC ECM, with the ability to retain large amount of PBS for 48 hours. The investigated hydrogels had an interconnected porous morphology with a mean pore size in the range 100-200  $\mu\text{m}$  suitable for both cells migration and nutrient transport in AC regeneration. Also, they had a pore size distribution ranging from 50 to 400  $\mu\text{m}$  resembling AC hierarchical porosity. The addition of gelatin made pore morphology to appear more regular when compared to the other formulations. The four hydrogels exhibited an E mean value comparable to other natural hydrogels for soft tissue and/or cartilage regeneration. GG3 showed the highest E value ( $24.6 \pm 1.8$  kPa), followed by GG2 ( $19.7 \pm 1.2$  kPa), GG/GEL ( $18.0 \pm 1.6$  kPa) and GG/MH ( $16.2 \pm 2.8$  kPa). At the same GGMA concentration, the incorporation of MH did not lead to an increase of E. GG2- and GG/MH-double-crosslinked bioinks were successfully bioprinted with a Y201-C concentration of  $7 \times 10^6$  cells/ml in order to mimic the chondrocyte concentration in AC middle layer. Live and dead analysis demonstrated the high cell viability, suggesting that the printing process was relatively not harmful to cells and that these hydrogels provided a 3D environment resembling soft tissue ECM ensuring cell survival. Also, DAPI/Phalloidin showed that cells tended to aggregate in both bioprinted hydrogels. The final stage of the thesis dealt with the manufacturing of OA in vitro models, via culturing healthy models in cytokine-enriched culture medium, for future analysis on novel OA therapeutic treatments. The GAGs quantification

assay showed that Y201-C GAGs production increased over time in healthy and pathological constructs, that may be associate to the production of a cartilage-like ECM; also after 14 days of culture in GG2-P GAGs content was lower than in GG2-H, a situation comparable to OA condition. Finally, SEM analysis confirmed that cells tended to agglomerate in GG2 bioprinted constructs, suggesting that these hydrogels may provide a suitable environment for cell migration and interaction, and also that Y201-C had a spherical morphology, typical of AC middle layer chondrocytes.

It is important to note that this work possess some aspects to be studied in depth and that further tests will be performed in the future. Regarding the physico-chemical characterisation, an evaluation of the investigated hydrogels porosity degree would provide a better understanding of porosity influence on mechanical properties and swelling behaviour of the gels. For what concerns mechanical properties, rheological characterisation tests, such as Temperature Sweep and Time Sweep tests may be carried on to exactly assess the sol-gel transition temperature and time of GGMA-based hydrogels. From the biological point of view, analysis on metabolic activity (Cell Titer®) and ATP production (Presto Blue®) should be performed to better evaluate the Y201-C behaviour after bioprinting. Concerning the characterisation of healthy and pathological in vitro models, SEM morphological analysis will be performed on all the investigated constructs; also histological analysis (Sirius Red® and Alcian Blue® assays) should be performed to further evaluate Y201-C deposition of collagen and GAGs, while Dimethylmethylene Blue Assay should be carried on to quantify GAGs released in the cell culture medium. Moreover, the difference in terms of viscoelastic properties between healthy and pathological in vitro models should be performed via stress-relaxation tests.

Finally, we demonstrated GG2 and GG/MH bioprinted constructs may be used to bio-mimic the middle zone of the AC tissue. In the future, the investigated constructs will be inserted as a part of a complete AC zonal in vitro model, designed and manufactured by Annachiara Scalzone in her PhD work, resembling the superficial, the middle and the deep zone of the tissue



## Appendix: Immunofluorescence analysis

IF staining was used to assess the deposition of Coll II within the bioprinted healthy and pathological in vitro models. After removing cell culture medium/cytokine cocktail, cell-laden constructs were rinsed twice with pre-warmed Hanks' Balanced Salt Solution (HBSS) without phenol red (Thermo Fisher Scientific, UK) and fixed in pre-warmed 4% w/v PFA solution in PBS for 30 minutes at 4°C. Bioprinted constructs were washed twice with HBSS and subsequently blocked with 2% w/v bovine serum albumin (BSA; Thermo Fisher Scientific, UK) in PBS for 1h at RT to diminish non-specific binding. Constructs were rinsed twice in PBS-Tween and treated with 800 µl of anti-collagen II primary antibody (Abcam, UK) solution 1:200 in PBS-Tween overnight at 4°C. Then, hydrogels were washed twice in PBS-Tween and incubate covered from light in 800 µl of secondary antibody AlexaFluor 594-coniugated goat antirabbit IgG (Thermo Fisher Scientific, UK) solution 1:1000 in PBS-Tween for 1 hour at 4°C. Thereafter, constructs were washed twice with PBS-Tween and incubated protected from light in a 1:2500 DAPI (Vector Laboratories) solution in PBS-Tween for 20 minutes at 4°C. Thereafter, hydrogels were rinsed twice again with PBS-Tween and images were acquired using a Nikon A1R inverted confocal microscope as detailed in section 2.5.4. Analysis were performed at day 7 and day 14 for GG2-P and GG/MH-P constructs and at day 14 for GG/MH-H.

Figure A illustrates the volumetric stack of 3D constructs, demonstrating the presence of Coll II in al the investigated species. As regards to GG-MH constructs, the secreted collagen was found mainly in the pericellular region surrounding Y201-C (Figure A a, b, c). Cell aggregation, visualized as clustered nuclei, could be observed in GG/MH-P at day 14 (Figure A c). This last finding is consistent with the results at day 7 of immunostaining test (Figure A d). The red spots found in GG/MH-P at day 14 may be attributed to residues of MH not uniformly dispersed within the hydrogel. From day 7 to day 14, a slight decrease in collagen staining was observed in GG/MH-P models (Figure A a, c). Some red isolated dots were visualized within GG/MH-P at day 7 (Figure A a). Coll II content appeared to be comparable within GG/MH-H and GG/MH-P at day 14 (Figure A b, c). Concerning GG2-P model at day 14 (Figure A d), the presence of Coll II was minimal and reduced in respect with GG/MH-P at the same time point (Figure A c).

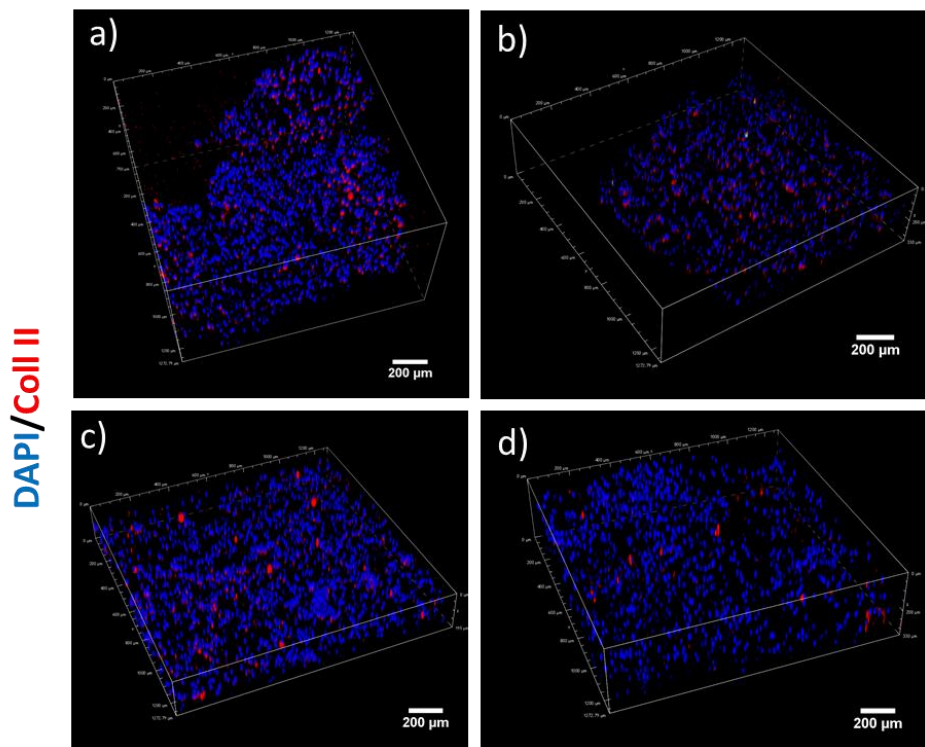


**Figure A:** Confocal microscopy 3D stack showing immunofluorescence staining of Y201-C in healthy and pathological in vitro models. Cell nuclei were stained in blue (DAPI) and collagen type II is visualized in red (AlexaFluor 594). (a) GG/MH-P at day 7 after printing; (b) GG/MH-H at day 14 after printing; (c) GG/MH-P at day 14 after printing; (d) GG2-P at day 14 after printing; (10x Magnification, Z-stack of 15 µm). Scale bar = 200 µm.



## Bibliography

- Agibayeva, L. E. *et al.* (2020) 'Gellan gum and its methacrylated derivatives as in situ gelling mucoadhesive formulations of pilocarpine: In vitro and in vivo studies', *International Journal of Pharmaceutics*, 577(January). doi: 10.1016/j.ijpharm.2020.119093.
- Ahadian, S. *et al.* (2018) 'Organ-On-A-Chip Platforms: A Convergence of Advanced Materials, Cells, and Microscale Technologies', *Advanced Healthcare Materials*, 7(2), p. 1700506. doi: doi:10.1002/adhm.201700506.
- Ahmed, E. M. (2015) 'Hydrogel: Preparation, characterisation, and applications: A review', *Journal of Advanced Research*, 6(2), pp. 105–121. doi: <https://doi.org/10.1016/j.jare.2013.07.006>.
- Akizuki, S. *et al.* (1986) 'Tensile properties of human knee joint cartilage: I. Influence of ionic conditions, weight bearing, and fibrillation on the tensile modulus', *Journal of Orthopaedic Research*, 4(4), pp. 379–392. doi: 10.1002/jor.1100040401.
- Akkouch, A., Yu, Y. and Ozbolat, I. T. (2015) 'Microfabrication of scaffold-free tissue strands for three-dimensional tissue engineering', *Biofabrication*. IOP Publishing, 7(3), p. 31002.
- Albright, J. C. and Daoud, A. K. (2017) 'Microfracture and Microfracture Plus', *Clinics in Sports Medicine*. Elsevier, 36(3), pp. 501–507. doi: 10.1016/J.CSM.2017.02.012.
- ALWAN, W. H. *et al.* (1991) 'Glycosaminoglycans in horses with osteoarthritis', *Equine Veterinary Journal*, 23(1), pp. 44–47. doi: 10.1111/j.2042-3306.1991.tb02712.x.
- An, Y. H. *et al.* (2001) 'Regaining chondrocyte phenotype in thermosensitive gel culture', *The Anatomical Record*, 263(4), pp. 336–341. doi: 10.1002/ar.1114.
- Ando, W. *et al.* (2007) 'Cartilage repair using an in vitro generated scaffold-free tissue-engineered construct derived from porcine synovial mesenchymal stem cells', *Biomaterials*. Elsevier, 28(36), pp. 5462–5470.
- Armiento, A. R. *et al.* (2018) 'Biomaterials for articular cartilage tissue engineering: Learning from biology', *Acta Biomaterialia*. Acta Materialia Inc., 65, pp. 1–20. doi: 10.1016/j.actbio.2017.11.021.
- Asakawa, N. *et al.* (2010) 'Pre-vascularization of in vitro three-dimensional tissues created by cell sheet engineering', *Biomaterials*. Elsevier, 31(14), pp. 3903–3909.
- Atala, A. and Yoo, J. J. (2015) *Essentials of 3D biofabrication and translation*. Academic Press.
- Athanasίου, K. A. *et al.* (2013) 'Self-organization and the self-assembling process in tissue engineering', *Annual review of biomedical engineering*. 2013/05/20, 15, pp. 115–136. doi: 10.1146/annurev-bioeng-071812-152423.
- Autissier, A. *et al.* (2010) 'Fabrication of porous polysaccharide-based scaffolds using a combined freeze-drying/cross-linking process', *Acta Biomaterialia*. Acta Materialia Inc., 6(9), pp. 3640–3648. doi: 10.1016/j.actbio.2010.03.004.
- Ávila, H. M. *et al.* (2016) '3D bioprinting of human chondrocyte-laden nanocellulose hydrogels for patient-specific auricular cartilage regeneration', *Bioprinting*. Elsevier, 1, pp. 22–35.
- Axpe, E. and Oyen, M. L. (2016) 'Applications of alginate-based bioinks in 3D bioprinting', *International Journal of Molecular Sciences*, 17(12). doi: 10.3390/ijms17121976.
- Bacelar, A. H. *et al.* (2016) 'Recent progress in gellan gum hydrogels provided by functionalization strategies', *Journal of Materials Chemistry B*, 4(37), pp. 6164–6174. doi: 10.1039/c6tb01488g.
- Bae, D. K., Yoon, K. H. and Song, S. J. (2006) 'Cartilage Healing After Microfracture in Osteoarthritic Knees', *Arthroscopy: The Journal of Arthroscopic & Related Surgery*. W.B. Saunders, 22(4), pp. 367–374. doi: 10.1016/J.ARTHRO.2006.01.015.
- Ballyns, J. J. *et al.* (2009) 'An Optical Method for Evaluation of Geometric Fidelity for Anatomically Shaped Tissue-Engineered Constructs', *Tissue Engineering Part C: Methods*. Mary Ann Liebert, Inc., publishers, 16(4), pp. 693–703. doi: 10.1089/ten.tec.2009.0441.
- Barbani, N. *et al.* (2012) 'Hydroxyapatite/gelatin/gellan sponges as nanocomposite scaffolds for bone reconstruction', *Journal of Materials Science: Materials in Medicine*. Springer, 23(1), pp. 51–61.
- Bartnikowski, M. *et al.* (2015) 'Protective effects of reactive functional groups on chondrocytes in photocrosslinkable hydrogel systems', *Acta Biomaterialia*, 27, pp. 66–76. doi: <https://doi.org/10.1016/j.actbio.2015.08.038>.
- Basu, B. and Ghosh, S. (2017) 'Chapter 8 Case Study: 3D Printed Cartilage 8.1, Biomaterials for Musculoskeletal Regeneration', pp. 173–189. doi: 10.1007/978-981-10-3017-8.
- Beck, E. C. *et al.* (2016a) 'Approaching the compressive modulus of articular cartilage with a decellularized cartilage-based hydrogel', *Acta Biomaterialia*. Acta Materialia Inc., 38, pp. 94–105. doi: 10.1016/j.actbio.2016.04.019.
- Beck, E. C. *et al.* (2016b) 'Approaching the compressive modulus of articular cartilage with a decellularized cartilage-based hydrogel', *Acta Biomaterialia*. Acta Materialia Inc., 38, pp. 94–105. doi: 10.1016/j.actbio.2016.04.019.
- Beldowski, P. *et al.* (2018) 'Physical crosslinking of hyaluronic acid in the presence of phospholipids in an aqueous nano-environment', *Soft matter*. The Royal Society of Chemistry, 14(44), pp. 8997–9004.

- Di Bella, C. *et al.* (2015) '3D Bioprinting of Cartilage for Orthopedic Surgeons: Reading between the Lines', *Frontiers in Surgery*, 2(August), pp. 1–7. doi: 10.3389/fsurg.2015.00039.
- Benito, M. J. *et al.* (2005) 'Synovial tissue inflammation in early and late osteoarthritis', *Annals of the Rheumatic Diseases*, 64(9), pp. 1263–1267. doi: 10.1136/ard.2004.025270.
- Benthien, J. P. and Behrens, P. (2010) 'Autologous matrix-induced chondrogenesis (AMIC): Combining microfracturing and a collagen I/III matrix for articular cartilage resurfacing', *Cartilage*, 1(1), pp. 65–68. doi: 10.1177/1947603509360044.
- Berger, J. *et al.* (2004) 'Structure and interactions in covalently and ionically crosslinked chitosan hydrogels for biomedical applications', *European Journal of Pharmaceutics and Biopharmaceutics*, 57(1), pp. 19–34. doi: [https://doi.org/10.1016/S0939-6411\(03\)00161-9](https://doi.org/10.1016/S0939-6411(03)00161-9).
- Bessa, P. C., Casal, M. and Reis, R. L. (2008) 'Bone morphogenetic proteins in tissue engineering: the road from laboratory to clinic, part II (BMP delivery)', *Journal of Tissue Engineering and Regenerative Medicine*, 2(2-3), pp. 81–96. doi: 10.1002/term.74.
- Bhattacharjee, M. *et al.* (2015) 'Tissue engineering strategies to study cartilage development, degeneration and regeneration', *Advanced Drug Delivery Reviews*. Elsevier B.V., 84, pp. 107–122. doi: 10.1016/j.addr.2014.08.010.
- Bhosale, A. M. and Richardson, J. B. (2008a) 'Articular cartilage: Structure, injuries and review of management', *British Medical Bulletin*, 87(1), pp. 77–95. doi: 10.1093/bmb/ldn025.
- Bhosale, A. M. and Richardson, J. B. (2008b) 'Articular cartilage: Structure, injuries and review of management', *British Medical Bulletin*, 87(1), pp. 77–95. doi: 10.1093/bmb/ldn025.
- Billiet, T. *et al.* (2014) 'The 3D printing of gelatin methacrylamide cell-laden tissue-engineered constructs with high cell viability', *Biomaterials*. Elsevier, 35(1), pp. 49–62.
- Bischoff, D. S., Makhijani, N. S. and Yamaguchi, D. T. (2012) 'Constitutive expression of human telomerase enhances the proliferation potential of human mesenchymal stem cells', *BioResearch Open Access*, 1(6), pp. 273–279. doi: 10.1089/biores.2012.0252.
- Bonifacio, M. A. *et al.* (2017) 'Insight into halloysite nanotubes-loaded gellan gum hydrogels for soft tissue engineering applications', *Carbohydrate Polymers*. Elsevier Ltd., 163, pp. 280–291. doi: 10.1016/j.carbpol.2017.01.064.
- Bonifacio, Maria A *et al.* (2018) 'Antibacterial effectiveness meets improved mechanical properties: Manuka honey/gellan gum composite hydrogels for cartilage repair', *Carbohydrate Polymers*, 198, pp. 462–472. doi: <https://doi.org/10.1016/j.carbpol.2018.06.115>.
- Bonifacio, Maria A. *et al.* (2018) 'Antibacterial effectiveness meets improved mechanical properties: Manuka honey/gellan gum composite hydrogels for cartilage repair', *Carbohydrate Polymers*. Elsevier, 198(April), pp. 462–472. doi: 10.1016/j.carbpol.2018.06.115.
- Bonifacio, M. A., Cochis, A., Cometa, S., Scalzone, A., *et al.* (2020) 'Advances in cartilage repair: The influence of inorganic clays to improve mechanical and healing properties of antibacterial Gellan gum-Manuka honey hydrogels', *Materials Science and Engineering C*. Elsevier, 108(August 2019), p. 110444. doi: 10.1016/j.msec.2019.110444.
- Bonifacio, M. A., Cochis, A., Cometa, S., Gentile, P., *et al.* (2020) 'From the Sea to the Bee: Gellan gum-Honey-Diatom composite to deliver resveratrol for cartilage regeneration under oxidative stress conditions', *Carbohydrate Polymers*. Elsevier, 245(May), p. 116410. doi: 10.1016/j.carbpol.2020.116410.
- Boschetti, F. *et al.* (2004) 'Biomechanical properties of human articular cartilage under compressive loads', *Biorheology*, 41(3–4), pp. 159–166.
- Bosetti, M. *et al.* (2012) 'Chondrogenic induction of human mesenchymal stem cells using combined growth factors for cartilage tissue engineering', *Journal of Tissue Engineering and Regenerative Medicine*, 6(3), pp. 205–213. doi: 10.1002/term.416.
- Boyan, B. D., Doroudi, M. and Schwartz, Z. (2011) 'Cartilage', *Vitamin D*, pp. 507–519. doi: 10.1016/B978-0-12-381978-9.10028-9.
- Brama, P. A. J. *et al.* (2009) 'Effect of loading on the organization of the collagen fibril network in juvenile equine articular cartilage', *Journal of Orthopaedic Research*. Wiley Online Library, 27(9), pp. 1226–1234.
- Brittberg, M. *et al.* (1994) 'Treatment of Deep Cartilage Defects in the Knee with Autologous Chondrocyte Transplantation', *New England Journal of Medicine*. Massachusetts Medical Society, 331(14), pp. 889–895. doi: 10.1056/NEJM199410063311401.
- Buckley, C. T. *et al.* (2009) 'The effect of concentration, thermal history and cell seeding density on the initial mechanical properties of agarose hydrogels', *Journal of the mechanical behavior of biomedical materials*. Elsevier, 2(5), pp. 512–521.
- Buckwalter, JA ; Mankin,HJ; Grodzinsky, A. (2005) '26\_BuckwalterArticularCartilage.pdf', *Articular Cartilage and Osteoarthritis*, pp. 466–480.
- Buckwalter, J. A. and Mankin, H. J. (1998) 'Articular cartilage: degeneration and osteoarthritis, repair, regeneration, and transplantation.', *Instructional course lectures*, pp. 487–504.
- Caddeo, S., Boffito, M. and Sartori, S. (2017) 'Tissue engineering approaches in the design of healthy and pathological in vitro tissue models', *Frontiers in Bioengineering and Biotechnology*, 5(AUG), pp. 1–22. doi: 10.3389/fbioe.2017.00040.
- Camarero-Espinosa, S. *et al.* (2016) 'Articular cartilage: From formation to tissue engineering', *Biomaterials Science*. Royal Society of Chemistry, 4(5), pp. 734–767. doi: 10.1039/c6bm00068a.
- Caron, M. M. J. *et al.* (2012) 'Redifferentiation of dedifferentiated human articular chondrocytes: Comparison of 2D and 3D cultures',

- Osteoarthritis and Cartilage*. W.B. Saunders, 20(10), pp. 1170–1178. doi: 10.1016/j.joca.2012.06.016.
- Carson, J. R. (2018) 'Articular Cartilage Repair', *Science Insights*, 2018(2018), pp. 1–4. doi: 10.15354/si.18.re082.
- Carver, S. E. and Heath, C. A. (1999) 'Increasing extracellular matrix production in regenerating cartilage with intermittent physiological pressure', *Biotechnology and Bioengineering*, 62(2), pp. 166–174. doi: 10.1002/(SICI)1097-0290(19990120)62:2<166::AID-BIT6>3.0.CO;2-K.
- Catros, S. *et al.* (2011) 'Effect of laser energy, substrate film thickness and bioink viscosity on viability of endothelial cells printed by Laser-Assisted Bioprinting', *Applied Surface Science*, 257(12), pp. 5142–5147. doi: <https://doi.org/10.1016/j.apsusc.2010.11.049>.
- Cencetti, C. *et al.* (2011) 'Preparation and characterisation of a new gellan gum and sulphated hyaluronic acid hydrogel designed for epidural scar prevention', *Journal of Materials Science: Materials in Medicine*. Springer, 22(2), pp. 263–271.
- Chang, C. C. *et al.* (2011) 'Direct-write bioprinting three-dimensional biohybrid systems for future regenerative therapies', *Journal of Biomedical Materials Research Part B: Applied Biomaterials*, 98B(1), pp. 160–170. doi: 10.1002/jbm.b.31831.
- Chawla, S. *et al.* (2018) 'Silk-Based Bioinks for 3D Bioprinting', *Advanced Healthcare Materials*, 7(8), pp. 1–23. doi: 10.1002/adhm.201701204.
- Chen, F. H., Rousche, K. T. and Tuan, R. S. (2006) 'Technology insight: Adult stem cells in cartilage regeneration and tissue engineering', *Nature Clinical Practice Rheumatology*, 2(7), pp. 373–382. doi: 10.1038/ncprheum0216.
- Chen, H. *et al.* (2018) 'Bone Marrow-Derived Mesenchymal Stem Cells Encapsulated in Functionalized Gellan Gum/Collagen Hydrogel for Effective Vascularization', *ACS Applied Bio Materials*, 1(5), pp. 1408–1415. doi: 10.1021/acsbm.8b00361.
- Cheng, J. *et al.* (2008) 'Rheological Properties of Cell-Hydrogel Composites Extruding Through Small-Diameter Tips', *Journal of Manufacturing Science and Engineering*, 130(2). doi: 10.1115/1.2896215.
- Chimene, D. *et al.* (2016) 'Advanced bioinks for 3D printing: a materials science perspective', *Annals of biomedical engineering*. Springer, 44(6), pp. 2090–2102.
- Cho, D.-W. *et al.* (2019) '3D Bioprinting', *3D Bioprinting*, pp. 5–12. doi: 10.1007/978-3-030-32222-9.
- Chung, C. and Burdick, J. A. (2008a) 'Engineering cartilage tissue', *Advanced Drug Delivery Reviews*, 60(2), pp. 243–262. doi: 10.1016/j.addr.2007.08.027.
- Chung, C. and Burdick, J. A. (2008b) 'Engineering cartilage tissue', *Advanced Drug Delivery Reviews*. Elsevier, pp. 243–262. doi: 10.1016/j.addr.2007.08.027.
- Ciardelli, G. *et al.* (2010) 'Enzymatically crosslinked porous composite matrices for bone tissue regeneration', *Journal of Biomedical Materials Research Part A: An Official Journal of The Society for Biomaterials, The Japanese Society for Biomaterials, and The Australian Society for Biomaterials and the Korean Society for Biomaterials*. Wiley Online Library, 92(1), pp. 137–151.
- Clair, B. L., Johnson, A. R. and Howard, T. (2009) 'Cartilage Repair: Current and Emerging Options in Treatment', *Foot & Ankle Specialist*, 2(4), pp. 179–188. doi: 10.1177/1938640009342272.
- Coburn, J. M. *et al.* (2013) 'Short-Chain Fatty Acid-Modified Hexosamine for Tissue-Engineering Osteoarthritic Cartilage', *Tissue Engineering Part A*. Mary Ann Liebert, Inc., publishers, 19(17–18), pp. 2035–2044. doi: 10.1089/ten.tea.2012.0317.
- Cohen, N. P., Foster, R. J. and Mow, V. C. (1998) 'Composition and dynamics of articular cartilage: Structure, function, and maintaining healthy state', *Journal of Orthopaedic and Sports Physical Therapy*, 28(4), pp. 203–215. doi: 10.2519/jospt.1998.28.4.203.
- Cope, P. J. *et al.* (2019) 'Models of osteoarthritis: the good, the bad and the promising', *Osteoarthritis and Cartilage*, 27(2), pp. 230–239. doi: 10.1016/j.joca.2018.09.016.
- Correa, D. and Lietman, S. A. (2017) 'Articular cartilage repair: Current needs, methods and research directions', *Seminars in Cell and Developmental Biology*. Elsevier Ltd, 62, pp. 67–77. doi: 10.1016/j.semcdb.2016.07.013.
- Costa, L. *et al.* (2018) 'Gellan Gum-Based Hydrogels for Osteochondral Repair', *Advances in Experimental Medicine and Biology*, 1058, pp. 281–304. doi: 10.1007/978-3-319-76711-6\_13.
- Cotter, E. J. *et al.* (2017) 'Bone Marrow Aspirate Concentrate for Cartilage Defects of the Knee: From Bench to Bedside Evidence', *CARTILAGE*. SAGE Publications Inc, 9(2), pp. 161–170. doi: 10.1177/1947603517741169.
- Coutinho, D. F. *et al.* (2010a) 'Modified Gellan Gum hydrogels with tunable physical and mechanical properties', *Biomaterials*. doi: 10.1016/j.biomaterials.2010.06.035.
- Coutinho, D. F. *et al.* (2010b) 'Modified Gellan Gum hydrogels with tunable physical and mechanical properties', *Biomaterials*. Elsevier Ltd, 31(29), pp. 7494–7502. doi: 10.1016/j.biomaterials.2010.06.035.
- Coutinho, D. F. *et al.* (2012) 'Microfabricated photocrosslinkable polyelectrolyte-complex of chitosan and methacrylated gellan gum', *Journal of Materials Chemistry*, 22(33), pp. 17262–17271. doi: 10.1039/c2jm31374j.
- Croisier, F. and Jérôme, C. (2013) 'Chitosan-based biomaterials for tissue engineering', *European Polymer Journal*, 49(4), pp. 780–792. doi: <https://doi.org/10.1016/j.eurpolymj.2012.12.009>.

- Cucchiari, M. and Madry, H. (2019) 'Biomaterial-guided delivery of gene vectors for targeted articular cartilage repair', *Nature Reviews Rheumatology*, 15(1), pp. 18–29. doi: 10.1038/s41584-018-0125-2.
- Cushing, M. C. and Anseth, K. S. (2007) 'Hydrogel cell cultures', *Science*. American Association for the Advancement of Science, 316(5828), pp. 1133–1134.
- Dababneh, A. B. and Ozbolat, I. T. (2014) 'Bioprinting technology: a current state-of-the-art review', *Journal of Manufacturing Science and Engineering*. American Society of Mechanical Engineers Digital Collection, 136(6).
- Dai, T. et al. (2011) 'Chitosan preparations for wounds and burns: antimicrobial and wound-healing effects', *Expert review of anti-infective therapy*. Taylor & Francis, 9(7), pp. 857–879.
- Das, R. K. et al. (2016) 'Stress-stiffening-mediated stem-cell commitment switch in soft responsive hydrogels', *Nature Materials*. Nature Publishing Group, 15(3), pp. 318–325. doi: 10.1038/nmat4483.
- Dave, P. N. and Gor, A. (2018) 'Chapter 3 - Natural Polysaccharide-Based Hydrogels and Nanomaterials: Recent Trends and Their Applications', in Mustansar Hussain, C. B. T.-H. of N. for I. A. (ed.) *Micro and Nano Technologies*. Elsevier, pp. 36–66. doi: <https://doi.org/10.1016/B978-0-12-813351-4.00003-1>.
- Davies, M. E. et al. (2004) 'Time dependency of osteoarthritis-like metabolic changes in mechanically loaded articular cartilage', in *Bone*, pp. S32–S33.
- Davison, T. et al. (2002) 'Static and dynamic compression modulate matrix metabolism in tissue engineered cartilage', *Journal of Orthopaedic Research*, 20(4), pp. 842–848. doi: doi:10.1016/S0736-0266(01)00160-7.
- DeFail, A. J. et al. (2006) 'Controlled release of bioactive TGF- $\beta$ 1 from microspheres embedded within biodegradable hydrogels', *Biomaterials*, 27(8), pp. 1579–1585. doi: <https://doi.org/10.1016/j.biomaterials.2005.08.013>.
- DeLise, A. M., Fischer, L. and Tuan, R. S. (2000) 'Cellular interactions and signaling in cartilage development', *Osteoarthritis and Cartilage*, 8(5), pp. 309–334. doi: 10.1053/joca.1999.0306.
- Démarteau, O. et al. (2003) 'Dynamic compression of cartilage constructs engineered from expanded human articular chondrocytes', *Biochemical and Biophysical Research Communications*, 310(2), pp. 580–588. doi: <https://doi.org/10.1016/j.bbrc.2003.09.099>.
- Demirtaş, T. T., Irmak, G. and Gümüşderelioğlu, M. (2017) 'A bioprintable form of chitosan hydrogel for bone tissue engineering', *Biofabrication*. IOP Publishing, 9(3), p. 35003.
- Demoor, M. et al. (2014) 'Cartilage tissue engineering: Molecular control of chondrocyte differentiation for proper cartilage matrix reconstruction', *Biochimica et Biophysica Acta (BBA) - General Subjects*, 1840(8), pp. 2414–2440. doi: <https://doi.org/10.1016/j.bbagen.2014.02.030>.
- DeRogatis, M. et al. (2019) 'Non-operative treatment options for knee osteoarthritis', *Annals of Translational Medicine*. AME Publishing Company, 7(S7), pp. S245–S245. doi: 10.21037/atm.2019.06.68.
- Dhawan, A. et al. (2019) 'Three-dimensional bioprinting for bone and cartilage restoration in orthopaedic surgery', *Journal of the American Academy of Orthopaedic Surgeons*, 27(5), pp. E215–E226. doi: 10.5435/JAAOS-D-17-00632.
- Diekmann, B. O. et al. (2012) 'Cartilage tissue engineering using differentiated and purified induced pluripotent stem cells', *Proceedings of the National Academy of Sciences of the United States of America*, 109(47), pp. 19172–19177. doi: 10.1073/pnas.1210422109.
- Douglas, T. E. L. et al. (2016) 'Generation of composites for bone tissue-engineering applications consisting of gellan gum hydrogels mineralized with calcium and magnesium phosphate phases by enzymatic means', *Journal of tissue engineering and regenerative medicine*. Wiley Online Library, 10(11), pp. 938–954.
- Duarte Campos, D. F. et al. (2015) 'The stiffness and structure of three-dimensional printed hydrogels direct the differentiation of mesenchymal stromal cells toward adipogenic and osteogenic lineages', *Tissue Engineering Part A*. Mary Ann Liebert, Inc. 140 Huguenot Street, 3rd Floor New Rochelle, NY 10801 USA, 21(3–4), pp. 740–756.
- Dudman, J. P. R. et al. (2020) 'Reliable inkjet printing of chondrocytes and MSCs using reservoir agitation', *Biofabrication*. IOP Publishing, 12(4), p. 45024.
- Dunkin, B. S. (2013) 'New and Emerging Techniques in Cartilage Repair: Matrix-Induced Autologous Chondrocyte Implantation', *Operative Techniques in Sports Medicine*. W.B. Saunders, 21(2), pp. 100–107. doi: 10.1053/J.OTSM.2013.03.003.
- Duval, K. et al. (2017) 'Modeling physiological events in 2D vs. 3D cell culture', *Physiology*, 32(4), pp. 266–277. doi: 10.1152/physiol.00036.2016.
- Ebert, J. R. et al. (2017) 'A Prospective Clinical and Radiological Evaluation at 5 Years After Arthroscopic Matrix-Induced Autologous Chondrocyte Implantation', *The American Journal of Sports Medicine*. SAGE Publications Inc., 45(1), pp. 59–69. doi: 10.1177/0363546516663493.
- Edmondson, R. et al. (2014) 'Three-Dimensional Cell Culture Systems and Their Applications in Drug Discovery and Cell-Based Biosensors', *ASSAY and Drug Development Technologies*, 12(4), pp. 207–218. doi: 10.1089/ad.2014.573.
- Eggl, P. S., Hunziker, E. B. and Schenk, R. K. (1988) 'Quantitation of structural features characterizing weight- and less-weight-bearing regions in articular cartilage: A stereological analysis of medial femoral condyles in young adult rabbits', *The Anatomical Record*, 222(3), pp. 217–227. doi: 10.1002/ar.1092220302.

- Eyre, D. R. and Wu, J. J. (1995) 'Collagen structure and cartilage matrix integrity', *The Journal of rheumatology. Supplement*, 43, p. 82–85. Available at: <http://europepmc.org/abstract/MED/7752147>.
- Fan, J. *et al.* (2010) 'In vitro engineered cartilage using synovium-derived mesenchymal stem cells with injectable gellan hydrogels', *Acta Biomaterialia*. Elsevier, 6(3), pp. 1178–1185.
- Fan, J. C. Y. and Waldman, S. D. (2010) 'The Effect of Intermittent Static Biaxial Tensile Strains on Tissue Engineered Cartilage', *Annals of Biomedical Engineering*, 38(4), pp. 1672–1682. doi: 10.1007/s10439-010-9917-5.
- Fecek, C. *et al.* (2008) 'Chondrogenic Derivatives of Embryonic Stem Cells Seeded into 3D Polycaprolactone Scaffolds Generated Cartilage Tissue In Vivo', *Tissue Engineering Part A*. Mary Ann Liebert, Inc., publishers, 14(8), pp. 1403–1413. doi: 10.1089/ten.tea.2007.0293.
- Felson, D. T. (2006) 'Osteoarthritis of the knee', *New England Journal of Medicine*. Massachusetts Medical Society, 354(8), pp. 841–848. doi: 10.1056/NEJMc051726.
- Fergg, F., Keil, F. J. and Quader, H. (2001) 'Investigations of the microscopic structure of poly(vinyl alcohol) hydrogels by confocal laser scanning microscopy', *Colloid and Polymer Science*, 279(1), pp. 61–67. doi: 10.1007/s003960000398.
- Ferris, Cameron J *et al.* (2013) 'Bio-ink for on-demand printing of living cells', *Biomaterials Science*. Royal Society of Chemistry, 1(2), pp. 224–230.
- Ferris, Cameron J. *et al.* (2013) 'Modified gellan gum hydrogels for tissue engineering applications', *Soft Matter*, 9(14), pp. 3705–3711. doi: 10.1039/c3sm27389j.
- Ficat, R. P. *et al.* (1979) 'Spongialization: a new treatment for diseased patellae', *Clinical orthopaedics and related research*, (144), p. 74–83. Available at: <http://europepmc.org/abstract/MED/535254>.
- Filardo, G. *et al.* (2016) 'Stem cells in articular cartilage regeneration', *Journal of Orthopaedic Surgery and Research*. Journal of Orthopaedic Surgery and Research, 11(1). doi: 10.1186/s13018-016-0378-x.
- Francioli, S. *et al.* (2011) 'Engineered Cartilage Maturation Regulates Cytokine Production and Interleukin-1 $\beta$  Response', *Clinical Orthopaedics and Related Research*, 469(10), pp. 2773–2784. doi: 10.1007/s11999-011-1826-x.
- Francis, S. L. *et al.* (2018) 'Cartilage Tissue Engineering Using Stem Cells and Bioprinting Technology—Barriers to Clinical Translation', *Frontiers in Surgery*, 5(November), pp. 1–12. doi: 10.3389/fsurg.2018.00070.
- Francis Suh, J.-K. and Matthew, H. W. . (2000) 'Application of chitosan-based polysaccharide biomaterials in cartilage tissue engineering: a review', *Biomaterials*. Elsevier, 21(24), pp. 2589–2598. doi: 10.1016/S0142-9612(00)00126-5.
- Freed, L. E., Martin, I. and Vunjak-Novakovic, G. (1999) 'Frontiers in tissue engineering: In vitro modulation of chondrogenesis', in *Clinical Orthopaedics and Related Research*. Lippincott Williams and Wilkins. doi: 10.1097/00003086-199910001-00006.
- Friedman, M. J. *et al.* (1984) 'Preliminary results with abrasion arthroplasty in the osteoarthritic knee', *Clinical orthopaedics and related research*, (182), p. 200–205. Available at: <http://europepmc.org/abstract/MED/6692614>.
- Frontera, W. R. *et al.* (2020) 'Osteoarthritis', *Essentials of Physical Medicine and Rehabilitation*. Content Repository Only!, pp. 792–798. doi: 10.1016/B978-0-323-54947-9.00140-1.
- Fukumoto, T. *et al.* (2003) 'Combined effects of insulin-like growth factor-1 and transforming growth factor- $\beta$ 1 on periosteal mesenchymal cells during chondrogenesis in vitro', *Osteoarthritis and Cartilage*, 11(1), pp. 55–64. doi: 10.1053/joca.2002.0869.
- Gabriel, N. *et al.* (2010) 'Development of an in vitro model of feline cartilage degradation', *Journal of Feline Medicine and Surgery*. No longer published by Elsevier, 12(8), pp. 614–620. doi: 10.1016/j.jfms.2010.03.007.
- Galuzzi, M. *et al.* (2018) 'Human engineered cartilage and decellularized matrix as an alternative to animal osteoarthritis model', *Polymers*, 10(7), pp. 1–16. doi: 10.3390/polym10070738.
- Gantar, A. *et al.* (2014) 'Nanoparticulate bioactive-glass-reinforced gellan-gum hydrogels for bone-tissue engineering', *Materials Science and Engineering: C*. Elsevier, 43, pp. 27–36.
- Gasperini, L., Mano, J. F. and Reis, R. L. (2014) 'Natural polymers for the microencapsulation of cells', *Journal of the Royal Society Interface*. The Royal Society, 11(100), p. 20140817.
- Geng, L. *et al.* (2005) 'Direct writing of chitosan scaffolds using a robotic system', *Rapid Prototyping Journal*. Emerald Group Publishing Limited.
- Gentile, P. *et al.* (2016) 'Localised controlled release of simvastatin from porous chitosan–gelatin scaffolds engrafted with simvastatin loaded PLGA-microparticles for bone tissue engineering application', *Materials Science and Engineering: C*. Elsevier, 59, pp. 249–257.
- Gentile, P. *et al.* (2017) 'Alginate-based hydrogels functionalised at the nanoscale using layer-by-layer assembly for potential cartilage repair', *Biomaterials science*. Royal Society of Chemistry, 5(9), pp. 1922–1931.
- Gerhardt, L.-C. and Boccaccini, A. R. (2010) 'Bioactive Glass and Glass-Ceramic Scaffolds for Bone Tissue Engineering', *Materials*, 3(7), pp. 3867–3910. doi: 10.3390/ma3073867.
- Gering, C. (2015) 'Functionalization of the Polysaccharide Hydrogel', (December).

- Gering, C. *et al.* (2019) 'Design of modular gellan gum hydrogel functionalized with avidin and biotinylated adhesive ligands for cell culture applications', *PLoS one*. Public Library of Science San Francisco, CA USA, 14(8), p. e0221931.
- Ghosh, S. *et al.* (2009) 'In vitro model of mesenchymal condensation during chondrogenic development', *Biomaterials*. Elsevier Ltd, 30(33), pp. 6530–6540. doi: 10.1016/j.biomaterials.2009.08.019.
- De Giglio, E. *et al.* (2018) 'Multi-compartment scaffold fabricated via 3D-printing as in vitro co-culture osteogenic model', *Scientific Reports*. Springer US, 8(1), pp. 1–13. doi: 10.1038/s41598-018-33472-1.
- Glyn-Jones, S. *et al.* (2015) 'Osteoarthritis', *The Lancet*, 386(9991), pp. 376–387. doi: 10.1016/S0140-6736(14)60802-3.
- Gong, Y. *et al.* (2009) 'An improved injectable polysaccharide hydrogel: modified gellan gum for long-term cartilage regeneration in vitro', *Journal of Materials Chemistry*. Royal Society of Chemistry, 19(14), pp. 1968–1977.
- Goodstone, N. J., Cartwright, A. and Ashton, B. (2004) 'Effects of high molecular weight hyaluronan on chondrocytes cultured within a resorbable gelatin sponge', *Tissue engineering*, 10(3–4), p. 621–631. doi: 10.1089/107632704323061979.
- Gopinathan, J. and Noh, I. (2018) 'Recent trends in bioinks for 3D printing', *Biomaterials Research*. Biomaterials Research, 22(1), pp. 1–15. doi: 10.1186/s40824-018-0122-1.
- Goycoolea, F. M. *et al.* (2003) 'Effect of chemical crosslinking on the swelling and shrinking properties of thermal and pH-responsive chitosan hydrogels', *Macromolecular Bioscience*. Wiley Online Library, 3(10), pp. 612–619.
- Grenier, S., Bhargava, M. M. and Torzilli, P. A. (2014) 'An in vitro model for the pathological degradation of articular cartilage in osteoarthritis', *Journal of Biomechanics*, 47(3), pp. 645–652. doi: <https://doi.org/10.1016/j.jbiomech.2013.11.050>.
- Griffith, L. G. and Swartz, M. A. (2006) 'Capturing complex 3D tissue physiology in vitro', *Nature Reviews Molecular Cell Biology*, 7(3), pp. 211–224. doi: 10.1038/nrm1858.
- Groll, J. *et al.* (2016) 'Biofabrication: Reappraising the definition of an evolving field', *Biofabrication*, 8(1). doi: 10.1088/1758-5090/8/1/013001.
- Guilak, F. (2000) 'The deformation behavior and viscoelastic properties of chondrocytes in articular cartilage', in *Biorheology*, pp. 27–44.
- Guillemot, F. *et al.* (2010) 'High-throughput laser printing of cells and biomaterials for tissue engineering', *Acta Biomaterialia*, 6(7), pp. 2494–2500. doi: <https://doi.org/10.1016/j.actbio.2009.09.029>.
- Gungor-Ozkerim, P. S. *et al.* (2018) 'Bioinks for 3D bioprinting: An overview', *Biomaterials Science*. Royal Society of Chemistry, 6(5), pp. 915–946. doi: 10.1039/c7bm00765e.
- Guvendiren, M., Lu, H. D. and Burdick, J. A. (2012) 'Shear-thinning hydrogels for biomedical applications', *Soft matter*. Royal Society of Chemistry, 8(2), pp. 260–272.
- Guzman, R. E. *et al.* (2003) 'Mono-Iodoacetate-Induced Histologic Changes in Subchondral Bone and Articular Cartilage of Rat Femorotibial Joints: An Animal Model of Osteoarthritis', *Toxicologic Pathology*. SAGE Publications Inc, 31(6), pp. 619–624. doi: 10.1080/01926230390241800.
- Hall, B. K. (2005) *Bones and Cartilage: Developmental and Evolutionary Skeletal Biology*, *Bones and Cartilage: Developmental and Evolutionary Skeletal Biology*. doi: 10.1016/B978-0-12-319060-4.X5000-3.
- Hall, B. K. and Miyake, T. (1992) 'The membranous skeleton: the role of cell condensations in vertebrate skeletogenesis', *Anatomy and Embryology*, 186(2), pp. 107–124. doi: 10.1007/BF00174948.
- Harley, B. A. *et al.* (2006) 'Fabricating tubular scaffolds with a radial pore size gradient by a spinning technique', *Biomaterials*, 27(6), pp. 866–874. doi: 10.1016/j.biomaterials.2005.07.012.
- Hartung, T. (2008) 'Thoughts on limitations of animal models', *Parkinsonism and Related Disorders*, 14(SUPPL.2), pp. 83–85. doi: 10.1016/j.parkreldis.2008.04.003.
- Haseeb, A. and Haqqi, T. M. (2013) 'Immunopathogenesis of osteoarthritis', *Clinical Immunology*. Academic Press, 146(3), pp. 185–196. doi: 10.1016/J.CLIM.2012.12.011.
- Häuselmann, H. J. *et al.* (1992) 'Synthesis and Turnover of Proteoglycans by Human and Bovine Adult Articular Chondrocytes Cultured in Alginate Beads', *Matrix*, 12(2), pp. 116–129. doi: [https://doi.org/10.1016/S0934-8832\(11\)80053-3](https://doi.org/10.1016/S0934-8832(11)80053-3).
- Haycock, J. W. (2011) 'Chapter 1 and Techniques', *3D Cell Culture: Methods and Protocols, Methods in Molecular Biology*, 695(2), pp. 1–15. doi: 10.1007/978-1-60761-984-0.
- Hayes, W. C. *et al.* (1972) 'A mathematical analysis for indentation tests of articular cartilage', *Journal of Biomechanics*. Elsevier, 5(5), pp. 541–551. doi: 10.1016/0021-9290(72)90010-3.
- Hayes, W. C. and Mockros, L. F. (1971) 'Viscoelastic properties of human articular cartilage.', *Journal of applied physiology*, 31(4), pp. 562–568. doi: 10.1152/jappl.1971.31.4.562.
- Haywood, L. *et al.* (2003) 'Inflammation and angiogenesis in osteoarthritis', *Arthritis & Rheumatism*, 48(8), pp. 2173–2177. doi: 10.1002/art.11094.

- He, B. *et al.* (2014) 'High-resolution measurements of the multilayer ultra-structure of articular cartilage and their translational potential', *Arthritis Research and Therapy*, 16(2). doi: 10.1186/ar4506.
- He, Y. *et al.* (2016) 'Research on the printability of hydrogels in 3D bioprinting', *Scientific Reports*, 6(1), p. 29977. doi: 10.1038/srep29977.
- Heinegård, D. and Saxne, T. (2011) 'The role of the cartilage matrix in osteoarthritis', *Nature Reviews Rheumatology*. Nature Publishing Group, 7(1), pp. 50–56. doi: 10.1038/nrrheum.2010.198.
- Hemmati-Sadeghi, S. *et al.* (2019) 'Biomimetic sulfated polyethylene glycol hydrogel inhibits proteoglycan loss and tumor necrosis factor- $\alpha$ -induced expression pattern in an osteoarthritis in vitro model', *Journal of Biomedical Materials Research - Part B Applied Biomaterials*, 107(3), pp. 490–500. doi: 10.1002/jbm.b.34139.
- Hendrikson, W. J. *et al.* (2017) 'Towards 4D printed scaffolds for tissue engineering: exploiting 3D shape memory polymers to deliver time-controlled stimulus on cultured cells', *Biofabrication*. {IOP} Publishing, 9(3), p. 31001. doi: 10.1088/1758-5090/aa8114.
- Hinckel, B. B., Gomoll, A. H. and Farr, J. (2017) 'Cartilage restoration in the patellofemoral joint', *Am J Orthop*, 46, pp. 217–222.
- Hockaday, L. A. *et al.* (2012) 'Rapid 3D printing of anatomically accurate and mechanically heterogeneous aortic valve hydrogel scaffolds', *Biofabrication*. IOP Publishing, 4(3), p. 35005.
- Holland, T. A., Tabata, Y. and Mikos, A. G. (2005) 'Dual growth factor delivery from degradable oligo(poly(ethylene glycol) fumarate) hydrogel scaffolds for cartilage tissue engineering', *Journal of Controlled Release*, 101(1), pp. 111–125. doi: <https://doi.org/10.1016/j.jconrel.2004.07.004>.
- Hözl, K. *et al.* (2016) 'Bioink properties before, during and after 3D bioprinting', *Biofabrication*. IOP Publishing, 8(3). doi: 10.1088/1758-5090/8/3/032002.
- Homan, K. A. *et al.* (2016) 'Bioprinting of 3D Convoluted Renal Proximal Tubules on Perfusable Chips', *Biomaterials*, 6(1), pp. 45–59. doi: <https://doi.org/10.1016/j.biomaterials.2016.09.003>.
- Horváth, L. *et al.* (2015) 'Engineering an in vitro air-blood barrier by 3D bioprinting', *Scientific Reports*, 5(1), p. 7974. doi: 10.1038/srep07974.
- Hospodiuk, M. *et al.* (2017) 'The bioink: A comprehensive review on bioprintable materials', *Biotechnology Advances*. Elsevier Inc., 35(2), pp. 217–239. doi: 10.1016/j.biotechadv.2016.12.006.
- Hoyer, B. *et al.* (2014) 'Jellyfish collagen scaffolds for cartilage tissue engineering', *Acta Biomaterialia*. Elsevier, 10(2), pp. 883–892. doi: 10.1016/j.actbio.2013.10.022.
- Hsu, S. *et al.* (2004) 'Evaluation of chitosan-alginate-hyaluronate complexes modified by an RGD-containing protein as tissue-engineering scaffolds for cartilage regeneration', *Artificial Organs*. Wiley Online Library, 28(8), pp. 693–703.
- Hu, J. C. and Athanasiou, K. A. (2006) 'A Self-Assembling Process in Articular Cartilage Tissue Engineering', *Tissue Engineering*. Mary Ann Liebert, Inc., publishers, 12(4), pp. 969–979. doi: 10.1089/ten.2006.12.969.
- Huang, C. Y. *et al.* (2005) 'Anisotropy, inhomogeneity, and tension-compression nonlinearity of human glenohumeral cartilage in finite deformation', *Journal of Biomechanics*. Elsevier, 38(4), pp. 799–809. doi: 10.1016/j.jbiomech.2004.05.006.
- Huang, Q. *et al.* (2002) 'In vivo mesenchymal cell recruitment by a scaffold loaded with transforming growth factor TGF- $\beta$ 1 and the potential for in situ chondrogenesis', *Tissue Engineering*. Mary Ann Liebert, Inc., 8(3), pp. 469–482.
- Huang, Y. *et al.* (2017) '3D bioprinting and the current applications in tissue engineering', *Biotechnology Journal*, 12(8). doi: 10.1002/biot.201600734.
- Huh, D. *et al.* (2010) 'Reconstituting organ-level lung functions on a chip', *Science*. American Association for the Advancement of Science, 328(5986), pp. 1662–1668.
- Hunziker, E. B., Michel, M. and Studer, D. (1997) 'Ultrastructure of adult human articular cartilage matrix after cryotechnical processing', *Microscopy Research and Technique*. John Wiley & Sons, Ltd, 37(4), pp. 271–284. doi: 10.1002/(SICI)1097-0029(19970515)37:4<271::AID-JEMT3>3.0.CO;2-O.
- Hunziker, E. B., Quinn, T. M. and Häuselmann, H. J. (2002) 'Quantitative structural organization of normal adult human articular cartilage', *Osteoarthritis and Cartilage*, 10(7), pp. 564–572. doi: 10.1053/joca.2002.0814.
- Huser, C. A. M. and Davies, M. E. (2006) 'Validation of an in vitro single-impact load model of the initiation of osteoarthritis-like changes in articular cartilage', *Journal of Orthopaedic Research*, 24(4), pp. 725–732. doi: 10.1002/jor.20111.
- Ihalainen, P., Määttä, A. and Sandler, N. (2015) 'Printing technologies for biomolecule and cell-based applications', *International Journal of Pharmaceutics*, 494(2), pp. 585–592. doi: <https://doi.org/10.1016/j.ijpharm.2015.02.033>.
- Imparato, G., Urciuolo, F. and Netti, P. A. (2015) 'In vitro three-dimensional models in cancer research: A review', *International Materials Reviews*, 60(6), pp. 297–311. doi: 10.1179/1743280415Y.0000000003.
- Jia, J. *et al.* (2014) 'Engineering alginate as bioink for bioprinting', *Acta biomaterialia*. Elsevier, 10(10), pp. 4323–4331.
- Jiang, Y., Lin, H. and Tuan, R. (2017) 'Overview: State of the Art and Future Prospectives for Cartilage Repair', in *Cartilage*, p. pp 1-34. doi: 10.1007/978-3-319-53316-2\_1.

- Jin, M. *et al.* (2001) 'Tissue Shear Deformation Stimulates Proteoglycan and Protein Biosynthesis in Bovine Cartilage Explants', *Archives of Biochemistry and Biophysics*, 395(1), pp. 41–48. doi: <https://doi.org/10.1006/abbi.2001.2543>.
- Jin, R. *et al.* (2009) 'Injectable chitosan-based hydrogels for cartilage tissue engineering', *Biomaterials*, 30(13), pp. 2544–2551. doi: <https://doi.org/10.1016/j.biomaterials.2009.01.020>.
- Johnson, C. I., Argyle, D. J. and Clements, D. N. (2016) 'In vitro models for the study of osteoarthritis', *Veterinary Journal*. Elsevier Ltd, 209, pp. 40–49. doi: [10.1016/j.tvjl.2015.07.011](https://doi.org/10.1016/j.tvjl.2015.07.011).
- Johnstone, B. *et al.* (1998) 'In Vitro Chondrogenesis of Bone Marrow-Derived Mesenchymal Progenitor Cells', *Experimental Cell Research*, 238(1), pp. 265–272. doi: <https://doi.org/10.1006/excr.1997.3858>.
- Jones, N. (2012) 'Science in three dimensions: the print revolution', *Nature*, 487(7405), p. 22–23. doi: [10.1038/487022a](https://doi.org/10.1038/487022a).
- Jutila, A. A. *et al.* (2015) 'Encapsulation of Chondrocytes in High-Stiffness Agarose Microenvironments for In Vitro Modeling of Osteoarthritis Mechanotransduction', *Annals of Biomedical Engineering*, 43(5), pp. 1132–1144. doi: [10.1007/s10439-014-1183-5](https://doi.org/10.1007/s10439-014-1183-5).
- Kaklamani, G. *et al.* (2014) 'Mechanical properties of alginate hydrogels manufactured using external gelation', *Journal of the Mechanical Behavior of Biomedical Materials*, 36, pp. 135–142. doi: <https://doi.org/10.1016/j.jmbbm.2014.04.013>.
- Kalamegam, G. *et al.* (2018) 'A comprehensive review of stem cells for cartilage regeneration in osteoarthritis', *Advances in Experimental Medicine and Biology*, 1089(May), pp. 23–36. doi: [10.1007/978-94-007-5584-2\\_205](https://doi.org/10.1007/978-94-007-5584-2_205).
- Kambe, Y. *et al.* (2010) 'Effects of RGDS sequence genetically interfused in the silk fibroin light chain protein on chondrocyte adhesion and cartilage synthesis', *Biomaterials*. Elsevier, 31(29), pp. 7503–7511.
- Kavalkovich, K. W. *et al.* (2002) 'Chondrogenic differentiation of human mesenchymal stem cells within an alginate layer culture system', *In Vitro Cellular & Developmental Biology - Animal*, 38(8), pp. 457–466. doi: [10.1290/1071-2690\(2002\)038<0457:CDOHMS>2.0.CO;2](https://doi.org/10.1290/1071-2690(2002)038<0457:CDOHMS>2.0.CO;2).
- Kean, W. F., Kean, R. and Buchanan, W. W. (2004) 'Osteoarthritis: Symptoms, signs and source of pain', *Inflammopharmacology*, 12(1), pp. 3–31. doi: [10.1163/156856004773121347](https://doi.org/10.1163/156856004773121347).
- Kelly, T. A. N. *et al.* (2013) 'Tissue-engineered articular cartilage exhibits tension-compression nonlinearity reminiscent of the native cartilage', *Journal of Biomechanics*. doi: [10.1016/j.jbiomech.2013.05.017](https://doi.org/10.1016/j.jbiomech.2013.05.017).
- Kesti, M. *et al.* (2015) 'Bioprinting Complex Cartilaginous Structures with Clinically Compliant Biomaterials', *Advanced Functional Materials*, 25(48), pp. 7406–7417. doi: [10.1002/adfm.201503423](https://doi.org/10.1002/adfm.201503423).
- Khademhosseini, A. *et al.* (2006) 'Microscale technologies for tissue engineering and biology', *Proceedings of the National Academy of Sciences of the United States of America*, 103(8), pp. 2480 LP – 2487. doi: [10.1073/pnas.0507681102](https://doi.org/10.1073/pnas.0507681102).
- Khang, G. *et al.* (2015) 'Biological evaluation of intervertebral disc cells in different formulations of gellan gum-based hydrogels', *Journal of tissue engineering and regenerative medicine*. Wiley Online Library, 9(3), pp. 265–275.
- Kim, M. and Evans, D. (2005) 'Tissue Engineering : The Future of Stem Cells', *Topics in Tissue Engineering*, pp. 1–22.
- Kim, S. E. *et al.* (2003) 'Porous chitosan scaffold containing microspheres loaded with transforming growth factor- $\beta$ 1: Implications for cartilage tissue engineering', *Journal of Controlled Release*, 91(3), pp. 365–374. doi: [https://doi.org/10.1016/S0168-3659\(03\)00274-8](https://doi.org/10.1016/S0168-3659(03)00274-8).
- Kim, W. K. *et al.* (2019) 'Evaluation of cartilage regeneration of chondrocyte encapsulated gellan gum-based hyaluronic acid blended hydrogel', *International journal of biological macromolecules*. Elsevier, 141, pp. 51–59.
- Kloppenburg, M. and Berenbaum, F. (2020) 'Osteoarthritis year in review 2019: epidemiology and therapy', *Osteoarthritis and Cartilage*. Elsevier Ltd, 28(3), pp. 242–248. doi: [10.1016/j.joca.2020.01.002](https://doi.org/10.1016/j.joca.2020.01.002).
- Klotz, Barbara J. *et al.* (2016) 'Gelatin-Methacryloyl Hydrogels: Towards Biofabrication-Based Tissue Repair', *Trends in Biotechnology*. Elsevier Ltd, 34(5), pp. 394–407. doi: [10.1016/j.tibtech.2016.01.002](https://doi.org/10.1016/j.tibtech.2016.01.002).
- Klotz, Barbara J. *et al.* (2016) 'Gelatin-Methacryloyl Hydrogels: Towards Biofabrication-Based Tissue Repair', *Trends in Biotechnology*, 34(5), pp. 394–407. doi: <https://doi.org/10.1016/j.tibtech.2016.01.002>.
- Knight, E. and Przyborski, S. (2015) 'Advances in 3D cell culture technologies enabling tissue-like structures to be created in vitro', *Journal of Anatomy*. Blackwell Publishing Ltd, pp. 746–756. doi: [10.1111/joa.12257](https://doi.org/10.1111/joa.12257).
- Knowlton, S. and Tasoglu, S. (2016) 'A Bioprinted Liver-on-a-Chip for Drug Screening Applications', *Trends in Biotechnology*, 34(9), pp. 681–682. doi: <https://doi.org/10.1016/j.tibtech.2016.05.014>.
- Ko, C.-S. *et al.* (2009) 'Type II collagen-chondroitin sulfate-hyaluronan scaffold cross-linked by genipin for cartilage tissue engineering', *Journal of Bioscience and Bioengineering*. Elsevier, 107(2), pp. 177–182. doi: [10.1016/J.JBIOSEC.2008.09.020](https://doi.org/10.1016/J.JBIOSEC.2008.09.020).
- Koay, E. J. and Athanasiou, K. A. (2008) 'Hypoxic chondrogenic differentiation of human embryonic stem cells enhances cartilage protein synthesis and biomechanical functionality', *Osteoarthritis and Cartilage*. Elsevier Ltd, 16(12), pp. 1450–1456. doi: [10.1016/j.joca.2008.04.007](https://doi.org/10.1016/j.joca.2008.04.007).
- Koay, E. J., Hoben, G. M. B. and Athanasiou, K. A. (2007) 'Tissue Engineering with Chondrogenically Differentiated Human Embryonic Stem Cells', *Stem Cells*, 25(9), pp. 2183–2190. doi: [10.1634/stemcells.2007-0105](https://doi.org/10.1634/stemcells.2007-0105).

- Kobayashi, K., Huang, C. and Lodge, T. P. (1999) 'Thermoreversible gelation of aqueous methylcellulose solutions', *Macromolecules*. ACS Publications, 32(21), pp. 7070–7077.
- Kock, L., Van Donkelaar, C. C. and Ito, K. (2012) 'Tissue engineering of functional articular cartilage: The current status', *Cell and Tissue Research*, 347(3), pp. 613–627. doi: 10.1007/s00441-011-1243-1.
- Koga, H. *et al.* (2008) 'Comparison of mesenchymal tissues-derived stem cells for in vivo chondrogenesis: suitable conditions for cell therapy of cartilage defects in rabbit', *Cell and tissue research*. Springer, 333(2), pp. 207–215.
- Kolesky, D. B. *et al.* (2016) 'Three-dimensional bioprinting of thick vascularized tissues', *Proceedings of the National Academy of Sciences*. National Academy of Sciences, 113(12), pp. 3179–3184. doi: 10.1073/pnas.1521342113.
- Korhonen, R. K. *et al.* (2002) 'Comparison of the equilibrium response of articular cartilage in unconfined compression, confined compression and indentation', *Journal of Biomechanics*, 35(7), pp. 903–909. doi: 10.1016/S0021-9290(02)00052-0.
- Korhonen, R. K. *et al.* (2002) 'Superficial Collagen Network Modifies Differently Equilibrium Response of Articular Cartilage in Unconfined Compression and Indentation', *Transactions of the Orthopaedic Research Society*, 27(79), pp. 903–909. Available at: <http://luotain.uef.fi/content/abstracts/ORS/0079.pdf>.
- Kosik-Kozioł, A. *et al.* (2017) 'PLA short sub-micron fiber reinforcement of 3D bioprinted alginate constructs for cartilage regeneration', *Biofabrication*, 9(4). doi: 10.1088/1758-5090/aa90d7.
- Kouhi, M. *et al.* (2020) 'Injectable gellan gum/lignocellulose nanofibrils hydrogels enriched with melatonin loaded forsterite nanoparticles for cartilage tissue engineering: Fabrication, characterisation and cell culture studies', *Materials Science and Engineering: C*. Elsevier, p. 111114.
- Krogstad, D. V. *et al.* (2013) 'Effects of polymer and salt concentration on the structure and properties of triblock copolymer coacervate hydrogels', *Macromolecules*. ACS Publications, 46(4), pp. 1512–1518.
- Kuettner, K. E. (1992) 'Biochemistry of articular cartilage in health and disease', *Clinical Biochemistry*, 25(3), pp. 155–163. doi: 10.1016/0009-9120(92)90224-G.
- Kumar, A. *et al.* (2016) 'Low temperature additive manufacturing of three dimensional scaffolds for bone-tissue engineering applications: Processing related challenges and property assessment', *Materials Science and Engineering: R: Reports*, 103, pp. 1–39. doi: <https://doi.org/10.1016/j.mser.2016.01.001>.
- Kundu, B. *et al.* (2013) 'Silk fibroin biomaterials for tissue regenerations', *Advanced drug delivery reviews*. Elsevier, 65(4), pp. 457–470.
- Kundu, J. *et al.* (2015) 'An additive manufacturing-based PCL–alginate–chondrocyte bioprinted scaffold for cartilage tissue engineering', *Journal of tissue engineering and regenerative medicine*. Wiley Online Library, 9(11), pp. 1286–1297.
- Kusuhara, H. *et al.* (2009) 'Tissue engineering a model for the human ear: assessment of size, shape, morphology, and gene expression following seeding of different chondrocytes', *Wound Repair and Regeneration*. Wiley Online Library, 17(1), pp. 136–146.
- Kwon, H. *et al.* (2016a) 'Articular cartilage tissue engineering: The role of signaling molecules', *Cellular and Molecular Life Sciences*. Springer International Publishing, 73(6), pp. 1173–1194. doi: 10.1007/s00018-015-2115-8.
- Kwon, H. *et al.* (2016b) 'Articular cartilage tissue engineering: The role of signaling molecules', *Cellular and Molecular Life Sciences*. Springer International Publishing, 73(6), pp. 1173–1194. doi: 10.1007/s00018-015-2115-8.
- Kwon, H. *et al.* (2019) 'Surgical and tissue engineering strategies for articular cartilage and meniscus repair', *Nature Reviews Rheumatology*. Springer US, 15(9), pp. 550–570. doi: 10.1038/s41584-019-0255-1.
- Labat-Robert, J., Bihari-Varga, M. and Robert, L. (1990) 'Extracellular matrix', *FEBS Letters*, 268(2), pp. 386–393. doi: 10.1016/0014-5793(90)81291-U.
- Lai, W. M., Hou, J. S. and Mow, V. C. (1991) 'A triphasic theory for the swelling and deformation behaviors of articular cartilage', *Journal of Biomechanical Engineering*, 113(3), pp. 245–258. doi: 10.1115/1.2894880.
- Lancaster, M. A. *et al.* (2013) 'Cerebral organoids model human brain development and microcephaly', *Nature*. Nature Publishing Group, 501(7467), p. 373.
- Lane, N. E. and Schnitzer, T. J. (2012) 'Osteoarthritis', *Goldman's Cecil Medicine*. W.B. Saunders, pp. 1672–1676. doi: 10.1016/B978-1-4377-1604-7.00270-0.
- Langer, R. and Vacanti, J. P. (1993) 'Tissue engineering', *Science*, 260(5110), pp. 920 LP – 926. doi: 10.1126/science.8493529.
- Lee, H. *et al.* (2011) 'Optimizing gelling parameters of gellan gum for fibrocartilage tissue engineering', *Journal of Biomedical Materials Research Part B: Applied Biomaterials*. Wiley Online Library, 98(2), pp. 238–245.
- Lee, H. J. *et al.* (2008) 'Enhanced Chondrogenesis of Mesenchymal Stem Cells in Collagen Mimetic Peptide-Mediated Microenvironment', *Tissue Engineering Part A*. Mary Ann Liebert, Inc., publishers, 14(11), pp. 1843–1851. doi: 10.1089/ten.tea.2007.0204.
- Lee, J. E. *et al.* (2004) 'Effects of a Chitosan Scaffold Containing TGF- $\beta$ 1 Encapsulated Chitosan Microspheres on In Vitro Chondrocyte Culture', *Artificial Organs*, 28(9), pp. 829–839. doi: doi:10.1111/j.1525-1594.2004.00020.x.
- LEHMAN, T. (2011) 'Textbook of Pediatric Rheumatology, 6th Edition', *The Journal of Rheumatology*, 38(10), pp. 2285 LP – 2285. doi:

10.3899/jrheum.110630.

Lenas, P., Moos, M. and Luyten, F. P. (2009) 'Developmental Engineering: A New Paradigm for the Design and Manufacturing of Cell-Based Products. Part I: From Three-Dimensional Cell Growth to Biomimetics of In Vivo Development', *Tissue Engineering Part B: Reviews*. Mary Ann Liebert, Inc., publishers, 15(4), pp. 381–394. doi: 10.1089/ten.teb.2008.0575.

Levato, R. *et al.* (2014) 'Biofabrication of tissue constructs by 3D bioprinting of cell-laden microcarriers', *Biofabrication*. IOP Publishing, 6(3). doi: 10.1088/1758-5082/6/3/035020.

Levato, R. *et al.* (2017) 'The bio in the ink: cartilage regeneration with bioprintable hydrogels and articular cartilage-derived progenitor cells', *Acta Biomaterialia*. Acta Materialia Inc., 61, pp. 41–53. doi: 10.1016/j.actbio.2017.08.005.

Li, Z. and Zhang, M. (2005) 'Chitosan–alginate as scaffolding material for cartilage tissue engineering', *Journal of Biomedical Materials Research Part A*, 75A(2), pp. 485–493. doi: 10.1002/jbm.a.30449.

Liao, E. *et al.* (2007) 'Tissue-Engineered Cartilage Constructs Using Composite Hyaluronic Acid/Collagen I Hydrogels and Designed Poly(Propylene Fumarate) Scaffolds', *Tissue Engineering*, 13(3), pp. 537–550. doi: 10.1089/ten.2006.0117.

Lien, S.-M., Ko, L.-Y. and Huang, T.-J. (2009) 'Effect of pore size on ECM secretion and cell growth in gelatin scaffold for articular cartilage tissue engineering', *Acta Biomaterialia*, 5(2), pp. 670–679. doi: <https://doi.org/10.1016/j.actbio.2008.09.020>.

Lien, S.-M., Li, W.-T. and Huang, T.-J. (2008) 'Genipin-crosslinked gelatin scaffolds for articular cartilage tissue engineering with a novel crosslinking method', *Materials Science and Engineering: C*. Elsevier, 28(1), pp. 36–43. doi: 10.1016/j.MSEC.2006.12.015.

Lima, E. G. *et al.* (2006) 'The Effect of Applied Compressive Loading on Tissue-Engineered Cartilage Constructs Cultured with TGF- $\beta$ 3', in *2006 International Conference of the IEEE Engineering in Medicine and Biology Society*, pp. 779–782.

Linn, F. C. and Sokoloff, L. (1965) 'Movement and composition of interstitial fluid of cartilage', *Arthritis & Rheumatism*. John Wiley & Sons, Ltd, 8(4), pp. 481–494. doi: 10.1002/art.1780080402.

Liu, L. *et al.* (2013) 'Chitosan fibers enhanced gellan gum hydrogels with superior mechanical properties and water-holding capacity', *Carbohydrate polymers*. Elsevier, 97(1), pp. 152–158.

Loessner, D. *et al.* (2016) 'Functionalization, preparation and use of cell-laden gelatin methacryloyl–based hydrogels as modular tissue culture platforms', *Nature protocols*. Nature Publishing Group, 11(4), p. 727.

Loh, Q. L. and Choong, C. (2013) 'Three-dimensional scaffolds for tissue engineering applications: Role of porosity and pore size', *Tissue Engineering - Part B: Reviews*, 19(6), pp. 485–502. doi: 10.1089/ten.teb.2012.0437.

Lozano, R., Stevens, L., Thompson, Brianna C., *et al.* (2015) '3D printing of layered brain-like structures using peptide modified gellan gum substrates', *Biomaterials*. Elsevier Ltd, 67, pp. 264–273. doi: 10.1016/j.biomaterials.2015.07.022.

Lozano, R., Stevens, L., Thompson, Brianna C., *et al.* (2015) '3D printing of layered brain-like structures using peptide modified gellan gum substrates', *Biomaterials*. Elsevier, 67, pp. 264–273.

Lu, H. T. *et al.* (2019) 'Development of injectable fucoidan and biological macromolecules hybrid hydrogels for intra-articular delivery of platelet-rich plasma', *Marine Drugs*, 17(4). doi: 10.3390/md17040236.

Lu, X. L. and Mow, V. C. (2008) 'Biomechanics of articular cartilage and determination of material properties', *Medicine and Science in Sports and Exercise*, 40(2), pp. 193–199. doi: 10.1249/mss.0b013e31815cb1fc.

M. Iliescu, C.D. Hoemann, M.S. Shive, A.Chenite, M. D. B. (2008) 'Ultrastructure of Hybrid Chitosan–Glycerol Phosphate Blood Clots by Environmental Scanning Electron Microscopy', *Microscopy Research and Technique*, 71, pp. 236–247. doi: 10.1002/jemt.20545.

Ma, X. *et al.* (2018) '3D bioprinting of functional tissue models for personalized drug screening and in vitro disease modeling', *Advanced Drug Delivery Reviews*. Elsevier B.V., 132, pp. 235–251. doi: 10.1016/j.addr.2018.06.011.

Macrory, L. *et al.* (2009) 'An exploration of the ability of tepoxalin to ameliorate the degradation of articular cartilage in a canine in vitro model', *BMC Veterinary Research*. BioMed Central, 5(1), p. 25. doi: 10.1186/1746-6148-5-25.

Maitra, J. and Shukla, V. K. (2014) 'Cross-linking in Hydrogels - A Review', *American Journal of Polymer Science*, 4(2), pp. 25–31. doi: 10.5923/j.ajps.20140402.01.

Makris, E. A. *et al.* (2014) 'Developing functional musculoskeletal tissues through hypoxia and lysyl oxidase-induced collagen cross-linking', *Proceedings of the National Academy of Sciences*, 111(45), p. E4832 LP-E4841. doi: 10.1073/pnas.1414271111.

Makris, E. A. *et al.* (2015) 'Repair and tissue engineering techniques for articular cartilage', *Nature Reviews Rheumatology*. Nature Publishing Group, 11(1), pp. 21–34. doi: 10.1038/nrrheum.2014.157.

Malda, J. *et al.* (2003) 'Cartilage Tissue Engineering: Controversy in the Effect of Oxygen', *Critical Reviews in Biotechnology*. CRC Press LLC, pp. 175–194. doi: 10.1080/bty.23.3.175.

Malda, J. *et al.* (2013) '25th Anniversary Article: Engineering Hydrogels for Biofabrication', *Advanced Materials*, 25(36), pp. 5011–5028. doi: 10.1002/adma.201302042.

Maldonado, M. and Nam, J. (2013) 'The role of changes in extracellular matrix of cartilage in the presence of inflammation on the pathology of osteoarthritis', *BioMed Research International*, 2013. doi: 10.1155/2013/284873.

- Manda-Guiba, G. M. *et al.* (2012) 'Gellan gum: hydroxyapatite composite hydrogels for bone tissue engineering'. Wiley.
- Mandrycky, C. *et al.* (2016) '3D bioprinting for engineering complex tissues', *Biotechnology Advances*. Elsevier Inc., 34(4), pp. 422–434. doi: 10.1016/j.biotechadv.2015.12.011.
- Mangine, B., Rauch, J. T. and Middendorf, W. A. (2012) 'Physiologic Factors in Rehabilitation', *Physical Rehabilitation of the Injured Athlete*. W.B. Saunders, pp. 11–31. doi: 10.1016/B978-1-4377-2411-0.00002-2.
- Mansour, J. M. (2003) 'Biomechanics of Cartilage in: Kinesiol. Mech. pathomechanics Hum. Mov.', *Kinesiology: the mechanics and pathomechanics of human movement*, pp. 66–75. Available at: [http://web.mit.edu/cortiz/www/3.052/3.052CourseReader/27\\_BiomechanicsofCartilage.pdf](http://web.mit.edu/cortiz/www/3.052/3.052CourseReader/27_BiomechanicsofCartilage.pdf).
- Mansour, J. M. (2013) 'Biomechanics of cartilage', *Kinesiology: The Mechanics and Pathomechanics of Human Movement: Second Edition*, pp. 69–83.
- March, L. and Little, C. (2010) *Articular cartilage in health and disease*. Second Edi, *The Musculoskeletal System: Systems of the Body Series*. Second Edi. Elsevier Limited. doi: 10.1016/B978-0-7020-3377-3.00006-8.
- der Mark, K. *et al.* (1992) 'Type X collagen synthesis in human osteoarthritic cartilage. Indication of chondrocyte hypertrophy', *Arthritis & Rheumatism: Official Journal of the American College of Rheumatology*. Wiley Online Library, 35(7), pp. 806–811.
- Markstedt, K. *et al.* (2015) '@article{avila20163d, title={3D bioprinting of human chondrocyte-laden nanocellulose hydrogels for patient-specific auricular cartilage regeneration}, author={{\A}vila, H{{\e}ctor Mart{{\i}nez and Schwarz, Silke and Rotter, Nicole and Gatenholm, Paul},', *Biomacromolecules*. ACS Publications, 16(5), pp. 1489–1496.
- Maroudas, A. and Bullough, P. (1968) 'Permeability of articular cartilage [24]', *Nature*. Nature Publishing Group, pp. 1260–1261. doi: 10.1038/2191260a0.
- Martens, P. J., Bryant, S. J. and Anseth, K. S. (2003) 'Tailoring the Degradation of Hydrogels Formed from Multivinyl Poly(ethylene glycol) and Poly(vinyl alcohol) Macromers for Cartilage Tissue Engineering', *Biomacromolecules*. American Chemical Society, 4(2), pp. 283–292. doi: 10.1021/bm025666v.
- Martin, I. *et al.* (2001) 'Enhanced cartilage tissue engineering by sequential exposure of chondrocytes to FGF-2 during 2D expansion and BMP-2 during 3D cultivation', *Journal of Cellular Biochemistry*, 83(1), pp. 121–128. doi: 10.1002/jcb.1203.
- Matsusue, Y., Yamamuro, T. and Hama, H. (1993) 'Arthroscopic multiple osteochondral transplantation to the chondral defect in the knee associated with anterior cruciate ligament disruption', *Arthroscopy*. Elsevier, 9(3), pp. 318–321. doi: 10.1016/S0749-8063(05)80428-1.
- Melchels, F. P. W. *et al.* (2012) 'Additive manufacturing of tissues and organs', *Progress in Polymer Science*. Elsevier, 37(8), pp. 1079–1104.
- Melchels, F. P. W. *et al.* (2014) 'Development and characterisation of a new bioink for additive tissue manufacturing', *Journal of Materials Chemistry B*, 2(16), pp. 2282–2289. doi: 10.1039/c3tb21280g.
- Mescher, A. L. (2016) 'Junqueira's Basic Histology Text & Atlas (14th ed.)', (January), pp. 295–304.
- Meyer, U. *et al.* (2012) 'Cartilage defect regeneration by ex vivo engineered autologous microtissue - Preliminary results', *In Vivo*. International Institute of Anticancer Research, 26(2), pp. 251–257.
- Min, D. *et al.* (2018) 'Bioprinting of biomimetic skin containing melanocytes', *Experimental Dermatology*, 27(5), pp. 453–459. doi: 10.1111/exd.13376.
- Mironi-Harpaz, I. *et al.* (2012) 'Photopolymerization of cell-encapsulating hydrogels: Crosslinking efficiency versus cytotoxicity', *Acta Biomaterialia*, 8(5), pp. 1838–1848. doi: <https://doi.org/10.1016/j.actbio.2011.12.034>.
- Mironov, V., Prestwich, G. and Forgacs, G. (2007) 'Bioprinting living structures', *Journal of Materials Chemistry*. Royal Society of Chemistry, 17(20), pp. 2054–2060.
- Mitchell, N. and Shepard, N. (1976) 'The resurfacing of adult rabbit articular cartilage by multiple perforations through the subchondral bone', *JBJS*, 58(2). Available at: [https://journals.lww.com/jbjsjournal/Fulltext/1976/58020/The\\_resurfacing\\_of\\_adult\\_rabbit\\_articular.12.aspx](https://journals.lww.com/jbjsjournal/Fulltext/1976/58020/The_resurfacing_of_adult_rabbit_articular.12.aspx).
- Mithoefer, K. *et al.* (2009) 'Clinical Efficacy of the Microfracture Technique for Articular Cartilage Repair in the Knee: An Evidence-Based Systematic Analysis', *The American Journal of Sports Medicine*, 37(10), pp. 2053–2063. doi: 10.1177/0363546508328414.
- Miyagawa, Y. *et al.* (2011) 'A Microfabricated Scaffold Induces the Spheroid Formation of Human Bone Marrow-Derived Mesenchymal Progenitor Cells and Promotes Efficient Adipogenic Differentiation', *Tissue Engineering Part A*. Mary Ann Liebert Inc., 17(3–4), pp. 513–521. doi: 10.1089/ten.tea.2009.0810.
- Miyaki, S. *et al.* (2009) 'MicroRNA-140 is expressed in differentiated human articular chondrocytes and modulates interleukin-1 responses', *Arthritis & Rheumatism*, 60(9), pp. 2723–2730. doi: 10.1002/art.24745.
- Mizrahi, J. *et al.* (1986) 'The "instantaneous" deformation of cartilage: Effects of collagen fiber orientation and osmotic stress', *Biorheology*. IOS Press, 23(4), pp. 311–330. doi: 10.3233/BIR-1986-23402.
- Mizuno, S. *et al.* (2002) 'Hydrostatic fluid pressure enhances matrix synthesis and accumulation by bovine chondrocytes in three-dimensional culture', *Journal of Cellular Physiology*, 193(3), pp. 319–327. doi: 10.1002/jcp.10180.

- Mobasheri, A. *et al.* (2014) 'Chondrocyte and mesenchymal stem cell-based therapies for cartilage repair in osteoarthritis and related orthopaedic conditions', *Maturitas*. Elsevier Ireland Ltd, 78(3), pp. 188–198. doi: 10.1016/j.maturitas.2014.04.017.
- Mohd Azam, N. A. N. and Amin, K. A. M. (2017) 'The Physical and Mechanical Properties of Gellan Gum Films Incorporated Manuka Honey as Wound Dressing Materials', *IOP Conference Series: Materials Science and Engineering*, 209(1). doi: 10.1088/1757-899X/209/1/012027.
- Mollon, B. *et al.* (2013) 'The clinical status of cartilage tissue regeneration in humans', *Osteoarthritis and Cartilage*. Elsevier Ltd, 21(12), pp. 1824–1833. doi: 10.1016/j.joca.2013.08.024.
- Montembault, A. *et al.* (2006) 'A material decoy of biological media based on chitosan physical hydrogels: application to cartilage tissue engineering', *Biochimie*, 88(5), pp. 551–564. doi: <https://doi.org/10.1016/j.biochi.2006.03.002>.
- Moroni, L., Boland, T., *et al.* (2018) 'Biofabrication: a guide to technology and terminology', *Trends in biotechnology*. Elsevier, 36(4), pp. 384–402.
- Moroni, L., Burdick, J. A., *et al.* (2018) 'Biofabrication strategies for 3D in vitro models and regenerative medicine', *Nature Reviews Materials*. Springer US, 3(5), pp. 21–37. doi: 10.1038/s41578-018-0006-y.
- Morris, E. R., Nishinari, K. and Rinaudo, M. (2012) 'Gelation of gellan – A review', *Food Hydrocolloids*, 28(2), pp. 373–411. doi: <https://doi.org/10.1016/j.foodhyd.2012.01.004>.
- Mota, C. *et al.* (2015) 'Additive manufacturing techniques for the production of tissue engineering constructs', *Journal of tissue engineering and regenerative medicine*. Wiley Online Library, 9(3), pp. 174–190.
- Mouser, V. H. M. *et al.* (2016a) 'Yield stress determines bioprintability of hydrogels based on gelatin-methacryloyl and gellan gum for cartilage bioprinting', *Biofabrication*. doi: 10.1088/1758-5090/8/3/035003.
- Mouser, V. H. M. *et al.* (2016b) 'Yield stress determines bioprintability of hydrogels based on gelatin-methacryloyl and gellan gum for cartilage bioprinting', *Biofabrication*, 8(3), pp. 1–24. doi: 10.1088/1758-5090/8/3/035003.
- Mouser, V. H. M. *et al.* (2017) 'Three-Dimensional Bioprinting and Its Potential in the Field of Articular Cartilage Regeneration', *Cartilage*, 8(4), pp. 327–340. doi: 10.1177/1947603516665445.
- Mouser, V. H. M. *et al.* (2020) 'Bio-ink development for three-dimensional bioprinting of hetero-cellular cartilage constructs', *Connective Tissue Research*. Taylor & Francis, 61(2), pp. 137–151. doi: 10.1080/03008207.2018.1553960.
- Mow, V. C. *et al.* (1980) 'Biphasic creep and stress relaxation of articular cartilage in compression: Theory and experiments', *Journal of Biomechanical Engineering*, 102(1), pp. 73–84. doi: 10.1115/1.3138202.
- Muir, H., Bullough, P. and Maroudas, A. (1970) 'The distribution of collagen in human articular cartilage with some of its physiological implications.', *Journal of Bone and Joint Surgery - Series B*. The British Editorial Society of Bone and Joint Surgery, 52(3), pp. 554–563. doi: 10.1302/0301-620X.52B3.554.
- Müller, F. A. *et al.* (2006) 'Cellulose-based scaffold materials for cartilage tissue engineering', *Biomaterials*. Elsevier, 27(21), pp. 3955–3963. doi: 10.1016/j.biomaterials.2006.02.031.
- Müller, M. *et al.* (2015) 'Nanostructured Pluronic hydrogels as bioinks for 3D bioprinting', *Biofabrication*. IOP Publishing, 7(3). doi: 10.1088/1758-5090/7/3/035006.
- Müller, M. *et al.* (2017) 'Alginate sulfate--nanocellulose bioinks for cartilage bioprinting applications', *Annals of biomedical engineering*. Springer, 45(1), pp. 210–223.
- Murakami, S. *et al.* (2000) 'Up-regulation of the chondrogenic *Sox9* gene by fibroblast growth factors is mediated by the mitogen-activated protein kinase pathway', *Proceedings of the National Academy of Sciences*, 97(3), pp. 1113 LP – 1118. doi: 10.1073/pnas.97.3.1113.
- Murphy, S. V. and Atala, A. (2014a) '3D bioprinting of tissues and organs', *Nature Biotechnology*. Nature Publishing Group, pp. 773–785. doi: 10.1038/nbt.2958.
- Murphy, S. V. and Atala, A. (2014b) '3D bioprinting of tissues and organs', *Nature Biotechnology*. Nature Publishing Group, 32(8), pp. 773–785. doi: 10.1038/nbt.2958.
- Musumeci, G. *et al.* (2011) 'Oa cartilage derived chondrocytes encapsulated in poly(ethylene glycol) diacrylate (PEGDA) for the evaluation of cartilage restoration and apoptosis in an in vitro model', *Histology and Histopathology*, 26(10), pp. 1265–1278. doi: 10.14670/HH-26.1265.
- Nandagiri, V. K. *et al.* (2011) 'Incorporation of PLGA nanoparticles into porous chitosan-gelatin scaffolds: Influence on the physical properties and cell behavior', *Journal of the Mechanical Behavior of Biomedical Materials*. Elsevier Ltd, 4(7), pp. 1318–1327. doi: 10.1016/j.jmbbm.2011.04.019.
- Natoli, R. M., Revell, C. M. and Athanasiou, K. A. (2009) 'Chondroitinase ABC Treatment Results in Greater Tensile Properties of Self-Assembled Tissue-Engineered Articular Cartilage', *Tissue Engineering Part A*, 15(10), pp. 3119–3128. doi: 10.1089/ten.tea.2008.0478.
- Nguyen, D. *et al.* (2017) 'Cartilage Tissue Engineering by the 3D Bioprinting of iPS Cells in a Nanocellulose/Alginate Bioink', *Scientific Reports*, 7(1), pp. 1–10. doi: 10.1038/s41598-017-00690-y.
- Norotte, C. *et al.* (2009) 'Scaffold-free vascular tissue engineering using bioprinting', *Biomaterials*, 30(30), pp. 5910–5917. doi:

<https://doi.org/10.1016/j.biomaterials.2009.06.034>.

O'Connell, C. D. *et al.* (2016) 'Development of the Biopen: a handheld device for surgical printing of adipose stem cells at a chondral wound site', *Biofabrication*. {IOP} Publishing, 8(1), p. 15019. doi: 10.1088/1758-5090/8/1/015019.

Okay, O. (2009) 'General properties of hydrogels', in *Hydrogel sensors and actuators*. Springer, pp. 1–14.

Oliveira, J. T. *et al.* (2009) 'Performance of new gellan gum hydrogels combined with human articular chondrocytes for cartilage regeneration when subcutaneously implanted in nude mice', *Journal of tissue engineering and regenerative medicine*. Wiley Online Library, 3(7), pp. 493–500.

Oliveira, J. T., Martins, L., *et al.* (2010a) 'Gellan gum: A new biomaterial for cartilage tissue engineering applications', *Journal of Biomedical Materials Research - Part A*. doi: 10.1002/jbm.a.32574.

Oliveira, J. T., Martins, L., *et al.* (2010b) 'Gellan gum: A new biomaterial for cartilage tissue engineering applications', *Journal of Biomedical Materials Research - Part A*, 93(3), pp. 852–863. doi: 10.1002/jbm.a.32574.

Oliveira, João T., Santos, T. C., *et al.* (2010) 'Gellan gum injectable hydrogels for cartilage tissue engineering applications: In vitro studies and preliminary in vivo evaluation', *Tissue Engineering - Part A*. doi: 10.1089/ten.tea.2009.0117.

Oliveira, João T., Gardel, L. S., *et al.* (2010) 'Injectable gellan gum hydrogels with autologous cells for the treatment of rabbit articular cartilage defects', *Journal of Orthopaedic Research*. doi: 10.1002/jor.21114.

Oliveira, M. B. *et al.* (2016) 'Autonomous osteogenic differentiation of hASCs encapsulated in methacrylated gellan-gum hydrogels', *Acta Biomaterialia*. Acta Materialia Inc., 41, pp. 119–132. doi: 10.1016/j.actbio.2016.05.033.

Onofrillo, C. *et al.* (2018) 'Biofabrication of human articular cartilage: A path towards the development of a clinical treatment', *Biofabrication*. IOP Publishing, 10(4), p. 45006. doi: 10.1088/1758-5090/aad8d9.

Osmalek, T., Froelich, A. and Tasarek, S. (2014) 'Application of gellan gum in pharmacy and medicine', *International Journal of Pharmaceutics*, 466(1–2), pp. 328–340. doi: 10.1016/j.ijpharm.2014.03.038.

Ovalle, W. K. and Nahirney, P. C. (2008) *Netter's essential histology* /. 1st ed. Philadelphia : Saunders/Elsevier,. Available at: <http://www.loc.gov/catdir/toc/ecip079/2007003957.html>.

Ozbolat, I. T. and Hospodiuk, M. (2016) 'Current advances and future perspectives in extrusion-based bioprinting', *Biomaterials*, 76, pp. 321–343. doi: <https://doi.org/10.1016/j.biomaterials.2015.10.076>.

Ozbolat, I. T., Peng, W. and Ozbolat, V. (2016) 'Application areas of 3D bioprinting', *Drug Discovery Today*. Elsevier Ltd, 21(8), pp. 1257–1271. doi: 10.1016/j.drudis.2016.04.006.

Ozbolat, I. T. and Yu, Y. (2013) 'Bioprinting toward organ fabrication: challenges and future trends', *IEEE Transactions on Biomedical Engineering*. IEEE, 60(3), pp. 691–699.

Ozeki, M. and Tabata, Y. (2005) 'In vivo degradability of hydrogels prepared from different gelatins by various cross-linking methods', *Journal of Biomaterials Science, Polymer Edition*. Taylor & Francis, 16(5), pp. 549–561. doi: 10.1163/1568562053783731.

Pacelli, S. *et al.* (2015) 'Injectable and photocross-linkable gels based on gellan gum methacrylate: A new tool for biomedical application', *International Journal of Biological Macromolecules*. Elsevier B.V., 72, pp. 1335–1342. doi: 10.1016/j.ijbiomac.2014.10.046.

Pacelli, S. *et al.* (2016) 'Gellan gum methacrylate and laponite as an innovative nanocomposite hydrogel for biomedical applications', *European Polymer Journal*. Elsevier Ltd, 77, pp. 114–123. doi: 10.1016/j.eurpolymj.2016.02.007.

Pantani, R. and Turng, L. S. (2015) 'Manufacturing of advanced biodegradable polymeric components', *Journal of Applied Polymer Science*, 132(48). doi: 10.1002/app.42889.

Panwar, A. and Tan, L. P. (2016) 'Current status of bioinks for micro-extrusion-based 3D bioprinting', *Molecules*, 21(6). doi: 10.3390/molecules21060685.

Park, H. *et al.* (2015) 'Regeneration of intervertebral disc using gellan sponge loading PLGA microspheres', *Polymer Korea*. The Polymer Society of Korea, 39(1), pp. 144–150.

Parsons, J. R. and Black, J. (1977) 'The viscoelastic shear behavior of normal rabbit articular cartilage', *Journal of Biomechanics*. Elsevier, 10(1), pp. 21–29. doi: 10.1016/0021-9290(77)90026-4.

Parvizi, J. (2010) *High Yield Orthopaedics E-Book*. Elsevier Health Sciences.

ParviziMD, J. and KimMD, G. (2010) 'Chapter 39 Cartilage', *High Yield Orthopaedics*, 1, pp. 80–81. doi: 10.1016/B978-1-4160-0236-9/00050-X.

Pati, F., Gantelius, J. and Svahn, H. A. (2016) '3D Bioprinting of Tissue/Organ Models', *Angewandte Chemie - International Edition*, 55(15), pp. 4650–4665. doi: 10.1002/anie.201505062.

Pavelka, M. and Roth, J. (2010) 'Articular Cartilage', in *Functional Ultrastructure*. Vienna: Springer Vienna, pp. 294–295. doi: 10.1007/978-3-211-99390-3\_151.

Paxton, N. *et al.* (2017a) 'Proposal to assess printability of bioinks for extrusion-based bioprinting and evaluation of rheological properties

- governing bioprintability', *Biofabrication*. IOP Publishing, 9(4), p. 44107.
- Paxton, N. *et al.* (2017b) 'Proposal to assess printability of bioinks for extrusion-based bioprinting and evaluation of rheological properties governing bioprintability', *Biofabrication*. IOP Publishing, 9(4). doi: 10.1088/1758-5090/aa8dd8.
- Pearle, A. D., Warren, R. F. and Rodeo, S. A. (2005) 'Basic Science of Articular Cartilage and Osteoarthritis', *Clinics in Sports Medicine*. Elsevier, 24(1), pp. 1–12. doi: 10.1016/J.CSM.2004.08.007.
- Perdisa, F. *et al.* (2019) 'Biologic Solutions for Articular Cartilage Healing', in Doral, M. N. *et al.* (eds) *Intraarticular Fractures: Minimally Invasive Surgery, Arthroscopy*. Cham: Springer International Publishing, pp. 31–40. doi: 10.1007/978-3-319-97602-0\_5.
- Pereira, D. R. *et al.* (2018) 'Nanocellulose reinforced gellan-gum hydrogels as potential biological substitutes for annulus fibrosus tissue regeneration', *Nanomedicine: Nanotechnology, Biology and Medicine*. Elsevier, 14(3), pp. 897–908.
- Pereira, R. F., Almeida, H. A. and Bártolo, P. J. (2013) 'Biofabrication of hydrogel constructs', in *Drug Delivery Systems: Advanced Technologies Potentially Applicable in Personalised Treatment*. Springer, pp. 225–254.
- Petta, D. *et al.* (2018) '3D bioprinting of a hyaluronan bioink through enzymatic-and visible light-crosslinking', *Biofabrication*. IOP Publishing, 10(4). doi: 10.1088/1758-5090/aadf58.
- Pierog, M., Gierszewska-Drużyńska, M. and Ostrowska-Czubenko, J. (2009) 'Effect of ionic crosslinking agents on swelling behavior of chitosan hydrogel membranes', *Progress on Chemistry and Application of Chitin and its Derivatives*. Polish Chitin Society, Łódź, 75, p. 82.
- Pitarresi, G. *et al.* (2020) 'New gellan gum-graft-poly(D,L-lactide-co-glycolide) copolymers as promising bioinks: Synthesis and characterisation', *International Journal of Biological Macromolecules*. Elsevier B.V, 162, pp. 1653–1667. doi: 10.1016/j.ijbiomac.2020.07.254.
- Pogue, R. and Lyons, K. (2006) 'BMP Signaling in the Cartilage Growth Plate', *Current Topics in Developmental Biology*. Academic Press, 76, pp. 1–48. doi: 10.1016/S0070-2153(06)76001-X.
- POOLE, C. A. (1997) 'Review. Articular cartilage chondrons: form, function and failure', *Journal of Anatomy*. Cambridge University Press, 191(1), pp. 1–13. doi: 10.1046/j.1469-7580.1997.19110001.x.
- Poole, C. A., Flint, M. H. and Beaumont, B. W. (1987) 'Chondrons in cartilage: Ultrastructural analysis of the pericellular microenvironment in adult human articular cartilages', *Journal of Orthopaedic Research*, 5(4), pp. 509–522. doi: 10.1002/jor.1100050406.
- Pritzker, K. P. H. (2011) 'Osteoarthritis: Joint instability and OA: Do animal models provide insights?', *Nature Reviews Rheumatology*. Nature Publishing Group, pp. 444–445. doi: 10.1038/nrrheum.2011.104.
- Pullig, O. *et al.* (2000) 'Chondrocyte differentiation in human osteoarthritis: expression of osteocalcin in normal and osteoarthritic cartilage and bone', *Calcified tissue international*. Springer, 67(3), pp. 230–240.
- Quinn, F. X. *et al.* (1993) 'The conformational properties of gellan gum hydrogels', *Polymer gels and networks*. Elsevier, 1(2), pp. 93–114.
- Raghunath, J. *et al.* (2007) 'Biomaterials and scaffold design: key to tissue-engineering cartilage', *Biotechnology and Applied Biochemistry*, 46(2), p. 73. doi: 10.1042/ba20060134.
- Ramaiahgari, S. C. *et al.* (2014) 'A 3D in vitro model of differentiated HepG2 cell spheroids with improved liver-like properties for repeated dose high-throughput toxicity studies', *Archives of toxicology*. Springer, 88(5), pp. 1083–1095.
- Raucci, M. G. *et al.* (2019) 'Bioactivation routes of gelatin-based scaffolds to enhance at nanoscale level bone tissue regeneration', *Frontiers in bioengineering and biotechnology*. Frontiers, 7, p. 27.
- Redman, S. N. *et al.* (2005) 'Current strategies for articular cartilage repair', *European Cells and Materials*, 9(0), pp. 23–32. doi: 10.22203/eCM.v009a04.
- Rencsok, M. *et al.* (2017) 'Double printing of hyaluronic acid / poly ( glycidol ) hybrid hydrogels with poly (  $\epsilon$ -caprolactone ) for MSC chondrogenesis', *Biofabrication*. IOP Publishing, 9, p. 044108.
- Ribeiro, A. *et al.* (2018) 'Assessing bioink shape fidelity to aid material development in 3D bioprinting', *Biofabrication*. IOP Publishing, 10(1). doi: 10.1088/1758-5090/aa90e2.
- Rodriguez, M. J. *et al.* (2017) 'Silk based bioinks for soft tissue reconstruction using 3-dimensional (3D) printing with in vitro and in vivo assessments', *Biomaterials*, 117, pp. 105–115. doi: https://doi.org/10.1016/j.biomaterials.2016.11.046.
- Roseti, L. *et al.* (2018) 'Three-dimensional bioprinting of cartilage by the use of stem cells: A strategy to improve regeneration', *Materials*, 11(9). doi: 10.3390/ma11091749.
- Russell, W. M. S. and Burch, R. L. (1959) *The principles of humane experimental technique*. Methuen.
- Sakkas, L. I. and Platsoucas, C. D. (2007) 'The role of T cells in the pathogenesis of osteoarthritis', *Arthritis & Rheumatism*, 56(2), pp. 409–424. doi: doi:10.1002/art.22369.
- Santos, A. R. C., Almeida, H. A. and Bártolo, P. J. (2013) 'Additive manufacturing techniques for scaffold-based cartilage tissue engineering: A review on various additive manufacturing technologies in generating scaffolds for cartilage tissue engineering', *Virtual and Physical Prototyping*. Taylor & Francis, 8(3), pp. 175–186. doi: 10.1080/17452759.2013.838825.

- Sasikala, L., Rathinamoorthy, R. and Dhurai, B. (2018) 'Optimization of process conditions for chitosan-manuka honey film as wound contact layer for wound dressings', *Wound medicine*. Elsevier, 23, pp. 11–21.
- Sauerland, K., Raiss, R. X. and Steinmeyer, J. (2003) 'Proteoglycan metabolism and viability of articular cartilage explants as modulated by the frequency of intermittent loading', *Osteoarthritis and Cartilage*, 11(5), pp. 343–350. doi: [https://doi.org/10.1016/S1063-4584\(03\)00007-4](https://doi.org/10.1016/S1063-4584(03)00007-4).
- Scalzone, A. *et al.* (2019) 'The interplay between chondrocyte spheroids and mesenchymal stem cells boosts cartilage regeneration within a 3D natural-based hydrogel', *Scientific Reports*, 9(1), pp. 1–12. doi: [10.1038/s41598-019-51070-7](https://doi.org/10.1038/s41598-019-51070-7).
- Scalzone, A. *et al.* (2020) 'pH-Triggered Adhesiveness and Cohesiveness of Chondroitin Sulfate-Catechol Biopolymer for Biomedical Applications', *Frontiers in bioengineering and biotechnology*. Frontiers, 8, p. 712.
- Schacht, K. *et al.* (2015) 'Biofabrication of Cell-Loaded 3D Spider Silk Constructs', *Angewandte Chemie International Edition*, 54(9), pp. 2816–2820. doi: [doi:10.1002/anie.201409846](https://doi.org/10.1002/anie.201409846).
- Schinagl, R. M. *et al.* (1997) 'Depth-dependent confined compression modulus of full-thickness bovine articular cartilage', *Journal of Orthopaedic Research*. Raven Press Ltd, 15(4), pp. 499–506. doi: [10.1002/jor.1100150404](https://doi.org/10.1002/jor.1100150404).
- Schubert, T. *et al.* (2009) 'Long-term effects of chondrospheres on cartilage lesions in an autologous chondrocyte implantation model as investigated in the SCID mouse model', *International Journal of Molecular Medicine*. Spandidos Publications, 23(4), pp. 455–460. doi: [10.3892/ijmm.00000151](https://doi.org/10.3892/ijmm.00000151).
- Schulz, R. M. and Bader, A. (2007) 'Cartilage tissue engineering and bioreactor systems for the cultivation and stimulation of chondrocytes', *European Biophysics Journal*, 36(4), pp. 539–568. doi: [10.1007/s00249-007-0139-1](https://doi.org/10.1007/s00249-007-0139-1).
- Scotti, C. *et al.* (2010) 'Effect of in vitro culture on a chondrocyte-fibrin glue hydrogel for cartilage repair', *Knee Surgery, Sports Traumatology, Arthroscopy*, 18(10), pp. 1400–1406. doi: [10.1007/s00167-009-1014-7](https://doi.org/10.1007/s00167-009-1014-7).
- Setton, L. A., Elliott, D. M. and Mow, V. C. (1999) 'Altered mechanics of cartilage with osteoarthritis: Human osteoarthritis and an experimental model of joint degeneration', *Osteoarthritis and Cartilage*, 7(1), pp. 2–14. doi: [10.1053/joca.1998.0170](https://doi.org/10.1053/joca.1998.0170).
- Shetty, A. A. *et al.* (2014) *Techniques in cartilage repair surgery, Techniques in Cartilage Repair Surgery*. doi: [10.1007/978-3-642-41921-8](https://doi.org/10.1007/978-3-642-41921-8).
- Shin, H., Olsen, B. D. and Khademhosseini, A. (2012) 'The mechanical properties and cytotoxicity of cell-laden double-network hydrogels based on photocrosslinkable gelatin and gellan gum biomacromolecules', *Biomaterials*. Elsevier, 33(11), pp. 3143–3152.
- Shin, H., Olsen, B. D. and Khademhosseini, A. (2014) 'Gellan gum microgel-reinforced cell-laden gelatin hydrogels', *Journal of Materials Chemistry B*. Royal Society of Chemistry, 2(17), pp. 2508–2516.
- Silva-Correia, J. *et al.* (2011) 'Gellan gum and its methacrylated derivatives as in situ gelling mucoadhesive formulations of pilocarpine: In vitro and in vivo studies', *Journal of tissue engineering and regenerative medicine*. Wiley Online Library, 5(6), pp. e97–e107.
- Silva-Correia, J. *et al.* (2013) 'Biocompatibility evaluation of ionic- and photo-crosslinked methacrylated gellan gum hydrogels: In vitro and in vivo study', *Advanced Healthcare Materials*, 2(4), pp. 568–575. doi: [10.1002/adhm.201200256](https://doi.org/10.1002/adhm.201200256).
- da Silva, L. P. *et al.* (2014) 'Engineering cell-adhesive gellan gum spongy-like hydrogels for regenerative medicine purposes', *Acta biomaterialia*. Elsevier, 10(11), pp. 4787–4797.
- Simon, T. M. and Jackson, D. W. (2018) 'Articular Cartilage: Injury Pathways and Treatment Options', *Sports Medicine and Arthroscopy Review*, 26(1), pp. 31–39.
- Singh, M. *et al.* (2010) 'Inkjet Printing—Process and Its Applications', *Advanced Materials*, 22(6), pp. 673–685. doi: [doi:10.1002/adma.200901141](https://doi.org/10.1002/adma.200901141).
- Singh, Y. P., Bhardwaj, N. and Mandal, B. B. (2016) 'Potential of Agarose/Silk Fibroin Blended Hydrogel for in Vitro Cartilage Tissue Engineering', *ACS Applied Materials & Interfaces*. American Chemical Society, 8(33), pp. 21236–21249. doi: [10.1021/acsami.6b08285](https://doi.org/10.1021/acsami.6b08285).
- Sittinger, M. *et al.* (1996) 'Resorbable polyesters in cartilage engineering: Affinity and biocompatibility of polymer fiber structures to chondrocytes', *Journal of Biomedical Materials Research*, 33(2), pp. 57–63. doi: [doi:10.1002/\(SICI\)1097-4636\(199622\)33:2<57::AID-JBM1>3.0.CO;2-K](https://doi.org/10.1002/(SICI)1097-4636(199622)33:2<57::AID-JBM1>3.0.CO;2-K).
- Skaalure, S. C., Chu, S. and Bryant, S. J. (2015) 'An Enzyme-Sensitive PEG Hydrogel Based on Aggrecan Catabolism for Cartilage Tissue Engineering', *Advanced Healthcare Materials*, 4(3), pp. 420–431. doi: [10.1002/adhm.201400277](https://doi.org/10.1002/adhm.201400277).
- Smith, A. M. *et al.* (2007) 'An initial evaluation of gellan gum as a material for tissue engineering applications', *Journal of Biomaterials Applications*, 22(3), pp. 241–254. doi: [10.1177/0885328207076522](https://doi.org/10.1177/0885328207076522).
- Sodupe-Ortega, E. *et al.* (2018) 'Accurate calibration in multi-material 3D bioprinting for tissue engineering', *Materials*, 11(8), pp. 1–19. doi: [10.3390/ma11081402](https://doi.org/10.3390/ma11081402).
- Sohn, D. H. *et al.* (2012) 'Plasma proteins present in osteoarthritic synovial fluid can stimulate cytokine production via Toll-like receptor 4', *Arthritis Research and Therapy*, 14(1), pp. 1–13. doi: [10.1186/ar3555](https://doi.org/10.1186/ar3555).
- Sommar, P. *et al.* (2010) 'Engineering three-dimensional cartilage- and bone-like tissues using human dermal fibroblasts and macroporous gelatine microcarriers', *Journal of Plastic, Reconstructive and Aesthetic Surgery*. Elsevier Ltd, 63(6), pp. 1036–1046. doi: [10.1016/j.bjps.2009.02.072](https://doi.org/10.1016/j.bjps.2009.02.072).

- Sophia Fox, A. J., Bedi, A. and Rodeo, S. A. (2009) 'The basic science of articular cartilage: Structure, composition, and function', *Sports Health*, 1(6), pp. 461–468. doi: 10.1177/1941738109350438.
- Spiller, K. L., Maher, S. A. and Lowman, A. M. (2011) 'Hydrogels for the repair of articular cartilage defects', *Tissue Engineering - Part B: Reviews*, 17(4), pp. 281–299. doi: 10.1089/ten.teb.2011.0077.
- Squires, G. R. *et al.* (2003) 'The pathobiology of focal lesion development in aging human articular cartilage and molecular matrix changes characteristic of osteoarthritis', *Arthritis & Rheumatism*, 48(5), pp. 1261–1270. doi: doi:10.1002/art.10976.
- Sridhar, B. V. *et al.* (2014) 'Covalently tethered TGF- $\beta$ 1 with encapsulated chondrocytes in a PEG hydrogel system enhances extracellular matrix production', *Journal of biomedical materials research. Part A*. 2014/02/26, 102(12), pp. 4464–4472. doi: 10.1002/jbm.a.35115.
- Steadman, J. R., Rodkey, W. G. and Rodrigo, J. J. (2001) 'Microfracture: Surgical Technique and Rehabilitation to Treat Chondral Defects', *A Publication of The Association of Bone and Joint Surgeons® | CORR®*, 391. Available at: [https://journals.lww.com/clinorthop/Fulltext/2001/10001/Microfracture\\_\\_Surgical\\_Technique\\_and.33.aspx](https://journals.lww.com/clinorthop/Fulltext/2001/10001/Microfracture__Surgical_Technique_and.33.aspx).
- Stevens, L. R. *et al.* (2016a) 'Gellan gum: A new biomaterial for cartilage tissue engineering applications', *Biomaterials Science*, 4(9), pp. 1276–1290. doi: 10.1039/c6bm00322b.
- Stevens, L. R. *et al.* (2016b) 'Tissue engineering with gellan gum', *Biomaterials Science*, 4(9), pp. 1276–1290. doi: 10.1039/c6bm00322b.
- Sun, L., Wang, X. and Kaplan, D. L. (2011) 'A 3D cartilage - Inflammatory cell culture system for the modeling of human osteoarthritis', *Biomaterials*. Elsevier Ltd, 32(24), pp. 5581–5589. doi: 10.1016/j.biomaterials.2011.04.028.
- Sun, X. *et al.* (2018) 'Collagen-based porous scaffolds containing PLGA microspheres for controlled kartogenin release in cartilage tissue engineering', *Artificial Cells, Nanomedicine and Biotechnology*. Informa UK Limited, trading as Taylor & Francis Group, 46(8), pp. 1957–1966. doi: 10.1080/21691401.2017.1397000.
- Sydney Gladman, A. *et al.* (2016) 'Biomimetic 4D printing', *Nature Materials*, 15(4), pp. 413–418. doi: 10.1038/nmat4544.
- Szymańska, E. *et al.* (2015) 'The effect of  $\beta$ -glycerophosphate crosslinking on chitosan cytotoxicity and properties of hydrogels for vaginal application', *Polymers*, 7(11), pp. 2223–2244. doi: 10.3390/polym7111510.
- Tanaka, N. *et al.* (2016) 'Microcasting with agarose gel via degassed polydimethylsiloxane molds for repellency-guided cell patterning', *RSC advances*. Royal Society of Chemistry, 6(60), pp. 54754–54762.
- Thakker, R. V. *et al.* (2017) *Genetics of bone biology and skeletal disease*. Academic Press.
- Theodoropoulos, J. S. *et al.* (2011) 'Integration of tissue-engineered cartilage with host cartilage: An in vitro model', *Clinical Orthopaedics and Related Research*, 469(10), pp. 2785–2795. doi: 10.1007/s11999-011-1856-4.
- Thirumala, S., Gimble, J. M. and Devireddy, R. V. (2013) 'Methylcellulose based thermally reversible hydrogel system for tissue engineering applications', *Cells*. Multidisciplinary Digital Publishing Institute, 2(3), pp. 460–475.
- Thorvaldsson, A. *et al.* (2013) 'Development of nanofiber-reinforced hydrogel scaffolds for nucleus pulposus regeneration by a combination of electrospinning and spraying technique', *Journal of applied polymer science*. Wiley Online Library, 128(2), pp. 1158–1163.
- Tian, H. *et al.* (2013) 'Construction of self-assembled cartilage tissue from bone marrow mesenchymal stem cells induced by hypoxia combined with GDF-5', *Journal of Huazhong University of Science and Technology [Medical Sciences]*, 33(5), pp. 700–706. doi: 10.1007/s11596-013-1183-y.
- van Tienen, T. G. *et al.* (2002) 'Tissue ingrowth and degradation of two biodegradable porous polymers with different porosities and pore sizes', *Biomaterials*, 23(8), pp. 1731–1738. doi: [https://doi.org/10.1016/S0142-9612\(01\)00280-0](https://doi.org/10.1016/S0142-9612(01)00280-0).
- Titmarsh, D. *et al.* (2011) 'Optimization of flowrate for expansion of human embryonic stem cells in perfusion microbioreactors', *Biotechnology and Bioengineering*, 108(12), pp. 2894–2904. doi: doi:10.1002/bit.23260.
- Tonda-Turo, C. *et al.* (2020) 'Photocurable chitosan as bioink for cellularized therapies towards personalized scaffold architecture', *Bioprinting*. Elsevier Ltd, 18(December 2019), p. e00082. doi: 10.1016/j.bprint.2020.e00082.
- Tuan, R. S., Boland, G. and Tuli, R. (2002) 'Adult mesenchymal stem cells and cell-based tissue engineering', *Arthritis Res Ther*, 5(1), p. 32. doi: 10.1186/ar614.
- Unagolla, J. M. and Jayasuriya, A. C. (2020) 'Hydrogel-based 3D bioprinting: A comprehensive review on cell-laden hydrogels, bioink formulations, and future perspectives', *Applied Materials Today*. Elsevier Ltd, 18, p. 100479. doi: 10.1016/j.apmt.2019.100479.
- Vanderburgh, J., Sterling, J. A. and Guelcher, S. A. (2017) '3D Printing of Tissue Engineered Constructs for In Vitro Modeling of Disease Progression and Drug Screening', *Annals of Biomedical Engineering*. Springer US, 45(1), pp. 164–179. doi: 10.1007/s10439-016-1640-4.
- Varghese, S. *et al.* (2008) 'Chondroitin sulfate based niches for chondrogenic differentiation of mesenchymal stem cells', *Matrix Biology*, 27(1), pp. 12–21. doi: <https://doi.org/10.1016/j.matbio.2007.07.002>.
- Vepari, C. and Kaplan, D. L. (2007) 'Silk as a biomaterial', *Progress in polymer science*. Elsevier, 32(8–9), pp. 991–1007.
- Vetter, U. *et al.* (1986) 'Human fetal and adult chondrocytes. Effect of insulinlike growth factors I and II, insulin, and growth hormone on clonal growth.', *The Journal of Clinical Investigation*. The American Society for Clinical Investigation, 77(6), pp. 1903–1908. doi: 10.1172/JCI112518.

- Vieira, S. *et al.* (2015) 'Gellan gum-coated gold nanorods: an intracellular nanosystem for bone tissue engineering', *RSC Advances*. Royal Society of Chemistry, 5(95), pp. 77996–78005.
- Vinatier, C. and Guicheux, J. (2016) 'Cartilage tissue engineering: From biomaterials and stem cells to osteoarthritis treatments', *Annals of Physical and Rehabilitation Medicine*. Elsevier Masson SAS, 59(3), pp. 139–144. doi: 10.1016/j.rehab.2016.03.002.
- Visser, J. *et al.* (2013) 'Biofabrication of multi-material anatomically shaped tissue constructs', *Biofabrication*, 5(3). doi: 10.1088/1758-5082/5/3/035007.
- Van Vlierberghe, S. *et al.* (2007) 'Porous gelatin hydrogels: 1. Cryogenic formation and structure analysis', *Biomacromolecules*, 8(2), pp. 331–337. doi: 10.1021/bm060684o.
- Waldman, S. D. *et al.* (2003) 'Long-term intermittent shear deformation improves the quality of cartilaginous tissue formed in vitro', *Journal of Orthopaedic Research*, 21(4), pp. 590–596. doi: 10.1016/S0736-0266(03)00009-3.
- Walter, S. G., Ossendorff, R. and Schildberg, F. A. (2019) 'Articular cartilage regeneration and tissue engineering models: a systematic review', *Archives of Orthopaedic and Trauma Surgery*. doi: 10.1007/s00402-018-3057-z.
- Wang, L. *et al.* (2009) 'A Comparison of Human Bone Marrow–Derived Mesenchymal Stem Cells and Human Umbilical Cord–Derived Mesenchymal Stromal Cells for Cartilage Tissue Engineering', *Tissue Engineering Part A*. Mary Ann Liebert, Inc., publishers, 15(8), pp. 2259–2266. doi: 10.1089/ten.tea.2008.0393.
- Wang, Y. *et al.* (2005) 'In vitro cartilage tissue engineering with 3D porous aqueous-derived silk scaffolds and mesenchymal stem cells', *Biomaterials*, 26(34), pp. 7082–7094. doi: 10.1016/j.biomaterials.2005.05.022.
- Wang, Y. *et al.* (2006) 'Cartilage tissue engineering with silk scaffolds and human articular chondrocytes', *Biomaterials*. Elsevier, 27(25), pp. 4434–4442. doi: 10.1016/j.biomaterials.2006.03.050.
- Wang, Y. *et al.* (2015) 'In vitro model of the blood-brain barrier established by co-culture of primary cerebral microvascular endothelial and astrocyte cells', *Neural regeneration research*. Wolters Kluwer--Medknow Publications, 10(12), p. 2011.
- Wayne, J. S. *et al.* (2005) 'In vivo response of polylactic acid–alginate scaffolds and bone marrow-derived cells for cartilage tissue engineering', *Tissue engineering*. Mary Ann Liebert, Inc. 2 Madison Avenue Larchmont, NY 10538 USA, 11(5–6), pp. 953–963.
- Weber, M.-C. *et al.* (2018) 'Simulating osteoarthritis in vitro with human scaffold-free 3D cartilage transplants', *Osteoarthritis and Cartilage*. Elsevier Ltd, 26(2018), p. S103. doi: 10.1016/j.joca.2018.02.223.
- Weber, M.-C. *et al.* (2019) 'In vitro and in silico modeling of cellular and matrix-related changes during the early phase of osteoarthritis', *Osteoarthritis and Cartilage*. doi: 10.1101/725317.
- Woodfield, T. B. F. *et al.* (2005) 'Polymer scaffolds fabricated with pore-size gradients as a model for studying the zonal organization within tissue-engineered cartilage constructs', *Tissue Engineering*, 11(9–10), pp. 1297–1311. doi: 10.1089/ten.2005.11.1297.
- Woolf, A. D. and Pfleger, B. (2003) 'Burden of major musculoskeletal conditions', *Bulletin of the World Health Organization*. World Health Organization, pp. 646–656. doi: 10.1590/S0042-96862003000900007.
- Wu, D. *et al.* (2018) '3D bioprinting of gellan gum and poly (ethylene glycol) diacrylate based hydrogels to produce human-scale constructs with high-fidelity', *Materials and Design*, 160. doi: 10.1016/j.matdes.2018.09.040.
- Xia, W. *et al.* (2004) 'Tissue engineering of cartilage with the use of chitosan-gelatin complex scaffolds', *Journal of Biomedical Materials Research Part B: Applied Biomaterials*, 71B(2), pp. 373–380. doi: 10.1002/jbm.b.30087.
- Xu, Z. *et al.* (2018) 'Chemically Modified Gellan Gum Hydrogels with Tunable Properties for Use as Tissue Engineering Scaffolds', *ACS Omega*, 3(6), pp. 6998–7007. doi: 10.1021/acsomega.8b00683.
- Yamaoka, H. *et al.* (2006) 'Cartilage tissue engineering using human auricular chondrocytes embedded in different hydrogel materials', *Journal of Biomedical Materials Research Part A: An Official Journal of The Society for Biomaterials, The Japanese Society for Biomaterials, and The Australian Society for Biomaterials and the Korean Society for Biomaterials*. Wiley Online Library, 78(1), pp. 1–11.
- Yang, J. *et al.* (2017) 'Cell-laden hydrogels for osteochondral and cartilage tissue engineering', *Acta Biomaterialia*. Acta Materialia Inc., 57, pp. 1–25. doi: 10.1016/j.actbio.2017.01.036.
- Yang, X. *et al.* (2018) 'Collagen-alginate as bioink for three-dimensional (3D) cell printing based cartilage tissue engineering', *Materials Science and Engineering C*. Elsevier, 83(June 2017), pp. 195–201. doi: 10.1016/j.msec.2017.09.002.
- Ye, K. *et al.* (2014) 'Chondrogenesis of infrapatellar fat pad derived adipose stem cells in 3D printed chitosan scaffold', *PLoS One*. Public Library of Science, 9(6).
- Yeung, P. *et al.* (2019) 'Collagen microsphere based 3D culture system for human osteoarthritis chondrocytes (hOACs)', *Scientific Reports*. Springer US, 9(1), pp. 1–14. doi: 10.1038/s41598-019-47946-3.
- You, F., Eames, B. Frank and Chen, X. (2017) 'Application of extrusion-based hydrogel bioprinting for cartilage tissue engineering', *International Journal of Molecular Sciences*, 18(7), pp. 8–14. doi: 10.3390/ijms18071597.
- You, F., Eames, B. Frank and Chen, X. (2017) 'Application of Extrusion-Based Hydrogel Bioprinting for Cartilage Tissue Engineering', *International Journal of Molecular Sciences*, 18(7). doi: 10.3390/ijms18071597.

- Youn, I. *et al.* (2006) 'Zonal variations in the three-dimensional morphology of the chondron measured in situ using confocal microscopy', *Osteoarthritis and Cartilage*. W.B. Saunders, 14(9), pp. 889–897. doi: 10.1016/J.JOCA.2006.02.017.
- Yu, I., Kaonis, S. and Chen, R. (2017) 'A Study on Degradation Behavior of 3D Printed Gellan Gum Scaffolds', *Procedia CIRP*. The Author(s), 65, pp. 78–83. doi: 10.1016/j.procir.2017.04.020.
- Yu, Y. *et al.* (2016) 'Three-dimensional bioprinting using self-assembling scalable scaffold-free "tissue strands" as a new bioink', *Scientific Reports*, 6(1), p. 28714. doi: 10.1038/srep28714.
- Yue, K. *et al.* (2015) 'Synthesis, properties, and biomedical applications of gelatin methacryloyl (GelMA) hydrogels', *Biomaterials*. Elsevier, 73, pp. 254–271.
- Zehentner, B. K., Dony, C. and Burtscher, H. (1999) 'The Transcription Factor Sox9 Is Involved in BMP-2 Signaling', *Journal of Bone and Mineral Research*, 14(10), pp. 1734–1741. doi: 10.1359/jbmr.1999.14.10.1734.
- Zhang, L. *et al.* (2012) 'An in vitro study of collagen hydrogel to induce the chondrogenic differentiation of mesenchymal stem cells', *Journal of Biomedical Materials Research - Part A*, 100 A(10), pp. 2717–2725. doi: 10.1002/jbm.a.34194.
- Zhang, Q. *et al.* (2014) 'Pore size effect of collagen scaffolds on cartilage regeneration', *Acta Biomaterialia*. Acta Materialia Inc., 10(5), pp. 2005–2013. doi: 10.1016/j.actbio.2013.12.042.
- Zhang, W. *et al.* (2008) 'OARSI recommendations for the management of hip and knee osteoarthritis, Part II: OARSI evidence-based, expert consensus guidelines.', *Osteoarthritis and cartilage*. Elsevier, 16(2), pp. 137–62. doi: 10.1016/j.joca.2007.12.013.
- Zhang, W. *et al.* (2016) 'Current research on pharmacologic and regenerative therapies for osteoarthritis', *Bone Research*, 4(October 2015). doi: 10.1038/boneres.2015.40.
- Zhang, X. *et al.* (2004) 'Primary murine limb bud mesenchymal cells in long-term culture complete chondrocyte differentiation: TGF- $\beta$  delays hypertrophy and PGE2 inhibits terminal differentiation', *Bone*. Elsevier, 34(5), pp. 809–817. doi: 10.1016/J.BONE.2003.12.026.
- Zhang, Y. S. *et al.* (2016) 'Bioprinting 3D microfibrinous scaffolds for engineering endothelialized myocardium and heart-on-a-chip', *Biomaterials*, 110, pp. 45–59. doi: <https://doi.org/10.1016/j.biomaterials.2016.09.003>.
- Zhao, W. *et al.* (2013a) 'Degradable natural polymer hydrogels for articular cartilage tissue engineering', *Journal of Chemical Technology & Biotechnology*. Wiley Online Library, 88(3), pp. 327–339.
- Zhao, W. *et al.* (2013b) 'Degradable natural polymer hydrogels for articular cartilage tissue engineering', *Journal of Chemical Technology and Biotechnology*, 88(3), pp. 327–339. doi: 10.1002/jctb.3970.
- Zheng, Z. *et al.* (2018) '3D bioprinting of self-standing silk-based bioink', *Advanced healthcare materials*. Wiley Online Library, 7(6), p. 1701026.
- Zhu, J. and Marchant, R. E. (2011) 'Design properties of hydrogel tissue-engineering scaffolds', *Expert Review of Medical Devices*, 8(5), pp. 607–626. doi: 10.1586/erd.11.27.
- Zhuang, P. *et al.* (2019) 'Layer-by-layer ultraviolet assisted extrusion-based (UAE) bioprinting of hydrogel constructs with high aspect ratio for soft tissue engineering applications', *PLoS ONE*, 14(6), pp. 1–21. doi: 10.1371/journal.pone.0216776.
- Zustiak, S. P. and Leach, J. B. (2010) 'Hydrolytically degradable poly (ethylene glycol) hydrogel scaffolds with tunable degradation and mechanical properties', *Biomacromolecules*. ACS Publications, 11(5), pp. 1348–1357.